Habilitation à Diriger des Recherches Présentée devant L'Université Joseph Fourier -Grenoble I:

Jean Christophe Gabriel

Habilitation à Diriger des Recherches

NANO-STRUCTURES ANISOTROPES : DE LA SYNTHESE A L'INTEGRATION

Présentée devant

L'Université Joseph Fourier - Grenoble I

Par Jean-Christophe P. Gabriel

Soutenance prévue le 20 Mai 2009

Jury :

Valérie Cabuil	Professeur (U.M.P.C.),	Rapporteur
Alain Ibanez	D.R. CNRS (Institut Néel)	Rapporteur
Annick Loiseau	D.R. ONERA (L.E.M.)	Rapporteur
Jacques Livage	Professeur (Collège de France)	Examinateur
Jean-Claude MOUTET	Professeur (U.J.F.)	Examinateur
Thomas Zemb	D.R. CEA Marcoule, I.C.S.M.	Examinateur

Table des Matières

I. CURRICULUM VITAE

Keywords: Multidisciplinarity, Broad knowledge base, Catalysis, Characterization, organic-inorganic Hybrid and Composite Materials, Hydrogen storage, Micro- Mesoporous materials, Nanotechnoologies, Nanomaterials, Nanofabrication, product & process development, Semi-conductors, Chimie douce, Self-assembly, Characterization, Engineering, Catalysis, Silicates.

A. Cursus Universitaire - Education

02/94-04/94 **HERCULES Training**, Grenoble (France)
Higher European Research Course for Users of Large Scale Experimental Equipment.
Training and development of International Networking with Large facility users

1991-1993 **Ph.D. in Inorganic Chemistry**, University of Orsay, France (Mention Très Honorable avec Félicitations)
Exfoliation of all-inorganic materials; Self assembly of molecular nanowires.
Nanomaterials synthesis via solid state and solution chemistry.
Hybrid organic-inorganic materials synthesized by electrocrystallization.
Magnetism..
Synthesis of C_{60} (Fall 1990) and study of its non linear optical properties.

1988-1992 **Ecole Normale Supérieure** (ENS) Paris (France)
Magistère de Chimie de l'Université d'Orsay (Mention Très Bien);
DEA de Chimie Inorganique, Paris VI (Mention Bien)

1985-1988 **Ecole Préparatoire to the Ecole Nationale d'Agronomie**:

B. Professional Experience

2007- CEA/LETI, Program Manager "Beyond CMOS"

2001-2007 ***Nanomix Inc.*** (Emeryville, California, USA)
Senior Scientist, Manager (2001-2002) , Ass. Director NanoEngineering (2004), Director Product Development (2006**), Senior Director, Product Development (2007) & Chemical Hygiene Officer (2001-present)**

- Report directly to VP Product development or CEO (depending on subjects).
- Currently program and technical lead on Nanomix's next commercial product.
- Lead Nanomix's grant writing effort to raise public money. High success rate (total of $4.1MM awarded)
- Co-leader for the development of Nanomix's future biosensor in the field of blood testing.
- Key Scientist in the development of Nanomix's Emergency Response Monitor (Capnometer).
- Technical leader for the first commercial electronic device based on carbon nanotube delivered Q1 2005: hydrogen sensor (ref. **33**[1], patents).
- Played an executive role in defining the scientific focus and vision for the delivery of the first products & revenues and developed the foundation of the IP portfolio. Direct advisor to

[1] Highlighted references pinpoint publications that I regard as my most important (usually based on number of citations and/or the journal impact factor).

current CEO during Nanomix's transition from a R&D company to a commercial enterprise. Advised against development of materials projects with little added value. Hired more than 20 people to build performing multidisciplinary and cross-functional teams. Directly involved in the recruitment of more than 70 people.

- Performed and supervised materials synthesis R&D; built two nanomaterials laboratories; developed proprietary processes for the:
- Synthesis, purification, solubilization and functionalization of monodispersed nanoparticles, single wall carbon nanotubes as well as BN nanotubes (ref. 30, 36, 37, 40 patents).
- Organic functionalization and polymer wrapping of nanotubes on 4" wafers (ref. **30**, **37**, patents)
- Synthesis of high surface area materials (oxides, nitrides) for hydrogen storage (ref. 36, patents).
- Growth of single wall carbon nanotubes on 100 & 150 mm silicon wafers (ref. **33**, patents)
- Process development for sensor production (scale up).
- Co-inventor of new capnography technology for medical applications (ref. 42, patents)
- Co-inventor on applications of our platform for the detection of biomolecules (patents)
- Studied electronic behavior of nanostructure based electronic devices (ref. **30**, 31, **35**, **37**, 38, **39**; patents)
- Led the development of plastic electronics based on networks of carbon nanotubes (ref. **35**, patents)
- Co-discoverer of a new class of materials for storing H_2 at higher temperatures than carbon (patents).
- Nanomaterial synthesis for lubrication, low-K dielectric constant and dye applications (ref. 36).
- Negotiated the integration of our materials into Alfa Aesar line of products (BN Nanotubes).
- Involved in fund raising and in contacts with Venture Capital firms. Our efforts have allowed us to rise up to $34 MM.
- Invited lecturer for Haas School of Business, University of California, Berkeley.
- Supervised/managed Nanomix's users of the Berkeley microfabrication facility.

1997-2001 Institut des Matériaux Jean Rouxel (Nantes, France)
Chargé de recherche 1ère classe, CNRS.

- Biomaterials for applications in ophthalmology (artificial cornea and vitreous fluids).
- Use of inorganic mesophases for the measurement of residual dipolar couplings of biomolecules by NMR (ref. **22**, **24**, 32).
- Electrosynthesis in conventional and supercritical fluids (ref. **17**).
- Synthesis of highly ordered nanocomposite and mesoporous materials (oxides) using self-assembly properties of nanomaterials (ref. 27, **29**).
- Functionalization of rhenium nanoclusters (ref. **2**, 3, 10, 15, 18, **23**). Investigation of their possible use in radio-immunotherapy.
- Characterization of the self-assembly of clays (ref. **26**).

- Exfoliation of inorganic materials for the synthesis of nanostructures. This allowed us to discover highly flexible inorganic polymers as well as polymers that coil into nanotubes (ref. **22**, **25**).
- Synthesis of all-inorganic liquid crystals based on nanotubes, nanowires, nanorods and nanosheets (oxides, sulfides). Characterization by SAXS, TEM, rheometry (ref. **1**, **4**, 13, **21**, **24**, 26, **28**, **34**).
- Synthesis of nanosized oxides using "Chimie Douce" techniques.
- Synchrotron User. Beam time awarded at LURE and ESRF synchrotron (for the later, extra time was awarded due to the excellence of the proposal).
- Supervision of 4 Ph.D. students and numerous interns.

1995-1996 ***Materials Research Laboratory*** (U.C. Santa Barbara)
Postdoc, with Professor A. K. Cheetham.

- Studied self-assembly of clay nanosheets: First clear-cut demonstration of the mesogenic (liquid crystal) properties of clay minerals. This work has been considered a milestone in the field as it generated a refutation of the house of cards model for aqueous clay suspensions (ref. **8**, 26).
- Structure determination of high surface area nanoporous materials (and their templates) for catalytic applications (ref. **7**, **9**, 12).
- Purification, ion exchange and study of natural zeolites (Laumontite, Goosecreekite).
- X-ray Diffraction study of Stable Free Radical salts as well as $C_{59}N$ (ref. 11).

1994 ***Nuclear Research Center of Risø*** (Denmark)
Postdoc, with Professor K. Bechgaard,

- Synthesis and study of self-assembled organic photoconductive monolayers by AFM, Small Angle Neutron Scattering and neutron reflectivity (ref. **6**).
- Synthesis and characterization of Si-Phtalocyanin.

C. Skills

Grant writing, IP generation & Strategy, Expertise in molecular chemistry, including inorganic & nanomaterials synthesis, catalysis, purification, biomaterials and biocompatible materials, radio-immunotherapy (^{188}Re), composite materials, inorganic polymers, HPLC and GPC, chemical vapor deposition, surfactants (soaps), soft matter, supercritical fluids, crystal growth, electrocristallization, electrodeposition, thin films; clean room and microfabrication processes, characterization methods of materials and polymers: diffraction (X-rays and neutrons – small angles, powder and single crystals), IR, Raman, UV spectroscopies, ESR, NMR, magnetic studies and microscopy (optical, electronic, STM-AFM). Knowledge in Rheology.

D. Awards, Grants and other forms of scientific recognition

2002-2006: Principal investigator in 4 Nanomix funded projects; Principal investigator of four awarded NSF SBIR ($1,250k), one NIH ($100k), Key scientist for another 4 granted phase I SBIR ($800k total), one granted DOE grant ($990k); one TSA grant ($1.0 MM), one Biostar grant awarded with F. Wudl, UCLA.

2002-2003: Nanomix: Promoted Sr. Director Product Development (March 2007), Promoted Director Product Development (Aug. 2006); Promoted Asso. Director NanoEngineering Sept 2004; Promoted Manager, process engineering and member of the executive board in Sept. 2003-Sept 2004; Promoted Manager, Chemistry and Materials Development in Sept 2002.

2002: Three internal awards at Nanomix for the integration of nanotubes into semiconductor processes.

1999: CNRS-INSERM Grant for the development of materials for artificial cornea. Collaboration with Hotel Dieu.

1997: Young scientist grant from the Pays de Loire region. Electrocrystallization in supercritical fluids

1996: Treasurer of the Californian Catalysis Society, 1996.

1995: Lavoisier Fellowship from the French Foreign Office.

1994: E.U. Human Capital and Mobility program's Fellowship.

1992-93: "Bourse de Formation par la Recherche", a 2 year French Research Ministry fellowship.

E. Memberships (past and current)

Member of the American Chemical Society (ACS), the Materials Research Society (MRS), the Société Française de Chimie (SFC), International Association for the Promotion of Supercritical Fluids (IAPSF).

F. Responsabilités administratives/Gestion de la recherche

- Trésorier de la Califonia Catalysis Society, 1996
- Referee pour le JACS, Langmuir, Proceeding of the National Academy of Science, J. Phys. Chem., JCS Chem. Comm., ChemPhysChem.
- Reviewer SNSF
- Membre du Scientific Advisory Board de l'*International Journal of Nanotechnology*, depuis sa création.
- Expert en Electronique Moléculaire à l'OMNT.
- Expert à l'OSEO - Agence Française de Sécurité Sanitaire de l'Environnement et du Travail, sur la saisine « Expertise Oséo - Evaluation des risques des Nanotubes de Carbone ».
- Seul Expert Européen pour l'Advanced Energy Consortium, Nov. 2008. 17 projets de demandes de financements expertisés.
- Février 2009 : rapporteur d'une thèse de doctorat de Chimie de l'Université de Montpellier, directeur : P. Batail.
- Membre du conseil scientifique du GDR Graphène et Nanotube (01/2009).

G. Activités d'enseignements

- 1989-1991 : Examinateur oral Physique/Chimie (Kholles) au lycée Chaptal en Mathématique Spéciale Biologie (Paris 17ème) de 1989 à 1991.
- 1993 : Chargé de TD (thermodynamique), Licence de Physique et Applications, Université d'Orsay.
- 2003 : Intervenant Invité à l'Université de Californie, Davis :
- 2001-2003: Intervenant invité à Haas School of Business, Université de Californie, Berkeley; Titre de l'intervention : « Etude d'un cas pratique de startup "Nanomix". »
- 2007 : Intervenant à l'INSTN dans le cadre de la formation « Nano Objets et Technologies », Titrte du cours (1h30) :
- 2008: Intervenant Invité au Collège Polytechnique dans le cadre de leur formation sur « l'électronique de demain » ; titre du cours (2h) : Au delà de la Road Map. Depuis 2008.
- Nov. 2008 : Chairman de la formation sur la Valorisation des travaux de recherche dans le cadre de CHEMTRONICS.

II. FONCTIONS D'ENCADREMENT ET DE FORMATION A LA RECHERCHE

A. Encadrement d'étudiants en Licence/Maitrise/DEA/Magistère ou de visiteurs étrangers :

- L. Hill (visiting Ph.D. Student from Cornell University, training to electrocrystallization technics), L. Rayburn (visiting Ph.D. Student from Cornell University, training to electrocrystallization technics), S. Lenain (Technical College, Nantes), C. Chaudemanche (Technical College, Nantes), E. Geraud (Technical College, Nantes), K. Hériau (Masters in Chemistry), Y. Bouret (1st year training period of the Ecole Normale Supérieure, Paris), D. Latremolière (1st year training period of the Ecole Normale Supérieure, Paris), T. Devic (1st year training period of the Ecole Normale Supérieure of Lyon), K. Herriau (Masters in Chemistry, Nantes University). Stéphane Baudron (Masters in Chemistry, Nantes University)
- While at UCSB, I supervised on a daily basis the following Ph.D. student : S. Wiegel, J. MacLeod et B. Campbell; I also trained Dr. Srinivasan Natarajan to single crystal X-ray diffraction.

B. Encadrement d'étudiants en Thèse spécialité chimie:

(1998-2001) : Co-direction de la thèse de Franck Camerel soutenue le 29 octobre 2001 à l'Université de Nantes intitulée «Nouveaux fluides complexes minéraux : Aspects structuraux, organisation macroscopique, aspects synthétiques» direction : JCP Gabriel /P. Batail. Jury M. Corriu Robert (Président), M. Livage Jacques (rapporteur), M. Levitz Pierre (rapporteur), M. Zemb Thomas (rapporteur), M. Davidson Patrick (examinateur), M. Palvadeau Pierre (examinateur), M. Gabriel Jean-Christophe (examinateur), M. Batail Patrick (examinateur). Ce travail a fait l'objet de sept publications III.A.22 (Angew. Chem.), III.A.24 (Nature) ; III.A.25 (NanoLetters) ; III.A.27 (J Chem. Soc. Chem. Commun.) ; III.A.29 (Adv. Funct. Mater.) ; III.A.32 (Carbohyd. Res.) ; III.A.34 (Langmuir). Mon activité d'encadrement a consisté à former Franck Camerel : (i) Aux concepts et méthodes de caractérisation de la matière molle ; (ii) à la recherche et à la synthèse de phase cristal liquides minérales ; (iii) à la synthèse et caractérisation de matériaux poreux ; (iv) à l'électrocristallisation ; (v) à la résolution de structure cristalline par diffraction des rayons X sur monocristaux ; (vi) à la rédaction d'articles dans des journaux à fort IF, et plus généralement aux techniques de valorisation des travaux effectués ; (vii) à la rédaction de projets (financements et ESRF) ; (viii) à la présentation orale.

(1999-2000) : Co-direction à Nantes pendant un an (avant mon départ pour les USA) de la thèse de Stéphane Baudron, soutenue à l'université d'Angers le 24 Juin 2002, intitulée « Liaisons hydrogène à l'interface organique-inorganique comme outils de construction de matériaux moléculaires cristallins ». Direction : JCP Gabriel (un an) /P. Batail. Jury : Didier Astruc, Eugenio Coronado, Patrick Batail, Claude Coulon, Alain Gorgues, Gérard Jaouen. Lors de cette première année de thèse j'ai formé Stéphane Baudron à l'utilisation de fluide supercritique et aux techniques d'électrocristallisation et de résolution de structures cristallines par diffraction des rayons X sur monocristaux. Son sujet initial concernait l'électrosynthèse en milieu supercritique. Suite à mon départ aux UXA, son sujet s'est recentré sur l'électrocristallisation en milieu classique de matériaux à base de donneurs organiques et du rôle de la liaison hydrogène dans les édifices moléculaires créés. N'ayant pas été particulièrement impliqué dans ces travaux, je n'ai pas jouer de rôle d'encadrement lors des deux dernières années de cette thèse.

C. Autres encadrements de Recherche

Membres de mon équipe de recherche à Nanomix (2001-2007) :
Prakash Gandhi (ingénieur), Shripal Gandhi (ingénieur), Shapour Golzar (ingénieur), Sean Kiluk (ingénieur), Willem-Jan Ouborg (ingénieur), Theo Paran, Steve Snaith, Charlene Sun (Senior ingénieur), Lap Tam (senior ingénieur), Amy Ye (ingénieur), Karen Chu (ingénieur), Jacob Sprunck, Dr. Maria Virginia P. Altoe (Senior Scientist), Vikram Joshi, Serena Kwan, Darin, Dr. Darin Olson (Manager Process), Michael Thai (Ingénieur), J. Loren Passmore, Lisa Baracker, Kanchan Joshi.
La nature de l'encadrement fourni à ces ingénieurs a été diverse et varie de la synthèse, manipulation, purification et caractérisation de nanotubes de carbone et autres nanomatériaux (C60, peapods, nanotubes de BN, nanoparticules, oxydes de bore à haute surface spécifique) , à leur utilisation comme matériaux de stockage par physisorption de l'hydrogène, à leur intégration dans des dispositif électronique ; à l'étude des dispositifs électroniques associés comme senseur chimique ; à la fonctionalisation de ces dispositifs. Notons, qu'en tant de « Chemical Hygiene Officer » à Nanomix, dans le cadre de leur formation à la manipulation de ces objets de taille nanométrique, une attention particulière a été mise sur les règles de manutention et de sécurités associées.

III. PRODUCTION SCIENTIFIQUE

A. Publications dans des journaux à comités de lecture

1 - *« A New Nematic Suspension Based on All-Inorganic Polymer Rods. »*
P. Davidson, J.-C. Gabriel, A.-M. Levelut, P. Batail, ***Europhys. Lett.*** **21**(3)317-322, 1993.

2 - *« Molecular Hexanuclear Clusters in the System Rhenium Sulfur Chlorine - Solid State Synthesis, Solution Chemistry, and Redox Properties. »*
J.-C. Gabriel, K. Boubekeur, P. Batail, ***Inorg. Chem.*** **32**(13)2894-2900, 1993.

3 - *« A Novel Type of 2-Dimensional Pattern of Association of Mixed-Valence Dimers in the Structures of 2 Cation Radical Salts of Thieno[3,4-D]-1,3-Dithiol-2-Ylidene and a Monovalent Hexanuclear Chalcohalide Rhenium Cluster. »*
J.-C. Gabriel, I. Johannsen, P. Batail, C. Coulon, ***Acta Cryst.*** **C49**, 1052-1056,1993.

4 - *« Nematic liquid crystalline mineral polymers. »*
P. Davidson, J.-C. Gabriel, A.-M. Levelut, P. Batail, ***Adv. Mater.*** **5**(9)665-668, 1993.

5 - *« The Construction of Electroactive Ordered Molecular Assemblies of Organic-Inorganic Character. »*
P. Batail, K. Boubekeur, M. Fourmigue, A. Dolbecq, J.-C. Gabriel, A. Guirauden, C. Livage, S. Uriel, ***New J. Chem.*** **18**(10) 999-1006, 1994 (Review article).

6 - *« Ordering of the Disk-like Hexakis(hexylthio)triphenylene in Solution and at a Liquid-Solid Interface. »*
J.-C. Gabriel, N.B. Larsen, M. Larsen, N. Harrit, J.S. Pedersen, K. Schaumburg, K. Bechgaard. ***Langmuir***, **12**(6) 1690-1692, 1996.

7 - *« Structure-Directing Effects In Zeolite Synthesis - A Single-Crystal X-Ray Diffraction, Si-29 Mas Nmr, and Computational Study of the Competitive Formation of Siliceous Ferrierite and Dodecasil-3c (ZSM-39). »*
S.J. Weigel, J.-C. Gabriel, E.G. Puebla, A.M. Bravo, N.J. Henson, L.M. Bull, A.K. Cheetham, ***J. Am. Chem. Soc.*** **118**(10)2427-2435, 1996.

8 - *« Observation of Nematic Liquid-Crystal Textures in Aqueous Gels of Smectite Clays. »*
J.-C.P. Gabriel, C. Sanchez, P. Davidson. ***J. Phys. Chem.*** **100**(26) 11139-11143, 1996.

9 - *« Synthesis ans Structure of a Three-Dimensional Open-framework Aluminophosphate $[NH_2(CH_2)_3NH_3]^+[HAl_3P_3O_{14}]^-.H2O$, Containing AlO_5 and AlO_6 Polyhedra. »*

S. Natarajan, J.-C.P. Gabriel, A.K. Cheetham, ***J. Chem. Soc., Chem. Commun.*** 1415-1416, 1996.

10 - *« A Concave, Cubic Diamond Coordination Polymer in the Versatile Chemistry of the Aqua-alkaline-earth Complex salts of Molecular hexanuclear Chalcohalide Rhenium Clusters, $[Ca(H_2O)_n]Re_6Q_6Cl_8.mH_2O$ and $[Mg(H_2O)_6]Re_6S_6Cl_8.2H_2O$ (Q=S, Se). »*
S.Uriel, K.Boubekeur, J.-C. Gabriel, P.Batail, J.Orduna, ***Bull. Soc. Chim. Fr.*** **133**, 783-794, 1996.

11 - *« A Pressure Sensitive Two-Dimensional Tetracyanoquinodimethane (TCNQ) Salt of a Stable Free Radical. »*
K.A. Hutchinson, G. Srdanov, R. Menon, J.-C.P. Gabriel, B. Knight, F. Wudl, ***J. Am. Chem. Soc.*** **118**(51) 13081-13082, 1996.

12 - *« Hydrothermal Synthesis and Structure of a Mixed Valent Heteropoly-oxometallate Keggin Salt: $[PMo_{4.27}W_{7.73}O_{40}^{6-}][H_3N(CH_2)_6NH_3^{2+}]_3$. »*
J.-C.P. Gabriel, R. Nagarajan, S. Natarajan, A.K. Cheetham, C.N.R. Rao, ***J. Solid State Chem.*** **129**, 257-262, 1997.

13 - *« Mineral Liquid Crystalline Polymers »*
P. Davidson, P. Batail, J.-C.P. Gabriel, J. Livage, C. Sanchez, C. Bourgaux, ***Prog. Polym. Sc.*** **22**(5) 913-936, 1997 (Review article).

14 - *« A Stable Free Radical as Donor: A Layer-Structure Organic Pressure Sensor. »*
K.A. Huchinson, G. Srdanov, R. Menon, J.-C. P. Gabriel, B. Knight, F. Wudl, ***Synth. Metals*** **86**(1-3) 2147-2148, 1997.

15 - *« $(nBu_4N)_4[Re_6S_5OCl_7]_2O$, An Oxo-Bridged Siamese Twin Cluster of Two Hexanuclear Oxochalcohalide Rhenium Clusters »*
F.Simon, K.Boubekeur, J.-C.P. Gabriel and P.Batail, ***J. Chem. Soc., Chem. Commun.*** **1998**(7) 845-846, 1998.

16 - *« Complex Fluids Based on the Flexible One-Dimensional Mineral Polymers, $[K(MPS_4)]_\infty$ (M = Ni, Pd); AutoFragmentation to Concave, Cyclic $(PPh_4)_3[(NiPS_4)_3]$.»*
J.Sayettat, L.M. Bull, J.-C.P. Gabriel, S.Jobic, F. Camerel, A.-M. Marie, M.Fourmigué, P.Batail, R.Brec, R.-L.Inglebert, ***Angew.Chem. Int. Ed.*** **37**(12) 1711-1714, 1998.

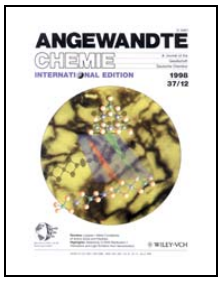

17 - *«* Electrocrystallization, an Invaluable Tool for the Construction of Ordered, Electroactive Molecular Solids*. »*
P.Batail, K.Boubekeur, M.Fourmigué, J.-C.P. Gabriel, **Chem. Mater.** ***10****(10) 3005-3015, 1998 (*Review article*).*

18 - *« $Cs_3Re_6S_7Cl_7$, the Missing, Water Soluble Octahedral Chalcohalide Rhenium(III) Cluster Mineral Salt »*
C.B. Guilbaud, J.-C. P. Gabriel, K.Boubekeur and P.Batail, ***C. R. Acad. Sci. IIc***, **1**, 765-770, 1998.

19 - *« Behaviour of the One-Dimensional, Inorganic Polymer $^1{}_\infty[MPS_4]^-$ Anions (M = Ni, Pd) in Organic Solutions »*
J.Sayettat, L.M. Bull, S.Jobic, J.-C.P. Gabriel, M.Fourmigué, P.Batail, R.Brec, R.-L.Inglebert, C.Sourisseau, ***J. Mater. Chem.*** **9**(1) 143-153, 1999.

20 - *«Lyotropic Mineral Liquid Crystals. »*
J.-C. P. Gabriel, P. Batail, ***Actualité Chim.***, **8-9**, 13-21, 1999 (Review article).

21 - « *New Trends in Colloidal Liquid Crystals Based on Mineral Moieties.* »
J.-C. P. Gabriel, P. Davidson, ***Adv. Mater.*** **12**(1) 9-20, 2000 (Review article).

22 - « *The First Use of a Mineral Liquid Crystal to Induce Residual Dipolar Couplings in a NMR Study of a Non-Labeled Biomolecule.* »
H. Desvaux, J.-C. P. Gabriel, P. Berthault, F. Camerel, ***Angew. Chem. Int. Ed.*** **40**(2) 373-376, 2001.

23 - « *The Chemistry of Hexanuclear Chalcohalide rhenium Clusters.* »
J.-C. P. Gabriel, K. Boubekeur, S. Uriel, P. Batail, ***Chem. Rev.*** **101**, 2037-2066, 2001 (Review article).

24 - « *Swollen Liquid-Crystalline Lamellar Phase Based on Extended Solid-Like Sheets.* »
J.-C. P. Gabriel, F. Camerel, B. J. Lemaire, H. Desvaux, P. Davidson, P. Batail, ***Nature*** **413**, 504-508, 2001.

25 - « *Solvent-induced Folding of the Mineral Chains* $^{1}{}_{\infty}[Nb_2PS_{10}]^{-}$ *into Nanotubes.* »
Franck Camerel, Jean-Christophe P. Gabriel, Patrick Davidson, Marc Schmutz, Thaddée Gulik-Krzywicki, Bruno Lemaire, Claudie Bourgaux, Patrick Batail, **Nano Letters** , **2**(4) 403-407, 2002.

26- *« The measurement by SAXS of the nematic order parameter of laponite gels »*
B. J. Lemaire, P. Panine, J.C.P. Gabriel and P. Davidson, ***Europhysic Letters***, **59**(1), 55–61. 2002.

27- *« Synthesis of a mesoporous composite material prepared by the self-assembly of mineral liquid crystals. »*
Franck Camerel, Jean-Christophe P. Gabriel and Patrick Batail, ***J. Chem. Soc., Chem. Commun.*** **2002**(17) 1926-1927, 2002.

28 - « *Mineral Liquid Crystals from Self-assembly of Anisotropic Nanosystems.* »
J.-C. P. Gabriel, P. Davidson ***Topics in Current Chemistry*** **226**, 119-172, 2003.

29 - « *Magnetically induced large mesoporous single-domain monoliths using a mineral liquid crystal as a template.* »
F. Camerel, J.-C. P. Gabriel, P. Batail ***Advanced Functional Materials 13***(5) 377-381, 2003.

30- « *Electronic Detection of Specific Protein Binding Using Nanotube FET Devices*. »
A. Star, J.-C. P. Gabriel, K. Bradley, G. Grüner, ***Nano Letters***, **3**(4) 459 - 463, 2003.

31 - « *Influence of Mobile Ions on Nanotube Based FET Devices.* »
K. Bradley, J. Cumings, A. Star, J.-C. P. Gabriel, G. Grüner, ***Nano Letters,*** **3**(5) 639-641, 2003.

32 - « *Dilute liquid crystals used to enhance residual dipolar couplings may alter conformational equilibrium in oligosaccharides.* »
P. Berthault, D. Jeannerat,Y. Camerel, F. Alvarez-Salgado, Y. Boulard, J.-C. P. Gabriel, H. Desvaux, ***Carbohydrate Research*** **338**, 1771-1785, 2003.

33 « *Large Scale Production of Carbon Nanotube Transistors: A Generic Platforms for Chemical Sensors.* » J.-C. P. Gabriel, ***Mat. Res. Soc. Symp. Proc.*** **762**, Q.12.7.1, 2003.

34 - « *Combined SAXS-rheology studies of liquid-crystalline colloidal suspensions of mineral moieties*.»
F. Camerel, J.-C. P. Gabriel, P. Panine, P. Davidson, ***Langmuir*** **19**(24); 10028-10035, 2003.

35 - « *Flexible nanotube transistors*.»
K. Bradley, J.-C. P. Gabriel, G. Grüner ***Nano Letters*** **3**(10) 1353, 2003. (Highlighted in Nanotech Alert and M.R.S. Bulletin).

36 - « *Nanococoon Seeds for BN Nanotube Growth*.»
M. V. P. Altoe, J. P. Sprunck, J.-C. P. Gabriel, K. Bradley, ***J. Mater. Science,* 38** (24): 4805-4810, 2003 (Cover).

37 - « *Interaction of Aromatic Compounds with Carbon Nanotubes: Correlation to the Hammett Parameter of the Substituent and Measured Carbon Nanotube FET Response.* »
A. Star, T.-R. Han, J.-C. P. Gabriel, K. Bradley, G. Grüner ***Nano Letters* 3**(10) 1421, 2003

38 - « *Short-channel effects in contact-passivated nanotube chemical sensors*.»
K. Bradley, J.-C. P. Gabriel, A. Star, G. Grüner ***Applied Phys. Lett*, 83**(18) 3821-3823, 2003.

39- « *Charge transfer from ammonia physisorbed on nanotubes*.»
K. Bradley, J.-C. P. Gabriel, M. Briman, A. Star, G. Grüner ***Phys. Rev. Lett.* 91**(21) 218301, 2003**.**

40- « *Quasi-Langmuir-Blodgett Thin Film Deposition of Carbon Nanotubes*. »
N. P. Armitage, J.-C. P. Gabriel, G. Grüner, ***J. Applied Phys.* 95**(6) 3228-3230, 2004.

41- «Hydrogen storage by physisorption: beyond carbon Strong hydrogen adsorbents for hydrogen storage.»
S.-H. Jhi, Y.-K. Kwon, K. Bradley, J.-C. P. Gabriel, ***Solid State Commun.* 129**, 769–773, 2004. (4th most downloaded article in the period Jan-March 2004).

42- « Nanoelectronic Carbon Dioxide Sensors.»
A. Star, T.-Ru Han, V. Joshi, J.-C. P. Gabriel, George Grüner ***Adv. Mater.*, 16**(22) 2049-2052**,** 2004 (Cover).

43- « Nanobioelectronics: integration of cell membranes and nanotube transistors.»
K. Bradley, A. Davis, J.-C. P. Gabriel, G. Grüner, ***Nano Letters*** 2005.

44- « Mineral Liquid Crystals.»
P. Davidson, J.-C. P. Gabriel ***Current Opinion Coll. Inter. Sciences* 9**, 377-383, 2005.

45- « Nanoelectronic CO_2 breath sensors.»
A. Star, V. Joshi, D. Thomas, J. Niemann, J.-C. P. Gabriel, C. Valcke, *Nanotech* **2005**, *1*, 104-107.

46- « Label-free detection of DNA hybridization using carbon nanotube network field-effect transistors.»
A. Star, E. Tu, J. Niemann, J.-C. P. Gabriel, C. S. Joiner, C. Valcke ***Proc. Nat. Acad. Sciences* 103**(4), 921–926, 2006.

47- « Gas Sensor Array Based on Metal-Decorated Carbon Nanotubes.»
Star, A.; Joshi, V.; Skarupo, S.; Thomas, D.; Gabriel, J.-C. P**. *J. Phys. Chem. B***. *110*(42); 21014-21020, 2006 (11th most downloaded article in Q4 2006 period)

B. Brevets

	Issued: PAT. NO.	Title
1	7,312,095	Modification of selectivity for sensing for nanostructure sensing device arrays
2	7,036,324	Hydrogen storage and supply system
3	6,991,773	Boron-oxide and related compounds for hydrogen storage

4	6,905,655	Modification of selectivity for sensing for nanostructure device arrays
5	6,894,359	Sensitivity control for nanotube sensors
6	6,834,508	Hydrogen storage and supply system
7	6,748,748	Hydrogen storage and supply system
8	6,672,077	Hydrogen storage in nanostructure with physisorption
	Applications: PUB.APP.NO.	Title
1	20070208243	Nanoelectronic glucose sensors
2	20070178477	Nanotube sensor devices for DNA detection
3	20070140946	Dispersed growth of nanotubes on a substrate
4	20070132043	Nano-electronic sensors for chemical and biological analytes, including capacitance and bio-membrane devices
5	20070114573	Sensor device with heated nanostructure
6	20070092437	Increasing hydrogen adsorption of nanostructured storage materials by modifying sp2 covalent bonds
7	20070048181	Carbon dioxide nanosensor, and respiratory CO2 monitors
8	20070048180	Nanoelectronic breath analyzer and asthma monitor
9	20070045756	Nanoelectronic sensor with integral suspended micro-heater
10	20060263255	Nanoelectronic sensor system and hydrogen-sensitive functionalization
11	20060228723	System and method for electronic sensing of biomolecules
12	20060165577	Boron oxide and related compounds for hydrogen storage
13	20060078468	Modification of selectivity for sensing for nanostructure device arrays
14	20060055392	Remotely communicating, battery-powered nanostructure sensor devices 1
5	20050279987	Nanostructure sensor device with polymer recognition layer
16	20050184641	Flexible nanostructure electronic devices
17	20050183424	Hydrogen storage and supply system
18	20050169798	Sensitivity control for nanotube sensors
19	20050157445	Nanostructures with electrodeposited nanoparticles
20	20050129573	Carbon dioxide nanoelectronic sensor

21	20040093874	HYDROGEN STORAGE AND SUPPLY SYSTEM
22	20040043527	Sensitivity control for nanotube sensors
23	20040031387	Boron-oxide and related compounds for hydrogen storage
24	20030226365	Hydrogen storage and supply system
25	20030175161	Modification of selectivity for sensing for nanostructure device arrays
26	20030167778	Hydrogen storage in nanostructures with physisorption
27	20030134433	Electronic sensing of chemical and biological agents using functionalized nanostructures

C. Conférences:

1. Conférences invitées répertoriées

- Mecatronic Connection 2008, Aix les Bains, 26/11/2008: « ***Nanocomposants, NEMS*** »
- Chimtronique 2007, Grenoble, 7/11/2007: « ***Nanomix, a Nanotube Startup !*** »
- Nanotech 2005, « ***Carbon Nanotube Field Effect Transistors and Sensors Based on Nanotube Networks.*** »
- Particles 2004, « **Nanotube Based Device Fabrication** »
- Materials Research Society Fall meeting 2004: « ***Commercial Carbon Nanotube Based Electronic Devices: a Reality.*** »
- Materials Research Society Fall meeting 2004: « ***Hydrogen storage by physisorption: beyond carbon.*** »
- **Keynote speaker** at the 8th International Symposium on metallomesogens (spring 2003)
- **Invited session organizer and speaker** at the Clay Minerals Society and Mineralogical Society of America joint meeting 2003.
- Complex Fluids based on Mineral Moieties, GDR 690 FORMES, May 17-20 1998, Forges-les-Eaux, France.
- Mineral Liquid Crystals, Galerne'98, October 4-10, 1998, La Rochette, France.
- Molecular Templates and Complex Fluids based on Mineral Moieties, GDR 690 FORMES, May 25-261999, Erdeven, France.

2. Autres présentations orales répertoriées à des Conférences:

- Structural Studies of Non-Conventional Nematic Phases, A.M. Levelut, P. Davidson, J.-C. Gabriel, P. Batail, J. Malthète. Congrès Annuel de la S.F.P. September 1992, Lille, France.
- C60: Production, Separation and Optical Properties, J.-C. Gabriel, M. Fourmigué, P. Batail, V. Dentan, P. Robin et J.P. Huignard. Congrès annuel de la S.F.P. September 1992, Lille, France.
- The Liquid Crystal Behavior of Some Smectites Clays. J.-C. P. Gabriel, C. Sanchez, P. Davidson. California Catalysis Society, Spring Meeting, 3-4 June 1996, U.C. Berkeley, California, USA.

- A Stable Free Radical as Donor: A Layer-Structure Organic Pressure Sensor. K. Hutchison, G. Srdanov, R. Menon, J.-C. Gabriel, B. Knight, F. Wudl. ACS meeting 1996.
- Behavior of the One-Dimensional, Inorganic Polymer 1∞[MPS4]- Anions (M = Ni, Pd) in Organic Solutions. J. Sayettat, L. M. Bull, S. Jobic, J.-C. P. Gabriel, M. Fourmigué, P. Batail, R. Brec, R.-L. Inglebert, C. Sourisseau, CNRS-RSC, 1st Materials Chemistry Discussion, Solid State Chemistry: Novel Synthesis and New Materials, 24-26 September 1998, Bordeaux, France.
- Complex Fluids with a Mineral Core and Associated Materials, J.-C. P. Gabriel, F. Camerel, P. Batail, Joint Workshop between the Institut des Matériaux Jean Rouxel and the Materials Research Laboratory, UCSB, 28 March – 1st April 1999, Nantes, France.
- Materials Research Society Spring Meeting 2003: **Nanotube Based Device Fabrication**

3. Séminaires invités répertoriés:

- Molecular Chemistry of Octahedral Clusters of Rhenium and Molybdenum, Solid State Physics Department, Risø National Laboratory, Denmark, December 1993.
- Liquid Crystals based on Mineral Moieties, Laboratoire Structure et Réactivité des Systèmes Interfaciaux, University Pierre et Marie Curie, Paris, France, 10th July 1998.
- Complex Fluids based on Mineral Moieties, Institut Charles Sadron, University Louis Pasteur, Strasbourg, France, 1st December 1998.
- Complex Fluids based on Mineral Moieties and Associated Materials, Laboratoire de Chimie de Coordination, University Paul Sabatier, Toulouse, France, 25th January 1999.
- Complex Fluids Based on Mineral Moieties, Mesoscopically Organized Composites, Institute of Theoretical Physics, Technical University of Berlin, Germany, 29th January 2000.
- Characterization Methods for the Study of Macromolecules at the Solid-Air Interface; Application to e-PTFE Used in Artificial Cornea, Hôtel Dieu, University Research Laboratory specializing in Substitutive therapy in Ophthalmology, Paris, France, 11th April 2000.
- Liquid Crystals and Complex Fluids Based on Mineral Moieties, Kodak Research Center, Chalon sur Saone, France, 8th June 2000.
- U.C. Berkeley, "**Nanotube Based Device Fabrication**" (02/2004).
- Parvis de la Science, Midi Minatec, Grenoble, 21/11/2008 : « *Les nanotechnologies, une discipline au carrefour des sciences* »

4. Communication par voie d'affiche

Non répertoriées

IV. ACTIVITES DE RECHERCHE

A. Travaux sur chimie, électrochimie de cluster moléculaires à cœur octaédrique

Mes activités de recherche dans ce domaine ont débutées lors de mon travail de thèse qui a permis de préciser la synthèse, les propriétés redox et la chimie en solution de ces molécules à cluster hexanucléaire de rhénium. L'article publié sur ce sujet à Inorganic Chemistry, suite à mon travail de thèse, a reçu un large nombre de citations. Il représente notamment le premier article décrivant la synthèse de ces clusters de façon reproductible. Ces travaux ont été ultérieurement poursuivis à l'IMN avec la synthèse de nouvelles molécules solubles et électroactives ainsi que de matériaux à

transferts de charges, notamment dans le cadre de ma participation à l'encadrement de la thèse de doctorat de Christophe Guilbaud. Mes activités dans ce domaine sont résumées dans un article publié dans la revue de l'ACS « Chemical Review » qui suit.

Chemistry of Hexanuclear Rhenium Chalcohalide Clusters

Jean-Christophe P. Gabriel, Kamal Boubekeur, Santiago Uriel,‡ and Patrick Batail*

Laboratoire Sciences Moléculaires aux Interfaces, CNRS FRE 2068, BP32229, 44322 Nantes, France

Received November 10, 2000

Contents

I. Introduction

The synthesis of $Re_6Q_4X_{10}$ (Q = Se, Te; X = Cl, Br)[1,2] by Fedorov in 1971 and, 12 years later, the work of Leduc, Perrin and Sergent[3] laid the foundation of an extensive high-temperature solid-state chemistry of hexanuclear rhenium chalcohalide clusters whose octahedral cores, $[Re_6Q_{4+n}X_{4-n}]^{(6-n)+}$ (Q = chalcogen, X = halogen, $n = 0-4$), are isostructural to the superconducting molybdenum chalcogenide analogues, the Chevrel−Sergent phases. The development of a molecular chemistry of their soluble cluster forms, whose inner core can only be prepared by high-temperature solid-state reactions, originates in the discovery, reported in 1987, of the solubility of $K[Re_6Se_5Cl_9]$ in ethanol.[4]

Today, the solution chemistry of hexanuclear rhenium chalcohalide clusters is in a stage of rapid development, an enhanced research activity driven by the opportunity to unravel the organic solution phase and redox chemistry of electron-rich mineral molecular forms and explore their substitution patterns and coordination chemistry which vary with the chalcogen/halogen ratio within the μ_3-ligand shell surrounding the octahedral metal cluster core.

Sizing up and assessing this burgeoning field in the present review, we seek to provide a perspective on a fruitful symbiosis among solid-state chemistry, which focuses on structural aspects, the chemistry

* Corresponding author. E-mail: batail@cnrs-imn.fr.
‡ Present address: Department of Inorganic and Organic Chemistry, Jaume I University, E-12080 Castellón, Spain.

10.1021/cr980058k CCC: $36.00
Published on Web 07/11/2001

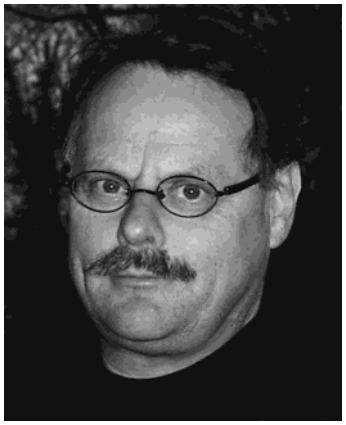

Patrick Batail was born in 1947 and obtained his Doctorat d'Etat (Inorganic Chemistry) at the University of Rennes I in 1976 where he became Assistant-Délégué (1973–1977) and then Chargé de Recherche CNRS from 1977 to 1985. He was an IBM postdoctoral fellow from 1978 to 1980 at the IBM Research Laboratory in San Jose, CA, where he worked with Jerry B. Torrance and Jim J. Mayerle on the neutral-to-ionic transition in TTF–chloranil. In 1985 he moved to the Laboratoire de Physique des Solides at the University of Paris-Sud at Orsay, France, to become Directeur de Recherche CNRS and create a molecular solid state chemistry group. In 1990 he also became Professeur Chargé de Cours at the Ecole Polytechnique in Palaiseau, France. In 1995 he moved to the Institut des Matériaux de Nantes, became its Director in 1998, and, following Jean Rouxel's sudden passing, went on to create a new CNRS Laboratory in 2000 (FRE 2068). His research interests concern the chemistry of molecular materials, especially long-range ordered hybrid solids whose collective conducting, magnetic, and optomagnetic properties are controlled by the nature of their organic–inorganic interface, the chemistry of organic solution soluble minerals, and lyotropic complex fluids with a mineral core. He has held visiting positions at the IBM Almaden Research Laboratory (1983), the Tokyo Institute of Technology (1989), and the Materials Research Laboratory at UCSB in 1996.

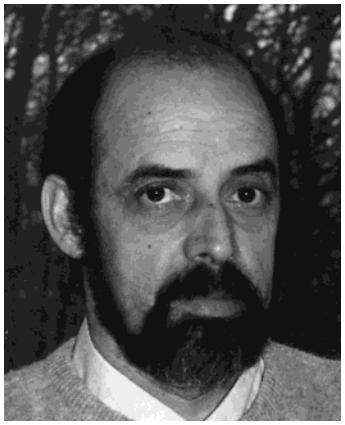

Kamal Boubekeur was born in Algiers, Algeria. He is a chemist engineer of the Ecole Supérieure de Chimie (Algiers) and a graduate of the University of Algiers (Doctorat 3ème cycle). His work dealt with the crystallographic studies of compounds of pharmaceutical interest. He served (1973–1985) at the University of Algiers as Assistant, then Maître-Assistant, and then Chargé de Cours. Simultaneously, he served (1985) as part time Chargé de Cours at the Ecole Nationale Polytechnique (Algiers). In 1985, he came in France and obtained a Ph.D. degree in 1989 from University of Rennes I where he has been also appointed guest Assistant Professor. His doctoral work with Patrick Batail shifted toward the synthesis, the crystal chemistry, and the electronic properties of radical cation salts of chalcohalide rhenium clusters. He then obtained a tenure position as Maître de Conférences in 1989 at the University of Paris XI, Orsay, France, where he joined the research group of Dr. Patrick Batail at the Laboratoire de Physique des Solides. After one year (1995) spent as Research Associate at the Centre National de la Recherche Scientifique, he moved to the Institut des Matériaux de Nantes at the University of Nantes where he is currently Maître de Conférences. His research interests include hybrid organic–inorganic materials, with focus on synthetic and structural chemistry of transition metal molecular ions and redox-active molecules based materials exhibiting electrical and magnetic properties.

Jean-Christophe P. Gabriel was born in Saint Nazaire, France. He is a graduate of the Ecole Normale Supérieure (Paris) and of the University of Paris Sud (Orsay, France). He received his Ph.D. degree in 1993 under the supervision of P. Batail. His doctoral work dealt with the molecular chemistry of octahedral rhenium and their association within organic–inorganic materials, as well as with the study of some lyotropic liquid crystals with a mineral core. After a first postdoctoral stay supported by an E.U. Human Capital and Mobility fellowship at the Risø National Laboratory (Denmark) with Professor K. Bechgaard, he was awarded a Lavoisier postdoctoral fellowship from the French Foreign Office and spend two years at the Materials Research Laboratory of the University of California, Santa Barbara, CA, with Professor Anthony K. Cheetham. In 1996, he was appointed in the position of "Chargé de Recherche" from the Centre National de la Recherche Scientifique at the Institut des Matériaux de Nantes, Nantes, France. His current research interests are in the study of complex fluids with a mineral core and to their use in the synthesis of nanocomposite materials.

Santiago Uriel was born in Madrid, Spain. He received his Ph.D. in 1992 from Zaragoza University, where he studied the synthesis of new (aminomethy)ltetrathiafulvalenes derivatives, under the direction of Dr. J. Garín. He spent two years (1993–1994) as a postdoctoral fellow with Dr. P. Batail under the E.U. Human Capital and Mobility Program at Laboratoire de Physique des Solides of the University of Paris XI (Orsay, France) and followed the group as Research Associate (1995) at the Centre National de la Recherche Scientifique at the Institut de Matériaux de Nantes. He worked in molecular chemistry of octahedral rhenium clusters and their association within organic–inorganic hybrid materials. He joined the research group of Dr. R. Llusar in 1997 at the Inorganic–Organic Chemistry Department at the University of Castellón. His research interest involve heterometallic clusters synthesis, optical and electrochemical properties, and hybrid organic–inorganic materials with electrical and magnetic properties.

of organic solution soluble minerals,[5] and synthetic methodologies and concepts of molecular inorganic chemistry, which altogether blend into one single chemistry at the organic−inorganic, solid-state−solution interface.

Part II travels through the entangled issues of phase formulations and structural principles, a journey guided by the concept of dimensionality in solid-state synthesis. Part III considers the cluster reactivity and molecular properties in organic solutions, and part IV singles out several current themes and serves to provide a perspective on promising area where developments are likely to continue to appear at a vigorous pace.

This review do not treat Bronger's seminal early work[6] and does not seek to encompass the all of rhenium sulfide chemistry, where trinuclear and tetranuclear clusters are also found and which was surveyed in recent papers by Saito[7] and others.[8] Some of the early developments of the high-temperature cluster chemistry of octahedral chalcohalides of molybdenum(II) and rhenium(III) were reviewed in 1988 by Perrin and Sergent.[9]

II. Cluster Core Synthesis

A. First Insight

The first synthesis of a series of hexanuclear rhenium chalcohalide cluster compounds, formulated $Re_3Q_2X_5$ (Q = Se, X = Cl, Br; Q = Te, X = Br), was reported by Opalovskii and Fedorov et al.[1,2] in 1971. The composition of these compounds was obtained by chemical analysis. Two synthetic pathways were explored which both involved the reduction of Re(IV) or Re(V) chalcogenides, either by gaseous halides ($ReSe_2 + Cl_2$ at 480 °C;[10] $ReSe_2 + Br_2$, starting reaction temperature 580 °C; $Re_2Te_5 + Br_2$, starting reaction temperature as low as 70 °C) or upon a redox reaction of Re(IV) diselenide with $ReCl_3$ or $ReBr_3$ at 700−720 °C.

B. A Chalcohalide with an Octahedral 24-Electron Re_6 Cluster Core

The 24-electron octahedral cluster core was first identified in chalcohalide hexarhenium compounds in 1983 by Leduc, Perrin, and Sergent within $Re_6Se_8Cl_2$ (Figure 1).[11,12] By this time, the success of partial substitution of molybdenum for rhenium atoms in Mo_6Q_8,[13] as well as the discovery by Brönger of metal chalcogenides with an octahedral rhenium cluster, such as $Na_4Re_6S_{12}$,[14] had led Sergent's group to search for chalcohalides with this hexanuclear core, hence Leduc's seminal thesis work defended in 1983 at the University of Rennes I.[3,15,16] The latter reports a large number of the known structural types of chalcohalides with an octahedral rhenium cluster, all of which obtained by high-temperature solid-state redox reaction between Re^0 and Re^V. Typically, a mixture of stoichiometric amounts of Re powder, $ReCl_5$, and Se (with a 10% excess of $ReCl_5$) is pressed into a pellet, sealed in a silica tube under ca. 10^{-5} Torr of residual pure argon, and then heated to 1300 K for 24 h.

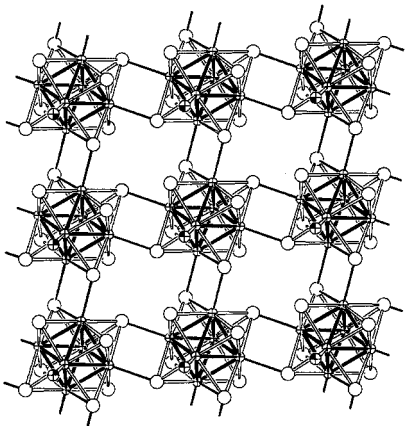

Figure 1. Projection of the 2-dimensional isomer of $Re_6Se_8Cl_2$, where a chalcohalide octahedral rhenium cluster was first revealed. Crossed, black-filled octant, and empty spheres represent Re, Cl, and Se atoms, respectively. The octahedral rhenium cluster as well as inter-$[Re_6Se_8]^{2+}$ core bonds are represented filled in black.

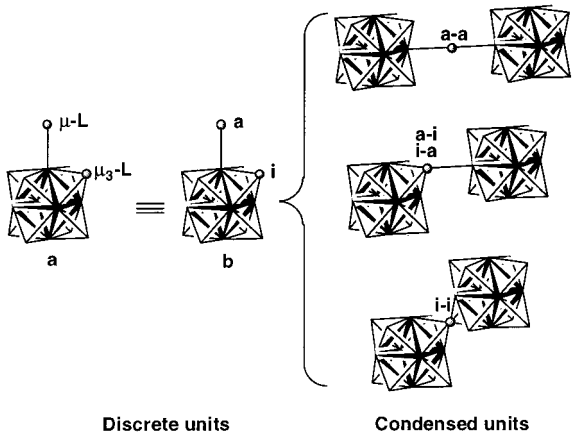

Figure 2. In Schäfer and von Schnering's notation, brackets designate the cluster core made out of 6 metal atoms forming the octahedral cluster and 8 *inner* ligands (μ_3) (the latter can be described as situated on the apex of a cube centered on the octahedral metal cluster), therefore labeled with a superscript "i". The outer/apical (*ausser* in German) ligands (μ) are not part of the core but are directly bonded to the metal atoms and, therefore, are listed outside the brackets and labeled with the superscript "a". Inner ligands that are also inner (μ_3-) or outer (μ-) ligands for a neighboring core are indexed with a superscript "i-i" or "i-a", respectively. Outer ligands that are also inner or outer ligands for a neighboring core are indexed with the superscript "a-i" or "a-a", respectively.

Within the two-dimensional polymer, $Re_6Se_8Cl_2$, the monomeric unit is readily apparent and underlined using Schäfer and von Schnering's nomenclature (Figure 2),[17] $[Re_6Se_4{}^{i}Se_{4/2}{}^{i-a}]Cl_2{}^{a}Se_{4/2}{}^{a-i}$. Thus, within the solid, $[Re_6Se_8]^{2+}$ cluster cores are linked by sharing four selenium ligands. The Re−Re distances, which range from 2.727 to 2.665 Å, have been associated with a 24-electron cluster core consisting of d^4 Re(III). Conductivity measurements performed on $Re_6Se_8Cl_2$, $Re_6Se_{8-x}Te_xCl_2$ ($0 \le x \le 1$) and $Re_6Se_{8-x}S_xCl_2$ ($0 \le x \le 1$) qualified these compounds as semiconductors.[16,18]

C. A $[Re_6Q_{4+n}X_{4-n}]^{(6-n)+}$ Core with a Tunable Charge

In addition to the former 2D polymer, Leduc synthesized a series of compounds whose inner core may be formulated, $[Re_6Se_{4+n}Cl_{4-n}]^{(6-n)+}$, where halide ligands substitute for a fraction of the eight inner chalcogen atoms. All these compounds have an isostructural 24-electron Re_6 cluster core, but as a consequence of the exchange of a divalent chalcogen atom by a monovalent halide, their core charge may vary between 6+ ($n = 0$) and 2+ ($n = 4$). In the solid state one find these motifs either isolated in discrete molecular forms, where each rhenium is capped by an apical, μ-ligand, or condensed into one-, two-, or three-dimensional polymers, where the motifs share one or several halogen and/or chalcogen "bridging" ligands, labeled "i-i", "a-a", "a-i", or "i-a", as exemplified in Figure 2.

D. Molecular Forms

1. Neutral

The single-crystal X-ray structure determination of $Re_6Se_4Cl_{10}$[3,15,19]—published in 1983 together with the unit cell of the isostructural phase $Re_6S_4Br_{10}$—revealed the molecular structure of the group of compounds previously synthesized and formulated $Re_3Q_2X_5$ by Opalovskii, Fedorov, and co-workers. The structure of $Re_6Se_4Cl_{10}$ at 153 K was also published independently by Fedorov and co-workers in 1984.[20,21] Other members of the series, namely $Re_6S_4Cl_{10}$,[22,23] $Re_6Te_4Cl_{10}$,[24] and $Re_6Q_4Br_{10}$ (Q = Se, Te),[1,25] have since been reported. All these triclinic compounds are isostructural with two geometrically similar, independent molecules per unit cell (Figure 3a). As expected for compounds with discrete, noninteracting molecular motifs, $Re_6Se_4Cl_{10}$ and $Re_6S_4Br_{10}$ are insulators.[16,19] However, an unusual voltage-dependent phase transition was observed in the study of their dielectric constant versus temperature. In addition, Opalovskii and co-workers demonstrated that some of these phases react with hot 50% potassium hydroxide solution.[2] No further studies on these solutions have since been performed.

Another neutral molecular chalcohalide with an octahedral rhenium cluster, namely, $[Re_6Te_6^{i}Cl_2^{i}]Cl_4^{a}(TeCl_2)_2^{a}$ (Figure 3b), has been reported recently by Ibers and co-workers.[26] The set of six outer ligands includes 4 chlorine atoms and 2 $TeCl_2$ groups, the latter being linked to the rhenium atoms through the Te atom. It should be noted that tellurohalide TeX_2 ligands were known only in the gas phase as unstable species[27,28] until Strähle (X = Br),[29] then Ibers' group (X = Cl),[26,30] and Fedin and co-workers (X = I)[31] were able to stabilize them on Re_4 cubane or Re_6 clusters. Another striking feature of this compound is that the six face-capping tellurium and two chlorine atoms are neatly ordered on the pseudocube surrounding the octahedral rhenium cluster. This unprecedented, precise registry of the eight mixed μ_3-ligands is likely to be favored by the large difference in size of the halide and tellurium atoms.

2. Monoanions

The synthesis and first single-crystal X-ray structure determination of a molecular monoanion, $[Re_6Q_5X_9]^-$, was achieved by Leduc with $K[Re_6Se_5Cl_9]$[3,15,32] (Figure 3c). The unit cell parameters of a series of $(M^+)[Re_6Q_5X_9]^-$ salts, based on the assignment of X-ray powder diffraction patterns, were also reported (Table 1). All these compounds were found to crystallize in the cubic $Pn\bar{3}$ space group and to be isostructural with $M^{2+}[Mo_6X_{14}]^{2-}$ (X = Cl, Br).[33] The structure is of the NaCl type with the Re_6 cluster anions located at the vertexes and at the center of the faces and the cations at both the center of the cell and the middle of the edges in the octahedral environment of the apical chlorine atoms of the six neighboring clusters. For a 1:1 stoichiometry, none of the accessible tetrahedral sites are occupied, as expected. A monoclinic distortion of this cubic structure has been identified from single-crystal X-ray diffraction data for $Rb[Re_6S_5Cl_9]$[23] (Figure 3d), $K[Re_6S_5Br_9]$,[34] and $Rb[Re_6Se_5Cl_9]$,[35] although $Rb[Re_6S_5Cl_9]$ and $Rb[Re_6Se_5Cl_9]$ were first reported as being cubic from an analysis of the powder X-ray diffraction patterns.[3,15,32] As expected, and similarly to $Re_6Se_4Cl_{10}$, $K[Re_6Se_5Cl_9]$ has been shown to be an electric insulator.[16]

Access to the organic solution chemistry of such mineral salts was demonstrated for the first time when $K[Re_6Se_5Cl_9]$ was found to be soluble in ethanol,[4] leaving the all-inorganic molecular anion intact (cf. section III). Cation exchange with tetrabutylammonium chloride yields $(Bu_4N^+)[Re_6Se_5Cl_9]^-$, which, in turn, is soluble in polar organic solvents. This prompted the synthesis of $Rb[Re_6S_5Cl_9]$ in order to prepare a soluble salt in the (Re, S, Cl) system.[23,36]

3. Dianions

An increase by 1 equiv of chalcogen in the synthesis of the monoanionic cluster salts, together with the use of a divalent cation, led to a series of compounds formulated $(M^{2+})\{[Re_6Q_6X_2]X_6\}$ (Table 1). These compounds, first synthesized and reported by Leduc and co-workers (M = Cd, Pb; Q = Se; X = Cl),[3,15] are isostructural to the cubic monoanion salts described above. Recently, it was reported that this structure is also obtained with other dications such as Zn^{2+}, Ca^{2+}, and Mg^{2+} in the (S, Cl) and (Se, Cl) systems.[37] A monoclinic distortion of the cubic structure, similar to the one described in the case of $(M^+)[Re_6Q_5X_9]^-$, is not observed for any of these hexanuclear rhenium clusters salts with dicationic metals.

Interestingly, these isostructural compounds present contrasted solubility properties. While a solvent able to dissolve the Cd^{2+}, Pb^{2+}, and Zn^{2+} salts has not been found, the Ca^{2+} and Mg^{2+} salts, which indeed were synthesized for that purpose, are readily soluble in a variety of organic solvents.[37] Thus, $[Ca(H_2O)_7][Re_6Q_6Cl_8]\cdot 3H_2O$ (Q = S, Se), $[Ca(H_2O)_8][Re_6S_6Cl_8]$, and $Mg(H_2O)_6[Re_6S_6Cl_8]\cdot 2H_2O$ readily crystallize out of the organic phase containing even minute amounts of water and are found to be in turn soluble in water.[37]

One should note that $Cs_2[Re_6Se_6Cl_8]$ has been reported[3] to crystallize in the hexagonal system and

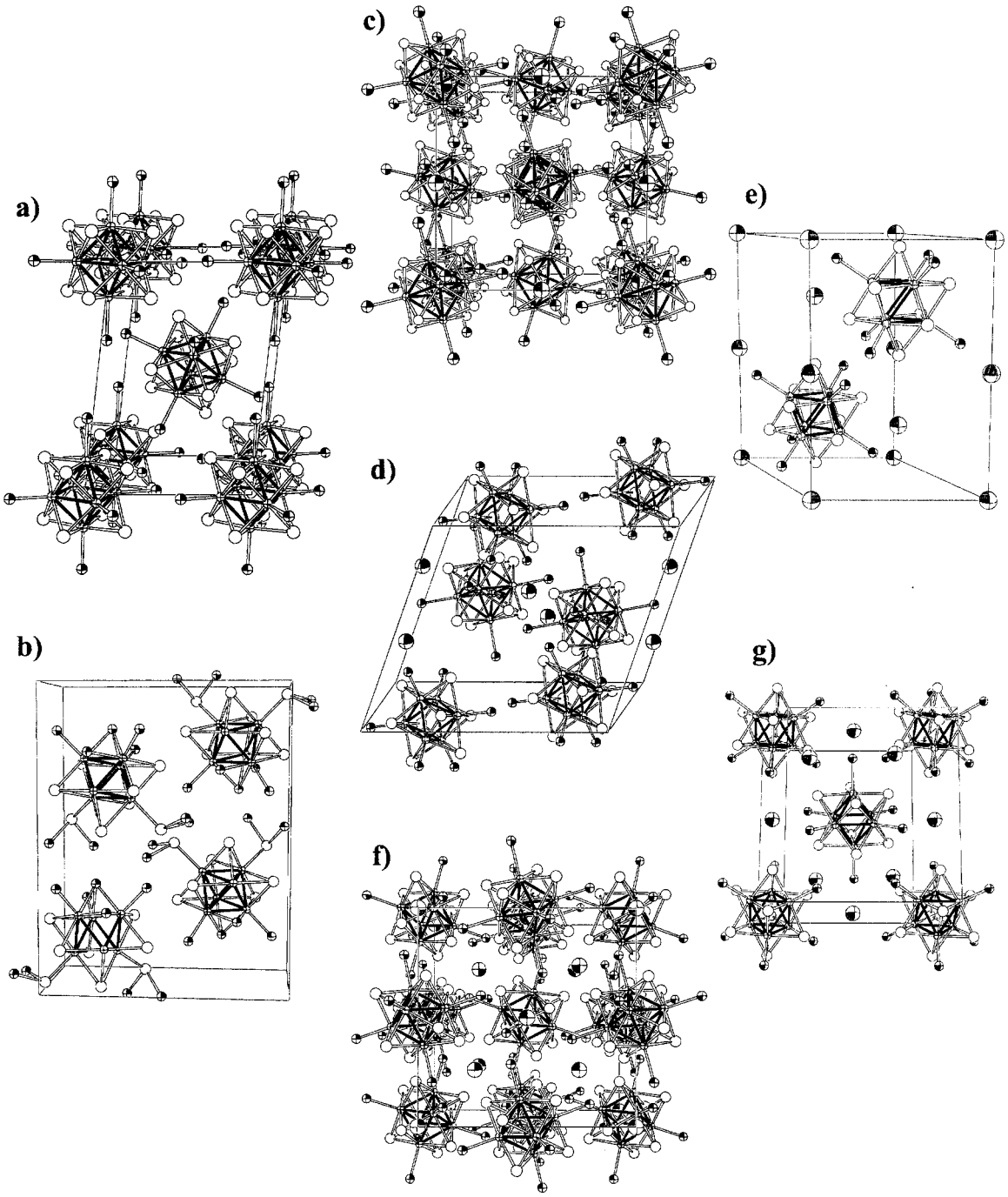

Figure 3. Unit cell content for the following compounds, all with discrete cluster motifs. (Empty and crossed atoms represent inner chalcogen or disordered chalcogen/halogen ligands and Re atoms, respectively; black-filled octant spheres represent apical or ordered inner halogen atoms as well as alkali-metal cations when present.). Key: (a) $Re_6S_4Cl_{10}$; (b) $Re_6Te_6Cl_6(TeCl_2)_2$; (c) $K[Re_6Se_5Cl_9]$; (d) $Rb[Re_6S_5Cl_9]$; (e) $Cs_2[Mo_6Cl_{14}]$; (f) $Rb_5[Re_6S_6Cl_8][Re_6S_7Cl_7]$; (g) $Cs_3[Re_6S_7Cl_7]$.

to be isostructural to $Cs_2[Mo_6Cl_{14}]$[38] (Figure 3e) although the structure was never fully reported. In addition, the hypothetical phase $K_2[Re_6Se_6Br_8]$ was postulated to have been formed as a soluble salt by reacting a mixture of Re_3Br_9, PbS, and KBr at 550 °C.[39] The formula of this salt was proposed on the basis that $[PPh_4^+]_2[Re_6Se_6Br_8]^{2-}$ is obtained upon cation exchange with tetraphenylphosphonium halide. However, the authors did not ruled out that the soluble inorganic salt could have been $Pb[Re_6Se_6Br_8]$. In that respect, a comparison of the X-ray powder pattern of the former raw material with that of $K_2[Re_6S_6Br_8]$, recently synthesized and characterized by single-crystal X-ray diffraction,[40] could help clarify the present uncertainty.

Both the dianionic and trianionic molecular forms $[Re_6S_6Cl_8]^{2-}$ and $[Re_6S_7Cl_7]^{3-}$ were found to coexist in a 1:1 ratio in $Rb_5[Re_6S_6Cl_8][Re_6S_7Cl_7]$.[23] This was the first example in this chemistry of a ternary, mixed-cluster salt. This salt crystallizes in the cubic system $Pn\bar{3}$ with an arrangement similar to the cubic structure obtained for $K[Re_6Se_5Cl_9]$, except that only the octahedral sites are filled in the latter whereas all octahedral as well as $^3/_4$ of the tetrahedral sites are occupied in $Rb_5[Re_6S_6Cl_8][Re_6S_7Cl_7]$ (Figure 3f). Thus, using Rb^+, a fraction of the tetrahedral sites

Table 1. Molecular, Inorganic, Hexanuclear Rhenium Chalcohalide Clusters Obtained by High-Temperature Reactions

charge	compd	Schäfer's notation	structure determination	refs
4−	$M^I_4[Re_6Q_8Cl_6]\cdot M^ICl$ (M^I = Tl, Y = S,Se; M^I = Cs, Q = S)	$n = 4$: $\{[Re_6Q_8{}^i]X_6{}^a\}^{4-}$	single crystal	45
	$Cs_4[Re_6S_8Br_6]\cdot CsBr$		single crystal	46
	$Cs_4[Re_6S_8I_6]\cdot Cs_2I_2$		single crystal	46
	$Cs_4[Re_6Se_8I_6]$		single crystal	46
	$Cs_{2.87}K_{1.13}[Re_6S_8Cl_6]$		single crystal	47
3−	$Cs_3[Re_6S_7Cl_7]$	$n = 3$: $\{[Re_6Q_7{}^iX^i]X_6{}^a\}^{3-}$	single crystal	43
	$Rb_3[Re_6S_7Br_7]$		single crystal	44a
2− and 3−	$Rb_5[Re_6S_6Cl_8][Re_6S_7Cl_7]$	$n = 2$ and 3	single crystal	23
2−	$Cs_2[Re_6Se_6Cl_8]$	$n = 2$: $\{[Re_6Q_6{}^iX_2{}^i]X_6{}^a\}^{2-}$	not specified	3
	$K_2[Re_6S_6Br_8]$		single crystal	40
	$Cd[Re_6Se_6Cl_8]$		powder	3
	$Pb[Re_6Se_6Cl_8]$		single crystal	15
	$M^{II}[Re_6Q_6Cl_8]$ (M = Ca, Mg; Q = S, Se)		powder	37
	$Zn[Re_6S_6Cl_8]$		single crystal	37
1−	$K[Re_6Se_5Cl_9]$	$n = 1$: $[Re_6Q_5{}^iX_3{}^i]X_6{}^a\}^-$	single crystal	15, 16, 32
	$M^I[Re_6Se_5Cl_9]$ (M = Li, Na, Rb, Cu, Ag)		powder	3
	$Rb[Re_6Se_5Cl_9]$		single crystal	35
	$M^I[Re_6S_5X_9]$ (M = Ag, X = Cl, Br; M = Rb, X = Cl)		powder	15
	$K[Re_6S_5Br_9]$		single crystal	34
	$Rb[Re_6S_5Cl_9]$		single crystal	23
neutral	"$Re_3Se_2Br_5$"	$n = 0$: $[Re_6Q_4{}^iX_4{}^i]X_6{}^a\}$	none	1, 2
	"$Re_3Se_2Cl_5$"		none	2
	"$Re_3Te_2Br_5$"		none	2
	$Re_6S_4Cl_{10}$		single crystal	23
	$Re_6Se_4Cl_{10}$		single crystal	15, 16, 19, 21
	$Re_6Te_4Cl_{10}$		single crystal	24
	$Re_6S_4Br_{10}$		powder	15, 16, 19
	$Re_6Q_4Br_{10}$ (Q = S, Se, Te)		powder and single crystal	25
	$[Re_6Te_6Cl_2]Cl_4(TeCl_2)_2$	n =2: $[Re_6Q_6{}^iX_2{}^i]X_4{}^aZ_2{}^a\}^a$	single crystal	26
2+	$[Re_6Te_8(TeBr_2)_6]Br_2$	$n = 4$: $\{[Re_6Q_8i]\ Z_6a\}^a$	single crystal	26
	$[Re_6Te_8(TeI_2)_6]I_2$		single crystal	31

[a] Z represents neutral ligands.

of the prototype cubic phase $K[Re_6Se_5Cl_9]$ must then be occupied or else the structure would collapse into the denser monoclinic arrangement described for $Rb[Re_6S_5Cl_9]$. Solid solutions, $M^+_{1+x}Re_6S_{4+x}Br_{10-2x}$ have been developed in the M−Re−S−Br (M = Na, K, Rb, Cs) system.[41]

4. Trianions

The series of compounds[15] with the formula $(M^{3+})\{[Re_6Q_7X]X_6\}^{3-}$ (M = Cr, Mn, Fe, Co, Eu; Q = Se; X = Cl) has been synthesized by Leduc, who did not ultimately ruled out an ambiguity in the oxidation state of the cation. This can be understood as Re metal is used in the synthesis, inducing a reductive atmosphere, prone to eventually reduce less electropositive metal cations along the course of the reaction. Indeed, most characterization results obtained in our group on compounds obtained by this route point toward the occurrence of mixtures of M^{2+} and M^{3+} cluster salts in the final product.[42] Hence, on the basis of the successful synthesis of $Cs_2[Re_6Se_6Cl_8]$,[3] the use of a monocation in the synthesis was subsequently favored. The viability of this alternative route was sustained by the fact that $(Bu_4N)_3[Re_6S_7Cl_7]$ was found to crystallize out of the aqueous mother liquor obtained from the washing of the reaction products of a typical $Rb[Re_6S_5Cl_9]$ synthesis,[23] thereby indicating that some amounts of $Rb_3[Re_6S_7Cl_7]$ are formed. The main problem with this "monocation" pathway is to avoid the synthesis of lower charged anion salts such as those described previously. This can be significantly overcome by optimizing the starting composition. Thus, a first attempt led us to synthesize the mixed-anion salt $Rb_5[Re_6S_6Cl_8][Re_6S_7Cl_7]$, described above, in which $[Re_6S_7Cl_7]^{3-}$ was unambiguously characterized for the first time in a mineral salt. Another indication that some amounts of $(M^+)_3[Re_6Y_7X_7]^{3-}$ might have actually been formed is that $(PPh_4)_3[Re_6S_7Br_7]$ could be recrystallized in low yield after reacting $Re_6S_4Br_{10}$ with KSCN at 550 °C, extraction in CH_3CN, and addition of PPh_4Br.[39] Further attempts, using Cs^+ instead of Rb^+ or K^+, resulted in the synthesis in good yield of the novel phase $Cs_3[Re_6S_7Cl_7]$ (Figure 3g).[43] This deep red colored salt has a novel monoclinic structure (space group $P2_1/c$). As expected, it is found to be highly soluble in water where cation exchange with tetrabutylammonium chloride affords pristine $(Bu_4N^+)_3[Re_6S_7Cl_7]^{3-}$, which in turn is soluble in numerous polar organic solvents.

One may have expected that $(M^+)_3[Re_6S_7Cl_7]^{3-}$ would have adopted the cubic structure of, with all the tetrahedral sites now fully occupied. A close look at two vacant tetrahedral sites in $Rb_5[Re_6S_6Cl_8][Re_6S_7Cl_7]$ reveals however that they are too small to allow for insertion of an additional cation as large as Cs^+ but may possibly allow for some amounts of Li^+ instead. This would lead to the yet unknown cubic phase $Rb_{2.5}Li_{0.5}[Re_6S_7Cl_7]$.

Finally, recent novel developments include the synthesis by direct high-temperature route of $Rb_3[Re_6Se_7Br_7]$, together with its recrystallized tetrahy-

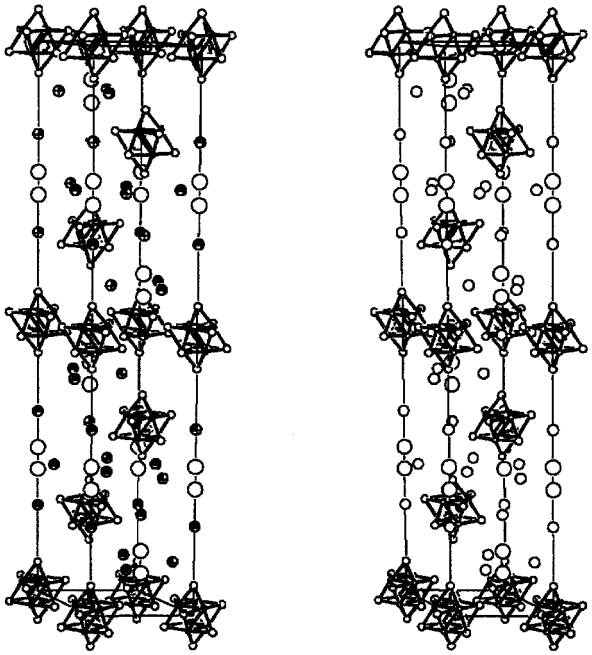

Figure 4. Stereoview of the unit cell content for $Cs_4[Re_6S_8Cl_6]$·CsCl. Isolated empty and black-filled octant spheres represent isolated chlorine and cesium atoms, respectively. To clarify this complex structure, apical halogen atoms have been removed.

drate $Rb_3[Re_6Se_7Br_7]\cdot 4H_2O$,[44a] and the synthesis of the hydrate $Rb_3[Re_6Se_7Br_7]\cdot H_2O$.[44b]

5. Tetraanions

Using a large excess of TlCl or CsCl in the initial pressed pellet mixture, Holm and co-workers succeeded in obtaining the first mineral salts containing the tetravalent molecular anion clusters ($n = 4$) in the $[Re_6Q_{4+n}X_{10-n}]^{n-}$ series, namely $M^I_4[Re_6Q_8Cl_6]\cdot M^ICl$ (M^I = Tl, Q = S, Se; M^I = Cs, Q = S) (Figure 4).[45] Further investigations led the same authors to the synthesis of other molecular salts containing an $[Re_6Q_8]^{2+}$ core, namely, $Cs_4[Re_6S_8Br_6]\cdot CsBr$ (hexagonal), $Cs_4[Re_6S_8I_6]\cdot 2CsI$ (cubic), and $Cs_4[Re_6Se_8I_6]$ (monoclinic).[46] Most of these salts are soluble in water, and ion exchange of the alkali metal cation by an alkylammonium cation affords salts soluble in common polar solvents (Table 1).

Note that a water-soluble potassium salt has recently been synthesized by Fedin et al.[47] by reaction of Re, S, S_2Cl_2, and KCl at 850 °C. Although this potassium salt has not been characterized yet, addition of CsCl to an aqueous solution of this water-soluble phase led the authors to isolate a crystalline product whose formulation, $Cs_{2.87}K_{1.13}[Re_6S_8Cl_6]$, was based on a single-crystal X-ray structure determination.

6. Dication

In addition to the synthesis of the neutral cluster $\{[Re_6Te_6Cl_2]Cl_4(TeCl_2)_2\}$ discussed in paragraph II.D.1, molecular compounds containing a $[Re_6Te_8]^{2+}$ core have also been prepared by high-temperature reactions (400−450 °C). Thus, a dicationic cluster formulated $\{[Re_6Te_8](TeBr_2)_6\}Br_2$ (Figure 5)[26] was synthesized in which each rhenium atom of the $[Re_6Te_8]^{2+}$ core is ligated by a $TeBr_2$ neutral group. This compound crystallized in the trigonal system.

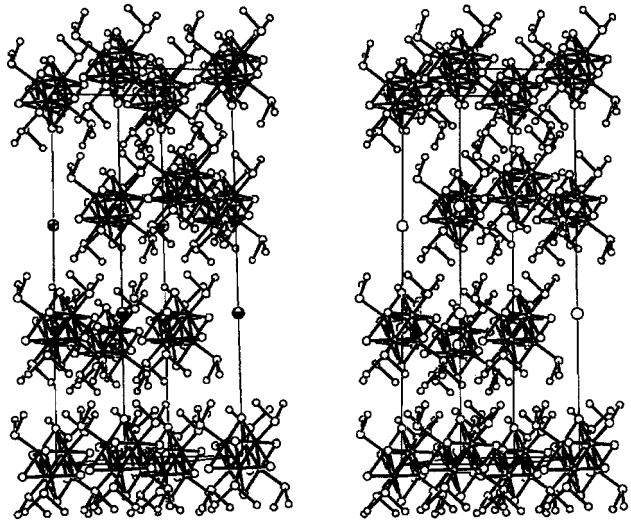

Figure 5. Stereoview of the unit cell content for $\{[Re_6Te_8](TeBr_2)_6\}Br_2$. (Isolated black-filled octant spheres represent bromine atoms.)

Its iodine analogue, $\{[Re_6Te_8](TeI_2)_6\}I_2$,[31] has also been synthesized. It is not isostructural to the bromine compound, crystallizes in the triclinic system, and appears to be diamagnetic as well as insoluble in usual solvents.

E. Polymeric Compounds

When $[Re_6Q_{4+n}X_{4-n}]^{(6-n)+}$ cores share any of the six outer or eight inner, halogen and/or chalcogen ligands, a wealth of polymeric cluster phases with all possible dimensionalities is generated (Table 2).

1. One-Dimensional

Thus, the structure of $Re_6Se_5Cl_8$ (Figure 6a)[3,15] reveals[48] that the compound contains a $[Re_6Se_5Cl_3]^{5+}$ core motif, identical to that identified within the molecular monoanion $[Re_6Se_5Cl_9]^-$. Two trans apical chlorine atoms are shared between neighboring cores, forming a neutral zigzag chain, hence, the compound formulation in Schäfer's nomenclature, $[Re_6Se_5^iCl_3^i]Cl_4^aCl_{2/2}^{a-a}$. $Re_6S_5Cl_8$ was later reported to be isostructural to its selenium analogue.[23] In both cases, the polymeric chains break into their neutral monomer components $\{[Re_6Q_5^iCl_3^i]Cl_5^a(solvent)^i\}$ in polar coordinating solvents such as acetonitrile,[23,49] as discussed in section III.A.2.

Negatively charged polymeric chains such as $Ag\{[Re_6Se_6^iCl_2^i]Cl_4^aCl_{2/2}^{a-a}\}$ and $Zn\{[Re_6Se_7^iCl^i]Cl_4^aCl_{2/2}^{a-a}\}$, isostructural with $Na[Mo_6Cl_{13}]$ (Figure 6b),[50] have been reported (p 78 of ref 15).

A strikingly different mode of linkage is that revealed by Holm and co-workers in the series $M^I_2[Re_6Q_8X_4]$ (M^I = Tl, Q = S, Se, X = Cl; M^I = Cs, Q = Se, X = Br),[45,46] where the $[Re_6Q_8]^{2+}$ cores are linked via inner chalcogen atoms in a symmetrical linkage mode; i.e., the outer ligand of a rhenium atom is one of the inner chalcogen of the adjacent cluster core and vice versa (Figure 6c,d). All these structures exhibit one-dimensional arrangements, whose explicit Schäfer formulation reads $M^I_2\{[Re_6Q_6^iQ_{2/2}^{i-a}]X_4^aQ_{2/2}^{a-i}\}$

Table 2. Inorganic Hexanuclear Rhenium Chalcohalide Cluster Polymers Obtained by High-Temperature Reactions

	compd	Schäfer's notation	(*n*, *m*, *l*) indices	refs
1D	$Re_6Se_5Cl_8$	$\{[Re_6Se_5^iCl_3^i]Cl_4^aCl_{2/2}^{a-a}\}$	(1, 0, 2)	15, 16, 48
	$Re_6S_5Cl_8$	$\{[Re_6S_5^iCl_3^i]Cl_4^aCl_{2/2}^{a-a}\}$	(1, 0, 2)	22
	$Ag[Re_6Se_6Cl_7]$	$\{[Re_6Se_6^iCl_2^i]Cl_4^aCl_{2/2}^{a-a}\}^-$	(2, 0, 2)	15
	$Zn[Re_6Se_7Cl_6]$	$\{[Re_6Se_7^iCl^i]Cl_4^aCl_{2/2}^{a-a}\}^{2-}$	(3, 0, 2)	15
	$M^I2[Re_6Q_8Cl_4]$ (M^I = Tl, Q = S, Se; M^I = Cs, Q = S)	$\{[Re_6Q_6^iQ_{2/2}^{i-a}]Cl_4^aQ_{2/2}^{a-i}\}^{2-}$	(4, 2, 0)	45
	$Cs_2[Re_6Se_8Br_4]$	$\{[Re_6Se_6^iSe_{2/2}^{i-a}]Br_4^aSe_{2/2}^{a-i}\}^{2-}$	(4, 2, 0)	46
2D	$Re_6Se_8Cl_2$	$\{[Re_6Se_4^iSe_{4/4}^{i-a}]Cl_2^aSe_{4/2}^{a-i}\}$	(4, 4, 0)	11, 15,18, 53, 55
	$Re_6Se_6Cl_6$	$\{[Re_6Se_6^iCl_2^i]Cl_2^aCl_{4/2}^{a-a}\}$	(2, 0, 4)	15, 48
	$Re_6Te_{16}Cl_6$	$\{[Re_6Te_8^i](TeCl_3)_2^a(Te_6)_{4/4}^{a-a}\}$	(4, 0, 4)*	56
	$Tl[Re_6Se_8Cl_3]$	$\{[Re_6Se_5^iSe_{3/2}^{i-a}]Cl_3^aSe_{3/2}^{a-i}\}^-$	(4, 3, 0)	45
	$Cs[Re_6Se_8I_3]$	$\{[Re_6Se_6^iSe_{2/2}^{i-a}]Cl_2^aCl_{2/2}^{a-a}Se_{2/2}^{a-i}\}^-$	(4, 2, 2)	46
3D	$Re_6S_7Br_4$	$\{[Re_6S_7^iBr^i]Br_{6/2}^{a-a}\}$	(3, 0, 6)	15, 48
	$Re_6Se_7Br_4$	$\{[Re_6Se_7^iBr^i]Br_{6/2}^{a-a}\}$	(3, 0, 6)	15, 48, 57
	$Re_6Q_8Br_2$ (Q = S, Se)	$\{[Re_6Q_6^iQ_{2/2}^{i-a}]Br_{4/2}^{a-a}Q_{2/2}^{a-i}\}$	(4, 2, 4)	25, 58
	$Re_6S_8Cl_2$	$\{[Re_6S_6^iS_{2/2}^{i-a}]Cl_{4/2}^{a-a}S_{2/2}^{a-i}\}$	(4, 2, 4)	60
	$Re_6Te_{16}Cl_{18}$	$\{[Re_6Te_8^i](Te_8Cl_{18})_{6/6}^{a-a}\}$	(4, 0, 6)[a]	56

[a] Here, because the apical ligands are different, the net charge of the cluster motif reads ($m - n + l/2$).

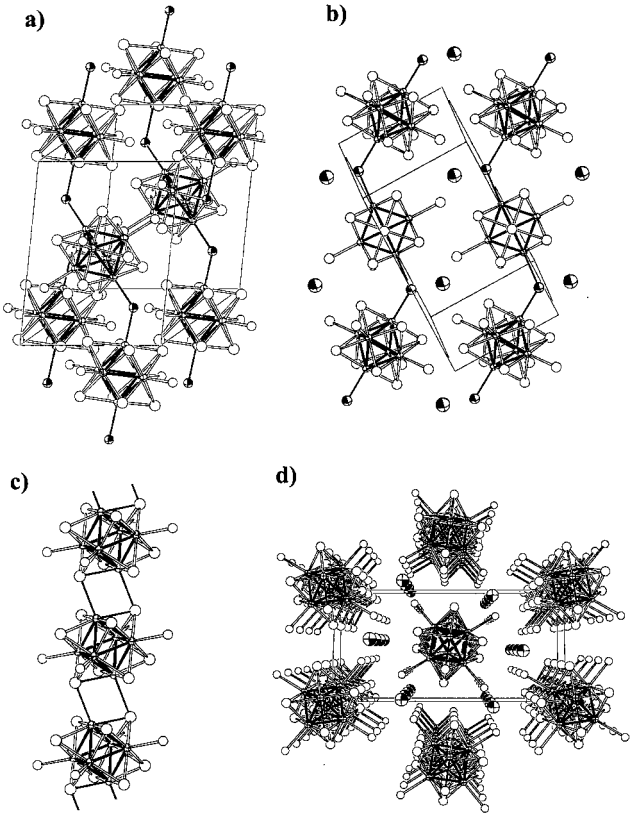

Figure 6. Variety of chains within the one-dimensional compound series. (Empty spheres represent inner μ_3-chalcogen or μ_3-halogen ligands or nonbridging apical μ-halogen atoms; crossed spheres represent metal atoms; black-filled octant spheres represent apical bridging "a-a" (μ_2) halogen as well as alkali-metal atoms; metal−metal as well as bridging bonds are filled in black.) One type is illustrated by (a) $Re_6S_5Cl_8 = [Re_6Se_5^iCl_3^i]Cl_4^aCl_{2/2}^{a-a}$ and (b) $Na[Mo_6Cl_{13}] = Na\{[Mo_6Cl_8^i]Cl_4^aCl_{2/2}^{a-a}\}$. Another type of chain can be observed within $M^I_2[Re_6Q_8Cl_4] = M^I_2\{[Re_6Q_6^iQ_{2/2}^{i-a}]Cl_4^aQ_{2/2}^{a-i}\}$ (M^I = Tl, Q = S, Se, X = Cl; M^I = Cs, Q = S, X = Br); (c) presents detail of this chain, and (d) shows a perspective representation of the structure viewed along the chain axis.

and where the lack of X^{a-a} (μ_2-) halogen bridges brings the $[Re_6Q_8]^{2+}$ cores closer to each other than within the chains in $Re_6Q_5Cl_8$. One consequence is

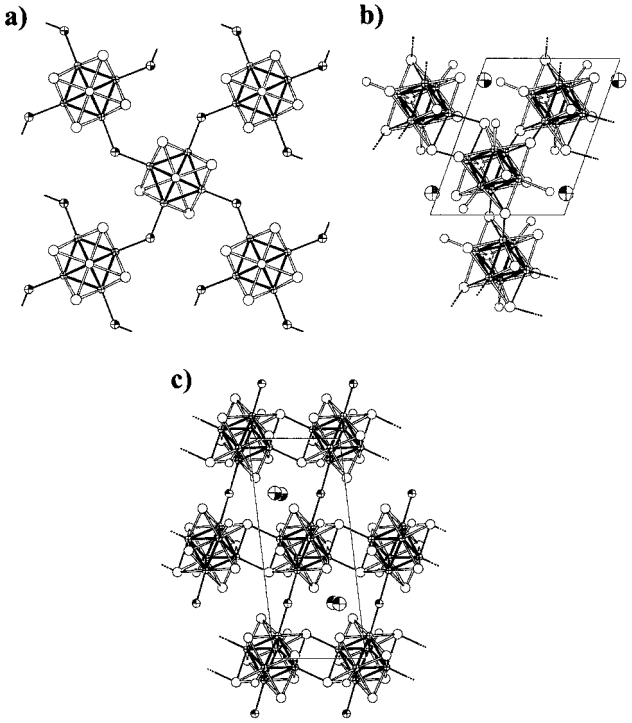

Figure 7. Projection normal to the mean plan of the 2-dimensional network of clusters within (same assignment as in Figure 6): (a) $Re_6Se_6Cl_6 = [Re_6Se_6^iCl_2^i]Cl_2^aCl_{4/2}^{a-a}$; (b) the triclinic structure, $Tl[Re_6Se_8Cl_3] = Tl_3\{[Re_6Se_5^iSe_{3/2}^{i-a}]Cl_3^aSe_{3/2}^{a-i}\}$; (c) the monoclinic structure, $Cs[Re_6Se_8I_3] = Cs\{[Re_6Se_6^iSe_{2/2}^{i-a}]I_2^aI_{2/2}^{a-a}Se_{2/2}^{a-i}\}$.

that such chains can neither be dissolved in usual solvents nor dissociated into their monomeric components.

2. Two-Dimensional

$Re_6Se_6Cl_6$ is the prototypical two-dimensional polymer. It is characterized by its distinctive, four coplanar μ_2-chloride ligands as shown (Figure 7a).[3,15,16] Its Schäfer−von Schnering formulation reads $[Re_6Se_6^iCl_2^i]Cl_2^aCl_{4/2}^{a-a}$, and it is isostructural to $MoCl_2$.[51] Just as the latter, this 24-electron cluster phase is

insulating[16] and, as shown for $MoCl_2$ by Sheldon in 1960,[52] it can be dismantled in polar solvents.[49]

Another pattern of two-dimensional association is revealed in $Re_6Se_8Cl_2$ where any given core is now linked to four adjacent neighbors via symmetrical linkage modes (Figure 1). Here, Se inner atoms of any cluster serve as outer ligands for neighboring clusters. Thus, face-capped octahedral $[Re_6Se_8]$ clusters, each with two trans terminal Cl ligands, are directly linked through intercluster Re−Se bonds to form eight connected sheets (see Figure 1). Photoelectrochemical investigations of $Re_6Se_8Cl_2$ single crystals have shown that it is an n-type semiconductor with a direct optical transition and a band gap of 1.42 eV.[53] Its electronic structure has been investigated and discussed (see section IV.G) with an emphasis on the structural relationship to the Chevrel−Sergent supraconducting phases[16,18] and because semiconducting behavior had been predicted for Chevrel−Sergent phases with 24 electrons/cluster unit.[54,55]

A remarkable example of framework isomerism in inorganic solid-state chemistry has been reported by Holm and co-workers while comparing the structures of the two-dimensional compounds $(Tl^+)[Re_6Se_8Cl_3]^-$ [45] and $(Cs^+)[Re_6Se_8I_3]^-$.[46] Thus, as exemplified in Figure 7b, any $[Re_6Se_8]^{2+}$ core within $Tl[Re_6Se_8Cl_3]$ is linked to *three* neighboring $[Re_6Se_8]^{2+}$ cores via three symmetrical linkage modes. Therefore, $[Re_6Se_8Cl_3]^-$ reads $\{[Re_6Se_5{}^iSe_{3/2}{}^{i-a}]Cl_3{}^aSe_{3/2}{}^{a-i}\}^-$. Now, for $Cs[Re_6Se_8I_3]$, each $[Re_6Se_8]^{2+}$ core is linked to *four* neighboring $[Re_6Se_8]^{2+}$ cores but via only two symmetrical linkage modes and two additional bridging apical chlorine atoms (Figure 7c). Hence the novel formulation now reads $\{[Re_6Se_6{}^iSe_{2/2}{}^{i-a}]I_2{}^aI_{2/2}{}^{a-a}Se_{2/2}{}^{a-i}\}^-$. As we shall see in section 3, structural isomers have been previously reported for hexarhenium chalcohalide clusters in the neutral $Re_6Q_8X_2$ series.

Finally, in their recent investigation of the Re−X−Te system, Ibers and co-workers obtained a two-dimensional phase, $Re_6Te_{16}Cl_6$ (Figure 8a),[56] in which two Re atoms at opposite vertexes of the Re_6 octahedron are capped by $[TeCl_3]^-$ ligands. The four remaining coplanar Re atoms are capped with neutral Te_6 ligands, any single Te_6 ligand being linked to four different $[Re_6Te_8]^{2+}$ cores, hence, the "4/4" indices in Schäfer's notation, $[Re_6Te_8{}^i](Te_6)_{4/4}{}^{a-a}(TeCl_3)_2{}^a$. In the latter, one chlorine atom has a longer Te−Cl bond (2.817(9) Å in comparison to 2.387(8) and 2.433(8) Å for the two others) and is in fact interacting with the Te^{2+} center of a $[TeCl_3]^-$ ligand belonging to an adjacent layer ($Cl_3Te\cdots Cl$ 3.028(9) Å), and the Te^{2+} ion adopts a square-planar coordination pattern (Figure 8b). Therefore, and even though no covalent bonding can be found between $[TeCl_3]^-$ ligands, it is suggested that the two-dimensional motifs are strongly interacting. Further theoretical work is necessary in order to evaluate the actual dimensionality of the chemical bonding in this system.

3. Three-Dimensional

The structure of $Re_6Q_7Br_4$ (Q = S, Se), initially reported by Leduc,[15,3] has been made available in full details only recently (Figure 9a).[57] It is to be considered as the prototypical, three-dimensional (dimensionality $d = 3$) halogen-bridged octahedral rhenium cluster architecture of general formula $Re_6Q_{4+d}X_{10-2d}$. Within the rhombohedral ($R\bar{3}c$) structure, each $[Re_6Se_7Br]^{3+}$ core is linked via halogen-bridged atoms to six $[Re_6Se_7Br]^{3+}$ neighboring cores located at the apex of an octahedron. The synthesis of $Re_6Se_7Cl_4$ has also been reported,[15,48] but systematic twinning precluded the structure determination. These three-dimensional phases, formulated $[Re_6Q^i7X^i]X_{6/3}{}^{a-a}$, proved to be insoluble.[49]

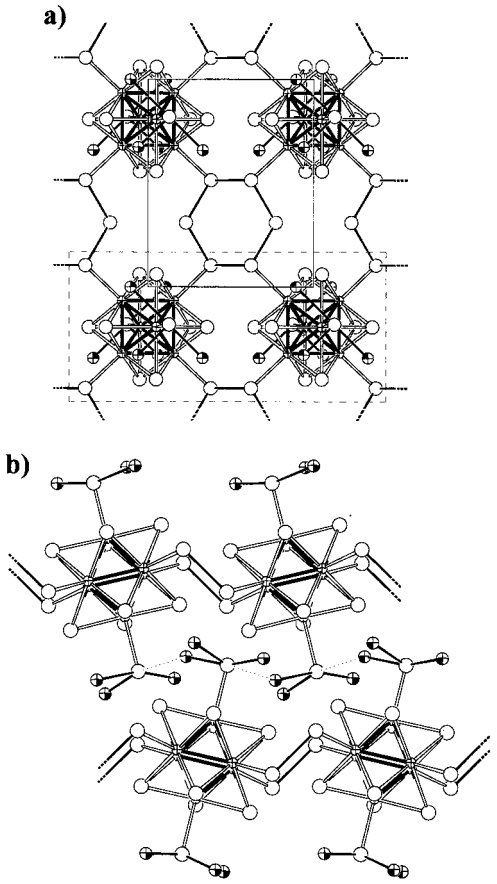

Figure 8. (a) Projection of the 2-dimensional network of clusters within $[Re_6Te_8{}^i](Te_6)_{4/4}{}^{a-a}(TeCl_3)_2{}^a$ perpendicularly to the mean plan of the sheet (same assignment as in Figure 6; Re−Re, Te−Te, and short Te−Cl bonds are filled in black). The area delimited by the dashed rectangle is shown in (b) in a perpendicular orientation involving two successive layers (the long Te−Cl contact is indicated here by a dotted line).

The mixed, intercluster core, three-dimensional bridging mode, in which both halogen bridges and symmetrical linkage modes coexist, is exemplified in $Re_6Q_8X_2$ (X = Cl, Q = S; X = Br, Q = S, Se) (Figure 9b).[58,59,60] A striking point is that these compounds have the same formulation as the two-dimensional prototype, $Re_6Se_8Cl_2$. In the present three-dimensional isomer, formulated $[Re_6Q_6{}^iQ_{2/2}{}^{i-a}]Q_{2/2}{}^{a-i}X_{4/2}{}^{a-a}$, one identifies infinite symmetrical linkage modes generating chains similar to the one observed in $M^I{}_2Re_6Q_8Cl_4$ (Figure 6c). The four remaining rhenium atoms, located in planes perpendicular to the chain axis, are linked to the adjacent chains via halogen bridges.

Table 3. Schäfer−von Schnering's Notation of All Known (*n*, *l*) Hexanuclear Rhenium Chalcohalide Clusters

l		*n* = 0	*n* = 1	*n* = 2	*n* = 3	*n* = 4
0	molecular, *d* = 0	$\{[Re_6Q_4{}^iX_4{}^i]X_6{}^a\}$	$\{[Re_6Q_5{}^iX_3{}^i]X_6{}^a\}^-$	$\{[Re_6Q_6{}^iX_2{}^i]X_6{}^a\}^{2-}$	$\{[Re_6Q_7{}^iX^i]X_6{}^a\}^{3-}$	$\{[Re_6Q_8{}^i]X_6{}^a\}^{4-}$
2	1D, *d* = 1		$\{[Re_6Q_5{}^iX_3{}^i]X_4{}^aX_{2/2}{}^{a-a}\}$	$\{[Re_6Q_6X_2{}^i]X_4{}^aX_{2/2}{}^{a-a}\}^-$	$\{[Re_6Q_7{}^iX^i]X_4{}^aX_{2/2}{}^{a-a}\}^{2-}$	
4	2D, *d* = 2			$\{[Re_6Q_6{}^iX_2{}^i]X_2{}^aX_{4/2}{}^{a-a}\}$		
6	3D, *d* = 3				$\{[Re_6Q_7{}^iX^i]X_{6/2}{}^{a-a}\}$	

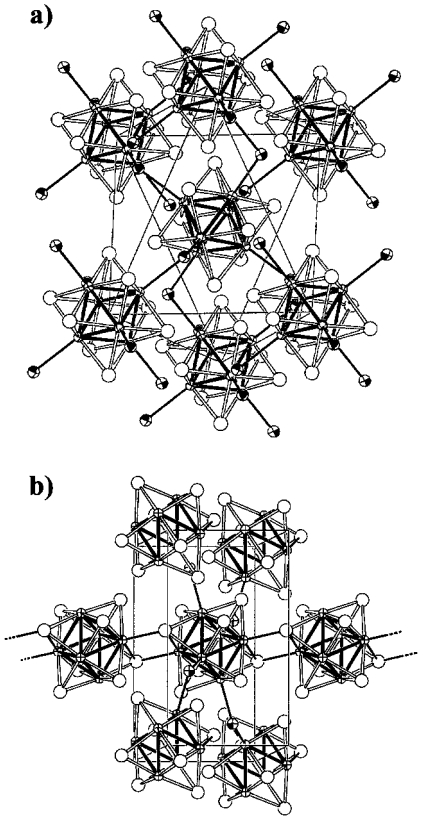

Figure 9. Prototypical structure for the 3-dimensional compounds (same assignment as in Figure 6; to simplify this complex structure, only the central *cluster* motif is shown complete with all bonds drawn) shown here in projection: (a) $Re_6Q_7Br_4 = [Re_6Q^i7Br^i]Br_{6/3}{}^{a-a}$ (Q = S, Se); (b) $Re_6Q_8X_2 = [Re_6Q_6{}^iQ_{2/2}{}^{i-a}]Q_{2/2}{}^{a-i}X_{4/2}{}^{a-a}$ (X = Cl, Q = S; X = Br, Q = S, Se).

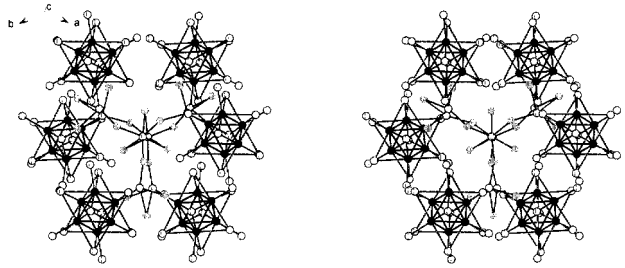

Figure 10. Stereoview of the $[Te_8Cl_{18}]^{2-}$ ligand environment in $Re_6Te_{16}Cl_{18} = [Re_6Te_8{}^i](Te_8Cl_{18})_{6/6}{}^{a-a}$. Each ligand chelates six $[Re_6Te_8]^{2+}$ cluster cores (Re, Te, and Cl atoms are drawn as black, crossed white, and gray hollow spheres, respectively).

The singularity of tellurium in these systems is again exemplified in the three-dimensional series by $Re_6Te_{16}Cl_{18}$ (Figure 10).[56] In this compound, one identifies $[Re_6Te_8]^{2+}$ cores, now bridged by a complex $[Te_8Cl_{18}]^{2-}$ apical ligand linking six cores together in a three-dimensional fashion, as shown by the formulation $[Re_6Te_8{}^i](Te_8Cl_{18})_{6/6}{}^{a-a}$. Thus, clusters cores and ligands are arranged in a rock-salt fashion.

F. Construction of a Virtual Library Spanning the Re–Q–X System

An analysis of the modes of linkages via apical chloride bridges for 1-, 2-, or 3-D networks within the five known types of molecular forms based on octahedral rhenium cluster cores formulated $[Re_6Q_{4+n}{}^iX_{4-n}{}^i]^{(6-n)+}$ led to the general formulation

$$\{[Re_6Q_{4+n}{}^iX_{4-n}{}^i]X_{6-l}{}^aX_{l/2}{}^{a-a}\}^{(l/2-n)} \quad (1)$$

where *l* is the number of bridging, outer halogen atoms and may take any value from 0 to 6 (*n* = 0−4). With this formula, the three polymers $Re_6Q_5X_8$, $Re_6Q_6X_6$, and $Re_6Q_7X_4$ are represented by the couple (*n*, *l*) of indices (1, 2), (2, 4), and (3, 6), respectively. Note that the dimensionality of these phases is given by *d* = *l*/2.

Once put aside cationic phases,[61] 14 different compounds can be formulated whose charges range from neutral to tetraanionic and dimensionality from 0- (molecular forms) to 3-dimensional (Table 3). Only in the Re−S−Cl system have all the molecular forms (first line of Table 3) now been synthesized. The *n* = 3 phase is still missing in the Re−Se−Cl system, and other systems have not been explored to any extent yet, not to mention their solubility properties. Besides, all halogen-bridged neutral polymers (main diagonal of Table 3) were fully characterized,[15] although essentially in the Re−Se−Cl system. If one considers halogen-bridged anionic polymers, apart from a brief mention of $Ag\{[Re_6Se_6{}^iCl_2{}^i]Cl_4{}^aCl_{2/2}{}^{a-a}\}$ (*n* = 2, *l* = 2) and $Zn\{[Re_6Se_7{}^iCl^i]Cl_4{}^aCl_{2/2}{}^{a-a}\}$ (*n* = 3, *l* = 2),[62] many new compounds await to be synthesized.

A more general formulation encompasses those phases, like $Re_6Se_8Cl_2$,[15,16] in which intercluster bonds are created by linking *m* inner ligands via symmetrical linkage modes:

$$\{[Re_6Q_{4+n-m}{}^iQ_{m/2}{}^{i-a}X_{4-n}{}^i] \times X_{6-m-l}{}^aX_{l/2}{}^{a-a}Q_{m/2}{}^{a-i}\}^{(m-n+l/2)} \quad (2)$$

Note that the following restrictions apply: $0 \le n \le 4$; *m* and *l* are positive integers with $m + l \le 6$ and $m - n + l/2 \le 0$, if one put aside cationic phases. The value of the (*n*, *m*, *l*) triplet for each known polymer type is given in Table 2. Thus, if one looks for neutral compounds ($m - n + l/2 = 0$) with a $[Re_6Q_8]^{2+}$ core (*n* = 4), and given the above restrictions, one ends up with only three possible (*n*, *m*, *l*) triplets of indices: (4, 4, 0); (4, 3, 2); (4, 2, 4). The first and latter correspond to the two known structural isomers of $Re_6Q_8X_2$, $[Re_6Se_4{}^iSe_{4/2}{}^{i-a}]Cl_2{}^aSe_{4/2}{}^{a-i}$, and $[Re_6Q_6{}^iQ_{2/2}{}^{i-a}]Br_{4/2}{}^{a-a}Q_{2/2}{}^{a-i}$ (Q = S, Se), respectively. Other known structural isomers are $Tl[Re_6Se_8Cl_3]$ and $Cs[Re_6Se_8I_3]$, with triplets indices of (4,

Table 4. Virtual Library of All Possible Hexarhenium Chalcohalide Clusters and Their Associated (*n*, *m*, *l*) Triplets, Compiled with Their Schäfer−von Schnering's Formulation

		n **= 4, *m* = 0**	
charge = 4− (*n*, *m*, *l*) = (4, 0, 0) formulation: $[Re_6Q_8X_6]^{4-}$ $\{[Re_6Q_8{}^{i}]X_6{}^{a}\}^{4-}$	charge = 4− (*n*, *m*, *l*) = (4, 0, 1) formulation: $[Re_6Q_8X_6]^{4-}$ $\{[Re_6Q_8{}^{i}]X_5{}^{a}X_{1/2}{}^{a-a}\}^{4-}$	charge = 3− (*n*, *m*, *l*) = (4, 0, 2) formulation: $[Re_6Q_8X_5]^{3-}$ $\{[Re_6Q_8{}^{i}]X_4aX_{2/2}{}^{a-a}\}^{3-}$	charge = 3− (*n*, *m*, *l*) = (4, 0, 3) formulation: $[Re_6Q_8X_5]^{3-}$ $\{[Re_6Q_8{}^{i}]X_3{}^{a}X_{3/2}{}^{a-a}\}^{3-}$
charge = 2− (*n*, *m*, *l*) = (4, 0, 4) formulation: $[Re_6Q_8X_4]^{2-}$ $\{[Re_6Q_8{}^{i}]X_2{}^{a}X_{4/2}{}^{a-a}\}^{2-}$	charge = 2− (*n*, *m*, *l*) = (4, 0, 5) formulation: $[Re_6Q_8X_4]^{2-}$ $\{[Re_6Q_8{}^{i}]X^{a}X_{5/2}{}^{a-a}\}^{2-}$	charge = 1− (*n*, *m*, *l*) = (4, 0, 6) formulation: $[Re_6Q_8X_3]^{-}$ $\{[Re_6Q_8{}^{i}]X_{6/2}{}^{a-a}\}^{-}$	
		m **= 1**	
charge = 3− (*n*, *m*, *l*) = (4, 1, 0) formulation: $[Re_6Q_8X_5]^{3-}$ $\{[Re_6Q_7{}^{i}Q_{1/2}{}^{i-a}]X_5{}^{a}Q_{1/2}{}^{a-i}\}^{3-}$	charge = 3− (*n*, *m*, *l*) = (4, 1, 1) formulation: $[Re_6Q_8X_5]^{3-}$ $\{[Re_6Q_7{}^{i}Q_{1/2}{}^{i-a}]X_4{}^{a}X_{1/2}{}^{a-a}Q_{1/2}{}^{a-i}\}^{3-}$	charge = 2− (*n*, *m*, *l*) = (4, 1, 2) formulation: $[Re_6Q_8X_4]^{2-}$ $\{[Re_6Q_7{}^{i}Q_{1/2}{}^{i-a}]X_3{}^{a}X_{2/2}{}^{a-a}Q_{1/2}{}^{a-i}\}^{2-}$	charge = 2− (*n*, *m*, *l*) = (4, 1, 3) formulation: $[Re_6Q_8X_4]^{2-}$ $\{[Re_6Q_7{}^{i}Q_{1/2}{}^{i-a}]X_2{}^{a}X_{3/2}{}^{a-a}Q_{1/2}{}^{a-i}\}^{2-}$
charge = 1− (*n*, *m*, *l*) = (4, 1, 4) formulation: $[Re_6Q_8X_3]^{-}$ $\{[Re_6Q_7{}^{i}Q_{1/2}{}^{i-a}]X^{a}X_{4/2}{}^{a-a}Q_{1/2}{}^{a-i}\}^{-}$	charge = 1− (*n*, *m*, *l*) = (4, 1, 5) formulation: $[Re_6Q_8X_3]^{-}$ $\{[Re_6Q_7{}^{i}Q_{1/2}{}^{i-a}]X_{5/2}{}^{a-a}Q_{1/2}{}^{a-i}\}^{-}$		
		m **= 2**	
charge = 2− (*n*, *m*, *l*) = (4, 2, 0) formulation: $[Re_6Q_8X_4]^{2-}$ $\{[Re_6Q_6{}^{i}Q_{2/2}{}^{i-a}]X_4{}^{a}Q_{2/2}{}^{a-i}\}^{2-}$	charge = 2− (*n*, *m*, *l*) = (4, 2, 1) formulation: $[Re_6Q_8X_4]^{2-}$ $\{[Re_6Q_6{}^{i}Q_{2/2}{}^{i-a}]X_3{}^{a}X_{1/2}{}^{a-a}Q_{2/2}{}^{a-i}\}^{2-}$	charge = 1− (*n*, *m*, *l*) = (4, 2, 2) formulation: $[Re_6Q_8X_3]^{-}$ $\{[Re_6Q_6{}^{i}Q_{2/2}{}^{i-a}]X_2{}^{a}X_{2/2}{}^{a-a}Q_{2/2}{}^{a-i}\}^{-}$	charge = 1− (*n*, *m*, *l*) = (4, 2, 3) formulation: $[Re_6Q_8X_3]^{-}$ $\{[Re_6Q_6{}^{i}Q_{2/2}{}^{i-a}]X^{a}X_{3/2}{}^{a-a}Q_{2/2}{}^{a-i}\}^{-}$
charge = 0 (*n*, *m*, *l*) = (4, 2, 4) formulation: $[Re_6Q_8X_2$ $\{[Re_6Q_6{}^{i}Q_{2/2}{}^{i-a}]X_{4/2}{}^{a-a}Q_{2/2}{}^{a-i}\}$			
		m **= 3**	
charge = 1− (*n*, *m*, *l*) = (4, 3, 0) formulation: $[Re_6Q_8X_3]^{-}$ $\{[Re_6Q_5{}^{i}Q_{3/2}{}^{i-a}]X_3{}^{a}Q_{3/2}{}^{a-i}\}^{-}$	charge = 1− (*n*, *m*, *l*) = (4, 3, 1) formulation: $[Re_6Q_8X_3]^{-}$ $\{[Re_6Q_5{}^{i}Q_{3/2}{}^{i-a}]X_2{}^{a}X_{1/2}{}^{a-a}Q_{3/2}{}^{a-i}\}^{-}$	charge = 0 (*n*, *m*, *l*) = (4, 3, 2) formulation: $[Re_6Q_8X_2$ $\{[Re_6Q_5{}^{i}Q_{3/2}{}^{i-a}]X^{a}X_{2/2}{}^{a-a}Q_{3/2}{}^{a-i}\}$	charge = 0 (*n*, *m*, *l*) = (4, 3, 3) formulation: $[Re_6Q_8X_2$ $\{[Re_6Q_5{}^{i}Q_{3/2}{}^{i-a}]X_{3/2}{}^{a-a}Q_{3/2}{}^{a-i}\}$
		m **= 4**	
charge = 0 (*n*, *m*, *l*) = (4, 4, 0) formulation: $[Re_6Q_8X_2]$ $\{[Re_6Q_4{}^{i}Q_{4/2}{}^{i-a}]X_2aQ_{4/2}{}^{a-i}\}$	charge = 0 (*n*, *m*, *l*) = (4, 4, 1) formulation: $[Re_6Q_8X_2]$ $\{[Re_6Q_4{}^{i}Q_{4/2}{}^{i-a}]X^{a}X_{1/2}{}^{a-a}Q_{4/2}{}^{a-i}\}$	charge = 0 (*n*, *m*, *l*) = (4, 4, 0) formulation: $[Re_6Q_8X_2]$ $\{[Re_6Q_4{}^{i}Q_{4/2}{}^{i-a}]X_2aQ_{4/2}{}^{a-i}\}$	charge = 0 (*n*, *m*, *l*) = (4, 4, 1) formulation: $[Re_6Q_8X_2]$ $\{[Re_6Q_4{}^{i}Q_{4/2}{}^{i-a}]X^{a}X_{1/2}{}^{a-a}Q_{4/2}{}^{a-i}\}$
		m **= 5, *m* = 6**	
		n **= 3, *m* = 0**	
charge = 3− (*n*, *m*, *l*) = (3, 0, 0) formulation: $[Re_6Q_7X_7]^{3-}$ $\{[Re_6Q_7{}^{i}X^{i}]X_6{}^{a}\}^{3-}$	charge = 3− (*n*, *m*, *l*) = (3, 0, 1) formulation: $[Re_6Q_7X_7]^{3-}$ $\{[Re_6Q_7{}^{i}X^{i}]X_5{}^{a}X_{1/2}{}^{a-a}\}^{3-}$	charge = 2− (*n*, *m*, *l*) = (3, 0, 2) formulation: $[Re_6Q_7X_6]^{2-}$ $\{[Re_6Q_7{}^{i}X^{i}]X_4{}^{a}X_{2/2}{}^{a-a}\}^{2-}$	charge = 2− (*n*, *m*, *l*) = (3, 0, 3) formulation: $[Re_6Q_7X_6]^{2-}$ $\{[Re_6Q_7{}^{i}X^{i}]X_3{}^{a}X_{3/2}{}^{a-a}\}^{2-}$
charge = 1− (*n*, *m*, *l*) = (3, 0, 4) formulation: $[Re_6Q_7X_5]^{-}$ $\{[Re_6Q_7{}^{i}X^{i}]X_2aX_{4/2}{}^{a-a}\}^{-}$	charge = 1− (*n*, *m*, *l*) = (3, 0, 5) formulation: $[Re_6Q_7X_5]^{-}$ $\{[Re_6Q_7{}^{i}X^{i}]X^{a}X_{5/2}{}^{a-a}\}^{-}$	charge = 0 (*n*, *m*, *l*) = (3, 0, 6) formulation: $[Re_6Q_7X_4]$ $\{[Re_6Q_7{}^{i}X^{i}]X_{6/2}{}^{a-a}\}$	
		m **= 1**	
charge = 2− (*n*, *m*, *l*) = (3, 1, 0) formulation: $[Re_6Q_7X_6]^{2-}$ $\{[Re_6Q_6{}^{i}Q_{1/2}{}^{i-a}X^{i}]X_5{}^{a}Q_{1/2}{}^{a-i}\}^{2-}$	charge = 2− (*n*, *m*, *l*) = (3, 1, 1) formulation: $[Re_6Q_7X_6]^{2-}$ $\{[Re_6Q_6{}^{i}Q_{1/2}{}^{i-a}X^{i}]X_4{}^{a}X_{1/2}{}^{a-a}Q_{1/2}{}^{a-i}\}^{2-}$	charge = 1− (*n*, *m*, *l*) = (3, 1, 2) formulation: $[Re_6Q_7X_5]^{-}$ $\{[Re_6Q_6{}^{i}Q_{1/2}{}^{i-a}X^{i}]X_3{}^{a}X_{2/2}{}^{a-a}Q_{1/2}{}^{a-i}\}^{-}$	charge = 1− (*n*, *m*, *l*) = (3, 1, 3) formulation: $[Re_6Q_7X_5]^{-}$ $\{[Re_6Q_6{}^{i}Q_{1/2}{}^{i-a}X^{i}]X_2aX_{3/2}{}^{a-a}Q_{1/2}{}^{a-i}\}^{-}$
charge = 0 (*n*, *m*, *l*) = (3, 1, 4) formulation: $[Re_6Q_7X_4]$ $\{[Re_6Q_6{}^{i}Q_{1/2}{}^{i-a}X^{i}]X^{a}X_{4/2}{}^{a-a}Q_{1/2}{}^{a-i}\}$	charge = 0 (*n*, *m*, *l*) = (3, 1, 5) formulation: $[Re_6Q_7X_4]$ $\{[Re_6Q_6{}^{i}Q_{1/2}{}^{i-a}X^{i}]X_{5/2}{}^{a-a}Q_{1/2}{}^{a-i}\}$		
		m **= 2**	
charge = 1− (*n*, *m*, *l*) = (3, 2, 0) formulation: $[Re_6Q_7X_5]^{-}$ $\{[Re_6Q_5{}^{i}Q_{2/2}{}^{i-a}X^{i}]X_4aQ_{2/2}{}^{a-i}\}^{-}$	charge = 1− (*n*, *m*, *l*) = (3, 2, 1) formulation: $[Re_6Q_7X_5]^{-}$ $\{[Re_6Q_5{}^{i}Q_{2/2}{}^{i-a}X^{i}]X_3aX_{1/2}{}^{a-a}Q_{2/2}{}^{a-i}\}^{-}$	charge = 0 (*n*, *m*, *l*) = (3, 2, 2) formulation: $[Re_6Q_7X_4]$ $\{[Re_6Q_5{}^{i}Q_{2/2}{}^{i-a}X^{i}]X_2{}^{a}X_{2/2}{}^{a-a}Q_{2/2}{}^{a-i}\}$	charge = 0 (*n*, *m*, *l*) = (3, 2, 3) formulation: $[Re_6Q_7X_4]$ $\{[Re_6Q_5{}^{i}Q_{2/2}{}^{i-a}X^{i}]X^{a}X_{3/2}{}^{a-a}Q_{2/2}{}^{a-i}\}$
		m **= 3**	
charge = 0 (*n*, *m*, *l*) = (3, 3, 0) formulation: $[Re_6Q_7X_4]$ $\{[Re_6Q_4{}^{i}Q_{3/2}{}^{i-a}X^{i}]X_3{}^{a}Q_{3/2}{}^{a-i}\}$	charge = 0 (*n*, *m*, *l*) = (3, 3, 1) formulation: $[Re_6Q_7X_4]$ $\{[Re_6Q_4{}^{i}Q_{3/2}{}^{i-a}X^{i}]X_2{}^{a}X_{1/2}{}^{a-a}Q_{3/2}{}^{a-i}\}$		
		m **= 4−6**	

Table 4 (Continued)

		***n* = 2**, $m = 0$	
charge = 2− $(n, m, l) = (2, 0, 0)$ formulation: $[Re_6Q_6X_8]^{2-}$ $\{[Re_6Q_6{}^iX_2{}^i]X_6{}^a\}^{2-}$	charge = 2− $(n, m, l) = (2, 0, 1)$ formulation: $[Re_6Q_6X_8]^{2-}$ $\{[Re_6Q_6{}^iX_2{}^i]X_5{}^aX_{1/2}{}^{a-a}\}^{2-}$	charge = 1− $(n, m, l) = (2, 0, 2)$ formulation: $[Re_6Q_6X_7]^-$ $\{[Re_6Q_6{}^iX_2{}^i]X_4{}^aX_{2/2}{}^{a-a}\}^-$	charge = 1− $(n, m, l) = (2, 0, 3)$ formulation: $[Re_6Q_6X_7]^-$ $\{[Re_6Q_6{}^iX_2{}^i]X_3{}^aX_{3/2}{}^{a-a}\}^-$
charge = 0 $(n, m, l) = (2, 0, 4)$ formulation: $[Re_6Q_6X_6]$ $\{[Re_6Q_6{}^iX_2{}^i]X_2{}^aX_{4/2}{}^{a-a}\}$	charge = 0 $(n, m, l) = (2, 0, 5)$ formulation: $[Re_6Q_6X_6]$ $\{[Re_6Q_6{}^iX_2{}^i]X^aX_{5/2}{}^{a-a}\}$		
		$m = 1$	
charge = 1− $(n, m, l) = (2, 1, 0)$ formulation: $[Re_6Q_6X_7]^-$ $\{[Re_6Q_5{}^iQ_{1/2}{}^{i-a}X_2{}^i]X_5{}^aQ_{1/2}{}^{a-i}\}^-$	charge = 1− $(n, m, l) = (2, 1, 1)$ formulation: $[Re_6Q_6X_7]^-$ $\{[Re_6Q_5{}^iQ_{1/2}{}^{i-a}X_2{}^i]X_4{}^aX_{1/2}{}^{a-a}Q_{1/2}{}^{a-i}\}^-$	charge = 0 $(n, m, l) = (2, 1, 2)$ formulation: $[Re_6Q_6X_6]$ $\{[Re_6Q_5{}^iQ_{1/2}{}^{i-a}X_2{}^i]X_3{}^aX_{2/2}{}^{a-a}Q_{1/2}{}^{a-i}\}$	charge = 0 $(n, m, l) = (2, 1, 3)$ formulation: $[Re_6Q_6X_6]$ $\{[Re_6Q_5{}^iQ_{1/2}{}^{i-a}X_2{}^i]X_2{}^aX_{3/2}{}^{a-a}Q_{1/2}{}^{a-i}\}$
		$m = 2$	
charge = 0 $(n, m, l) = (2, 2, 0)$ formulation: $[Re_6Q_6X_6]$ $\{[Re_6Q_4{}^iQ_{2/2}{}^{i-a}X_2{}^i]X_4{}^aQ_{2/2}{}^{a-i}\}$	charge = 0 $(n, m, l) = (2, 2, 1)$ formulation: $[Re_6Q_6X_6]$ $\{[Re_6Q_4{}^iQ_{2/2}{}^{i-a}X_2{}^i]X_3{}^aX_{1/2}{}^{a-a}Q_{2/2}{}^{a-i}\}$	charge = 0 $(n, m, l) = (2, 2, 0)$ formulation: $[Re_6Q_6X_6]$ $\{[Re_6Q_4{}^iQ_{2/2}{}^{i-a}X_2{}^i]X_4{}^aQ_{2/2}{}^{a-i}\}$	charge = 0 $(n, m, l) = (2, 2, 1)$ formulation: $[Re_6Q_6X_6]$ $\{[Re_6Q_4{}^iQ_{2/2}{}^{i-a}X_2{}^i]X_3{}^aX_{1/2}{}^{a-a}Q_{2/2}{}^{a-i}\}$
		$m = 3-6$	
		***n* = 1**, $m = 0$	
charge = 1− $(n, m, l) = (1, 0, 0)$ formulation: $[Re_6Q_5X_9]^-$ $\{[Re_6Q_5{}^iX_3i]X_6{}^a\}^-$	charge = 1− $(n, m, l) = (1, 0, 1)$ formulation: $[Re_6Q_5X_9]^-$ $\{[Re_6Q_5{}^iX_3{}^i]X_5{}^aX_{1/2}{}^{a-a}\}^-$	charge = 0 $(n, m, l) = (1, 0, 2)$ formulation: $[Re_6Q_5X_8]$ $\{[Re_6Q_5{}^iX_3{}^i]X_4{}^aX_{2/2}{}^{a-a}\}$	charge = 0 $(n, m, l) = (1, 0, 3)$ formulation: $[Re_6Q_5X_8]$ $\{[Re_6Q_5{}^iX_3{}^i]X_3{}^aX_{3/2}{}^{a-a}\}$
		$m = 1$	
charge = 0 $(n, m, l) = (1, 1, 0)$ formulation: $[Re_6Q_5X_8]$ $\{[Re_6Q_4{}^iQ_{1/2}{}^{i-a}X_3{}^i]X_5{}^aQ_{1/2}{}^{a-i}\}$	charge = 0 $(n, m, l) = (1, 1, 1)$ formulation: $[Re_6Q_5X_8]$ $\{[Re_6Q_4{}^iQ_{1/2}{}^{i-a}X_3{}^i]X_4{}^aX_{1/2}{}^{a-a}Q_{1/2}{}^{a-i}\}$		
		$m = 2-6$	
		***n* = 0**, $m = 0$	
charge = 0 $(n, m, l) = (0, 0, 0)$ formulation: $[Re_6Q_4X_{10}]$ $\{[Re_6Q_4{}^iX_4{}^i]X_6{}^a\}$	charge = 0 $(n, m, l) = (0, 0, 1)$ formulation: $[Re_6Q_4X_{10}]$ $\{[Re_6Q_4{}^iX_4{}^i]X_5{}^aX_{1/2}{}^{a-a}\}$		
		$m = 1-6$	

3, 0) and (4, 2, 2), respectively. Again, cationic phases not withstanding, 64 structurally different compounds, many of them still unknown, can be enumerated (Table 4), which decompose into 24, 19, 13, 6, and 2 for $n = 4$,[46] 3, 2, 1, and 0, respectively.

Furthermore, this formula remains valid for other M−Q−X systems where $M_6Q_nX_{8-n}$ cluster cores exist, for example the Mo−Q−X system, although the overall charge will depend on the nature of the metal and/or its oxidation state. A consequence is that changing the metal or its oxidation state allows for novel triplets that were explicitly excluded in the Re(III) series because they would have led to cationic species. This is the case, for example, of the triplet (4, 6, 0) which describes the Chevrel−Sergent phases. Such triplets can also be used in the case of apical bridging chalcogen instead of halogen. Once again, only the overall charge will change in the formula. Thus, $[Re_6S_{11}]^{4-}$ or $\{[Re_6S_8{}^i]S_{6/2}{}^{a-a}\}^{4-}$ would be represented by the triplet (4, 0, 6),[63] and the Siamese twin cluster, $\{[Re_6S_5OCl_7]_2O\}^{4-}$ (section III.A.1), by the triplet (2, 0, 1).[64]

G. Manipulating the Dimensionality of Solid-State Structures

Conceptually, one recognize how the 1-, 2-, and 3-dimensional, outer halide-bridged frameworks discussed above (section II.E) might be broken into small pieces by incorporating additional, bridge-terminating halide ligands in the structure. Here, one perceives a means of disrupting intercluster bonds through the insertion of intervening outer ligands. In a more or less implicit formulation, this strategy has prevailed for the syntheses designed by solid-state chemists of virtually all molecular anion cluster forms starting from $\{[Re_6Q_{4+n}{}^iX_{4-n}{}^i]X_{6-l}{}^aX_{l/2}{}^{a-a}\}^{(l/2-n)}$. Thus, from $Re_6Q_8X_2$, the cesium salts of discrete, molecular motifs, $[Re_6Q_8X_6]^{4-}$ (Q = S, Se; X = Cl, Br, I), and a set of compounds of intermediate dimensionalities (see Table 2) have been prepared by Holm and co-workers using this principle, formulated dimensional reduction.[45,46] Tulsky and Long recently proposed a practical formalism for the manipulation of the structures of solids using the dimensional reduction concept, very much in the spirit of the retrosynthesis paradigm.[65]

H. Practical Procedures for High-Temperature Solid-State Synthesis

All synthetic routes to octahedral chalcohalide rhenium clusters require high-temperature reactions. Most starting chemicals are given in Table 5. The synthesis usually starts either directly from the

Table 5. Starting Chemicals Used for the High-Temperature Synthesis of Hexanuclear Rhenium Chalcohalide Clusters

	Re	Q (S, Se, Te)	X (Cl, Br, I)
Re	Re powder	ReS_2, $ReSe_2$	"$ReCl_3$" = Re_3Cl_9, "$ReBr_3$" = Re_3Br_9
		"Re_2Te_5" = Re_6Te_{15}	"$ReCl_5$" = Re_2Cl_{10}, "$ReBr_5$" = Re_2Br_{10}
Q (S, Se, Te)		S, Se, Te powder	S_2Cl_2
		KSCN	
	$Re_6S_4Br_{10}$		
X (Cl, Br, I)			ICl_3, Cl_2, Br_2, I_2

elements or from binary phases. Only rarely has a ternary phase been used as a starting material.[39]

Given the complexity of the phase diagrams with the inherent close proximity of many different phases, it is of paramount importance to properly report[66] the following set of experimental data:

(i) The temperature, typically 800 to 850 °C, is obviously the most important parameter because small differences can lead to different ending products.[23]

(ii) The oven gradient should be registered, reported, and related to the position of the crystal growth when needed.

(iii) The actual thermal cycle[23] affects the crystalline quality of the products and may also influence the formulation of the final product. For example, two compounds being in equilibrium, a short thermal cycle would select the kinetic compound when a longer one yields the thermodynamic phase.

(iv) Since volatile materials are often used, the reaction is achieved under gaseous pressure; this pressure will also be of strong influence on the ending product; therefore, all papers should not only give the stoichiometry of the reaction but also the exact amount of reactants as well as the volume of the tube once sealed. For the sake of reproducibility, volume used during the synthesis should be carefully logged and reported.

(v) A consequence of the previous point is that tubes might explode when heated if their thickness is too small, creating a hazard. Therefore this thickness should also be reported.

III. Solution Chemistry

The remarkable developments of the solid-state and crystal chemistry of octahedral rhenium chalcohalide clusters discussed in the preceding sections had effectively flooded the pool of discrete or polymeric precursors of molecular forms of such cluster compounds. Thus, when the need for a *monoanionic* cluster form isosteric and isostructural to $[Mo_6Cl_{14}]^{2-}$ became necessary following our synthesis of $(TMTTF^{+\bullet})_2[Mo_6Cl_{14}]^{2-}$,[67] we turned to $(K^+)[Re_6Se_5Cl_9]^-$, hence, our initial discovery of the solubility of $K[Re_6Se_5Cl_9]$ in ethanol.[4]

A. From Soluble Mineral Cluster Compounds to a Large Series of Alkylammonium or Tetraphenylphosphonium Discrete Cluster Salts

1. Molecular Cluster Approach

All the salts collected in Table 1 have not been systematically tested for solubility yet. Instead, comparatively few have been reported to be soluble (Table 6) and most are alkali-metal or alkaline-earth cation salts.[42] The alkali-metal salts (Rb, K) of the monovalent cluster forms are soluble in ethanol, and although they are barely soluble in water, in the case of the potassium salt, the inner sphere, octacoordinated bis(aquo) potassium complex $[K(H_2O)_2][Re_6Se_5Cl_9]$ is obtained after dispersion of the initial salt in water and overnight stirring.[68] Note that the cluster core remains intact in solution and that, contrary to an earlier indication, no substitution of an inner, μ_3-core halogen ligand for OH^- occurs to yield $K[Re_6Se_5(\mu_3\text{-}OH)_2Cl_7]\cdot H_2O$.[69,70] The alkaline-earth salts of the divalent cluster forms are not soluble in water but are highly soluble in a variety of polar organic solvents such as alcohol, acetonitrile, tetrahydrofuran, dimethylformamide, dioxane, and acetone. In turn, the water-soluble, hydrated solid phases such as $[Ca(H_2O)_n][Re_6Q_6Cl_8]\cdot mH_2O$ crystallize out of the former organic phases containing even minute amounts of water (see section II.D.3).[37] It is only when the cluster anion charge reaches 3 and 4 that their alkali-metal salts become soluble in water. This is also true for the mixed cluster anion salt $Rb_5[Re_6S_6Cl_8][Re_6S_7Cl_7]$.

Cation exchange in alcohol or water with alkylammonium halides or tetraphenylphosphonium halides yields the extended series of organic solvent soluble salts of differently charged isosteric molecular cluster forms listed in Table 6. This route provides a ready access to the organic solution phase chemistry of a large set of molecular forms of mineral clusters.

Finally, by direct solid-state synthesis in the presence of minute amounts of water followed by cation exchange in ethanol, an oxo-bridged Siamese twin cluster of two dianion cluster units, $(Bu_4N)_4\{[Re_6S_5OCl_2]Cl_5\}_2O$ (Figure 11), the first (2, 0, 1) compound (section II.F), is obtained and recrystallized in acetonitrile.[64] Formally, a single μ-chloride is replaced by an oxo bridge across two identical cluster units; in addition, a single μ_3-core ligand is substituted by an oxygen atom. The X-ray structure determination has demonstrated that the inner μ_3-oxygen atom loci are perfectly defined and that no disorder with the other inner ligands can be observed. The chemistry of this oxo-bridged, twin cluster unit has not been explored to any extend yet. It is certainly conceivable, however, that it may in turn be subjected to reactions with water or with, for example, $(Me_3Si)_2O$ (see section B.1). One appealing objective would be to construct out of this twin monomer unprecedented oxo-bridged extended networks of increasing dimensionalities, from chains and slabs eventually all the way to, for example, augmented CaB_6 nets, in the spirit of design principles described by O'Keeffe et al.[71]

Table 6. Molecular Forms of Hexanuclear Chalcohalide Rhenium Clusters Derived in Solution

ion	ref	ion	ref
	Tetraanion		
$(Bu_4N)_4\{[Re_6S_5OCl_2]Cl_5\}_2O$	64	$(Bu_4N)_4[Re_6S_8X_6]\cdot H_2O$ (X = Br, I)	46
$(Bu_4N)_4[Re_6S_8Cl_6]$	46		
	Trianion		
$(Bu_4N)_3\{[Re_6S_7Cl]Cl_6\}$	23	$(Bu_4N)_3[Re^{III}_5Re^{IV}S_8Cl_6]$	112
$(PPh_4)_3\{[Re_6S_7Br]Br_6\}$	39	$Rb_3[Re_6S_7Br_7]\cdot 4\ H_2O$	44a
$(Bu_4N)_3\{[Re_6Q_8]Cl_6\}$	46,79	$Cs_3[Re_6Se_7Br_7]\cdot H_2O$	44b
$(Bu_4N)_3\{[Re_6Q_8]X_6\}\cdot 2Me_2CO$" (Q = S, X = Br, I; Q = Se, X = I)	46,79		
	Dianion		
$(Bu_4N)_2\{[Re_6S_6Cl_2]Cl_6\}$	23	$[Mg(H_2O)_6]\{[Re_6S_6Cl_2]Cl_6\}\cdot 2H_2O$	37
$(R_4N)_2\{[Re_6Se_6Cl_2]Cl_6\}$ (R = Et, Pr^n, Bu^n)	49, 68	$(R_4N)_2\{[Re_6Se_6Cl_2]Cl_6\}$ (R = Et, Pr, Bu)	49
$(Bu_4N)_2\{[Re_6Q_5ECl_2]Cl_6\}$ (Q = S, E = O, S, Se; Q = Se, E = S, Se, Te)	74	$(Pr_4N)_2\{[\alpha\text{-}Re_6Se_4O_2Cl_2]Cl_6\}\cdot 2DMF$	49
		$(Pr_4N)_2\{[\beta\text{-}Re_6Se_4O_2Cl_2]Cl_6\}$	49
$(PPh_4)_2\{[Re_6S_6Br_2]Br_6\}\cdot CH_3C_6H_5$	39	$(Bu_4N)_2[Re_6S_8(PEt_3)_2Br_4]$	80
$(Bu_4N)_2\{[Re_6Q_5(NR)Cl_2]Cl_6\}$ (Q = S, Se; R= Me, Bz)	75	$(Bu_4N)_2[Re_6S_8Cl_4(L)_2]$ (*cis* and *trans*); with L = py, pz, cpy, bpy, mpy, dmap)[a]	88, 111
$(Bu_4N)_2\{[Re_6Q_5(N^-SiMe_3)Cl_2]Cl_6\}$ (Q = S, Se)	75		
$(Bu_4N)_2\{[Re_6Q_5(NH)Cl_2]Cl_6\}$ (Q = S, Se)	75	$(Bu_4N)_2[Re_6Se_8(\mu\text{-dpph})\ I_4]$[a]	85
$[Ca(H_2O)_7][Re_6Q_6Cl_8]\cdot 3H_2O$ (Q = S, Se), $[Ca(H_2O)_8][Re_6S_6Cl_8]$	37		
	Monoanion		
$(Bu_4N)\{[Re_6Se_5Cl_3]Cl_6\}$	4	$(Bu_4N)[Re_6S_8(PEt_3)_3Br_3]$	80
$(Bu_4N)\{[Re_6S_5Cl_3]Cl_6\}$	23	$(Bu_4N)[mer\text{-}Re_6S_8Cl_3(py)_3]$[a]	83
$K(H_2O)_2[Re_6Se_5Cl_9]$	68	$(Bu_4N)[trans\text{-}Re^{III}_5Re^{IV}S_8Cl_4(L)_2]\cdot$ (L = py, py-CN)[a]	88
$(R_4N)\{[Re_6Se_5Cl_3]Cl_6\}$ (R = Et, Pr^n, Bu^n)	49		
$(Bu_4N)[Re_6Se_8(PEt_3)_3I_3]$	82		
	Neutral		
$[Re_6Se_8(PEt_3)_4I_2]\cdot 2CHCl_3$ (*trans*, cis)	82	$[mer\text{-}Re^{III}_5Re^{IV}S_8Cl_3(py)_3]\cdot$[a]	83
$[Re_6S_8(PEt_3)_4Br_2]$	80	(*cis* and *trans*)-$[Re_6Se_8(\mu\text{-dpph})_2I_2]$*	85
$[Re_6S_6E_2(PPr^n3)_6]$ (E = As, P)	89		
	Monocation		
$[Re_6Se_8(PEt_3)_5I]I\cdot 2CH_2Cl_2$	82	$[Re_6S_8(PEt_3)_5Br]Br$	80
	Dication		
$[Re_6Se_8(PEt_3)_n(MeCN)_{6-n}]A_2$ (n = 0, 5, 6, A= BF_4; n = 4, A = SbF_6)	82	$[Re_6S_8(H_2O)_6]^{2+}$	47
		Re_6Se_8(pyridyl functionality-bearing dendrons)$_6]^{2+}$	81
$[Re_6Se_8(PEt_3)_4(solv)_2](SbF_6)_2$ (solv = Bu^tCN, DMF, Me_2SO, py)[a]	83	$[Re_6Se_8(L)_6]^{2+}$ (L = py-R, py-OH)[a]	81, 82
trans-$[Re_6Se_8(PEt_3)_4(solv)_2](SbF_6)_2$ (solv = MeCN, DMF, Me_2SO)	84	$[Re_6Se_8(L)_6](SbF_6)_2$ (L = DMF, Me_2SO, py, bpy (*cis*, *trans*))	84
$[Re_6S_8(PEt_3)_6]Br_2$	80	$[Re_6Se_8(\mu\text{-dpph})_3](SbF_6)_2$[a]	85
$[Re_6S_6Y_2(PPr^n3)_6][Re_6S_6Cl_8]\cdot 2CH_3CN$ (E = NH, O, S)	89		
	Tetracation and Hexacation		
$[Re_{12}Se_{16}(PEt_3)_{10}](BF_4)_4\cdot 4CH_2Cl_2$	82	$\{[Re_6Se_8(PEt_3)_5]_2(py_2C_2H_2)\}(SbF_6)_4]$[a]	84
trans-$[Re_{12}Se_{16}(PEt_3)_8(MeCN)_2](SbF_6)_4\cdot 4\ CH_2Cl_2$	83	$\{[Re_6Se_8(PEt_3)_5]_2(py_2C_2H_4)\}(SbF_6)_4]$[a]	84
$\{[Re_6Se_8(PEt_3)_5]_2(bpy)\}(SbF_6)_4]$[a]	84	$[Re_{18}Se_{24}(PEt_3)_{14}(bpy)_2](SbF_6)_6]$[a]	84

[a] py = pyridine; pz = pyrazine; cpy = cyanopyridine; bpy = 4,4-bipyridine; mpy = 4-methylpyridine; dmap = (4-dimethylamino)pyridine; py-CN = 4-cyanopyridine; py-OH = 4-hydroxypyridine; $py_2C_2H_2$ = *trans*-1,2-bis(4-pyridyl)ethylene; $py_2C_2H_4$ = *trans*-1,2-bis(4-pyridyl)ethane; dpph = diphenylphosphine hexane.

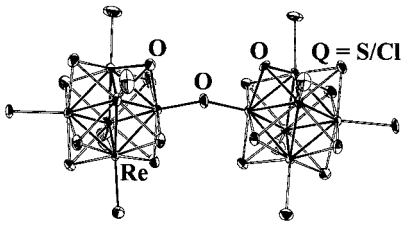

Figure 11. Oxo-bridged Siamese twin cluster in $(Bu_4N)_4[Re_6S_5OCl_7]_2O$.

2. Polymeric Clusters Approach

An alternative entry into the organic solution phase chemistry of the former monoanionic and dianionic molecular cluster forms starts from the corresponding neutral one- and two-dimensional, μ_2-halide-bridged polymers, $Re_6Q_5Cl_8$ and $Re_6Q_6Cl_6$

Scheme 1

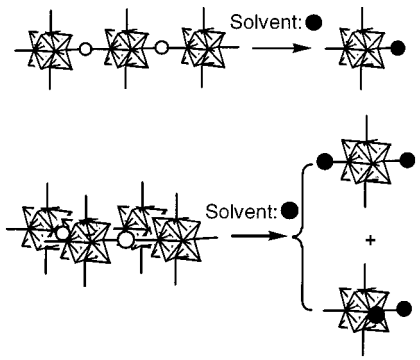

(Scheme 1). In the presence of coordinating solvent molecules such as acetonitrile or dimethylformamide, and along the progress of the excision of their

solvated molecular forms, $Re_6Q_5Cl_8(\mu_1\text{-solvent})$ and $Re_6Q_6Cl_6(\mu_1\text{-solvent})_2$, the μ_2-halide bridges are severed and yield μ-halide and μ-solvent ligand sites as shown in Scheme 1, prior to the reaction with appropriate alkylammonium halides.[49,23] This process, analogous to Sheldon's dissociation of $MoCl_2$ and reminiscent of our own observation that $(Bu_4N)_2[Mo_6Cl_{14}]$ is readily obtained from $Na[Mo_6Cl_{13}]$ in polar solvents,[72] has been recently developed in Holm's group.[73] In that respect, it would be of interest to explore the solubility properties of the one-dimensional anionic polymers $\{[Re_6Se_6{}^iCl_2{}^i]Cl_4{}^aCl_{2/2}{}^{a-a}\}^-$ and $\{[Re_6Se_7{}^iCl^i]Cl_4{}^aCl_{2/2}{}^{a-a}\}^{2-}$ (see section II.E.1) isostructural to $Na[Mo_6Cl_{13}]$.

Thus, the mono- and dianion molecular cluster salts are accessible from two different routes. However, the latter suffers from the inherent difficulty to prepare the neutral polymeric precursors as pure single phase materials because of their close proximity in the Re−Q−Cl phase diagram.[15] By contrast, the solid-state synthesis of the alkali-metal and alkaline-earth cation salts of the discrete molecular cluster anion forms proved to yield compounds that can be purified because of their different solubility.[23,37] Furthermore, the neutral polymeric clusters approach provides an access to solely the mono-and dianion cluster forms in solution since the neutral, halide-bridged three-dimensional polymers $Re_6Q_7Cl_4$ have so far proven to be insoluble.[49] In that respect, it is suggested that the yet unknown phases $M^+\{[Re_6Q_7{}^iCl^i]Cl_2{}^aCl_{4/2}{}^{a-a}\}^-$ and $M^{2+}\{[Re_6Q_8{}^i]Cl_2{}^aCl_{4/2}{}^{a-a}\}^{2-}$, where negatively charged two-dimensional inorganic polymers are effectively screened by metal cations, would both prove to be easier to synthesize as single phase materials and be readily soluble in coordinating solvents, thereby extending the polymeric clusters approach to the synthesis of the tri- and tetranionic cluster forms in solution.

B. Core Reactivity and Core Coordination: Toward Molecular Hybrids

1. μ_3-Functionalization

The first evidence of the lability of one face-capping, μ_3-chloride can be traced to our discovery, back in 1985, that cation exchange with Bu_4NCl of warm, aged overnight solutions of $K[Re_6Se_5Cl_9]$ in ethanol yields $(Bu_4N)_2[Re_6Se_6Cl_8]$ while cold, aged solutions consistently proved to afford the unreacted cluster core, $(Bu_4N)[Re_6Se_5Cl_9]$.[36] This was also consistent with a number of puzzling, essentially concomitant observations such as the diamagnetic character of single crystals of the putative mixed-valence cation radical salt $(TMTTF)_2[Re_6Se_5Cl_9]$, obtained by slow oxidation over several days at a platinum wire electrode of TMTTF solutions in acetonitrile containing $(Bu_4N)[Re_6Se_5Cl_9]$ as an electrolyte, and which proved to be $(TMTTF)_2[Re_6Se_6Cl_8]$ instead.[36] Thus, evidence was accumulating that the monoanionic cluster forms were prone to substitution of one μ_3-chloride by a chalcogenide element, both in the sulfur and selenium series.

This chemistry has been exemplified by Yaghi et al. with two sets of experiments (Figure 12).[49] First,

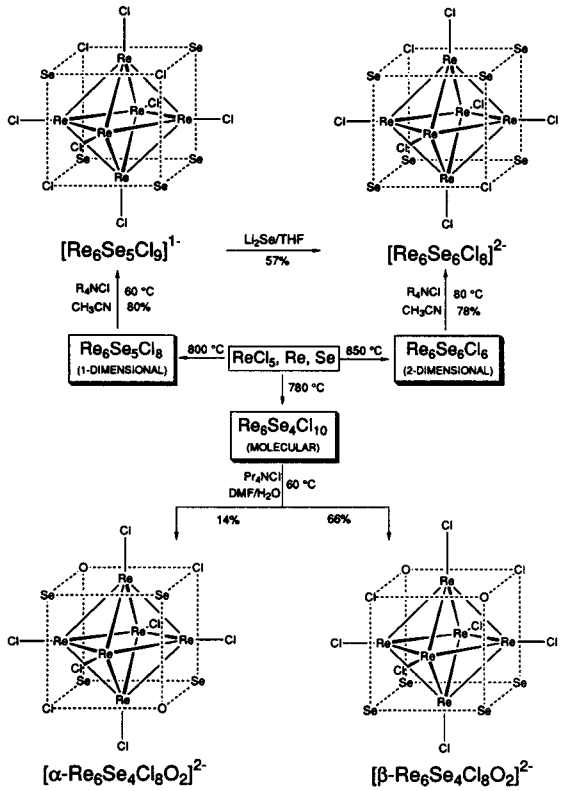

Figure 12. Reaction scheme illustrating the excision of clusters from the phase $Re_6Se_5Cl_8$ and $Re_6Se_6Cl_6$ and core conversion reactions in which chloride is substituted by selenide or oxide. For the sake of definiteness, core atom positions are specified, but some atoms are actually disordered. Reprinted from ref 49. Copyright 1992 American Chemical Society.

it was shown that the neutral molecular ($n = 0$) phase $Re_6Se_4Cl_{10}$ reacts with water in a DMF solution of $NPr^n{}_4Cl$ at 60 °C to give $\{[Re_6Se_4{}^iO_2{}^iCl_2{}^i]Cl_6{}^a\}^{2-}$, whose two isomers were isolated. Second, THF solutions of $[Re_6Se_5Cl_9]^-$ react with Li_2Se to afford $[Re_6Se_6Cl_8]^{2-}$.

A neat demonstration of the $[Re_6S_5Cl_3]^{5+}$ core reactivity in solution is offered by a key electrochemical experiment which follows the core transformation upon reaction with $(Me_3Si)_2S$, taking advantage that $[Re_6S_5Cl_9]^-$ and $[Re_6S_6Cl_8]^{2-}$ have markedly different redox behaviors (see section IV.B and Figure 13).

On the basis of these early results, the reaction in acetonitrile of sylilated reagents $(Me_3Si)_2E$ (E = O, S, Se, Te) with alkylammonium salts of the cluster monoanions forms has been explored and proved to provide a neat, efficient synthesis[74] of a series of alkylammonium salts of heterosubstituted cluster cores $(Bu_4N)_2[Re_6Q_5ECl_8]$ (Q = S, E = O, S, Se; Q = Se, E = S, Se, Te) (Table 6), as shown in Scheme 2. Among the former, the oxo chalcohalide cluster, $(Bu_4N)_2[Re_6S_5OCl_8]$, stands alone because its $[Re_6S_5O]^{2+}$ core is not disordered in the solid-state structure, a consequence of the ordering of the oxygen atom on one single μ_3-site only. In addition, the ordered, noncentrosymmetrical cluster proved to be distorted as a result of a contraction of the Re_3 face capped by the oxygen atom.[74] Similar structural features are observed for the Siamese twin oxo cluster case reported in section A.1.

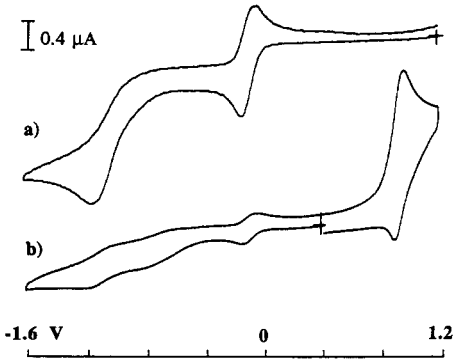

Figure 13. Cyclic voltammograms at a platinum electrode vs SCE in acetonitrile containing 0.1 M $(Bu_4N)PF_6$ (scan rate 0.1 V s^{-1}) of $(Bu_4N)[Re_6S_5Cl_9]$ (a) before and (b) after addition of $(Me_3Si)_2S$ and PPh_4Cl. Reprinted from ref 23. Copyright 1993 American Chemical Society.

Scheme 2

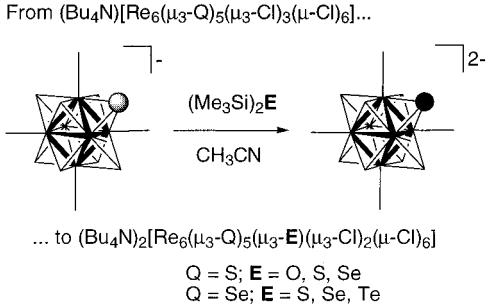

Among many attractive features[74] such as availability of large quantities in good yields, the latter silylated reagents route yields a wealth of novel compounds which include, for E = NR (R = H, Me, Bz), the μ_3-imido-functionalized Chevrel−Sergent-type molecular clusters $\{[Re_6Q_5^i(\mu_3\text{-}NR)^iCl_2^i]Cl_6^a\}^{2-}$ [75] and $\{[Re_6Q_5^i(NSiMe_3)^iCl_2^i]Cl_6^a\}^{2-}$ (Q = S, Se) (Figure 14). The nucleophilic conversion of the cluster-supported $NSiMe_3$ group into NH by reaction with Bu_4NF and the demonstration that the imido-functionalized core in turn reacts with electrophiles (Figure 14) are important new synthetic methods to prepare inorganic−organic hybrid compounds starting from cluster compounds which can only be prepared by high-temperature solid-state reactions.[75]

2. μ-Functionalization

$(Bu_4N^+)[Re_6S_5Cl_9]^-$ and $(Bu_4N^+)[Re_6Se_6Cl_9]^-$ do not react with $AgBF_4$ in refluxed acetonitrile,[76] indicating that the outer μ-Cl^- ligands held onto the hexarhenium chalcohalide cluster cores more strongly than in $[Mo_6Cl_{14}]^{2-}$.[77]

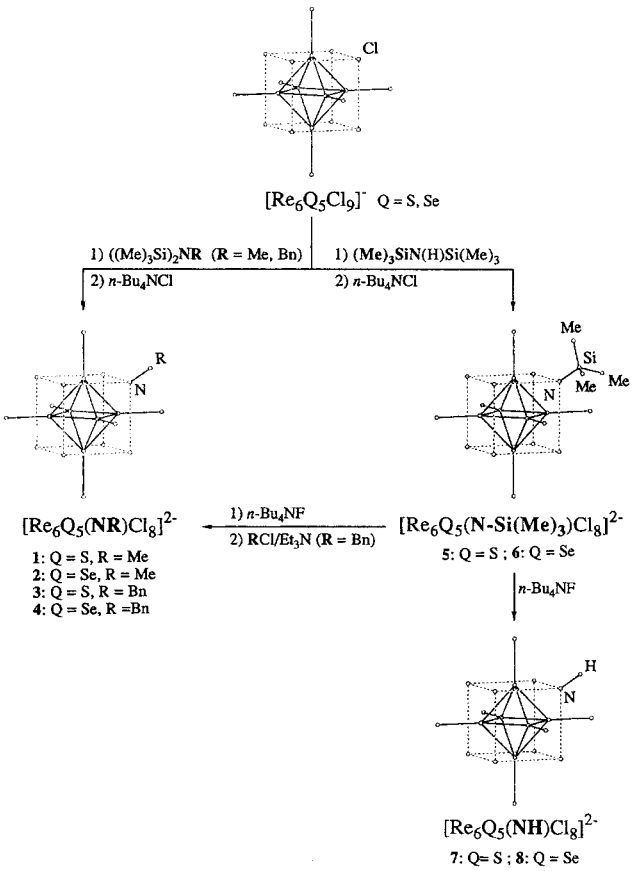

Figure 14. Reaction scheme for the preparation of compounds labeled here as **1**−**8**. In each case the counterions of the anionic cluster are Bu_4N^+ ions. Bn = benzyl. Reprinted from ref 75. Copyright 1996 Wiley-VCH.

The lability of outer iodides has been demonstrated recently by Zheng et al. for $(Bu_4N)_3[Re_6Se_7(SeH)I_6]$,[78] actually the oxidized, paramagnetic species, $(Bu_4N)_3[Re^{III}_5Re^{IV}Se_8I_6]$,[79] which is found to react with various amounts of PEt_3 in refluxed acetonitrile or DMF, to afford $[Re_6Se_8(PEt_3)_nI_{6-n}]^{(n-4)}$, $n = 3-6$ (Scheme 3).[82] This is not a simple μ-ligand exchange of $[Re_6Se_8I_6]^{3-}$ because simultaneous reductions of the 23-electron hexarhenium cores take place during the reaction.

The partially substituted clusters may be ultimately condensed upon thermolysis at 180 °C into dicluster species, such as $[Re_{12}Se_{16}(PEt_3)_{10}]^{4+}$ (Scheme 4).[82] Likewise, $(Bu_4N^+)_3[Re_6S_8Br_6]^{3-}$ reacts with PEt_3 to give $[Re_6S_8(PEt_3)_nBr_{6-n}]^{(n-4)+}$ ($n = 2-6$).[80] Also, a fraction up to the totality of the μ-iodide ligands may be stripped off $(Bu_4N^+)_3[Re_6S_8Br_6]^{3-}$ upon reaction with $AgBF_4$ in acetonitrile (see Table 6),[82] to yield

Scheme 3

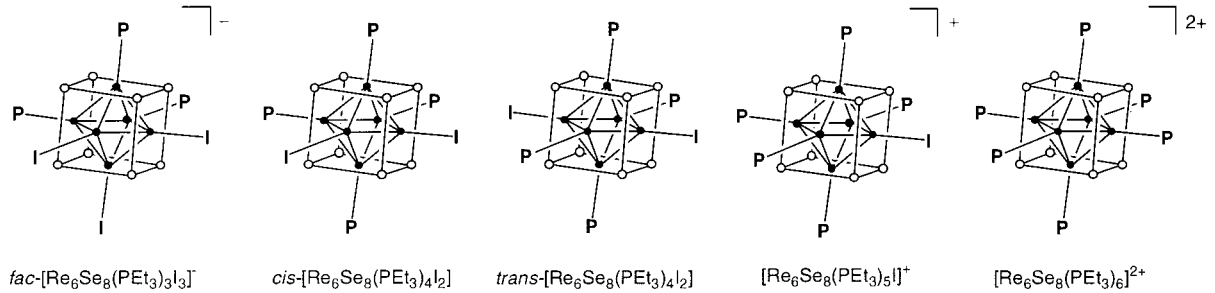

Scheme 4

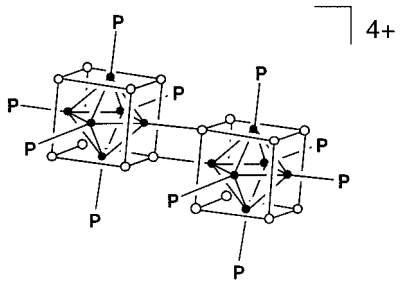

$[Re_6Se_8(MeCN)_6](BF_4)_2$. The latter solvated hexanuclear chalcogenide cluster core has been used recently to prepare pyridine- or 4-hydroxypyridine-ligated Re_6Se_8 complexes as well as the first dendrimers (Scheme 5) supported by a $[Re_6Q_8]^{2+}$ metal cluster core, based upon pyridyl functionality-bearing dendrons.[81,82] When *cis*-$[Re_6Se_8(PEt_3)_4I_2]$ is used as a starting material instead and dissolved in various solvents prior to the addition of $AgSbF_6$, additional phases have been obtained,[83] namely *cis*-$[Re_6Se_8(PEt_3)_4(solvent)_2](SbF_6)_2$ (Table 6). It should be noted that the iodide to solvent molecule exchange here occurs in the absence of any oxidation of the $[Re_6Se_8]^{2+}$ core. Thermolysis of *cis*-$[Re_6Se_8(PEt_3)_4(MeCN)_2](SbF_6)_2$ allowed another dicluster form, *trans*-$[Re_{12}Se_{16}(PEt_3)_{10}(MeCN)_2]^{4+}$, to be isolated.

This work has been extended to the synthesis of the SbF_6^- salts of *trans*-$[Re_6Se_8(PEt_3)_4(MeCN)_2]^{2+}$, $[Re_6Se_8(PEt_3)_5(4,4'\text{-bpy})]^{2+}$ (Scheme 6), and *trans*-$[Re_6Se_8(PEt_3)_4(4,4'\text{-bpy})_2]^{2+}$ (Scheme 6) and of the bridged diclusters $\{[Re_6Se_8(PEt_3)_5]_2(L-L)\}^{4+}$ (L−L = 4,4′-bpy, 4,4′-bipyridine (Scheme 7), 4,4′-$py_2C_2H_2$, *trans*-1,2-bis(4-pyridyl)ethylene, and 4,4′-$py_2C_2H_4$, 1,2-bis(4-pyridyl)ethane) (Scheme 8)), up to the quasi-linear tricluster $\{[Re_{18}Se_{24}(PEt_3)_{14}(4,4'\text{-bpy})_2]\}^{6+}$.[84] Further developments were recently disclosed where chelate embraces of the hexarhenium cluster core is achieved by the diphosphane 1,6-bis(diphenylphosphino)hexane (dpph) which substitutes for a fraction or the totality of μ-iodides in $(Bu_4N^+)_3[Re_6Se_8I_6]^{3-}$, to yield $[Re_6Se_8(\mu\text{-dpph})_nI_{6-2n}]^{2n-4}$ (n = 1−3), as shown in Scheme 9.[85]

Recently, Holm and Zheng have reported[86] the syntheses and characterization of three molecular squares by reacting *cis*-$[Re_6Se_8(PEt_3)_4(MeCN)_2](SbF_6)_2$ with ditopic ligands such as 4,4′-bipyridyl, 4,4′-$py_2C_2H_2$, and 4,4′-$py_2C_2H_4$.

The first aqua ion, $[Re_6S_8(H_2O)_6]^{2+}$,[47] was obtained in a parallel work by Fedin et co-workers by addition of a silver salt to an aqueous solution of $[Re_6S_8Cl_6]^{4-}$. However, no structural characterization of this dication have yet confirmed this interesting result.

Novel substitutions of μ-chlorine ligands of the one-electron-oxidized species $(Bu_4N)_3[Re^{III}_5Re^{IV}S_8Cl_6]$ have been reported recently by Sasaki and co-workers.[87] Thus, this paramagnetic 23-electron trianion reacts with pyridine (py) or 4-cyanopyridine (cpy) in DMF, leading, presumably upon an in-situ reduction, to a series of diamagnetic, 24-electron cluster salts, $(Bu_4N)_{4-n}[Re^{III}_6S_8Cl_{6-n}(py\text{-}R)_n]$ (n = 2−3, py-R = pyridine; n = 2, py-R = 4-cyanopyridine).[88] The attendant, one-electron-oxidized species have also been prepared upon electrochemical oxidation at constant potential, $(Bu_4N)_{3-n}[Re^{III}_5Re^{IV}S_8Cl_{6-n}(py\text{-}R)_n]$ (n = 2−3, py-R = pyridine; n = 2, py-R = 4-cyanopyridine).[93] The same authors have extended the series recently to include complexes with new N-heterocyclic ligands such as pyrazine (pz) (Scheme 10), 4,4′-bipyridine (bpy), 4-methylpyridine mpy), and (4-dimethylamino)pyridine (dmap) (see Table 6 and section IV.C).

Finally, when the number of substitutions of μ-halogen ligands reaches 2−4, two different isomers

Scheme 5

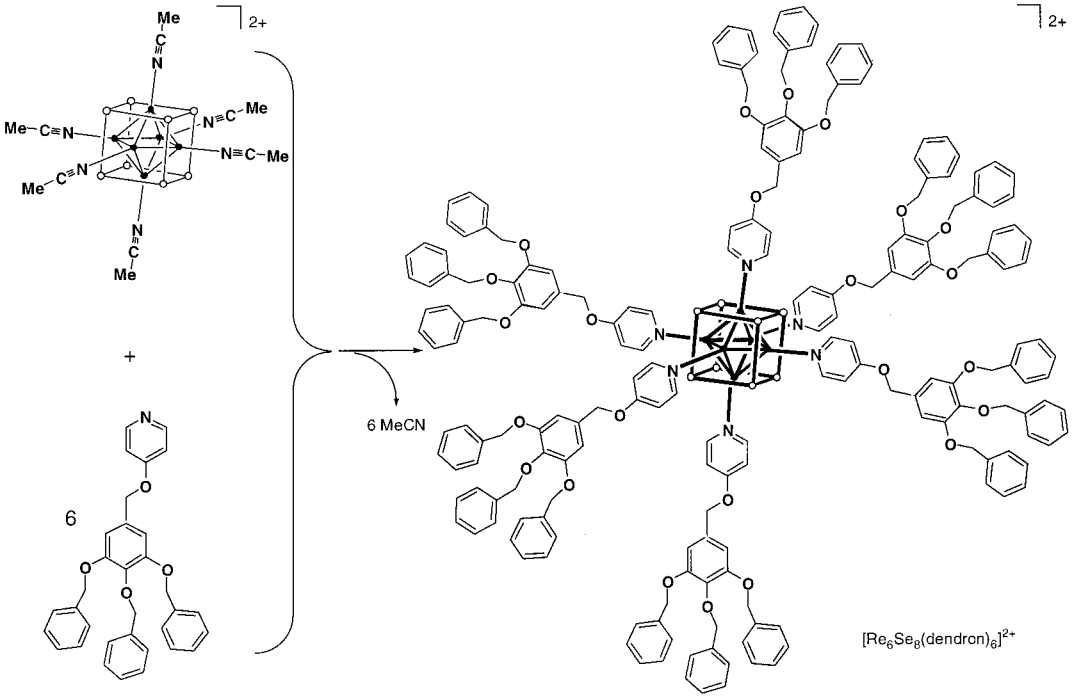

Scheme 6

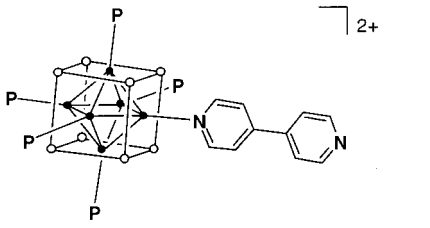

$[Re_6Se_8(PEt_3)_5(4,4'\text{-bpy})]^{2+}$

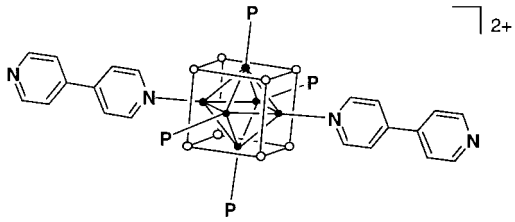

trans-$[Re_6Se_8(PEt_3)_4(4,4'\text{-bpy})_2]^{2+}$

Scheme 7

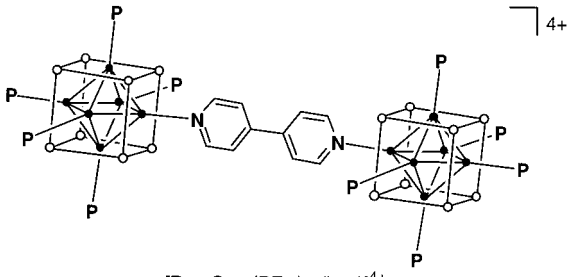

$[Re_{12}Se_{16}(PEt_3)_{10}(bpy)]^{4+}$

Scheme 8

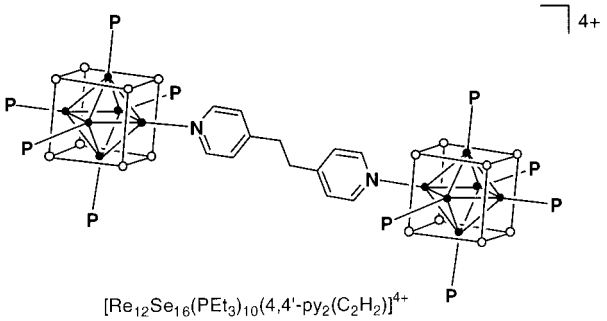

$[Re_{12}Se_{16}(PEt_3)_{10}(4,4'\text{-py}_2(C_2H_2)]^{4+}$

Scheme 9

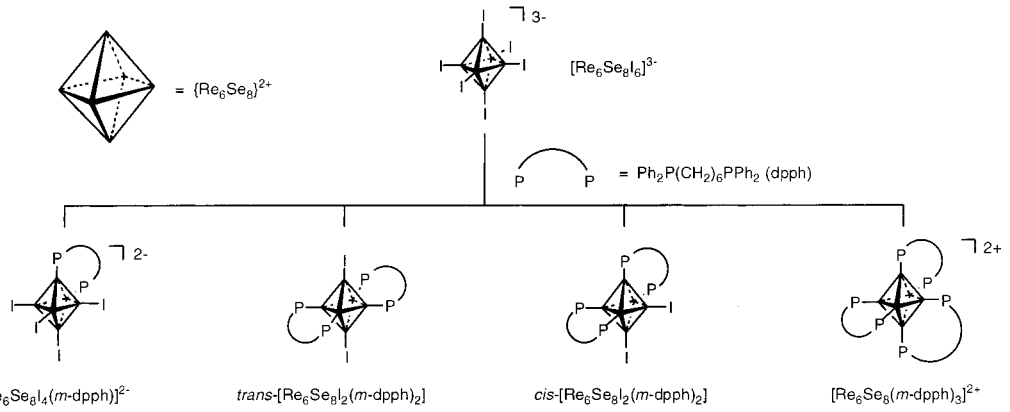

(Adapted from ref. 89. Copyright 2001 from Wiley-VCH)

are possible in each case. Their separation was achieved both in the $[Re_6Q_8(PEt_3)_nX_{6-n}]^{n-4}$ ($n = 2-4$, X = Br, Q = Se;[80] $n = 3-4$, X = I, Q = Se[82]) and $(Bu_4N)_{4-n}[Re^{III}{}_6S_8Cl_{6-n}(py\text{-}R)_n]$ ($n = 2-3$, py-R = pyridine; $n = 2$, py-R = 4-cyanopyridine)[88] series either by chromatography on silica/flash silica gel columns or by difference of solubility. The former proved to be most efficient for neutral and charged molecules alike, allowing for example to separate in good yield the cis and trans isomers of $[Re_6Y_8(PEt_3)_4X_2]$ as well as $(Bu_4N)_2[Re_6S_8Cl_4(py\text{-}R)_2]$.

3. Concomitant μ- and μ_3-Functionalization

Concomitant μ-Cl and μ_3-Cl displacement reactions have recently been achieved by reacting $Ca(THF)_6[Re_6S_6Cl_8]$,[89] instead of $(Bu_4N)_2[Re_6S_6Cl_8]$,[83] with $(Me_3Si)_2E$ (E = NH, O, S) or $(Me_3Si)_3E'$ (E′ = P, As) in the presence of $PPr^n{}_3$. Thus, unprecedented neutral and dicationic hexanuclear rhenium phosphine clusters with respectively μ_3-imido or oxo−chalcogenide heteroligand shells, $[Re_6S_6E_2(PPr^n{}_3)_6]^{2+}$ (E = NH, O, S), and μ_3-phosphido−chalcogenide or μ_3-arsenido−chalcogenide, $[Re_6S_6E_2(PPr^n{}_3)_6]$ (E = As, P), are obtained in good yields (Table 6 and Figure 15).[94]

4. Unsettled Mechanistic Issues

The cluster core inner and outer ligand-substitution chemistry in solution is still in its infancy, yet a number of key mechanistic questions may already be formulated and will have to be tackled by further reactivity and theoretical studies. One is the contrasted ease of μ- or μ_3-substitution as it would appear to depend on the presence of any halogen atom onto the eight inner cluster core μ_3-ligand sites within the $\{[Re_6(\mu_3\text{-}Q)_{4+n}(\mu_3\text{-}X)_{4-n}](\mu\text{-}X)_6\}^{n-}$ series. An analysis of the reaction products listed in Table 6 for which μ-functionalization occurred reveals that none of the latter retain an inner halogen ligand in its cluster core. Furthermore, when reactions were performed starting with those cluster forms having two to four inner halogen ligands, no purely μ-functionalization has been achieved. Either, purely μ_3-reactivity have been observed instead[23,49,74,75] or else all μ_3-halogen ligands were also substituted in the final compounds.[89]

Scheme 10

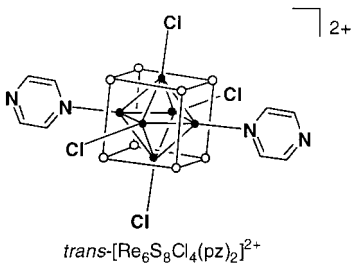

trans-$[Re_6S_8Cl_4(pz)_2]^{2+}$

It is perhaps too early to claim that the removal of all inner μ_3-halogen ligands and their replacement by chalcogen or pnictogen atoms might be required in order to activate the reactivity of the apical μ-halogen atoms.[90] Two experimental findings correlate with this assumption and are reformulated now. First, whenever any number of μ_3-halogen ligands are present onto the cluster core, the latter remains reluctant to oxidation, as discussed in section IV.C. Second, as reviewed in the preceding section (section III.B. 2), it is the oxidized, 23-electron forms, $[Re^{III}_5Re^{IV}Q_8X_6]^{3-}$ (Q = S, Se; X = Cl, Br, I), typically prepared by reacting the 24-electron precursors $[Re^{III}6Q_8X_6]^{4-}$ with $SOCl_2$ or $SOBr_2$, which are consistently engaged in the substitution reactions. Note that the latter are not simple μ-X substitution reactions of $[Re^{III}_5Re^{IV}Q_8X_6]^{3-}$ because simultaneous reduction of the hexarhenium cores takes place during the reactions. The mechanism for the latter has not been addressed yet. Note, also, the salient counterexample of the partially substituted, reduced cluster *cis*-$[Re_6Se_8(PEt_3)_4I_2]$ (Scheme 3), for which the remaining outer iodides can be exchanged by acetonitrile molecules in the absence of oxidant in the solution.

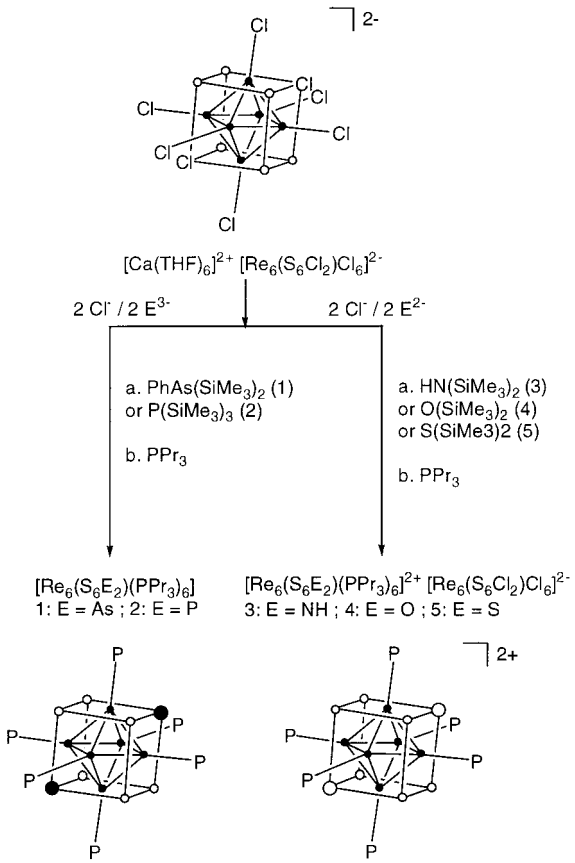

Figure 15. Synthetic scheme for the phosphine-substituted cluster labeled here as **1**−**5**. The μ_3-Cl and μ_3-E ligands are ordered (**2**, **4**, **5**) or disordered (**1**, **3**) over the μ_3-face-capping cluster sites and are therefore only presented schematically in the pictures. Adapted from ref 93. Copyright 2000 Wiley-VCH.

Another, elusive issue is the role of the nature, when relevant, of the cation in the starting material for inner or outer ligand exchange reactions in solution as Ca(THF)$[Re_6S_6Cl_8]$ reacts further than $(Bu_4N)[Re_6S_5Cl_9]$ (see section B.1).

Finally, one way to enter in the ligand exchange chemistry of the mixed-ligand cluster cores is to start from the one- or two-dimensional polymers, $Re_6Q_5Cl_8$ and $Re_6Q_6Cl_6$, respectively, as discussed earlier (section III.A.2). In turn, the solvent molecule μ-coordinated to the excised molecular forms $\{[Re_6Q_5Cl_3]Cl_5(\mu\text{-solvent})\}$ and $\{[Re_6Q_6Cl_2]Cl_4(\mu\text{-solvent})_2\}$ or the inner chloride atoms even could be substituted by other ligands such as phosphines or N-heterocycles.

IV. Special Topics

A. Structural Correlations

1. Constraints Imposed by the Ligands and Mechanochemical Response of the Re_6 Core

As readily exemplified by the analysis of the data collected in Table 7, the Re−Re bond lengths change with both the elements and the chalcogen/halogen ratio. Thus, in the Re−S−Cl system the Re−Re distance is slightly shorter than that calculated for a Re−Re single bond (2.609 Å) using the Pauling bond order expression,[91] with $d_n = d_1 - 0.6 \log n$, where n is Donnay and Allmann's bond-order value calculated as $n = |d_1/d_n|^5$ (d_n is the bond distance of order n; d_1 is the bond distance of order 1).[92] This core contraction, not observed for other systems such as Re−Se−Cl or Re−S−Br, is likely to reflect an internal pressure or constraint applied on the Re_6 octahedral core and which become significant for smaller ligands surroundings. This is further confirmed by the fact that, in the structures that contain one or two μ_3-oxo face-capping ligands, the averaged Re−Re distance within these cluster faces is even shorter, 2.530 Å for $(Bu_4N)_4[Re_6S_5OCl_7]_2O$,[64] 2.523 Å for $(Bu_4N)_2\{[Re_6S_5OCl_2]Cl_6\}$,[74] and 2.557 Å for $\{[Re_6S_6O_2](PPr_3)_6\}\{[Re_6S_6Cl_2]Cl_6\}\cdot 2CH_3CN$.[93] Consistently, larger Re−Re distances are obtained when tellurium ligands are involved, with for example 2.643 Å in $Re_6Te_4Br_{10}$.[25]

2. Re–L Distance as a Function of the X/Q Ratio

In the series $\{[Re_6Q_{4+n}X_{4-n}]X_6\}^{n-}$, where most structures are solved using a disordered mixed-ligand L = [(4 + n)/8Y + (4 − n)/8X], the averaged ⟨Re−L⟩ distance can be estimated in first approximation by applying the same weighting scheme to the actual Re−Q and Re−X bond lengths:

$$\langle d(\text{Re}-\mu_3\text{-L})\rangle = [(4+n)/8d(\text{Re}-\mu_3\text{-Q}) + (4-n)/8d(\text{Re}-\mu_3\text{-X})] \quad (3)$$

Table 7. Mean Interatomic Distances (Å) for the Series $[Re_6Q_{4+n}X_{10-n}]^{n-}$ ($n = 0-4$) in the Re−S−Cl, Re−S−Br, and Re−Se−Cl Systems

Re−S−Cl	$Re_6S_4Cl_{10}$[23]	(a) $(Bu_4N)[Re_6S_5Cl_9]$[2 3]	(a) $(Bu_4N)_2[Re_6S_6Cl_8]$[23]	(a) $(Bu_4N)_3[Re_6S_7Cl_7]$[23]	(a) $(Bu_4N)_4[Re_6S_8Cl_6]$[46]
		(b) $RbRe_6S_5Cl_9$23	(b) $ZnRe_6S_6Cl_8$37	(b) $Cs_3Re_6S_7Cl_7$43	(b) $Cs_4Re_6S_8Cl_6.Cs\ Cl$[46]
Re−Re	2.595(2)	(a) 2.589(7)	(a) 2.573(8)	(a) 2.570(10)	(a) 2.601(4)
		(b) 2.594(4)	(b) 2.593(3)	(b) 2.591(3)	(b) 2.596(4)
Re−L	2.422(12)	(a) 2.418(45)	(a) 2.401(9)	(a) 2.395(19)	(a) 2.403(9)
		(b) 2.416(14)	(b) 2.425(25)	(b) 2.408(11)	(b) 2.399(4)
Re−Cl[a]	2.319(11)	(a) 2.344(45)	(a) 2.362(12)	(a) 2.397(3)	(a) 2.451(4)
		(b) 2.358(7)	(b) 2.379(5)	(b) 2.407(10)	(b) 2.421(10)
Re−S−Br		$KRe_6S_5Br_9$[34]	$(PPh_4)_2[Re_6S_6Br_8]$[3 9]	$(PPh_4)_3[Re_6S_7Br_7]$[39]	$(Bu_4N)_4[Re_6S_8Br_6].H_2O$[46]
Re−Re		2.608(9)	2.601(10)	2.602(3)	2.594(7)
Re−L		2.502(43)	2.472(72)	2.444(19)	2.396(12)
Re−Br[a]		2.520(3)	2.534(13)	2.569(5)	2.595(10)
Re−Se−Cl	$Re_6Se_4Cl_{10}$[15]	(a) $KRe_6Se_5Cl_9$[15]	(a) $PbRe_6Se_6Cl_8$[15]		$Tl_4Re_6Se_8Cl_6.T\ lCl$[46]
		(b) $(Bu_4N)[Re_6Se_5Cl_9]$[4]	(b) $(NPr^n4)_2[Re_6Se_6Cl_8]$[49]		
Re−Re	2.615(5)	(a) 2.608(1)	(a) 2.611(1)		2.614(5)
		(b) 2.607(3)	(b) 2.613(3)		
Re−L	2.499(10)	(a) 2.501(13)	(a) 2.506(14)		2.523(3)
		(b) 2.499(8)	(b) 2.505(15)		
Re−Cl[a]	2.330(9)	(a) 2.373(6)	(a) 2.406(8)		2.431(8)
		(b) 2.353 (5)	(b) 2.379(12)		

Thus, knowing that $d(Re-\mu_3\text{-}S) < d(Re-\mu_3\text{-}Cl) < d(Re-\mu_3\text{-}Se) < d(Re-\mu_3\text{-}Br) < d(Re-\mu_3\text{-}Te) < d(Re-\mu_3\text{-}I)$, one expects that $d(Re-\mu_3\text{-}L)$ increases with n if $d(Re-\mu_3\text{-}Q) > d(Re-\mu_3\text{-}X)$ and decreases with n if $d(Re-\mu_3\text{-}Q) < d(Re-\mu_3\text{-}X)$. This turns out to be verified for the three systems for which sufficient data are available. Indeed, for two of them, Re−S−Cl and Re−S−Br, $d(Re-\mu_3\text{-}L)$ decreases when n increases, while, in the Re−Se−Cl system, the reverse is observed, in agreement with the above rule.

3. Re–μ-X Bond Length as a Function of the $[Re_6Q_{4+n}X_{4-n}]^{(6-n)+}$ Core Charge

A consistent observation for all Re−Q−X systems for which sufficient data are available (Table 7) has been that the Re−μ-X bond distance increases with n in the series $\{[Re_6Q_{4+n}X_{4-n}]X_6\}^{n-}$.[23,36] This can be explained in terms of Coulombic interactions between the net positive core charge of $[Re_6Q_{4+n}X_{4-n}]^{(6-n)+}$ and that of the negatively charged X^- apical ligand shell. As n increases, the net cluster core charge decreases from 6+ for $n = 0$ to 2+ for $n = 4$; thus, the attractive Coulombic interactions between the cluster core and its apical ligands decrease and the mean Re−μ-X distance increases. The same interpretation was given for a similar effect in the series $[Mo_6(Se_nCl_{8-n})Cl_6]^{(2+n)-}$ ($n = 0-2$),[93] by Ebihara and co-workers.[94]

4. Distribution of the Cluster Core Inner μ_3-Ligands

Most X-ray structure determinations of hexanuclear rhenium chalcohalide clusters salts of the type $\{[Re_6(\mu_3\text{-}Q)_{4+n}(\mu_3\text{-}X)_{4-n}](\mu\text{-}X)_6\}^{n-}$, where $0 \le n \le 3$, conclude to the occurrence of disordered chalcogen and halogen μ_3-ligands on the eight positions of the pseudocube. The origin of this disorder can be either geometric or orientational.[95] Indeed, there are 6, 3, and 3 geometric isomers for $n = 0$, 1, and 2, respectively (Figure 16), whose random distribution in the crystal generates geometrical disorder. When no geometric isomer exist ($n = 3$), the random orientation of a single isomer creates an orientational disorder in the crystal.

A few exceptions have, however, been reported. *Partial* ordering occurs for some of the ligands, as

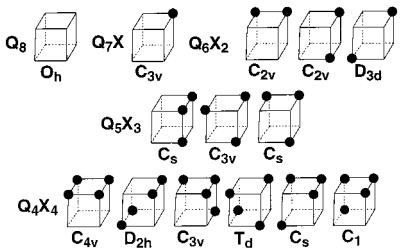

Figure 16. All possible geometric isomers for a $[Re_6(\mu_3\text{-}Q)_{4+n}(\mu_3\text{-}X)_{4-n}]^{(6-n)+}$ cluster core ($n = 0-4$) together with their Schönflies point group symmetry symbol.

for the oxo−chalcohalide derivatives (sections III.A.1 and III.B.1)[49,64,74] and the μ_3-imido-functionalized clusters (section III.B.1),[75] where solely the heteroatom loci proved to be neatly ordered in the solid-state structure refinements. Complete ordering of the inner ligands has been reported in the case of $[Re_6Te_6Cl_2]Cl_4(TeCl_2)_2$, an $n < 4$ cluster (section II.D.1).[26]

Finally, one should note that those instances where ordering has been observed correspond to situations of uttermost relative steric demands of the ligand set, i.e., oxygen versus sulfur and chlorine or tellurium versus chlorine.

B. Reactions in Molten Salts

Following the seminal observation by Fedorov, Mironov, and co-workers that the octahedral cluster is retained[2,96] upon reacting Re_6Te_{15} with bromine to afford $Re_6Te_4Br_{10}$, the reaction of octahedral chalcohalide rhenium cluster derivatives has been further explored in molten salts such as KSCN or KCN, thus, the reaction of Re_6Te_{15} in molten KSCN and subsequent treatment with an aqueous solution of CsCl which led to the first soluble cyanide-substituted octahedral rhenium cluster salt, $Cs_3K\{[Re_6S_6(Te_{0.66}S_{0.34})_2](CN)_6\}$.[97,98] Similarly, the reaction of $Re_6S_4Br_{10}$, $\{[Re_6S_4Br_4]Br_6\}$, with KSCN followed by cation exchange affords small amounts of $(PPh_4)_3[Re_6S_7Br_7]$ (see section II.D.4).[39]

Likewise, upon reaction in molten KCN at 600 °C, the 3D polymer $Re_6Se_8Br_2$ (see section II.E.3) breaks

into the water-soluble molecular salt $K_4\{[Re_6Se_8](CN)_6\}$[99] or, similarly, $NaCs_3[Re_6S_8(CN)_6]$ and $NaCs_3[Re_6Se_8(CN)_6]$ can be obtained by a high-temperature exchange reactions in molten NaCN of $Cs_4[Re_6S_8Br_6]\cdot CsBr$ and $Cs_4[Re_6Se_8I_6]$,[46] respectively.[100] In light of this success, it would be of interest to probe the reactivity of the halogen-bridged 3D polymers $\{[Re_6Q_7X]X_3\}$ in molten salts since all previous attempts to dismantle these sets of compounds have failed so far.

More recently, the reaction of KCN with either ReS_2 or $ReSe_2$ at 800 and 650 °C for 2 days gave the polymeric 1D and 2D phases $K_4[Re_6S_{10}(CN)_2]$ and $K_4[Re_6Se_{10}(CN)_4]$, respectively.[101]

Again, it is striking that in these molten salt reactions, and similarly to what was observed in organic solution reactions (see section III.B.3), apical halide substitution for μ-cyanide ligands are observed only on octahedral rhenium cluster compounds that have their inner ligand shells purely made of chalcogen atoms. Consistently, one observes that in the reaction of a cluster core containing μ_3-halogen ligands, such as in the $Re_6S_4Br_{10}$ vs KSCN case, it is the inner μ_3-bromide ligands which get substituted.[39]

Finally, a coordination chemistry[37,68] of these water-soluble cyanide-substituted octahedral rhenium cluster ligands[97,98] is developing rapidly. Novel coordination polymers constructed out of the alkaline-earth or metallic cations coordination spheres include $Cs_2Mn_3[Re_6Se_8(CN)_6]_2\cdot 15H_2O$ and $(H_3O)_2Co_3[Re_6Se_8(CN)_6]_2\cdot 14.5H_2O$[102] and $(Pr_4N)_2M(H_2O)_5[Re_6X_8(CN)_6]\cdot H_2O$ (X = S, Se; M = Mn, Ni)[103] and a new class of porous materials with $[Zn(H_2O)]_2[Re_6S_8(CN)_6]\cdot 7H_2O$, $Cs_2[trans\text{-}Fe(H_2O)_2]_3[Re_6S_8(CN)_6]_2\cdot 12\ H_2O$,[100] and $[Cd_2(H_2O)_4][Re_6S_8(CN)_6]\cdot 14H_2O$,[104] as well as 3D cluster-expanded Prussian blue analogues, $M_4[Re_6Q_8(CN)_6]_3\cdot xH_2O$ (M = Ga, Q = Se; M = Fe, Q = Te).[105] Two-dimensional compounds have also be prepared with $Cs_2[trans\text{-}Fe(H_2O)_2][Re_6S_8(CN)_6]$.[100] Recent results include the synthesis of $Na_2Zn_3[Re_6Se_8(CN)_6]_2\cdot 24H_2O$, a compound exhibiting a porous three-dimensional framework isotypic with that of $Na_2Zn_3[Fe(CN)_6]_2\cdot 9H_2O$, by reaction between $[Zn(H_2O)_6]^{2+}$ and $Na_4[Re_6Se_8(CN)_6]$. Upon using a slight excess of the zinc reactant, $[Zn(H_2O)_6]^{2+}$ incorporates instead of Na^+ to yield the ion-exhanged compound $[Zn(H_2O)_6]_2Zn_3[Re_6Se_8(CN)_6]_2\cdot 18H_2O$.[106] Also, the face-capped octahedral clusters $[Re_6Q_8(CN)_6]^{4-}$ (Q = S, Se) are used to space apart partially hydrated Co^{2+} ions, thus forming extended porous framework, that display strong and reversible color changes, from orange to intense blue-violet, upon exposure to certain organic solvents. Three phases have been reported: $[Co_2(H_2O)_4][Re_6S_8(CN)_6]\cdot 10\ H_2O$; $Cs_2[Co(H_2O)_2][Re_6S_8(CN)_6]\cdot 2H_2O$; $[Co(H_2O)_3]_4[Co_2(H_2O)_4][Re_6S_8(CN)_6]_3\cdot 44H_2O$.[107]

These developments now allow to envision the construction of ligand-bridged extended arrays in the solid state, thereby reassembling multicluster networks of diverse dimensionalities from divergent molecular precursors, taking advantage of the stereochemistry of the cluster core as well as of the diversity of shape, size, redox activity, and binding preferences of bridging, functional molecular spacers.

C. Diversity of the Redox Chemistry in the $\{[Re_6Q_{4+n}X_{4-n}]X_6\}^{n-}$ Series

The presently available electrochemical data on halides and chalcohalides of Mo_6, W_6, and Re_6 octahedral cluster anions have been collected in Table 8. The first report[23] described the cyclic voltammetry in acetonitrile of $(Bu_4N^+)_n[Re_6S_{4+n}Cl_{10-n}]^{n-}$ with n = 1−3. A striking difference of behavior was revealed when going from $[Re_6S_5Cl_9]^-$, which undergoes a quasi-reversible reduction at −0.075 V/ECS, to $[Re_6S_6Cl_8]^{2-}$ and $[Re_6S_7Cl_7]^{3-}$, which both proved to give up one electron upon a quasi-reversible process at ca. 1.0 V/ECS, while being inert to any kind of reduction process in the cathodic regime (Figure 17). This contrasted behavior which correlates with both the net cluster charge and the chalcogen/halogen ratio, suggests that significant modifications of the cluster core electronic structure underlie this redox chemistry. Another striking observation is the reversible one-electron oxidation process for $(Bu_4N)_4[Re_6S_8X_6]$ (X = Cl, Br), at potentials as low as ca. 0.3 V/ECS, hence providing an exquisite entry into the charge-transfer chemistry of open-shell cluster forms (Figure 17).[46,70,112] This was recently exemplified by the electrocrystallization[108] and structural characterization of paramagnetic $(Bu_4N^+)_3[Re_6S_8Cl_6]^{\bullet 3-}$ (g = 2.44) and the discovery of the luminescence properties of such open-shell, 23-electron species (see section IV.D.3).[112]

Sasaki and co-workers have significantly extended the electrochemistry of these systems to $(Bu_4N)_{4-n}[Re_6S_8Cl_{6-n}L_n]$ (L = py or cpy; n = 2−3, py = pyridine; n = 2, cpy = 4-cyanopyridine)[88] or $(Bu_4N)_4[Re_6Q_8(CN)_6]$,[109] whose cluster cores all exhibit a reversible oxidation wave at various potentials in CH_3CN, ranging from $E_{1/2}$ = 0.06 to 0.92 V vs SCE for $(Bu_4N)_4[Re_6Te_8(CN)_6]$ and $(Bu_4N)[mer\text{-}Re_6S_8Cl_3(py)_3]$, respectively (see Table 8).[110] Then, the study of the cpy derivative having revealed that the ligand-reduction waves of the two chemically equivalent cpy ligands coordinated in a cis or trans orientation to the $[Re_6(\mu_3\text{-}S)_8]^{2+}$ core are split in the cyclic voltammogram, these electrochemical studies have been extended to a series of *trans*- or *cis*-$[Re_6(\mu_3\text{-}S)_8Cl_4(L)_2]^{2-}$ complexes with N-heterocylic ligands (see Table 6 and section III.B).[111] Thus, the $E_{1/2}$ values for the $Re^{III}_6/Re^{III}_5Re^{IV}$ couple become more positive in the order L = dmap < mpy < py < bpy < cpy < pz suggesting that the coordination of electron-withdrawing groups make the $[Re_6(\mu_3\text{-}S)_8]^{2+}$ core more difficult to oxidize. A good linear correlation between the $E_{1/2}$ and pK_a values of the N-heterocylic ligands ($E_{1/2}$ = 0.8737 − 0.0197(pK_a)) demonstrates that the σ electrons of the latter affect the closely spaced HOMO levels of the rhenium clusters. It is further concluded that an electronic interaction through the $[Re_6(\mu_3\text{-}S)_8]^{2+}$ core is responsible for the observed 90−140 mV splitting of the ligand-reduction waves. In addition, the second ligand-reduction wave of the bpy complexes is quenched by traces of water as well as by addition of the proton donor imidazole (Scheme 4).

Table 8. Electrochemical Properties of Hexanuclear Cluster Molecules ($E_{1/2}$ vs SCE in V)[a]

redox system				$E_{1/2}$	solvent	ref
$[Mo_6Cl_{14}]^{-/2-}$			23/24 e$^-$	1.36	CH_3CN	120
		$[Re_6S_8Cl_6]^{2-/3-}$	22/23 e$^-$	1.09	CH_3CN	70
		$[Re_6S_7Cl_7]^{2-/3-}$	23/24 e$^-$	1.02	CH_3CN	23
		$[Re_6Se_8(\mu\text{-dpph})_2I_4]^{3+/2+}$	23/24 e$^-$	1.01	CH_2Cl_2	85
$[(Mo_6Br_7S)Cl_6]^{-/2-}$			22/23 e$^-$	1.01	CH_2Cl_2	94
	$[W_6Cl_8Br_6]^{-/2-}$		23/24 e$^-$	0.99	CH_2Cl_2	129
		$[Re_6S_6Cl_8]^{1-/2-}$	23/24 e$^-$	0.99	CH_3CN	23
	$[W_6Cl_{14}]^{-/2-}$		23/24 e$^-$	0.93	CH_2Cl_2	129
		mer-$[Re_6S_8Cl_3(py)_3]^{0/-}$	23/24 e$^-$	0.92	CH_3CN	88
		cis- and *trans*-$[Re_6S_8Cl_4(pz)_2]^{-/2-}$	23/24 e$^-$	0.81	CH_3CN	111
	$[W_6Br_{14}]^{-/2-}$		23/24 e$^-$	0.80	CH_2Cl_2	129
$[(Mo_6Br_7S)Cl_5(CH_3CN)]^{1-/2-}$			23/24 e$^-$	0.80	CH_2Cl_2	130
		cis- and *trans*-$[Re_6S_8Cl_4(cpy)_2]^{-/2-}$	23/24 e$^-$	0.78	CH_3CN	88
		cis- and *trans*-$[Re_6S_8Cl_4(bpy)_2]^{-/2-}$	23/24 e$^-$	0.74	CH_3CN	111
		cis-$[Re_6Se_8(\mu\text{-dpph})_2I_4]^{+/-}$	23/24 e$^-$	0.74	CH_2Cl_2	85
		cis- and *trans*-$[Re_6S_8Cl_4(py)_2]^{-/2-}$	23/24 e$^-$	0.72	CH_3CN	88
		trans-$[Re_6Se_8(\mu\text{-dpph})_2I_4]^{+/-}$	23/24 e$^-$	0.71	CH_2Cl_2	85
		cis- and *trans*-$[Re_6S_8Cl_4(mpy)_2]^{-/2-}$	23/24 e$^-$	0.70	CH_3CN	111
		cis- and *trans*-$[Re_6S_8Cl_4(dmap)_2]^{-/2-}$	23/24 e$^-$	0.63	CH_3CN	111
$[(Mo_6Cl_7S)Br_6]^{2-/3-}$			23/24 e$^-$	0.63	CH_2Cl_2	94
$[(Mo_6Cl_7Se)Br_6]^{2-/3-}$			23/24 e$^-$	0.62	CH_2Cl_2	94
		$[Re_6S_8(CN)_6]^{3-/4-}$	23/24 e$^-$	0.55	CH_3CN	109
$[(Mo_6Cl_7S)Cl_6]^{2-/3-}$			23/24 e$^-$	0.59	CH_2Cl_2	94
	$[W_6I_{14}]^{-/2-}$		23/24 e$^-$	0.57	CH_2Cl_2	129
	$[W_6I_8Br_6]^{-/2-}$		23/24 e$^-$	0.56	CH_2Cl_2	129
$[(Mo_6Cl_7Se)Cl_6]^{2-/3-}$			23/24 e$^-$	0.56	CH_2Cl_2	94
$[(Mo_6Cl_6Se_2)Cl_6]^{2-/3-}$ isomer B			22/23 e$^-$	0.53	CH_2Cl_2	93b
$[Mo_6Se_8(PEt_3)_6]^{1+/0}$			19/20 e$^-$	0.49	THF	131
$[Mo_6S_8(PEt_3)_6]^{1+/0}$			19/20 e$^-$	0.47	THF	131
$[(Mo_6Cl_6Se_2)Cl_6]^{2-/3-}$ isomer A			22/23 e$^-$	0.43	CH_2Cl_2	93b
		$[Re_6Se_8(CN)_6]^{3-/4-}$	23/24 e$^-$	0.33	CH_3CN	109
$[(Mo_6Br_7S)Cl_6]^{2-/3-}$			23/24 e$^-$	0.34	CH_2Cl_2	94
		$[Re_6Se_8(\mu\text{-dpph})I_4]^{-/2-}$	23/24 e$^-$	0.30	CH_2Cl_2	85
		$[Re_6S_8Br_6]^{3-/4-}$	23/24 e$^-$	0.29	CH_3CN	46, 84
		$[Re_6S_8Cl_6]^{3-/4-}$	23/24 e$^-$	0.30	CH_3CN	46, 112
$[Mo_6S_8(PEt_3)_6]^{1+/0}$			19/20 e$^-$	0.22	CH_2Cl_2	131
$[Mo_6Se_8(PEt_3)_6]^{1+/0}$			19/20 e$^-$	0.22	CH_2Cl_2	131
		$[Re_6Te_8(CN)_6]^{3-/4-}$	23/24 e$^-$	0.065	CH_3CN	109
		$[Re_6S_5Cl_9]^{1-/2-}$	24/25 e$^-$	−0.07	CH_3CN	23
		$[Re_6Se_5Cl_9]^{1-/2-}$	24/25 e$^-$	−0.22	CH_3CN	70
$[(Mo_6Cl_6Se_2)Cl_6]^{3-/4-}$ isomer B			23/24 e$^-$	−0.22	CH_2Cl_2	93b
$[(Mo_6Cl_6Se_2)Cl_6]^{3-/4-}$ isomer A			23/24 e$^-$	−0.29	CH_2Cl_2	93b
$[Mo_6Se_8(PEt_3)_6]^{0/1-}$			20/21 e$^-$	−0.93	THF	131
$[Mo_6S_8(PEt_3)_6]^{0/1-}$			20/21 e$^-$	−0.96	THF	131
$[Mo_6S_8(Pet_3)_6]^{0/1-}$			20/21 e$^-$	−1.05	CH_2Cl_2	131
$[Mo_6Se_8(PEt_3)_6]^{0/1-}$			20/21 e$^-$	−1.05	CH_2Cl_2	131
$[Mo_6Cl_{14}]^{2-/3-}$			24/25 e$^-$	−1.70	CH_2Cl_2	129
$[Mo_6Se_8(PEt_3)_6]^{1-/2-}$			21/22 e$^-$	−1.91	THF	131
$[Mo_6S_8(Pet_3)_6]^{1-/2-}$			21/22 e$^-$	−1.97	THF	131

[a] $E°(Fc/Fc^+) = 0.446$ (in CH_2Cl_2) and 0.543 V (in THF) vs KSCE (SCE).

Since no general trend can be easily driven out upon the influence of the number of μ_3-halide and the nature of μ-ligands on redox processes potentials, a thorough analysis of the electronic structures of the closed- and open-shell cluster cores is now needed to discuss further their rich redox and photochemistry.

D. IR and UV–Visible Spectroscopies

1. Infrared and Raman Spectroscopies

There is only one report of infrared and Raman data conducted on $Re_6Se_4Cl_{10}$ in the solid state.[21] The authors note that the simple spectra (Figure 18) indicate T_d symmetry for the molecule.[95] This implies μ_3-Cl and μ_3-Se ligands alternate at the vertexes of the $(\mu_3\text{-X})_8$ ligand set pseudocube which can be symbolized by two interpenetrating tetrahedra. Thus, the disordered motif refined in their crystallographic study would be the consequence of a random orientation disorder of the molecular units in the crystal.

2. UV–Visible Spectroscopy

The UV−vis absorbance spectra between 300 and 700 nm of DMF solutions of $(Bu_4N^+)_n[Re_6Q_{4+n}Cl_{10-n}]^{n-}$ (Q = S, $n = 1-3$; Q = Se, $n = 1, 2$) and $Re_6S_5Cl_8$ have been reported (Figure 19 and Table 9).[22,70] Absorption spectra of DMF solutions of $Re_6S_5Cl_8$ and (Bu_4N)-$[Re_6S_5Cl_9]$ are very similar with a single and small shoulder near 360−380 nm. This shoulder is much more pronounced in the case of the DMF solutions of $(Bu_4N)_2[Re_6S_6Cl_8]$ and $(Bu_4N)_3[Re_6S_7Cl_7]$ with, in addition, two other smaller ones at 330 and 460 nm. The absorbance spectra of the selenides are closely related to their sulfido analogues, albeit slightly shifted toward longer wavelengths. Thus, the spectra of $(Bu_4N)[Re_6Se_5Cl_9]$ have a small shoulder near

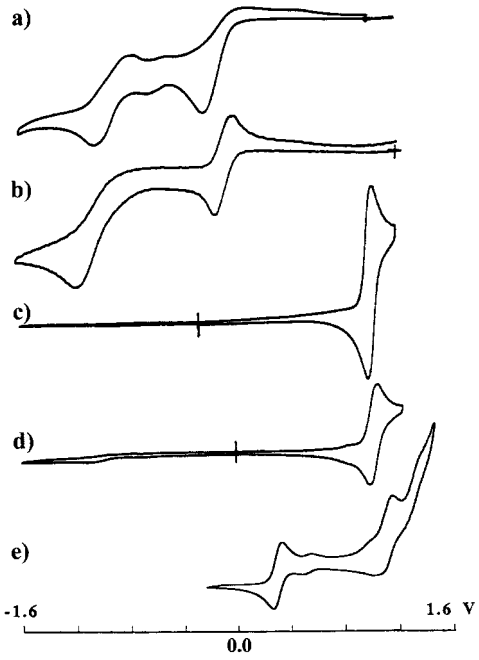

Figure 17. Cyclic voltammograms at a platinum electrode vs SCE in acetonitrile containing 0.1 M $(Bu_4N)PF_6$ (scan rate 0.1 V s^{-1}) of (a) $[Re_6S_5Cl_9(DMF)]$, (b) $(Bu_4N)[Re_6S_5Cl_9]$, (c) $(Bu_4N)_2[Re_6S_6Cl_8]$, (d) $(Bu_4N)_3[Re_6S_7Cl_7]$, and (e) $(Bu_4N)_4[Re_6S_8Cl_6]$. Modified—(e) has been added—from ref 23. Copyright 1993 American Chemical Society.

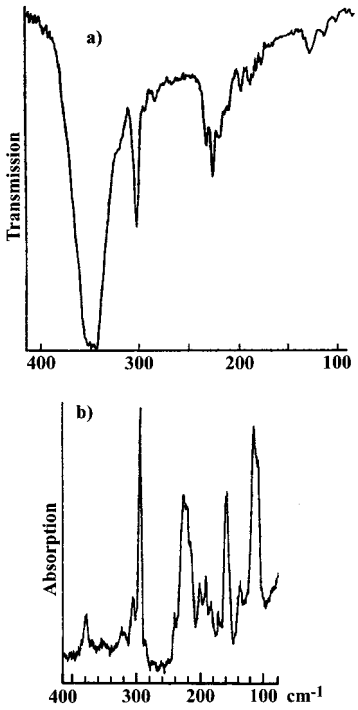

Figure 18. IR (a) and Raman (b) spectra for $Re_6Se_4Cl_{10}$. Reprinted from ref 21. Copyright 1985 Plenum Publishing Corp.

380−400 nm plus a weak additional one around 500 nm, and $(Bu_4N)_2[Re_6Se_6Cl_8]$ presents a main shoulder at 400 nm as well as two similar additional smaller ones.

The UV−visible spectra for acetonitrile solutions of $(Bu_4N^+)_4[Re_6Q_8X_6]^{4-}$ (X = Cl, Br, I; Q = S) have been reported by Holm et al.[46] and confirmed, in the case of $(Bu_4N^+)_4[Re_6S_8Cl_6]^{4-}$, by further studies,[70,87,112,113] except for the absence of a weak peak at 537 nm, whose occurrence likely indicates the presence of small amounts of $[Re_6S_8Cl_6]^{\bullet 3-}$ (Figure 20).[112] Within the series $[Re_6S_{4+n}Cl_{10-n}]^{n-}$ (n = 1−4), the intense absorption at 436 nm is observed for the tetraanion (n = 4) only.[22,70] In addition, this peak experiences a red shift upon going from μ-chlorine, to μ-bromide, and, finally, to μ-iodide ligands (see Table 9), perhaps an indication of halide ligand-to-metal charge transfer.[46] The spectrum for acetonitrile solutions of $(Bu_4N^+)_3[Re_6S_8Cl_6]^{\bullet 3-}$ (Figure 20) is strikingly different from any of the former. The occurrence of two large peaks at 490 and 540 nm and a large near-IR absorption (Figure 20) again demonstrate that a significant change of electronic structure of the cluster anion occurs upon the one-electron oxidation. The wide near-IR absorption band between 700 and 1800 nm (λ_{max} ~1254 nm, $\epsilon \sim 500$ L·mol^{-1}·cm^{-1})[70] may correspond to electronic transitions from a fully to a partially occupied metal orbital or to a charge-transfer band between localized Re^{III} and Re^{IV} states. A similar absorption band has been observed for the paramagnetic hexanuclear molybdenum clusters anions (Mo_6^{13+}) $[Mo_6(X_7Q)X'_6]^{\bullet 2-}$ (X = X′ = Cl, Br; Q = S, Se) and $[Mo_6(Cl_6Se_2)Cl_6]^{\bullet 3-}$.[93a,b]

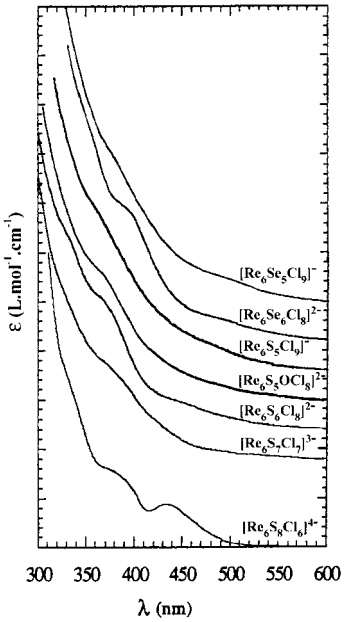

Figure 19. UV−vis absorbance spectra for $(Bu_4N^+)_n[Re_6Q_{4+n}Cl_{10-n}]^{n-}$ (in DMF for Q = S, n = 1; in CH_3CN for n = 2−4; Q = Se, n = 1, 2), as well as $(Bu_4N^+)_2[Re_6S_5OCl_8]^{2-}$. For each spectrum, the concentration was 3×10^{-4} mol·L^{-1}, and the extrema of absorbance are few tenths and 6000 L·mol^{-1}·cm^{-1}.

Finally, the UV−vis absorption spectrum of the solvated cluster core $[Re_6S_8(H_2O)_6]^{2+}$ in 1 M $HClO_4$ has been reported and shows four peaks ranging from 216 to 409 nm (see Table 9).[47]

3. NMR Spectroscopy

The majority of NMR studies of hexanuclear rhenium chalcohalide clusters have used the nuclei ^1H and ^{31}P to characterize the stereochemistry of clusters where organic ligands have partially substituted the terminal halogen ligands. ^{31}P NMR resonances

Table 9. λ_{max} (nm) of UV−Vis Absorbance Spectra for Various Hexanuclear Rhenium Chalcohalide Clusters

cluster (in CH_3CN)	λ_{max} abs (ϵ_M L·mol^{-1}·cm^{-1})	ref
$[Re_6S_8Cl_6]^{4-}$	377 (sh, 1860), 434 (1050), 537 (140)	46
$[Re_6S_8Br_6]^{4-}$	401 (sh, 1540), 443 (945), 545 (90)	46
$[Re_6S_8I_6]^{4-}$	393 (sh, 3290), 420 (2200), 507 (755)	46
$[Re_6S_8Cl_6]^{3-}$	378 (sh, 1820), 489 (785), 544 (1190)	46, 79
$[Re_6S_8Br_6]^{3-}$	395 (sh, 2380), 492 (781), 541 (1270)	46, 79
$[Re_6S_8I_6]^{3-}$	534 (590), 586 (sh, 353)	46, 79
$[Re_6Se_8I_6]^{3-}$	477 (sh, 2060), 525 (1180), 609 (1190)	46, 79
$[Re_6S_8Cl_6]^{3-\bullet}$	sh 381, 489 (850), 544 (1230), 1250 (400)	112
$[Re_6S_8(H_2O)_6]^{2+}$ [a]	216 (44 000), 260 (13 200), 360 (1540), 409 (875)	47
trans-$[Re_6S_8Cl_4(py)_2]^{2-}$	424 (sh, 1070), 373 (sh, 2400), 306 (sh, 10 400), 270 (sh, 25 100), 240 (sh, 38 300), 226 (52300)	88
cis-$[Re_6S_8Cl_4(py)_2]^{2-}$	422 (sh, 1260), 373 (sh, 2390), 303 (sh, 8350), 268 (sh, 16900), 239 (sh, 39 200), 227 (51 300)	88
trans-$[Re_6S_8Cl_4(cpy)_2]^{2-}$	521 (sh, 310), 320 (11 800), 269 (sh, 27 500), 239 (sh, 41 300), 222 (65 500)	88
cis-$[Re_6S_8Cl_4(cpy)_2]^{2-}$	529 (sh, 320), 316 (11 800), 240 (sh, 36 000), 223 (64 000)	88
mer-$[Re_6S_8Cl_3(cpy)_3]^{-}$	421 (1050), 374 (sh, 2320), 269 (sh, 28 400), 240 (sh, 36 600), 226 (49 000).	88
trans-$[Re_6S_8Cl_4(py)_2]^{\bullet-}$	1408 (370), 545 (1190), 494 (890), 269 (sh, 32 000), 252 (38 000), 227 (53 300)	88
trans-$[Re_6S_8Cl_4(cpy)_2]^{\bullet-}$ [b]	1417 (350), 545 (1180), 493 (890), 310 (sh, 14 700), 275 (sh, 30 000), 223 (66 000).	88
mer-$[Re_6S_8Cl_3(cpy)_3]^{\bullet}$ [b]	1380 (360), 547 (1210), 495 (850)	88

[a] In 1 M $HClO_4$. [b] In CH_2Cl_2.

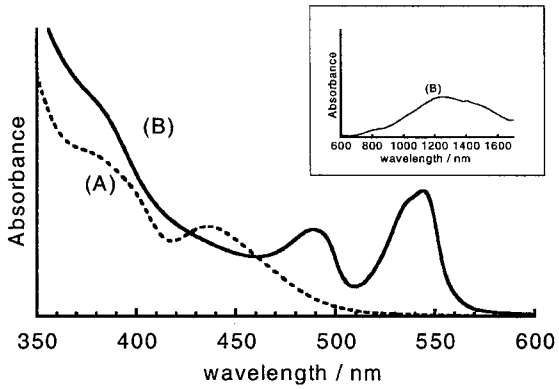

Figure 20. Electronic absorption spectra for acetonitrile solutions ($C = 2.8 \times 10^{-4}$ M) of $(Bu_4N)_4[Re_6S_8Cl_6]$ ((A) two poorly resolved shoulders at 335 and 380 nm and a peak of larger intensity at 436 nm ($\epsilon_M = 8.6 \times 10^2$ L·mol^{-1}·cm^{-1})) and $(Bu_4N)_3[Re_6S_8Cl_6]$ ((B) one poorly resolved shoulder (381 nm), two large peaks (489 nm, $\epsilon_M = 8.5 \times 10^2$ L·mol^{-1}·cm^{-1}; 544 nm, $\epsilon_M = 1.23 \times 10^3$ L·mol^{-1}·cm^{-1}), and a very wide band centered around 1250 nm (700−1750 nm, $\epsilon_M = 4 \times 10^2$ L·mol^{-1}·cm^{-1})). Reprinted from ref 112. Copyright 1999 Royal Society of Chemistry Journals U.K.

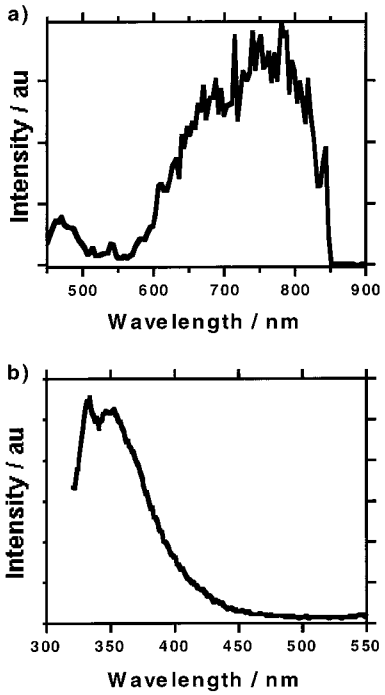

Figure 21. (a) Luminescence spectra for acetonitrile solutions of $(Bu_4N)_4[Re_6S_8Cl_6]$ (5.0×10^{-5} M) for excitations at 390 nm (maximum at 720 nm). (b) Luminescence spectra for acetonitrile solutions of $(Bu_4N)_3[Re_6S_8Cl_6]$ (2.0×10^{-5} M) for excitations at 270 nm (maxima at 320 and 355 nm).

have been observed within the ranges of −35.7 to −17.6 ppm and −23.1 to −16.2 ppm (with respect to an 85% solution of H_3PO_4 at 0 ppm) for the system Re−Se−I[82,83] and Re−S−Br,[80] respectively. By comparison of the shifts from isostructural molecules obtained in both systems, it was concluded that the peaks are shifted to higher frequency in the latter system. The highest frequency signals, −15.1 and −10.6 ppm, have been observed for the condensed clusters $[Re_{12}Se_{16}(PEt_3)_{10}](BF_4)_4 \cdot 4CH_2Cl_2$[82] and *trans*-$[Re_{12}Se_{16}(PEt_3)_8(MeCN)_2](SbF_6)_4 \cdot 4CH_2Cl_2$,[83] respectively.

A detailed ^{77}Se and ^{125}Te NMR investigation has also enabled the stereochemistry of the inner ligands in $\{[Re_6Te_{8-n}Se_n](CN)_6\}^{4-}$ ($n = 0-8$) to be studied.[30]

E. Luminescence Properties

As the difference with the mono-, di-, and trianions within the chalcohalide series $[Re_6S_{4+n}Cl_{10-n}]^{n-}$ (n = 1, 2, 3), the tetraanions $[Re_6Q_8X_6]^{4-}$ (Q = S, X = Cl, Br, I; Q = Se, X = Cl, Br, I)[88,112] as well as the paramagnetic 23-electron cluster trianion $[Re_6S_8Cl_6]^{\bullet 3-}$ [112] are luminescent, and the emission spectra of acetonitrile solutions of $(Bu_4N)_4[Re_6S_8Cl_6]$ and $(Bu_4N)_3[Re_6S_8Cl_6]$ are reported in Figure 21a,b,[114] respectively. The values of the maxima for the emission peaks are reported in Table 10. It should be noted that the luminescence of the tetraanions $[Re_6Q_8X_6]^{4-}$ occurs for excitation wavenumbers in the range of those of its singular large absorption band centered at 430 nm. Altogether, the luminescence for the tetraanions shifts slightly to a longer wavelength and their emission lifetimes (τ_{em}) as well as quantum yields (ϕ_{em}) decrease as the terminal halide changes from Cl to Br and I. Also, emission spectra are similar[112] to that for the hexanuclear molybdenum-

Table 10. Photophysical Data for Hexanuclear Chalcogenide and Halide Molecular Metal Clusters

salt	$\lambda_{excitation}$ (nm)	λ_{max} (nm)	τ_{em} (μs)	ϕ_{em}	ref
$(Bu_4N)_4[Re_6S_8Cl_6]^a$	390	720	5.1	0.037	112, 114
	436	750		0.031	113
$(Bu_4N)_4[Re_6S_8Cl_6]^a$	355	770	6.3	0.039	87
$(Bu_4N)_4[Re_6S_8Br_6]^a$	355	780	5.4	0.018	87
	436		3.9	0.012	113
$(Bu_4N)_4[Re_6S_8I_6]^a$	355	800	4.4	0.015	87
	436		2.6	0.011	113
$(Bu_4N)_3[Re_6S_8Cl_6]^a$	270	320, 350			112, 114
$(Bu_4N)_2[Re_6Se_8(\mu\text{-dpph})I_4]$	436	787	2.4	0.007	85
$(Bu_4N)\{mer\text{-}[Re_6S_8(PEt_3)_3Br_3]\}$	436	760	4.2	0.019	113
trans-$[Re_6S_8(PEt_3)_4Br_2]$	436	740	5.7	0.008	113
cis-$[Re_6S_8(PEt_3)_4Br_2]$	436	750	4.2	0.019	113
trans-$[Re_6Se_8(PEt_3)_4I_2]$	436	750	5.4	0.037	113
cis-$[Re_6Se_8(\mu\text{-dpph})_2I_2]$	436	790	3.2	0.012	85
trans-$[Re_6Se_8(\mu\text{-dpph})_2I_4]$	436	770	2.1	0.008	85
cis-$[Re_6Se_8(PEt_3)_4I_2]$	436	750	6.0	0.029	113
$[Re_6S_8(PEt_3)_5Br]Br$	436	740	7.0	0.043	113
$[Re_6Se_8(PEt_3)_5I]I$	436	740	6.5	0.085	113
$[Re_6S_8(PEt_3)_6]Br_2$	436	720	10.0	0.044	113
$[Re_6Se_8(PEt_3)_6]I_2$	436	730	10.8	0.068	113
$[Re_6Se_8(\mu\text{-dpph})_3](SbF_6)$	436	779	6.5	0.031	85
$[Re_6S_8(MeCN)_6](SbF_6)_2$	436	690	14.8	0.100	113
$[Re_6S_8(py)_6](SbF_6)_2$	436	690	14.0	0.163	113
$[Re_6S_8(DMF)_6](SbF_6)_2$	436	680	18.9	0.203	113
$[Re_6S_8(Me_2SO)_6](SbF_6)_2$	436	660	22.4	0.238	113
$(Bu_4N)_2[Mo_6Cl_8Cl_6]^a$	436	805	180	0.19	132, 133
$(Bu_4N)_2[Mo_6Br_8Br_6]^a$	436	825	130	0.23	132, 133
$(Bu_4N)_2[Mo_6Cl_8Br_6]$	355		140		134
$(Bu_4N)_2[Mo_6Cl_8I_6]$	355		86		134
$(Bu_4N)_2[W_6Cl_8Cl_6]^a$	355	833	1.5	0.02	135
$(Bu_4N)_2[W_6Cl_8Br_6]^a$	355	814	2.3	0.04	135
$(Bu_4N)_2[W_6Cl_8I_6]^a$	355	802	3.0	0.07	135
$(Bu_4N)_2[W_6Br_8Cl_6]^a$	355	766	9.7	0.10	135
$(Bu_4N)_2[W_6Br_8Br_6]^a$	355	758	15	0.15	135
$(Bu_4N)_2[W_6Br_8I_6]^a$	355	752	15	0.25	135
$(Bu_4N)_2[W_6I_8Cl_6]^a$	355	701	10	0.11	135
$(Bu_4N)_2[W_6I_8Br_6]^a$	355	698	22	0.25	135
$(Bu_4N)_2[W_6I_8I_6]^a$	355	698	30	0.39	135
$[P(C_6H_5)_4][Re_6S_8(CN)_6]^a$	355	720	11.2	0.056	110
$[P(C_6H_5)_4][Re_6Se_8(CN)_6]^a$	355	720	17.1	0.140	110
$[P(C_6H_5)_4][Re_6Te_8(CN)_6]^a$	355	750	0.57	0.004	110
$Cs_3K[Re_6S_8(CN)_6]^b$	355	720	1.2	0.009	110
$K_4[Re_6Se_8(CN)_6]^b$	355	720	1.9	0.015	110
$K_4[Re_6Te_8(CN)_6]^b$	355	750	0.42	0.004	110

[a] In CH_3CN. [b] In water.

(II) and tungsten(II) clusters,[132,133] although, in the case of the molybdenum one, both τ_{em} and ϕ_{em} are significantly larger (see Table 10). Further comparison of these systems show that the halide terminal dependences of τ_{em} and ϕ_{em} go in opposite trends for rhenium and molybdenum clusters on the one hand and the tungsten one on the other. In the molybdenum and tungsten cases, this was explained in terms of π-back-donation.[135]

Finally, the cyano-substituted chalcogenide hexanuclear rhenium(III) clusters $[Re_6Q_8(CN)_6]^{4-}$ (Q = S, Se, Te) also exhibit luminescence at room temperature with emission quantum yields and lifetimes decreasing in the order Se > S ≫ Te (see Table 10).[109]

The luminescence of the sulfidorhenium clusters was anticipated by Arratia-Pérez and Hernández-Acevedo,[115] who also predicted it recently for $[Re_6Se_8X_6]^{4-}$ (X = Cl, I),[116] on the basis of the similitude in their calculations of their electronic structures to that calculated for $[W_6Cl_{14}]^{2-}$ which also is luminescent. Now, just why are these M_6Q_8-based clusters luminescent is an open question which can only be tackled by further in-depth investigations of their electronic structures.

F. Subtle Ligand Shell Variations Neatly Characterized by Mass Spectrometry

It is only recently that high-resolution mass spectrometry has been applied to characterize all-inorganic species such as molybdenum halide cluster anions.[117] Liquid secondary ion mass spectrometry (LSIMS) proved to be efficient for identifying the present heterosubsituted rhenium clusters.[37,74,75] Since LSIMS, together with electrospray mass spectrometry (ESMS) or fast atom bombardment mass spectrometry (FABMS), is of high resolution, each low-resolution peak is the envelope of all the high resolution peaks that are due to the different isotopic composition and that can be simulated very accurately, hence providing a fingerprint for each cluster formulation. It is therefore a very efficient

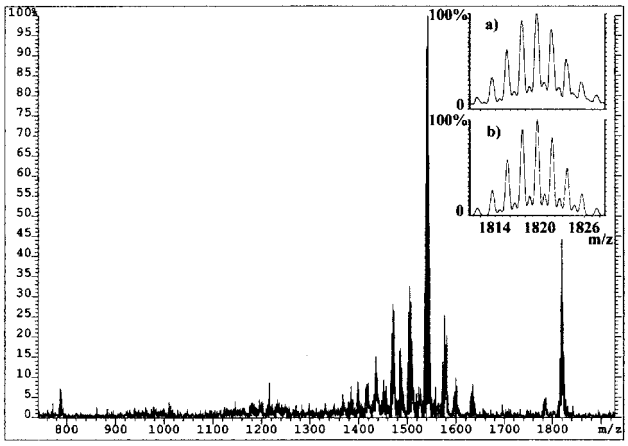

Figure 22. Negative LSIMS for $(Bu_4N)_2[Re_6S_5OCl_8]$, together with the (a) observed and (b) calculated isotopic ion distribution for the parent ion $\{(Bu_4N)[Re_6S_5OCl_8]\}^-$, at m/z = 1819.6. Reprinted from ref 74. Copyright 1995 American Chemical Society.

method to reveal the precise composition of such clusters, especially when an ambiguity remains on the nature of one of the elements (Figure 22).

G. Electronic Structure

An extensive analysis of the electronic structure of Mo_6Q_8 clusters, the fundamental unit of the Chevrel−Sergent phases, to which the electronic structure of $Re_6L_8L'_6$ is related, is to be found in a seminal paper by Hughbanks and Hoffmann.[118] Calculations of the electronic structure for a few $Re_6L_8L'_6$ cluster phases have been performed by Certain and Lissillour using tight-binding band-structure calculations and the "solidlike" extended Huckel method.[119] The authors used a three-band model which come from the observation that, in all calculations of the convoluted density of state (DOS), the electronic structures are very similar; thus, the Fermi level area is described by means of a general pattern of three bands, labeled from bottom to top B1, B2, and B3 (Figure 23). The B1 band is essentially based on L ligand p orbitals, and B2 together with B3 is mainly composed of 12 and 18 d rhenium levels, respectively. Since B1 and B2 are filled, the Fermi level of these compounds lies between B2 and B3 which explains, depending upon the extend of the gap, their insulator to semiconductor behavior. The authors anticipate

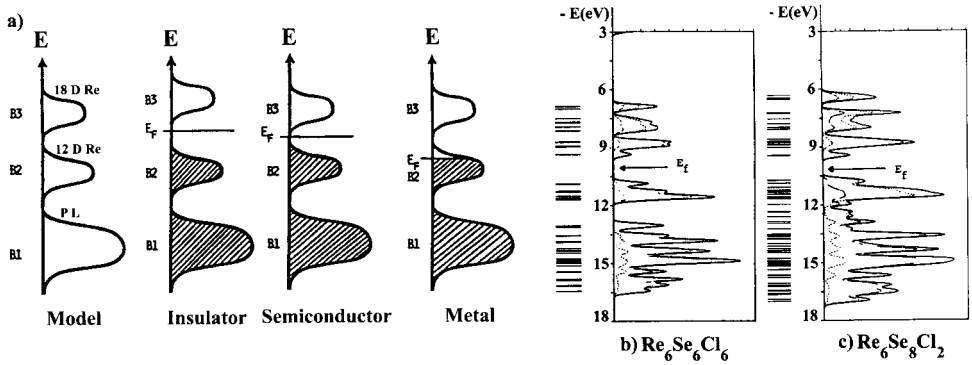

Figure 23. (a) Three band model for convoluted density of states (partial p L DOS in dotted line, partial d M DOS in dashed line, total DOS in continuous line) for (b) $Re_6Se_6Cl_6$ and (c) $Re_6Se_8Cl_2$. Reprinted from ref 119. Copyright 1986 from Wiley-VCH.

Table 11. Organic Radical Cations and Hexanuclear Rhenium Chalcohalide Cluster Anion Hybrid Salts

phase formulation	physical properties	ref
$(TMTTF)_2[Re_6Se_6Cl_8]$	insulator, diamagnetic	4
$(TMTTF)_2[Re_6Se_5Cl_9]$	semiconductor, spin Peierls	136
$(TMTSF)_2[Re_6S_5Cl_9]$	semiconductor	136
$(TTF)_3[Re_6Q_6Cl_8]Cl$ (Q = S, Se)	insulator, antiferromagnetic	4, 121
$(TSeF)_3[Re_6Se_6Cl_8]Cl$	insulator, antiferromagnetic	4
$(BEDT\text{-}TTF)_4^{\bullet+}[Re_6Se_5Cl_9]^-\cdot$guest	metal	122
$(BEDT\text{-}TTF)^{\bullet+}[Re_6Se_5Cl_9]^-\cdot$solvent	insulator with uniform, noninteracting antiferromagnetic chain of spins	125
$(cis\text{-}[10]TTFphane^{\bullet+})_2[Re_6S_6Cl_8]^{2-}$	insulator, diamagnetic	137
$(cis\text{-}[12\ TTFphane)_2^{\bullet+}[Re_6S_5Cl_9]^-$	insulator, paramagnetic	137
$(BET\text{-}TTF)_2^{\bullet+}[Re_6S_5Cl_9]^-$	semiconductor, paramagnetic	138
$(BES\text{-}TTF)_2^{\bullet+}[Re_6S_5Cl_9]^-$	semiconductor, paramagnetic	138
$[(MeS)_4\text{-}TTF]_2^{\bullet+}[Re_6S_5Cl_9]^-$	insulator, paramagnetic	120
$[(MeSe)_4\text{-}TTF]^{\bullet+}[Re_6S_5Cl_9]^-$	insulator, paramagnetic	120
$[(MeSe)_4\text{-}TTF]_2^{\bullet+}[Re_6S_6Cl_8]^-\cdot 2DMF$	insulator, diamagnetic	120
$[(MeTe)_4\text{-}TTF]^{\bullet+}[Re_6S_5Cl_9]^-\cdot 1.5DMF$	insulator, diamagnetic	120
$[(EtTe)_4\text{-}TTF]^{\bullet+}[Re_6S_5Cl_9]^-$	insulator, paramagnetic	120
$[(EtTe)_4\text{-}TTF]_2^{\bullet+}[Re_6S_5Cl_9]^-$	insulator, paramagnetic	120
$[bis(DMTTF)ethane]_3[Re_6Se_6Cl_8]$	spin Peierls transition	139
$[bis(DMTTF)ethane]_3[Re_6S_6Cl_8]$	spin ladder	139
$[bis(DMTTF)ethane]_2[Re_6S_5Cl_9]$ (Y = S, Se)	insulator, paramagnetic	139
$[bis(DMTTF)ethane]_5[Re_6Se_5Cl_9][Re_6Se_6Cl_8]$	insulator, paramagnetic	139
$[cryptophane]^{\bullet+}[Re_6S_5Cl_9]^-$	insulator	140
$\beta\text{-}[BDT\text{-}TTP)_6[Re_6S_6Cl_8]\cdot 2CH_2ClCHCl_2$	metal	127

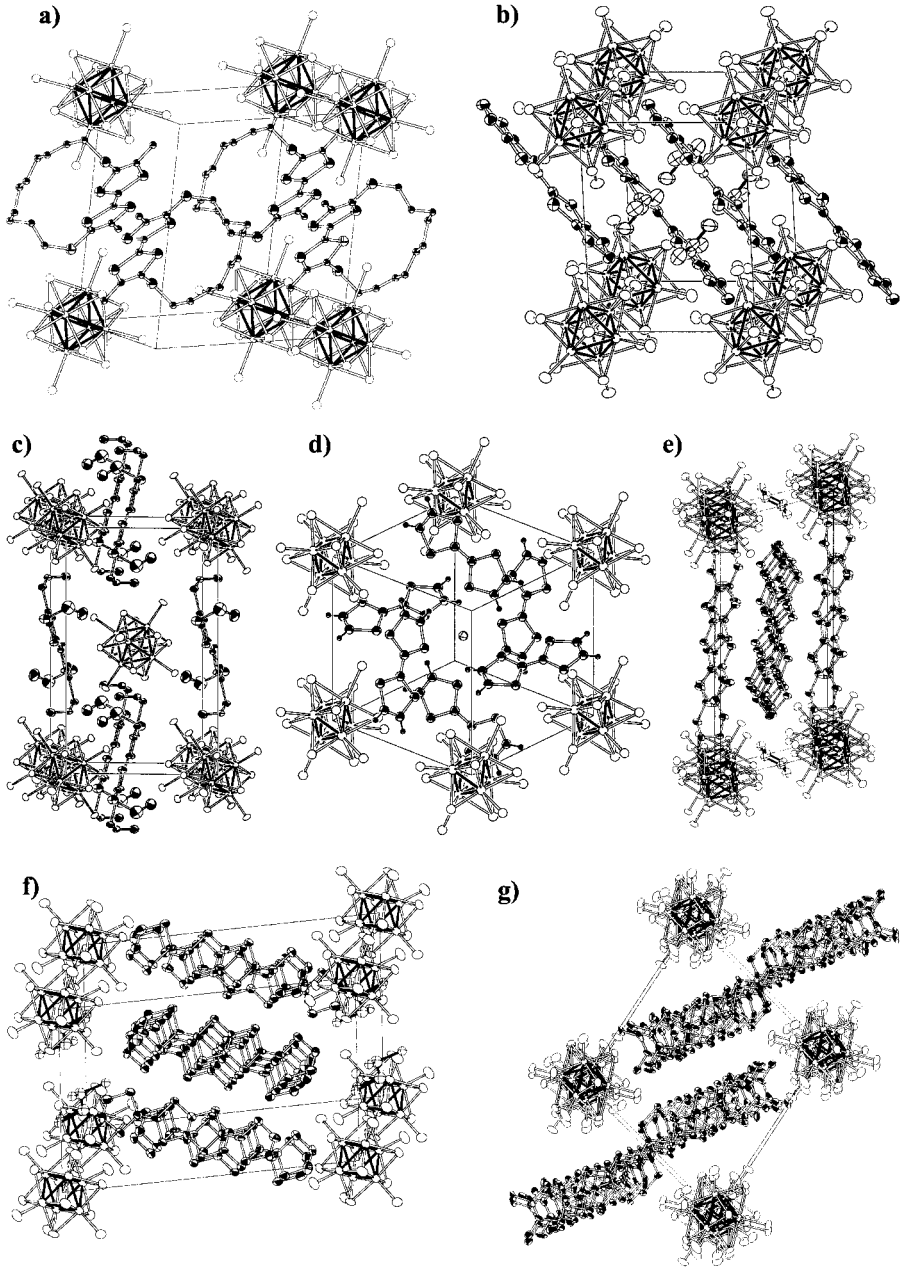

Figure 24. Organic radical cation arrays templated by rhenium chalcohalide cluster anions, as exemplified here by the projections of the unit cell content of a set of binary and ternary associations assembled by electrocrystallization: (a) (*cis*-[10]TTFphane)$_2$[$Re_6S_6Cl_8$]; (b) (BET-TTF)$_2$[$Re_6S_5Cl_9$]; (c) [($EtTe)_4$-TTF][$Re_6S_5Cl_9$]; (d) ($TSeF)_3$[$Re_6Se_6Cl_8$]Cl; (e) (BEDT-TTF)$_4$[$Re_6S_6Cl_8$]·guest; (f) β-(BDT-TTP)$_6$[$Re_6S_6Cl_8$]·($CH_2ClCHCl_2$)$_2$; (g) [bis(DMTTF)ethane]$_5$[$Re_6S_5Cl_9$][$Re_6S_6Cl_8$].

that removal of the intercalated metal cation (for example Pb in Pb[$Re_6Se_6Cl_8$]) would give a metal.

DFT calculations have been performed recently by Arratia-Pérez and Hernández-Acevedo on the octahedral [$Re_6Q_8X_6$]$^{4-}$ (Q = S, X = Cl, Br, I;[115] Q = Se, X = Cl, I)[116] cluster ions. Manifolds of closely space unoccupied energy levels are found to be mainly localized on the octahedral rhenium core with some contributions from the μ_3-Q ligands, while the cluster highest occupied molecular orbital (HOMO) for all calculated structures would appear to be largely centered on the terminal halide ligands. Note that, as far as the cluster reactivity is concerned, one should be aware of the difficulty at reasoning on one individual orbital since the orbital character may vary entirely from one to the other because the energy levels are so close to each other. In addition, calculations typically handle poorly the negative charge of molecular species. This is particularly relevant in the case of the tetranionic form, [$Re_6(\mu_3$-$Q)_8(\mu$-$X)_6$]$^{4-}$, where electrostatic contributions to the core−μ-ligand interactions are likely to be significant. Therefore, the sizable percentage of the terminal halide contribution to the cluster HOMO may well be an artifact altogether. Finally, the authors conclude that the hexarhenium cluster ions have the same singlet ground state as $W_6Cl_{14}^{2-}$ (spanning the Γ_6^+ symmetry) and should therefore be diamagnetic. Note that the calculated charge distributions are as follows: [$Re_6^{-0.21}S_8^{-0.16}Cl_6^{-0.24}$], [$Re_6^{-0.23}S_8^{-0.17}Br_6^{-0.21}$],

$[Re_6^{-0.26}S_8^{-0.21}I_6^{-0.12}]$, $[Re_6^{-0.34}Se_8^{+0.04}Cl_6^{-0.38}]$, and $[Re_6^{-0.43}Se_8^{-0.03}Cl_6^{-0.20}]$, with negatively charged rhenium atoms a rather unexpected outcome.

Several major questions remain unanswered and will require further theoretical work. For example, why are the potentials of the redox couples $[Re_6Q_8]^{2+}/[Re_6Q_8]^{3+}$ so much lower than those of their chalcohalide counterparts? Furthermore, a sound investigation and discussion of the electronic structures of the open-shell forms $[Re_6Q_8]^{3+}$ is in dire need. A prominent unsettled question concerns the reactivity of the oxidized, 23-electron cluster forms: why are the radical anions $[Re_6Q_8X_6]^{3-}$ more reactive toward the substitution of μ-halides by cyanides and phosphine ligands, or N-heterocycles, than their reduced forms or, rather, is it essentially the higher positive charge of the cluster core which favors outer ligand exchange (section III.B.4)? Then, what is the nature of the electronic transition responsible for the intense absorption at 430 nm in $[Re_6Q_8]^{2+}$? All of these interrogations relate to key issues for further developments of the many, yet unexplored facets of the chemistry and physics of these luminescent and magnetic, organic−inorganic hybrid molecules.

H. Opportunities in Chemistry of Molecular Materials by Manipulating a Rare Set of Isosteric Anions

Right from the initial discovery of their solution phase chemistry these chalcohalide hexanuclear rhenium cluster anions have been engaged (sections II.D.2 and III.A.1)[4] in the construction of ordered molecular assemblies upon their electrochemical association with tetrathiafulvalene-based cation radical molecules.[108] Thus, if one probes the interplay between the molecular properties (size, shape, functionality, charge, redox properties,...) of organic and inorganic electroactive precursors and the structural organization and functions of associated integrated O−I hybrid salts,[120] a large variety of binary or ternary salts have been obtained and shown to adopt remarkable molecular architectures (Table 11 and Figure 24), as exemplified by the series of molecular antiperovskite series $(TTF)_3[Re_6Q_6Cl_8]X$ (Q = S, Se, X = Cl, Br, I)[36,121] or the series of metallic pseudopolymorphs β''-(BEDT-TTF)$_4$(guest)·$[Re_6Q_6Cl_8]$,[70,122123,124] where a host of electronic and magnetic properties such as antiferromagnetism[36,121,125] or metallic behavior[127] are currently being explored.

A particularly interesting aspect of this solid-state chemistry of molecular ions lies in the opportunity now offered to unravel unprecedented situations where one concentrates on the template charge effect, for a given size and shape of the (all-inorganic) molecular anion. This contrasts with the classical approach in inorganic solid-state chemistry where the (organic) template size, volume, and shape is preferably tuned with less variability of its charge itself.[126] One particularly relevant example addresses the important issue of the manipulation of band filling in low-dimensional molecular metals. Thus, our capacity to change the cluster anion charge and hence to modify the band filling, Fermi surface, and therefore the metallic character of the robust organic slabs within the two-dimensional metal[127] β-(BDT-TTP)$_6$-$[Re_6S_6Cl_8]$·$2CH_2ClCHCl_2$ is nicely exemplified by the synthesis of β-(BDT-TTP)$_8[Re_6S_7Cl_7]$·$4CH_2Cl_2$. Regardless of their stoichiometries, the two compounds have essentially identical slab geometries and band structures. Therefore, different electron counts result in different Fermi levels and Fermi surfaces topologies, as expected.[128]

V. Acknowledgments

Our research on the chemistry of hexanuclear chalcohalide rhenium clusters has benefited from the talent and dedication of the following students or postdocs, in turn at Rennes, Orsay, and Nantes: L. Ouahab, A. Pénicaud, C. Lenoir, A. Decker, F. Simon, C. Guilbaud, T. Retailleau, A. Deluzet, B. Domercq, S. Baudron, and S. Perruchas. This paper is dedicated to M. Sergent whose contribution to the chemistry of chalcogenide metal clusters has inspired this work, and discussions with M. Sergent, A. Perrin, and C. Perrin at the early stage of our work at the University of Rennes I are gratefully acknowledged. We are grateful to Prof. Long, University of California, Berkeley, CA, and Prof. Sasaki, Hokkaido University, for kindly providing us with preprints of their work. We thank the Ministère de l'Education Nationale, de la Recherche et de la Technologie, the CNRS, and the Région des Pays-de-Loire for support.

VI. References

(1) Opalovskii, A. A.; Fedorov, V. E.; Lobkov, E. U. *Russ. J. Inorg. Chem.* **1971**, *16*, 790.
(2) Opalovskii, A. A.; Fedorov, V. E.; Lobkov, E. U.; Erenburg, B. G. *Russ. J. Inorg. Chem.* **1971**, *16*, 1685.
(3) Leduc, L.; Perrin, A.; Sergent, M. *C. R. Acad. Sci. Paris, Ser. 2* **1983**, *296*, 961.
(4) Batail, P.; Ouahab, L.; Pénicaud, A.; Lenoir, C.; Perrin, A. *C. R. Acad. Sci. Ser. 2* **1987**, *304*, 1111.
(5) Complementary approaches are currently emerging; see: (a) Sayettat, J.; Bull, L. M.; Gabriel, J.-C. P.; Jobic, S.; Camerel, F.; Marie, A.-M.; Fourmigué, M.; Batail, P.; Brec, R.; Inglebert, R.-L. *Angew. Chem., Int. Ed. Engl.* **1998**, *37*, 1711. (b) Kolesnichenko, V.; Swenson, D. C.; Messerle, L. *Inorg. Chem.* **1998**, *37*, 3257. (b) Kolesnichenko, V.; Messerle, L. *Inorg. Chem.* **1998**, *37*, 3660. (c) Kolesnichenko, V.; Luci, J. J.; Swenson, D. C.; Messerle, L. *J. Am. Chem. Soc.* **1998**, *120*, 13260. See also the seminal ongoing work of Roesky and co-workers on the chemistry on soluble metal fluorides: (d) Walawalkar, M. G.; Roesky, H. W.; Murugavel R. *Acc. Chem. Res.* **1999**, *32*, 117. (e) Yu, P.; Müller, P.; Roesky, H. W.; Noltemeyer, M.; Demsar, A.; Uson, I. *Angew. Chem., Int. Ed. Engl.* **1999**, *38*, 3319.
(6) (a) Bronger, W; Koppe, C; Loevenich, M; Schmitz, D; Schuster, T. *Z. Anorg. Chem. Allg. Chem.* **1997**, *623*, 695. (b) Bronger, W; Koppe, C; Schmitz, D. *Z. Anorg. Chem. Allg. Chem.* **1997**, *623*, 239. (c) Bronger, W.; Loevenich, M.; Schmitz, D. *J. Alloys Compd.* **1994**, *216*, 25. (d) Bronger, W.; Loevenich, M. *J. Alloys Compds.* **1994**, *216*, 29. (e) Bronger, W.; Kanert, M.; Loevenich, M.; Schmitz, D. *Z. Anorg. Chem. Allg. Chem.* **1993,** *619*, 2015. (f) Lutz, H. D.; Muller, B.; Bronger, W.; Loevenich, M. *J. Alloys Compds.* **1993**, *190*, 181. (g) Bronger W.; Schuster, T. *Z. Anorg. Chem. Allg. Chem.* **1990**, *587*, 74. (h) Bronger, W.; Loevenich, M.; Schmitz, D.; Schuster, T. *Z. Anorg. Chem. Allg. Chem.* **1990**, *587*, 91.
(7) Saito, T. *J. Chem. Soc., Dalton Trans.* **1999**, 97.
(8) See also the yearly reviews based on Chemical Abstracts searches, covering most rhenium compounds, with a focus on organometallic ones, and for the period 1991−1996: (a) Vites, J. C.; Lynam, M. *Coord. Chem. Rev.* **1994**, *94*, 127. (b) Vites, J. C.; Lynam, M. *Coord. Chem. Rev.* **1995**, *95*, 1. (c) Vites, J. C.; Lynam, M. *Coord. Chem. Rev.* **1995**, *95*, 207. (d) Vites, J. C.; Lynam, M. *Coord. Chem. Rev.* **1997**, *162*, 3319. (e) Vites, J. C.; Lynam, M. *Coord. Chem. Rev.* **1998**, *169*, 201. (g) Vites, J. C.; Lynam, M. *Coord. Chem. Rev.* **1998**, *172*, 357.
(9) Perrin, A; Sergent, M. *New. J. Chem.* **1988**, *12*, 337.

(10) Iodine trichlorine, ICl_3, which decomposes into ICl and chlorine when heated above 77 °C, was used as an in situ Cl_2 source.
(11) Preliminary structural data: (a) Perrin, A.; Sergent, M. *Bull. Soc. Chim. Fr.* **1980**, *11*−*12*, 66. (b) Leduc, L.; Perrin, A.; Sergent, M. *Bull. Soc. Chim. Fr.* **1981**, *11*−*12*, I-399.
(12) For a full report of the structure, see: Leduc, L.; Perrin, A.; Sergent, M. *Acta Crystallogr.* **1983**, *C59*, 1503.
(13) For the synthesis of $Mo_2Re_4X_8$ (X = S, Se), see: Perrin, A.; Sergent, M.; Fisher, Ø. *Mater. Res. Bull.* **1978**, *13*, 259.
(14) (a) Spangenberg, M.; Brönger, W. *Angew. Chem., Int. Ed. Engl.* **1978**, *17*, 368. (b) Chen, S.; Robinson, W. R. *J. Chem. Soc., Chem. Commun.* **1978**, *20*, 879.
(15) Leduc, L. Ph.D. Thesis, University of Rennes I, Rennes, France, 1983.
(16) Pilet, J.-C.; Le Traon, F.; Le Traon, A.; Perrin, C.; Perrin, A.; Leduc, L.; Sergent, M. *Surf. Sci.* **1985**, *156*, 359.
(17) Schäfer, H.; von Schnering, H. G. *Angew. Chem.* **1964**, *20*, 833.
(18) Leduc, L.; Padiou, J.; Perrin, A.; Sergent, M. *J. Less-Common Met.* **1983**, *95*, 73.
(19) Leduc, L.; Perrin, A.; Sergent, M.; Le Traon, F.; Pilet, J.-C.; Le Traon, A. *Mater. Lett.* **1985**, *3*, 209.
(20) Fedorov, V. E.; Mishchenko, A. V.; Kolesov, B. A.; Gubin, S. P.; Slovokhotov, Yu. L.; Struchkov, Yu. T. *Bull. Acad. Sci. USSR, Chem. Sci.* **1984**, *9*, 1976.
(21) Fedorov, V. E.; Mishchenko, A. V.; Kolesov, B. A.; Gubin, S. P.; Slovokhotov, Yu. L.; Struchkov, Yu. T. *Koord. Khim.* **1985**, *11*, 980.
(22) Gabriel, J.-C. Ph.D. Thesis, University of Paris-Sud, Orsay, France, 1993.
(23) Gabriel, J.-C.; Boubekeur, K.; Batail, P. *Inorg. Chem.* **1993**, *32*, 2894.
(24) Mironov, Y. V.; Cody, J. A.; Ibers, J. A. *Acta Crystallogr.* **1996**, *C52*, 281.
(25) Yarovoi, S. S.; Mironov, Yu. I.; Mironov, Yu. V.; Virovets, A. V.; Fedorov, V. E.; Paek, U−Hyon; Shin, Sung Chul; Seo, Moo-Lyong *Mater. Res. Bull.* **1997**, *32*, 1271.
(26) Mironov, Y. V.; Pell, M. A.; Ibers, J. A. *Inorg. Chem.* **1996**, *35*, 2709.
(27) Müller, A.; Krickemeyer, E.; Bögge, H. *Angew. Chem., Int. Ed. Engl.* **1986**, *25*, 485.
(28) Müller, A.; Krickemeyer, E.; Bögge, H. *Z. Anorg. Allg. Chem.* **1987**, *554*, 61.
(29) Schulz Lang, E.; Abram, U.; Strähle, J. *Z. Anorg. Allg. Chem.* **1996**, *622*, 251.
(30) Mironov, Y. V.; Albrecht-Schmitt, T. E.; Ibers, J. A. *Inorg. Chem.* **1997**, *36*, 944.
(31) Fedin, V. P.; Fedorov, V. E.; Imoto, H.; Saito, T. *Polyhedron* **1997**, *16*, 1615.
(32) For a full report of the structure, see: Perrin, A.; Leduc, L.; Potel, M.; Sergent, M. *Mater. Res. Bull.* **1990**, *25*, 1227.
(33) (a) von Schnering, H. G. *Z. Anorg. Allg. Chem.* **1971**, *385*, 75. (b) Potel, M.; Perrin, C.; Perrin, A.; Sergent, M. *Mater. Res. Bull.* **1986**, *21*, 1239.
(34) Slougui, A.; Perrin, A.; Sergent, M. *Acta Crystallogr.* **1992**, *C48*, 1917.
(35) Lenain, S.; Gabriel, J.-C. P, Batail, P. Unpublished results.
(36) Boubekeur, K. Ph.D. Thesis, University of Rennes I, Rennes, France, 1989.
(37) Uriel, S.; Boubekeur, K.; Gabriel, J.-C.; Batail, P.; Orduna, J. *Bull. Soc. Chim. Fr.* **1996**, *133*, 783.
(38) Healy, P. C.; Kepert, D. L.; Taylor, D.; White, A. H. *J. Chem. Soc., Dalton Trans.* **1973**, *6*, 646.
(39) Fedin, V. P.; Imoto, H.; Saito, T.; Fedorov, V. E.; Mironov, Y. V.; Yarovoi, S. S. *Polyhedron* **1996**, *15*, 1229.
(40) $K_2[Re_6S_6Br_8]$ crystallizes in the cubic system, space group $Pn\bar{3}$ (No. 201), with a = 13.433 Å: Slougui, A.; Ferron, S.; Perrin, A.; Sergent, M. *J. Cluster Sci.* **1997**, *8*, 349.
(41) Perricone, A.; Slougui, A.; Perrin, A. *Solid State Sci.* **1999**, *1*, 657.
(42) Reacting a mixture of Re, $ReCl_5$, S, and $FeCl_3$ yielded solid products that were found soluble in ethanol; cation exchange of the cation with a quaternary ammonium afforded $(Bu_4N)[Re_6S_6Cl_8]$. This therefore indicates that iron-based salts of octahedral rhenium cluster anions could be soluble: Retailleau, T.; Gabriel, J.-C. P.; Boubekeur, K.; Batail, P. Unpublished results.
(43) Guilbaud, C. B.; Boubekeur, K.; Gabriel, J.-C. P.; Batail, P. *C. R. Acad. Sci. Ser. 2c* **1998**, *1*, 765.
(44) (a) Slougui, A.; Perrin, A.; Sergent, M. *J. Solid State Chem.* **1999**, *147*, 358. (b) Yarovoi, S. S.; Mironov, Yu. V.; Solodovnikov, S. F.; Virovets, A. V.; Fedorov, V. E. *Mater. Res. Bull.* **1999**, *34*, 1245.
(45) Long, J. R.; Williamson, A. S.; Holm, R. H. *Angew. Chem., Int. Ed. Engl.* **1995**, *34*, 226.
(46) Long, J. R.; McCarty, L. S.; Holm, R. H. *J. Am. Chem. Soc.* **1996**, *118*, 4603.
(47) Fedin, V. P.; Virovets, A. A.; Sykes, A. G. *Inorg. Chim. Acta* **1998**, *271*, 228.
(48) Perrin, A.; Leduc, L.; Sergent, M. *Eur. J. Solid State Inorg. Chem.* **1991**, *28*, 919.
(49) Yaghi, O. M.; Scott, M. J.; Holm, R. H. *Inorg. Chem.* **1992**, *31*, 4778.
(50) (a) First mention of $M[Mo_6Cl_{13}]$ (M = Ag, Na): see ref 33b. (b) Full description of the structure: Boeschen, S.; Keller, H. L. *Z. Kristallogr.* **1991**, *196*, 159.
(51) Schäfer, H.; von Schnering, H. G.; Tillack, J.; Kuhnen, F.; Wohrle, H.; Baumann, H. *Z. Anorg. Allg. Chem.* **1967**, *353*, 281.
(52) Sheldon, J. C. *J. Chem. Soc.* **1960**, 1007.
(53) Le Nagard, N.; Perrin, A.; Sergent, M.; Levy-Clement, C. *Mater. Res. Bull.* **1985**, *20*, 835.
(54) Hughbanks, T.; Hoffmann, R. *J. Am. Chem. Soc.* **1983**, *105*, 1150.
(55) Fischer, C.; Colell, H.; Tributsch, H. *Surf. Sci. Lett.* **1993**, *280*, L267.
(56) Mironov, Y. V.; Pell, M. A.; Ibers, J. A. *Angew. Chem., Int. Ed. Engl.* **1997**, *35*, 2854.
(57) Pinheiro, C. B.; Speziali, N. L.; Berger, H. *Acta.Crystallogr. C* **1997**, *53*, 1178.
(58) Speziali, N. L.; Berger, H.; Leicht, G.; Sanjinés, R.; Chapuis, G.; Lévy, F. *Mater. Res. Bull.* **1988**, *23*, 1597.
(59) Fisher, C.; Alonso-Vante, N.; Fiechter, S.; Tributsch, H.; Reck, G.; Schultz, W. J. *J. Alloys Compd.* **1992**, *178*, 305.
(60) Fisher, C.; Fiechter, S.; Tributsch, H.; Reck, G.; Schultz, B. *Ber. Bunsen-Ges. Phys. Chem.* **1992**, *96*, 1652.
(61) The general formula encompasses, for $n < l/2$, cationic species which remain to be discovered.
(62) Page 78 of ref 15.
(63) Bronger, W.; Miessen, H.-J.; Müller, P.; Neugroschel, R. *J. Less-Common Met.* **1985**, *105*, 303.
(64) Simon, F.; Boubekeur, K.; Gabriel, J.-C. P.; Batail, P. *J. Chem. Soc., Chem. Commun.* **1998**, 845−846.
(65) Tulsky, E. G.; Long, J. R. *Chem. Mater.* **2001**, *13*, in press.
(66) Typically, high-temperature solid-state syntheses of hexanuclear rhenium chalcohalide clusters are carried out in our laboratory in ca. 0.4 g pellets/sealed batch tube, and several (up to 6) tubes are treated in a single oven cycle. See refs 23 and 37 for detailed procedures.
(67) Ouahab, L.; Batail, P.; Perrin, C.; Garrigou-Lagrange, C. *Mater. Res. Bull.* **1986**, *21*, 1223.
(68) Uriel, S.; Boubekeur, K.; Batail, P.; Orduna, J.; Perrin, A. *New J. Chem.* **2001**, *25*, 737.
(69) Perrin, A. *New. J. Chem.* **1990**, *14*, 561.
(70) Guilbaud, C. B. Ph.D. Thesis, University of Nantes, Nantes, France, 1998.
(71) O'Keeffe, M.; Eddaoudi, M.; Li, H.; Reineke, T.; Yaghi, O. M. *J. Solid State Chem.* **2000**, *153*, 3−20.
(72) Boubekeur, K.; Batail, P. Unpublished results.
(73) Lee, S. C.; Holm, R. H. *Angew. Chem., Int. Ed. Engl.* **1990**, *29*, 840.
(74) Uriel, S.; Boubekeur, K.; Batail, P.; Orduna, J.; Canadell, E. *Inorg. Chem.* **1995**, *34*, 5307.
(75) Uriel, S.; Boubekeur, K.; Batail, P.; Orduna, J. *Angew. Chem., Int. Ed. Engl.* **1996**, *35*, 1544.
(76) Gabriel, J.-C. P.; Boubekeur, K.; Batail, P. Unpublished result.
(77) Guirauden, A.; Johannsen, I.; Batail, P.; Coulon, C. *Inorg. Chem.* **1993**, *32*, 2446 and references therein.
(78) Zheng, Z.; Long, J. R.; Holm, R. H. *J. Am. Chem. Soc.* **1997**, *119*, 2163.
(79) Further studies on similar compounds have concluded that the protonated compounds $[Re^{III}_6Q_7(QH)X_6]^{3-}$ [46,82,80] are in fact the paramagnetic trianion $[Re^{III}_5Re^{IV}Q_8X_6]^{\bullet 3-}$ (Q = chalcogen, X = halogen) as shown for X = Cl and Q = S.[75,89,92,115]
(80) Willer, M. W.; Long, J. R.; McLauchlan, C. C.; Holm, R. H. *Inorg. Chem.* **1998**, *37*, 328.
(81) Wang, R.; Zheng, Z. *J. Am. Chem. Soc.* **1999**, *121*, 3549.
(82) The syntheses of compounds $[Re_6Se_8(py\text{-}R)_6]^{2+}$ (py-R = pyridine or 4-hydroxypyridine) are reported in a footnote of ref 81.
(83) Zheng, Z.; Holm, R. H. *Inorg. Chem.* **1997**, *36*, 5173.
(84) Zheng, Z.; Gray, T. G.; Holm, R. H. *Inorg. Chem.* **1999**, *38*, 4888.
(85) Chen, Z.-N.; Yoshimura, T.; Abe, M.; Sasaki, Y.; Ishizaka, S.; Kim, H.-B.; Kitamura, N. *Angew. Chem., Int. Ed. Engl.* **2001**, *40*, 239.
(86) Selby, H. D.; Zheng, Z.; Gray, T. G.; Holm, R. H. *Inorg. Chim. Acta* **2001**, *312*, 205.
(87) Yoshimura, T.; Ishizaka, S; Umakoshi, K.; Sasaki, Y; Kim, H.-B.; Kitamura, N. *Chem. Lett.* **1999**, 697.
(88) Yoshimura, T.; Umakoshi, K.; Sasaki, Y.; Sykes, A. G. *Inorg. Chem.* **1999**, *38*, 5557.
(89) Decker, A.; Simon, F.; Boubekeur, K.; Fenske, D.; Batail, P. *Z. Anorg. Allg. Chem.* **2000**, *626* (1), 309.
(90) Alternatively, and as pointed out by a reviewer, it could equally be argued that the higher positive charge of the oxidized cluster cores in $[Re_6Q_8]^{3+}$ leads to stronger bonding interactions with the anionic outer halides, rendering them less labile; besides, the monoanionic halide atoms in the inner core might be more readily replaced by dianionic chalcogenide atoms when the cluster core positive charge increases in the series, $[Re_6Q_8]^{2+}$ to $[Re_6Q_7X]^{3+}$ to $[Re_6Q_6X_2]^{4+}$ and $[Re_6Q_5X_3]^{5+}$. Both arguments are in favor of an increased susceptibility to μ-halide exchange for the reduced cluster cores. There is, however, a lack of experi-

mental evidence for the latter mechanism at the present stage of development of the chemistry.
(91) Pauling L. *The Nature of the Chemical Bond*, 3rd ed.; Cornell University Press: Ithaca, NY, 1960; pp 400, 403. $d_1 = 2.750 + 0.6 \log(7/12) = 2.609$ Å.
(92) Allmann, R. *Monatsh. Chem.* **1975**, *106*, 779. Donnay, G.; Donnay, J. H. *Acta Crystallogr.* **1973**, *B29*, 1417.
(93) (a) Ebihara, M.; Toriumi, K.; Saito, K. *Inorg. Chem.* **1988**, *27*, 13. (b) Ebihara, M.; Toriumi, K.; Sasaki, Y.; Saito, K. *Gazz. Chim. Ital.* **1995**, *125*, 87. See also for $[Mo_6Cl_{13}Q]^{3-}$ (Q = S, Te): (c) Michel, J. B.; McCarley, R. E. *Inorg. Chem.* **1982**, *21*, 1864. (d) Ebihara, M.; Imai, T.; Kawamura, T. *Acta Crystallogr., Sect. C* **1995**, *51*, 1743.
(94) Ebihara, M.; Isobe, K.; Sasaki, Y.; Saito, K. *Inorg. Chem.* **1992**, *31*, 1644.
(95) Geometrical disorder arises from the random distribution in the packing within the crystal of all different geometric isomers. Orientational disorder arises from random orientation of only one geometric isomer.
(96) Fedorov, V. E.; Podberezskaya, N. V.; Mischenko, A. V.; Khudorozko, G. F.; Asanov, I. P. *Mater. Res. Bull.* **1986**, *21*, 1335.
(97) Mironov, Y. V.; Virovets, A. V.; Fedorov, V. E.; Podberezskaya, N. V. *Polyhedron* **1995**, *14*, 3171.
(98) Development of this reaction[97] results in a series of tetraanions formulated as the following. (a) $(KCs_3)\{[Re_6S_8^i](CN)_6^a\}$: Slougui, A; Mironov, Y. V.; Perrin, A.; Fedorov, V. E. *Croat. Chem. Acta* **1995**, *68*, 885. (b) $(NMe_4)_4\{[Re_6(Te_{8-n}Se_n)^i](CN)_6^a\}$: Mironov, Y. V.; Cody, J. A.; Albrecht-Schmitt, T. E.; Ibers, J. A. *J. Am. Chem. Soc.* **1997**, *119*, 493.
(99) Naumov, N. G.; Virovets, A. V.; Podberezskaya, N. V.; Fedorov, V. E. *Zh. Strukt. Khim.* **1997**, *38*, 1020.
(100) Beauvais, L. G.; Shores, M. P.; Long, J. R. *Chem. Mater.* **1998**, *10*, 3783.
(101) Mironov, Y. V.; Fedorov, V. E.; McLauchlan, C. C.; Ibers, J. A. *Inorg. Chem.* **2000**, *39*, 1809.
(102) Naumov, N. G.; Virovets, A. V.; Sokolov, N. S.; Artemkina, S. B.; Fedorov, V. E. *Angew. Chem., Int. Ed. Engl.* **1998**, *37*, 1943.
(103) Naumov, N. G.; Artemkina, S. B.; Virovets, A. V.; Fedorov, V. E. *J. Solid State Chem.* **2000**, *153*, 195.
(104) This compound contains accessible cubelike cavities: Shores, M. P.; Beauvais, L. G.; Long, J. R. *Inorg. Chem.* **1999**, *38*, 1648.
(105) Shores, M. P.; Beauvais, L. G.; Long, J. R. *J. Am. Chem. Soc.* **1999**, *121*, 775.
(106) Bennett, M. V.; Shores, M. P.; Beauvais, L. G.; Long, J. R. *J. Am. Chem. Soc.* **2000**, *122*, 6664.
(107) Beauvais, L. G.; Shores, M. P.; Long, J. R. *J. Am. Chem. Soc.* **2000**, *122*, 2763.
(108) A review of the principles of the electrocrystallization technique and its application to the synthesis of electroactive molecular solids is to be found in the following: Batail, P.; Boubekeur, K.; Fourmigué, M.; Gabriel, J.-C. P. *Chem. Mater.* **1998**, *10*, 3005.
(109) Yoshimura, T.; Ishizaka, S.; Sasaki, Y.; Kim, H.-B.; Kitamura, N.; Naumov, N. G.; Sokolov, M. N.; Fedorov, V. E. *Chem. Lett.* **1999**, 1121.
(110) In original articles,[88,109] $E_{1/2}$ values were given vs Ag/AgCl.
(111) Yoshimura, T.; Umakoshi, K.; Sasaki, Y.; Ishizaka; S.; Kim, H.-B.; Kitamura, N. *Inorg. Chem.* **2000**, *39*, 1765.
(112) Guilbaud, C.; Deluzet, A.; Domercq, B.; Molinié, P.; Coulon, C.; Boubekeur, K.; Batail, P. *Chem. Commun.* **1999**, 1867.
(113) Gray, T. G.; Rudzinski, C. M.; Nocera, D. G.; Holm, R. H. *Inorg. Chem.* **1999**, *38*, 5932.
(114) It should be noted that $(Bu_4N)_4[Re_6S_8Cl_6]$ has one single luminescence only shown in Figure 21 and as observed by others (Table 10); the band B reported in Figure 3a of ref 115 proved to correspond to the luminescence of $(Bu_4N)_3[Re_6S_8Cl_6]$ generated in-situ upon UV irradiation of the $(Bu_4N)_4[Re_6S_8Cl_6]$ acetonitrile solution in the presence of oxygen: Deluzet, A.; Pansu, R.; Batail, P. Unpublished materials. Also, in Figure 3 of ref 115, the band at 796 nm upon excitation at 393 nm is an experimental artifact.
(115) Arratia-Pérez, R.; Hernández-Acevedo, L. *J. Chem. Phys.* **1999**, *110*, 2529.
(116) Arratia-Pérez, R.; Hernández-Acevedo, L. *J. Chem. Phys.* **1999**, *111*, 168.
(117) (a) Johnston, D. H.; Gaswick, D. C.; Lonergan, M. C.; Stern, C. L.; Shriver, D. F. *Inorg. Chem.* **1992**, *31*, 1869. (b) Holadi, H. A.; Hung, H.; Shriver, D. F. *Inorg. Chim. Acta* **1992**, *198−200*, 245.
(118) See ref 52 and refs 13 and 14 therein.
(119) Certain, D.; Lissillour, R. *Z. Phys. D* **1986**, *3*, 411.
(120) Batail, P.; Boubekeur, K.; Fourmigué, M.; Dolbecq, A.; Gabriel, J.-C.; Guirauden, A.; Livage, C.; Uriel, S. *New J. Chem.* **1994**, *18*, 999.
(121) (a) Batail, P.; Livage, C.; Parkin, S. S. P.; Coulon, C.; Martin, J. D.; Canadell, E. *Angew. Chem., Int. Ed. Engl.* **1991**, *30*, 1498. (b) Coulon, C.; Livage, C.; Gonzalvez, L.; Boubekeur, K.; Batail, P. *J. Phys. I (Paris)* **1993**, *3*, 1153.
(122) (a) Pénicaud, A.; Boubekeur, K.; Batail, P.; Canadell, E.; Auban-Senzier, P.; Jérome, D. *J. Am. Chem. Soc.* **1993**, *115*, 4101. (b) Canadell, E. *Chem. Mater.* **1998**, *10*, 2770.
(123) Deluzet, A. Ph.D. Thesis, University of Nantes, Nantes, France, 2000.
(124) Deluzet, A.; Guilbaud, C.; Boubekeur, K.; Batail, P.; Auban-Senzier, P.; Jérôme, D. Submitted for publication.
(125) Pénicaud, A.; Lenoir, C.; Batail, P.; Coulon, C.; Perrin, A. *Synth. Met.* **1989**, *32*, 25.
(126) Dolbecq, A.; Boubekeur, K.; Batail, P.; Canadell, E.; Auban-Senzier, P.; Coulon, C.; Lerstrup, K.; Bechgaard, K. *J. Mater. Chem.* **1995**, *5*, 1707.
(127) Deluzet, A.; Batail, P.; Misaki, Y.; Auban-Senzier, P.; Canadell, E. *Adv. Mater.* **2000**, *12*, 436.
(128) Perruchas, S.; Deluzet, A.; Boubekeur, K.; Batail, P.; Misaki, Y.; Canadell, E.; Auban-Senzier, P.; Jérôme, D. Unpublished results.
(129) Mussell, R. D.; Nocera, D. G. *Inorg. Chem.* **1990**, *29*, 3711.
(130) Ebihara, M.; Kawamura, T.; Isobe, K.; Saito, K. *Bull. Chem. Soc. Jpn.* **1994**, *67*, 3119.
(131) Saito, T.; Yamamoto, N.; Nagase, T.; Tsuboi, T.; Kobayashi, K.; Yamagata, T.; Imoto, H.; Unoura, K. *Inorg. Chem.* **1990**, *29*, 764.
(132) Maverick, A. W.; Gray, H. B. *J. Am. Chem. Soc.* **1981**, *103*, 1298.
(133) Maverick, A. W.; Najdzionek, J. S.; MacKenzie, D.; Nocera, D. G.; Gray, H. B. *J. Am. Chem. Soc.* **1983**, *105*, 1878.
(134) Jackson, J. A.; Turro, C.; Newsham, M. D.; Nocera, D. G. *J. Phys. Chem.* **1990**, *94*, 4500.
(135) Zietlow, T. C.; Nocera, D. G.; Gray, H. B. *Inorg. Chem.* **1986**, *25*, 1351.
(136) Renault, A.; Pouget, J.-P.; Parkin, S. S. P.; Torrance, J. B.; Ouahab, L.; Batail, P. *MCLC S&T, Sect. B: Nonlinear Opt.* **1988**, *161*, 329.
(137) Boubekeur, K.; Lenoir, C.; Batail, P.; Carlier, R.; Tallec, A.; Le Paillard, M.-P.; Lorcy, D.; Robert, A. *Angew. Chem., Int. Ed. Engl.* **1994**, *33*, 1379.
(138) Gabriel, J.-C.; Johannsen, I.; Batail, P.; Coulon C. *Acta. Crystallogr. C* **1993**, *49*, 1052.
(139) Dolbecq, A.; Boubekeur, K.; Batail, P.; Canadell, E.; Auban-Senzier, P.; Coulon, C.; Lerstrup, K.; Bechgaard, K. *J. Mater. Chem.* **1995**, *5*, 1707.
(140) Renault, A.; Talham, D.; Canceill, J.; Batail, P.; Collet, A.; Lajzerowicz, J. *Angew. Chem., Int. Ed. Engl.* **1989**, *28*, 1249.

CR980058K

B. Travaux sur les cristaux liquides à cœur minéral

Mes activités de recherche dans ce domaine ont débutées lors de mon travail de thèse avec la démonstration des propriétés mésogènes de $Li_2Mo_6Se_6$. Ma collaboration avec Patrick Davidson à continuer à UCSB avec la démonstration de la nature mésogène des argiles de la famille des smectites. Il est à noter que l'article publié à J. Phys. Chem. A reçu à ce jour plus d'une centaine de citations. Il remet notamment en cause le modèle du château de carte qui prévalait jusqu'alors et qui est présent dans la plupart des livres dédiés aux argiles. Ce travail à éveillé l'attention de la communauté des géologues, d'où l'invitation que j'ai reçu de la part de la société américaine des argiles pour l'organisation d'une session dédiée à la structure des gels à base d'argiles smectites. J'ai poursuivi mes travaux sur les cristaux liquides minéraux à l'IMN. J'y ai notamment démontré la nature smectique de matériaux lamellaires. Cette phase smectique est la première répertoriée dans laquelle les plans smectiques sont formés de plans covalents. Ces travaux ont fait l'objet d'une publication dans la revue Nature. L'ensemble de mes activités dans ce domaine sont résumées dans l'article de revue invité, publié dans la revue Topics in Current Chemistry, qui suit.

Top Curr Chem (2003) 226: 119 – 172
DOI 10.1007/b 10827

Mineral Liquid Crystals from Self-Assembly of Anisotropic Nanosystems

Jean-Christophe P. Gabriel[1], Patrick Davidson[2]

[1] Nanomix, Inc., 5980 Horton Street, Suite 600, Emeryville, CA 94608, USA
E-mail: jcgabriel@nano.com
[2] Laboratoire de Physique des Solides, Bât. 510, UMR 8502 CNRS, Université d'Orsay, 91405 Orsay, France, *E-mail: davidson@lps.u-psud.fr*

In this article we review the mesogenic properties of the mineral liquid crystals (MLCs) based on molecular nanowires: $Li_2Mo_6Se_6$; nanotubes: Imogolite and $NaNb_2PS_{10}$; molecular ribbons: V_2O_5; exfoliated single sheets: smectic clays and $H_3Sb_3P_2O_{14}$; nanorods: Boehmite (γ-AlOOH), Akaganeite (β-FeOOH), Goethite (α-FeOOH); platelets: Gibbsite ($Al(OH)_3$); disks: $Ni(OH)_2$; bio-mineral hybrids. We then propose numerous phases that could lead to the discovery of new MLCs. We finally review how the properties of these mesophases and their collective behavior have been used for making mesoporous composites with anisotropic properties, for making nanodevices and solar cells, as well as how they could be used to allow the measurement of residual dipolar couplings in NMR studies of biomolecules.

Keywords. Liquid crystals, Complex Fluids, Self-assembly, Mineral, Inorganic, Nanosystem, Nanoparticle, Nanotube, Nanowire, Nanorod, Anisotropy, NMR

List of Abbreviations

AAO	Anodic Aluminum oxide
AOT	(2-Ethylhexyl)sulfosuccinate
CNT	Carbon nanotube
CVD	Chemical vapor deposition
DLVO	Deryagin Landau Verwey Overbeek
DMF	Dimethylformamide
DMSO	Dimethylsulfoxide
FFEM	Freeze fracture electron microscopy
FWHM	Full width at half maximum
HFCVD	Hot filament chemical vapor deposition
HPC	Hydroxypropylcellulose
HT	High temperature
MLC	Mineral liquid crystals
NMF	*N*-Methylformamide
NR	Nanorod
NT	Nanotube
NW	Nanowire
PBLG	Poly(γ-benzyl-L-glutamate)
PDMS	Poly(dimethylsiloxane)
PVA	Poly(vinylalcohol)
SANS	Small Angle Neutron Scattering
SAXS	Small angle X-ray scattering
TEM	Transmission electron microscopy

TMV Tobacco Mosaic Virus
USAXS Ultra small angle X-ray scattering

1 Introduction

Liquid crystalline phases, which were discovered more than a century ago, are phases intermediate between crystalline and liquid ones [1]. They combine both the fluidity of the liquids and the anisotropy of crystals and they are usually based on anisotropic building blocks (molecules, polymers, micelles, aggregates etc...). Liquid crystalline materials are extremely diverse since they range from DNA to Kevlar (a high strength synthetic polymer) and from small organic molecules used in displays to self assembling amphiphilic soap molecules. A common feature of all these materials is that they are organic [2] or organometallic – ca. inorganic – and currently there are more than 80,000 examples of organic liquid crystalline compounds [3]. In contrast, there are only a dozen lyotropic mineral liquid crystals known and characterized to date [4]. One reason is that there are only a few low-dimensional (one-dimensional or two-dimensional) purely-inorganic objects known to dissolve or to be dispersed in water or in other organic solvents. The solubility criteria of mineral moieties, their interactions with solvents, and the structures and physical properties of such fluids are currently a subject of intense research activity [4, 5]. In addition, organic synthesis techniques allow numerous structural variations of liquid crystalline molecules to be made whereas the solution chemistry of molecular mineral objects, i.e., prepared by high temperatures solid state reactions, is still being developed [6].

Concerning the use of the term "mineral" to name this family of liquid crystals, one can argue that the term inorganic would be more appropriate. However, inorganic liquid crystals have long been used for organometallic liquid crystals [7]. Therefore in order to avoid any confusion between these fairly chemically different families, and taking into account that a large number of these liquid crystals occur naturally in nature, we think that the use of the old fashioned but adequate "mineral" adjective taken sensus largo is more specific that an alternative such as "purely inorganic", to name this subclass of the inorganic liquid crystals family.

In spite of their scarcity, lyotropic mineral liquid crystals have actually been known for many decades: Zocher, a German scientist, reported as early as 1925 the observation of the unusual behavior of colloidal aqueous suspensions of vanadium pentoxide (V_2O_5) [8]. He compared these suspensions with the newly discovered liquid crystalline phases and inferred that these colloids must be constituted from needle-like objects mutually oriented in the same direction. We know now that this behavior in fact arises from V_2O_5 ribbons forming a nematic phase. Later, in 1938, Langmuir examined suspensions of bentonite clay platelets and recognized their anisotropic and fluid-like properties [9]. However, the key theoretical development came with the theory that Onsager devised to describe the nematic ordering of suspensions of rod-like particles such as the Tobacco Mosaic Virus (TMV) [10]. This model provides an extremely useful frame to un-

derstand and predict this kind of phase transition in mineral and organic systems. This model which is based on simple assumptions describes in quantitative terms the phase diagram for any suspension of anisotropic rod-like (or disk-like) particles interacting solely through a hard-core potential and predicts that it should undergo a nematic/isotropic first-order transition (i.e., with phase coexistence) and that temperature has no effect on this transition. Numerical simulations have also proved to be very powerful techniques to gain insight into such phenomena [11].

From the experimental point of view, a simple way to identify a liquid crystalline phase is to observe its texture using polarized light microscopy. Unlike usual isotropic liquids, liquid crystalline phases are birefringent, interact with linearly polarized light, and can be observed between crossed polarizers. The detection of birefringence when the fluid phase is at rest proves that it is liquid crystalline. The textures observed under polarized light are due to the existence of topological defects and their analysis gives information on the symmetry of the phase. For instance, the most common defects of the nematic phase are called disclination lines. These are one-dimensional singularities in the local average direction (director) of the anisotropic moieties. Thus, unless special caution is taken to remove these defects, nematic samples are usually "powders" (i.e., random distributions) of small nematic domains (a "nematic domain" is defined as a region of the sample which shows ideal nematic orientational correlation).

Nematic phases can often be aligned by the action of a magnetic field. The alignment is due to the anisotropy of the mesophase that reorients to minimize its free energy in the field. Therefore, the director is aligned along or perpendicular to the field direction, depending on the sign of the magnetic anisotropy of the building blocks. The alignment of the phase in an external field suppresses the topological defects and produces a single domain that is suitable for more detailed physical studies. Electric fields produce similar effects: this is the basis of most applications of nematic phases in display technology.

Small angle X-ray scattering (SAXS) is a powerful technique [12] to study the molecular organization of lyotropic nematic phases on a length scale ranging from 3 to 300 nm. In this range, the detailed atomic structure of the particles is irrelevant and the scattering is sensitive to only the particle shape and its electronic contrast with the solvent. In this respect mineral liquid crystals are particularly convenient because their contrast is usually much larger than that of their organic counterparts. SAXS also allows a clear-cut demonstration of the symmetry and structure of a complex fluid, avoiding possible and usual pitfalls that can come when one restricts itself to only a texture analysis.

In contrast to organic liquid crystals, mineral liquid crystals can differ largely in size from one system to another. They actually range from molecular nanowires or nanotubes to anisotropic crystallites such as nanorods. Molecular nanowires can be considered as one-dimensional objects where the diameter is precisely defined by the molecular unit that makes up the chain (typically 5–25 Å). In contrast, molecular disks (nanosheets) are two-dimensional objects where the thickness of the disks is defined at the molecular scale but the diameter is polydisperse (100–10,000 Å). Finally, liquid crystalline suspensions may

be formed from anisotropic crystallites whose dimensions are all in the colloidal range (100–10,000 Å) so that these moieties are two to three orders of magnitude larger than usual organic liquid crystals. This classification defines the outline of this review article.

2 Molecular Nanowires

2.1 Dispersion of a Conducting Nanowire: $Li_2Mo_6Se_6$

Among all the phases that have been discovered after the report of high critical field superconductivity within the Chevrel-Sergent phases (MMo_6X_8–M=Cu, Pb, Sn, etc.; X=S, Se, Te), $Li_2Mo_6Se_6$ is singular since it contains $^1_\infty[Mo_6Se_6]^{2-}$ infinite conducting molecular nanowires [13, 14] and, it has been demonstrated to be soluble in highly polar solvents such as *N*-methylformamide (NMF) or dimethylsulfoxide (DMSO) [15][1]. It is this last property that prompted us to investigate such solutions and therefore led us to study mineral liquid crystals. The infinite mineral polymer $^1_\infty[Mo_6Se_6]^{2-}$ (Fig. 1d) can be regarded as a stack of dimerized $Mo_3Se_3^-$ units (Fig. 1a), and therefore is the end member (n=∞) of the $(Mo_3Y_3^-)_nY_2$ series (Y=chalcogen) (Fig. 1b, c). The study of static solutions of $Li_2Mo_6Se_6$ in NMF ($c>10^{-2}$ mol l^{-1}) with an optical microscope under polarized light (crossed polarizers) has demonstrated their birefringent and thus anisotropic nature. Both threaded and Schlieren textures were revealed [16], which are textures usually observed in the case of organic nematic phases and prove the mesogenic nature of these solutions.

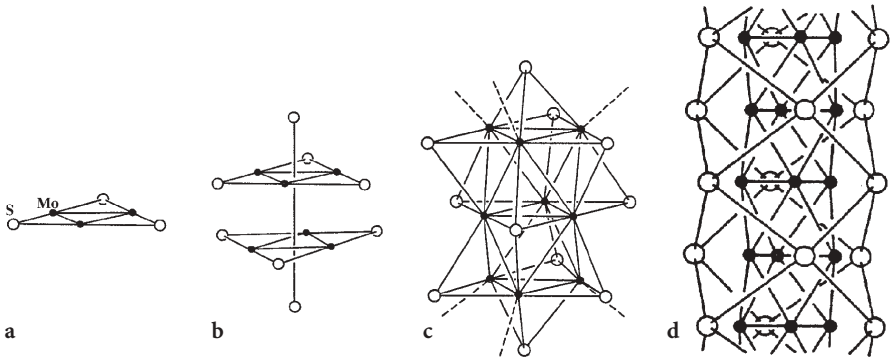

Fig. 1a–d. $Li_2Mo_6Se_6$ can be seen as the end member of the family $(Mo_3Se_3^-)_nSe_2$ made from the alternating stacking of $Mo_3Se_3^-$ motifs with an extra chalcogen capping each extremity: **a** n=1; **b** n=2; **c** n=4; **d** n=∞

[1] Note that $^1_\infty[Mo_6Se_6]^{2-}$ solutions are not stable for more than a few hours when in contact with dioxygen because of the decomposition of the chains. However, they can be kept for months and even years if kept or sealed under an inert atmosphere.

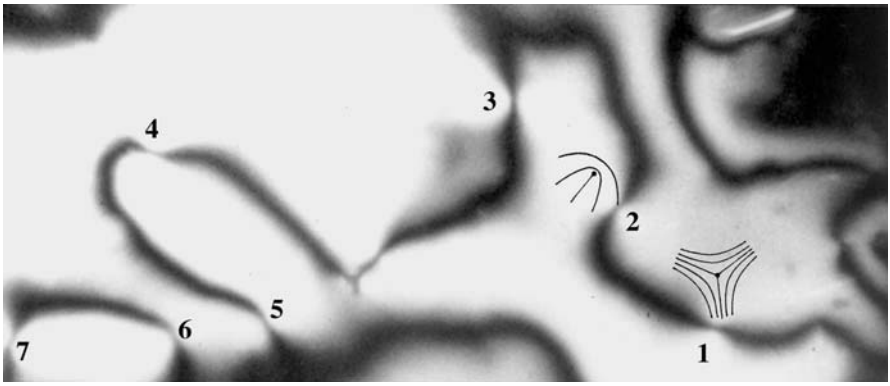

Fig. 2. Photograph of a typical Schlieren texture obtained from a 10^{-1} mol l^{-1} solution of $Li_2Mo_6Se_6$ in *N*-methylformamide in the nematic phase taken using an optical microscopy with crossed polarizers with a magnification of 1000x. (Reprinted from [4b], copyright (2000) from John Wiley and Sons)

For example, Fig. 2 shows a Schlieren texture, which is typical of nematic distortions of the director field (visible as dark branches usually named *brushes*). These distortions are induced by the perpendicular anchoring on the microscope slide of topological defects, called disclination lines, which are numbered from 1 to 7 in Fig. 2. These disclination lines can be classified into two groups according to their local topology as the dark brushes seen around these defects can rotate either clockwise or counterclockwise as the crossed polarizers are rotated simultaneously while the sample is kept fixed. This is due to the two different possible defect topologies illustrated in Fig. 2 for cases 1 and 2 [1].

The structure of these fluids was investigated by X-ray diffraction. When the chains are fully exfoliated the full width at half maximum (FWHM) of the (002) peak characteristic of the distance separating two $Mo_3Se_3^-$ moieties along the chain is of the same order as the experimental resolution; hence the coherence length of the chains is at least 1000 Å [17].

The anisotropic X-ray scattering pattern shows that there is no long-range three-dimensional positional order, demonstrating that this fluid is of a nematic liquid-crystalline nature (Fig. 3a). Moreover, the observation of an interference peak in Fig. 3b proves the existence of short-range positional correlations at ~70 Å, due to the separation of the chains, and probably arising from their repulsive electrostatic interactions. Indeed, charged particles confined in a finite volume at thermodynamic equilibrium repel each other and therefore stay at a well defined distance. Note that the diffuse ring of Fig. 3b appears anisotropic, indicating partial orientation of the chains along the capillary axis.

In addition to nematic ordering observed for the system $Li_2Mo_6Se_6$/solvent, the monodispersity in diameter of the wires should allow one to observe a nematic-hexagonal transition at high concentration. Note that, when the proper solvent is used (in order to avoid formation of bundles), one can expect to be able to tune the distance between the wires just by changing the concentration.

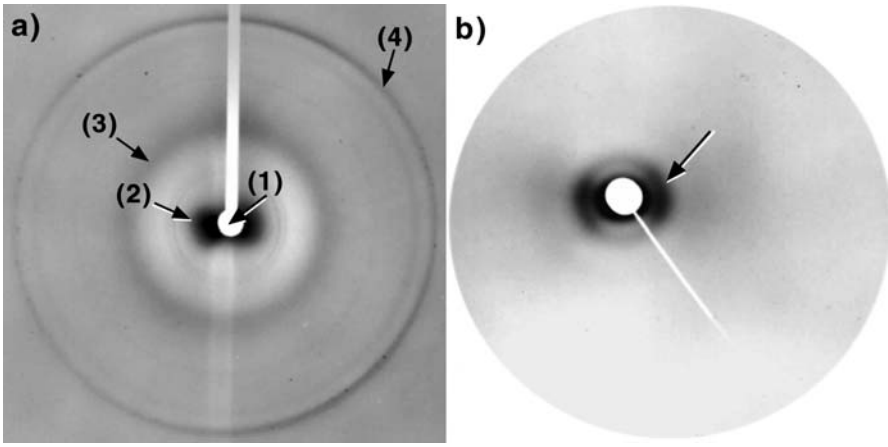

Fig. 3a,b. X-ray diffraction patterns obtained from a capillary filled with 10^{-1} mol l^{-1} solution of $Li_2Mo_6Se_6$/NMF: **a** using wide angle scattering. (**1** is the beam stop shadow, **2** the small angle scattering, **3** the diffuse scattering ring due to the solvent, **4** the 002 diffraction peak); **b** small angle scattering showing the presence of a diffuse ring at $q=9\cdot10^{-2}=2\pi/70$ $Å^{-1}$ (*arrow*)

This is indeed a typical behavior for dispersion of 1-D nanostructures (2-D swelling).

More recently, the molecular nanowire $Mo_6Se_6^{2-}$ has become a fairly popular subject of investigation due to the rise of nanotechnology [18] and the scarcity of well-defined molecular wires available that can be dispersed in solution. In one such study, $Mo_6Se_6^{2-}$ nanowires were dispersed and recondensed using a surfactant. Dense phases were obtained with lamellar or hexagonal ordering of the wires, depending upon the surfactant used. Furthermore, the distance between the $Mo_6Se_6^{2-}$ wires in these condensates could be adjusted by varying the number of carbon atoms in the aliphatic chain of the surfactant [19]. In a similar dispersion-recondensation study, P. Yang and co-workers used the self-assembly properties of $Li_2Mo_6Se_6$-solvent to perform a cation exchange of the Li with more bulky cations such as Na^+, K^+, Rb^+, Cs^+, NMe_4^+. This was performed by retaining the lithium cation in solution using 12-crown-4 ether [20].

Other studies focused on the electrical properties of discrete nanowires in a similar way that has been done with nanotubes. However the lack of stability of this phase when in contact with oxygen makes these studies experimentally difficult [21].

The example of $Li_2Mo_6Se_6$ illustrates one synthetic method towards low dimensional mineral compounds, commonly referred to as the "shake and bake" method. It usually implies the mixing of the starting materials followed by a high temperature treatment. Then, in order to obtain a liquid crystal, one needs to bring these charged low-dimensional mineral anions into solution. Thus, how can one control, within a given ternary or quaternary system, the dimensionality of the synthesized polymeric compounds? This problem has been addressed in the literature and an answer, based upon the 8-N electron rule, can be found

when using alkali metals (or other strong electropositive metals) as cations [22, 23]. Transferring electrons from the alkali metal to a 3-D polymeric covalent framework usually results in some of the covalent bonds being replaced by negative charges, hence the dimensionality of the framework is reduced, producing covalent negatively charged fragments, separated by alkali cations. By increasing the alkali metal content, further dismantling of the framework structure can be induced to the point where the residual framework is of molecular dimensions. This method is most efficient when large alkali metals such as cesium are used, because increasing the separation between the low dimension anionic moieties minimizes their electrostatic repulsion. A consequence of this is that a synthesis successful with cesium may not necessarily work with lithium (for example, the synthesis of $Li_2Mo_6Se_6$ differs from the one of $In_2Mo_6Se_6$ in the fact that it cannot be achieved directly at high temperature from the native element but required a two step synthesis, including an ion exchange procedure). This can be a problem in order to get soluble phases since it is empirically observed that in an alkali series of a given anion the highest solubility is obtained with the smallest cation [24]. Thus, a delicate balance needs to be found in order to synthesize new soluble low dimensional phases and, when the targeted phase cannot be directly synthesized with the smallest cation, a cation exchange additional step should be applied. This can either be tried in the solid state by a clever use of the different sublimation temperature to induce the cation exchange, or indirectly in solution by using high concentration of the replacing cation. In the latter case, it should be noted that the smallest cation that can be used is in fact H^+, for phases that can handle acidic conditions.

2.2
Imogolite: A Natural Nanotube, Aqueous Synthesis, and Composite Materials

Imogolite is a natural hydrated aluminum silicate first discovered in 1962 in the clay fraction of Japanese volcanic ash and it is found widely distributed in recent volcanic deposits. Since 1977, it is possible to synthesize it in the laboratory from dilute aqueous solutions of hydroxyaluminum cations and orthosilicic acid [25] or, by reaction of tetraethylorthosilicate with an aluminum source (aluminum chloride or aluminum *sec*-butoxide) [26, 27], at temperatures ranging from 25 to 100 °C.

This compound is made up of hollow rigid molecular tubes of diameter 25 Å and of variable length (Fig. 4). These can be dispersed in acidified water solutions [28]. A Japanese group has demonstrated that, in a specific range of concentrations, these suspensions phase separate into an isotropic liquid phase and a birefringent one [29]. Temperature has no influence on this phase transition. Fingerprint textures have been observed under polarized light, which, though highly reminiscent of cholesteric (i.e., chiral nematic) textures, have finally been attributed to the existence of a pleated structure on the basis of electron microscopy investigations of freeze-dried samples [30]. These studies show that the pleated sheets consist of a nematic organization of imogolite tubes. This prompts a comparison with the precholesteric states of DNA or collagen [31]. The phase transition could be explained on the basis of the Onsager

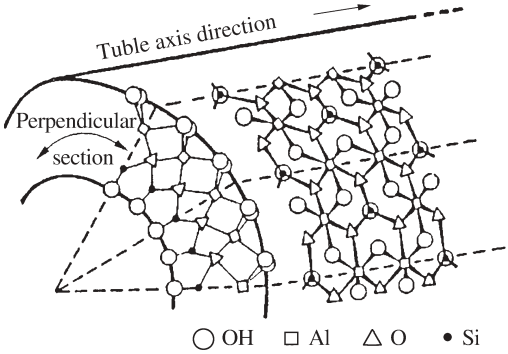

Fig. 4. Schematic view of part of an imogolite cylinder formed from twelve gibbsite structural type units, each corresponding to $(Al_2O_3 \cdot SiO_2 \cdot 2H_2O_2)_2$) and indicated by *dotted lines* (Reprinted from [29a], copyright (1986) from John Wiley and Sons)

model and the specific effects of polydispersity of the tube length were studied in detail.

The same group has also obtained composite materials based on imogolite and water-soluble polymers such as hydroxypropylcellulose (HPC) and poly (vinylalcohol) (PVA) [32]. HPC is a rigid rod polymer that has a cholesteric phase, whereas PVA is a random coil amorphous polymer. Significantly enhanced mechanical properties were only obtained in the case of the HPC composite materials.

2.3
Solvent Dependent Coiling of a Chain into a Nanotube: $NaNb_2PS_{10}$

In a recent search for other soluble mineral polymers, we discovered that KNb_2PS_{10} was soluble in hot DMSO. Our attention was drawn to this structure because we suspected the $^1_\infty[Nb_2PS_{10}]^-$ chain to be of intermediate rigidity between the rigid $Mo_6Se_6^{2-}$ molecular nanowire and the highly flexible $KPdPS_4$. The latter was shown to be highly flexible and behaving very similarly to organic flexible polymers [6]. In order to increase the solubility of KNb_2PS_{10} we synthesized its sodium equivalent $NaNb_2PS_{10}$ which, as expected, proved to be much more soluble in polar solvents. When observed under polarized light between crossed polarizers, concentrated solutions in NMF show strong flow birefringence. Such flow birefringence can arise either from a preferred orientation of anisotropic rigid molecules induced by the flow (like logs aligned with the flow in a river), or from stretching of entangled, folded, semi-flexible polymers (like drawn spaghetti).

SAXS investigation of the structure of these fluids showed a complex structure with two distinct features. The first signal demonstrated that upon dilution a 2-D swelling occurred, typical of suspensions of one-dimensional moieties. The second signal however was independent of the dilution and could not be explained by the chain structure; it is therefore the signature of a superstructure.

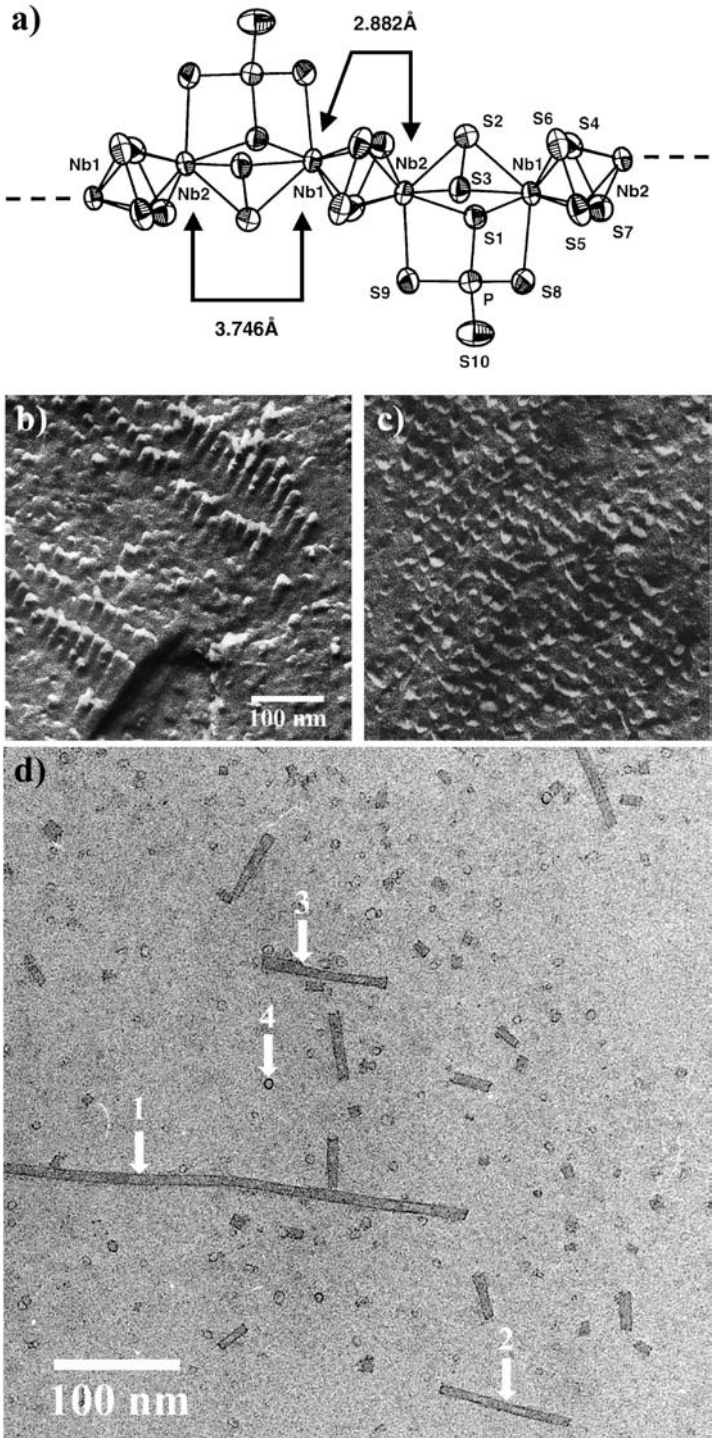
a)
2.882Å
Nb1
Nb2
Nb1
Nb2
S2
S6
S4
Nb1
Nb2
S3
S1
S5
S7
S9
P
S8
S10
3.746Å
b)
100 nm
c)
d)
3
4
1
2
100 nm

Furthermore, at higher concentration, thin diffraction lines were superimposed on the previously described signals, indicating that a first order transition toward a columnar mesophase (H) of hexagonal symmetry occurred. Partial alignment and even the melting (above 240 s^{-1}) of this hexagonal MLC could be obtained using a Couette shear cell. Such a melting had only been reported once prior to this study in the case of a hexagonal mesophase of a surfactant [33].

These results put together provide strong support for the presence in solution of cylinders having a well-defined diameter. However, a difference of behavior depending upon the solvent used was observed. If now DMF was used as the solvent, only the signature of 0-D moieties was detected. In addition no transition towards a hexagonal phase could be found.

To understand further and confirm our interpretation of the SAXS data, we complemented these results with a study using freeze fracture electron microscopy (FFEM) as well as low dose TEM (Fig. 5). This allowed us to show that in NMF $NaNb_2PS_{10}$ folds into single walled nanotubules having wall thickness of 1.6 nm (Fig. 5), whereas only globular coils can be observed in DMF. Furthermore, at high concentration in NMF these nanotubules tend to aggregate into bundles packed in a well-defined hexagonal arrangement [34].

A question still remains about the structure of the polymer within the walls of these nanotubules. The very low stability of theses tubes under TEM irradiation, even when applying low doses, precluded us so far from observing high-resolution images. An electron diffraction pattern highly reminiscent of a helicoidal organization of the polymer was observed but this still needs to be confirmed and studied in more detail.

3
Molecular Ribbons: V_2O_5, a MLC that Can be Readily Aligned in Both Magnetic and Electric Fields

Another way of obtaining suspensions of anisotropic mineral moieties is by the spontaneous condensation of dissolved molecular species. A typical example of this process is the synthesis of V_2O_5 ribbons by using "chimie douce" (soft chemistry) techniques (Fig. 6) [35, 36]. At pH≈2, V(V) species exist in an octahedral coordination with a V=O bond pointing along the Oz axis, three V-OH bonds in the xOy plane, and two bonded H_2O molecules to fill the coordination sphere. Beyond a concentration threshold of 10^{-3} mol l^{-1}, these vanadate species spontaneously condense in the xOy plane by two different reactions respectively called olation and oxolation reactions (olation: $V\text{-}OH+V\text{-}OH_2 \rightarrow V\text{-}OH\text{-}V+H_2O$; oxolation: $V\text{-}OH+V\text{-}OH \rightarrow V\text{-}O\text{-}V+H_2O$) to form ribbons 1 nm thick, about 25 nm

Fig. 5. **a** View of the $^1_\infty[Nb_2PS_{10}]^-$ chain showing the atom labeling and selected Nb-Nb bond lengths. **b,c** Arrays of nanotubules as observed by FFEM ($NaNb_2PS_{10}$ in NMF, 0.140 mol l^{-1}) with the cryofracture plane being arbitrary or perpendicular to the nanotubule axes for b and c, respectively. **d** Image obtained by low dose TEM of very dilute solutions of $NaNb_2PS_{10}$ in NMF showing single-wall nanotubules with: 10 nm ∅ (1), 7 nm ∅ (2), a 7–10 nm ∅ defect (3), and small rings corresponding to tubes seen along their principal axis (4). (Adapted from [34], copyright (2002) from the American Chemical Society)

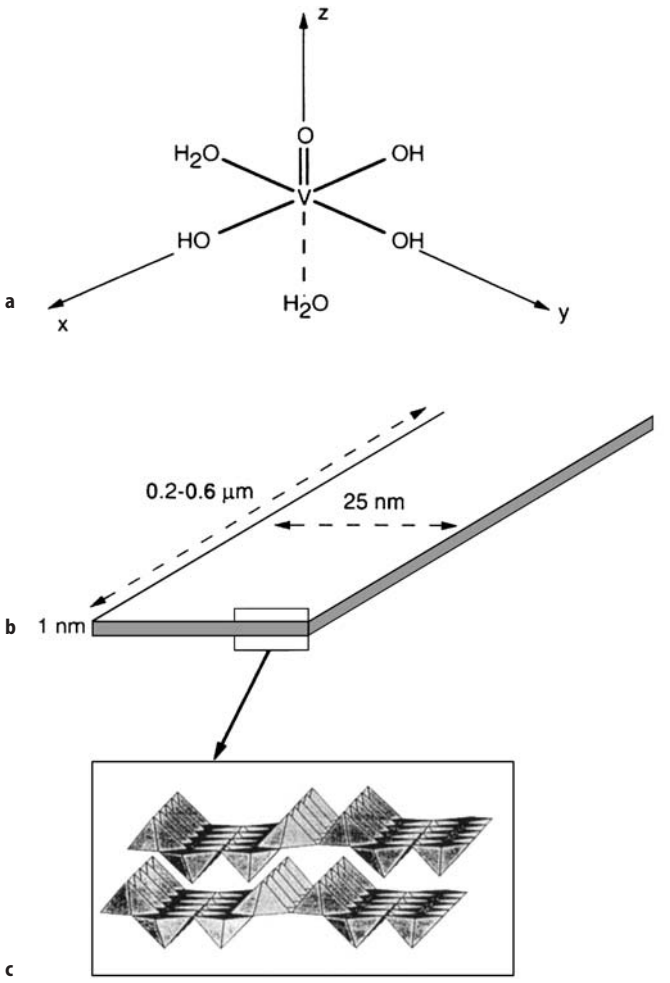

Fig. 6. **a** The molecular species that condense through olation and oxolation reactions into V_2O_5 ribbons **b** whose molecular structure is shown in **c**. (Reprinted from [4b], copyright (2000) from John Wiley and Sons)

wide, and about 200–600 nm long. The thickness is precisely defined by the ribbon molecular structure whereas both width and length is subject to some polydispersity, which is, however, usually rather small. The structure of these oxide ribbons is close to that of orthorhombic V_2O_5. The condensation reaction can be performed in several ways leading to similar ribbon structures. One of the most popular methods, as it avoids the introduction of foreign ions, consists of the acidification of an aqueous $NaVO_3$ solution by passing it through an ion-exchange resin column. The synthesis of V_2O_5 ribbons is a complex non-equilibrium process in which electrical charges play an important role. During the ola-

tion and oxolation reactions, V(V) charged molecular species are consumed and uncharged condensed moieties are produced. These condensed moieties do not experience electrostatic repulsion and hence flocculation of the suspension occurs under the influence of attractive Van der Waals interactions. However, this flocculation is only transient because subsequent adsorption and dissociation of water molecules produce V-OH groups, the ionization of which creates negative electrical charges on the surface of the ribbons and therefore repulsive electrostatic interactions become important again and ensure the stability of the colloid. Dark red gels and sols comprised of entangled ribbons dispersed in water are thus obtained.

The colloidal suspensions produced in this way are stable for years and, a few days after synthesis, their properties do not vary with time any more. In particular, they form a nematic liquid crystalline phase at volume fractions Φ larger than 0.7% [37]. Moreover, these suspensions undergo a sol/gel transition at Φ=1.2% which divides the nematic domain into a nematic sol and a nematic gel. The optical textures of samples sealed in flat glass capillaries and observed under polarized light microscopy are indeed typical of a nematic phase. The nematic sol phase readily displays Schlieren textures whereas the nematic gel often shows the so-called "banded texture" of sheared nematic polymers caused by filling the flat glass capillaries with gel samples. Moreover, at volume fractions larger than 5%, SAXS experiments with samples aligned by shear, proved that V_2O_5 suspensions are in a biaxial nematic gel state [38].

An outstanding feature of the V_2O_5 nematic sols is that they can be aligned in quite moderate magnetic fields [39]. For example, for samples 0.1 mm thick, at a volume fraction of $\Phi \approx 0.8\%$, a magnetic field larger than 0.3 Tesla will align the V_2O_5 ribbons parallel to the field. The defects observed by microscopy then vanish and the texture becomes completely homogeneous, as expected for a nematic single domain. This means that mineral non-ferromagnetic objects can thus be aligned by a purely external non-invasive action. Once the magnetic field has been removed, the samples still keep their nematic single domain properties, which makes them suitable for other physical studies. The alignment of a Φ=0.7% sample takes about 2 h at 0.3 T and about 5 min at 1 T. These times increase rapidly when Φ gets closer to the gelation threshold. Thus, V_2O_5 sols align as fast or even faster than usual lyotropic rigid rod polymers such as poly(*p*-benzamide) and poly(γ-benzyl-L-glutamate) (PBLG) which respectively take hours or fractions of hours to align under similar conditions [40]. The magnetization of the phase is very small however and has not even been determined by a Squid magnetometer or by torque measurements. This means that the magnetization of the phase is actually comparable to that of pure water, a result which is understandable if one remembers the very small V_2O_5 volume fraction (Φ=0.7%) involved. Consequently, the microscopic origin of the magnetic susceptibility and its anisotropy is still unknown. It has been proposed that the magnetization could arise either from a diamagnetism possibly related to the anisotropic shape of the ribbons or from the paramagnetism of V(IV) impurities always present at the level of a few percent. Nevertheless, this phenomenon illustrates a characteristic feature of "soft matter", namely that a very small perturbation can have a huge effect on the mesophase due to its collective nature. In other words, the

mineral building blocks of a nematic phase need not have strong magnetic properties for the phase to align in a magnetic field. In contrast, it was very difficult to induce any appreciable alignment in the isotropic phase of V_2O_5 ribbons.

An interesting application of the magnetic alignment is the following (Fig. 7). A single domain of the nematic phase can first be obtained by application of a magnetic field. Then, if this single domain is suddenly rotated in the field, it will undergo a transient hydrodynamic instability. This instability appears as a periodic pattern of microdomains in which the average direction of the ribbons is modulated. The pattern looks different depending upon the final magnetic field direction. This instability is classical in the field of liquid crystals and was thoroughly analyzed by Srajer et al. [41]. It can be used to micropattern a mineral material with periods in the range 10–100 μm in a very simple and cheap way. The lifetime of this instability varies from minutes to hours depending on the magnetic field intensity.

The production of nematic single domains also allows more detailed structural studies to be performed. For instance, the SAXS pattern (Fig. 8) of an aligned sample of V_2O_5 sol shows two diffuse spots located along a direction perpendicular to the director. These spots arise from the lateral interference between ribbons and their positions give the typical distance (~50 nm) between ribbons in the plane perpendicular to the director. This pattern is very similar to those of the nematic suspensions of the Tobacco Mosaic Virus (TMV), a typical example of rod-like organic polymer. Using a well-documented procedure, one can derive the nematic order parameter S from the distribution of scattered intensity [42]. This parameter takes values between 0, for a completely isotropic phase, and 1 for perfectly aligned moieties. The value obtained for V_2O_5, S=0.75, is in very good agreement with the predictions from the Onsager model and also, as expected, the nematic/isotropic phase transition is first order (with phase coexistence) and temperature has no influence on the nematic ordering (see also Sect. 5.1.). However, an increase of ionic strength, through salt (NaCl) addition had unexpected consequences. The nematic phase was actually stabilized with respect to the isotropic phase, in contrast to the behavior usually observed with this kind of lyotropic liquid crystals. This was attributed to Van der Waals interactions among ribbons that become increasingly important as electrostatic interactions are screened [43].

The anisotropy of the nematic phase also affects the properties of the solvent, in this case water. A recent ^2H NMR study of single domains of V_2O_5 sols has

Fig. 7a–d. Texture photographs in polarized light of transient hydrodynamic instabilities induced by a sudden change of the magnetic field orientation: **a** starting from a powder sample; **b** the magnetic field is applied along the main capillary axis; **c** the magnetic field direction is now perpendicular to the main capillary axis, but still in the plane of the figure. In consecutive stripes, the ribbons point in two different but symmetrical directions with respect to the polarizer-analyzer directions, giving rise to a zigzag pattern; **d** the magnetic field direction is now perpendicular to the plane of the figure. The dark regions are areas where the ribbons are perpendicular to the plane of the figure whereas the bright regions are areas where the ribbons still lie in the plane of the figure. (Reprinted from [39], copyright (1997) from John Wiley and Sons)

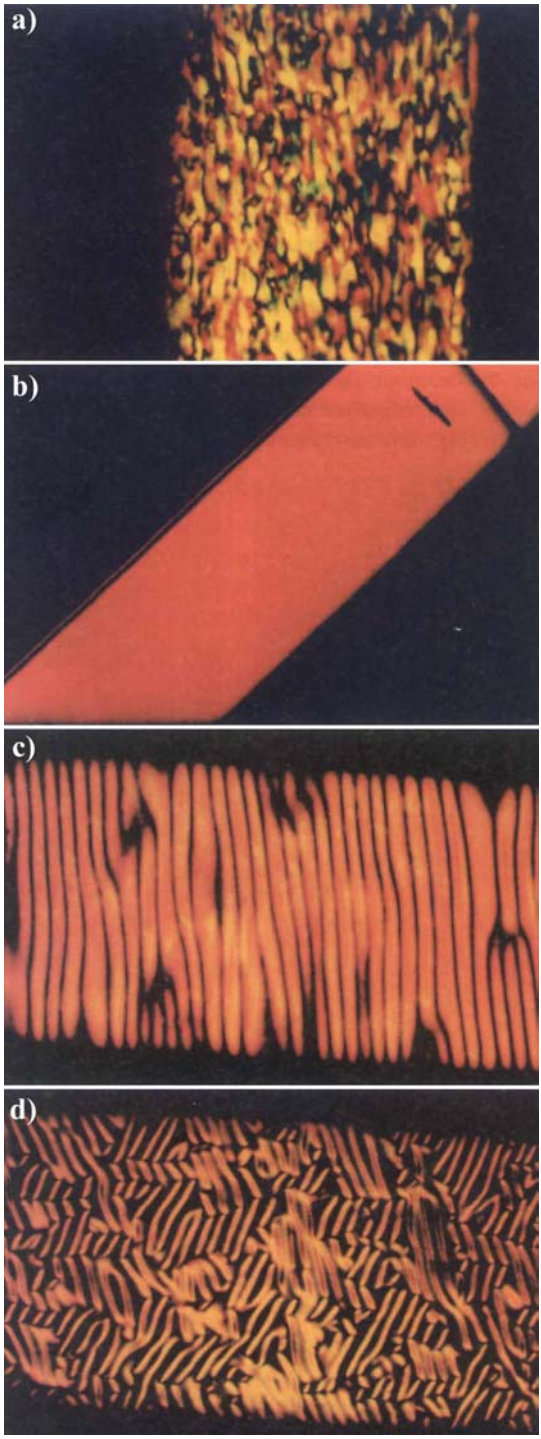
a)
b)
c)
d)

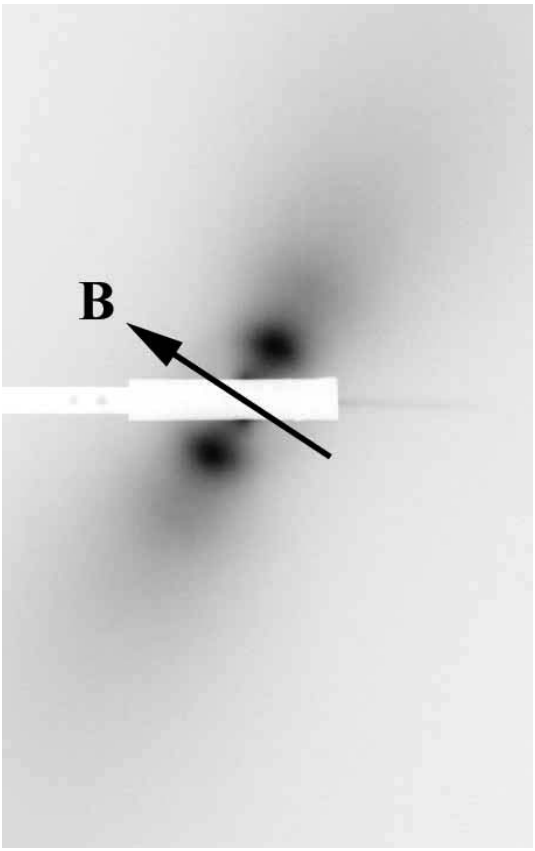

Fig. 8. Small angle X-ray scattering pattern of a sample aligned in a 1 T magnetic field. B is the field direction, which is set at an arbitrary angle of ≈40° to the main capillary axis. The *white rectangle* at the center of the figure is due to the beam stop

shown that, even at volume fractions as low as 0.7%, water molecules still experience a residual anisotropic interaction due to a situation of fast exchange between the bulk and sites located on the surface of the ribbons [44]. This is surprising and indicates that water molecules adsorbed on the surface of the ribbons still undergo fast motions. Thus, the behavior of the solvent faithfully reflects the anisotropy of the nematic phase, a feature that has subsequently been used to study the reorientation dynamics of the mesophase.

The magnetic alignment of these materials may be useful for applications when highly oriented samples are needed. V_2O_5 gels are classical host materials for the intercalation of guest species. For instance, the oxidative intercalation-polymerization of organic molecules, such as aniline or thiophene, has led to the synthesis of hybrid organic-inorganic materials, in which organic electrically conducting polymers are inserted between V_2O_5 ribbons giving rise to novel

sandwich compounds. This process, carried out in a magnetic field, may yield highly oriented conducting polymers of better quality.

Since one of the most important applications of liquid crystals lies in the electro-optic display industry, it was natural to examine the influence of an electric field on the nematic phase of V_2O_5 suspensions [45]. A major problem, due to the lyotropic nature of this liquid crystal, is the screening of the field by mobile ions. This was overcome by the use of a high frequency (300 kHz) a.c. field and of blocking electrodes. Home-made cells (thickness 10–75 μm) were prepared with glass plates coated with indium tin oxide electrodes covered with SiO_2 and polyimide layers. The cells were filled by capillarity. Applying fields of about 1 V μm^{-1} was enough to align the phase from an initially planar texture to a homeotropic one. This reorientation is reversible so that switching cycles could be produced, using effective voltages of about 10 V. The response times are in the region of 1 s. In addition, the isotropic phase shows a very strong birefringence induced by the electric field. These properties formally demonstrate that mineral liquid crystals would have the potential for simple slow display applications.

4
Molecular Disks

4.1
Clays, Nematic Ordering vs Gelation

Clays of the montmorillonite family are lamellar aluminosilicates [46] used in many industrial processes and in products such as paints, softeners, and composite materials [47]. They swell when brought into contact with water, which is due to the insertion of water molecules between the sheets. Complete exfoliation can be induced leading to dispersions of disk-like particles of 10 Å thickness and 300–3000 Å in diameter, depending on the variety of clay used. These clay platelets bear a rather large surface electrical charge so that electrostatic interactions between them must be considered and are actually responsible for the colloidal stability of these dispersions. These suspensions have been widely studied as model colloids and also because they form physical thixotropic gels.

As early as 1938, Langmuir observed the phase separation of clay suspensions into an isotropic phase and a birefringent gel at the macroscopic level in test-tubes [9]. However, in the same report, he noted that this property of phase separation was gradually lost with time, which he tentatively explained by the incorporation of impurities diffusing from the glass tubes. He also compared this system to normal liquid crystals. Later, in 1956, Emerson observed a banded texture similar to that displayed by the Tobacco Mosaic Virus [48]. The investigation of clay suspensions from the structural point of view has been recently resumed. However, the study of the nematic order of suspensions of montmorillonite clays is in fact complicated by their gel properties. In spite of sustained efforts to understand its nature, the gelation mechanism has not yet been fully elucidated [49].

The role of the surface electrical charge is certainly crucial because the properties of the suspensions vary considerably with their ionic strength.

Quite recently two systems of the montmorillonite family, namely bentonite $[Na_x(Al_{2-x}Mg_x)(Si_4O_{10})(OH)_2,zH_2O]$ and laponite B $[(Na_2Ca)_{x/2}(Li_xMg_{3-x})(Si_4O_{10})(OH)_2, z\ H_2O]$ (an industrial form of hectorite) have been studied under polarized light using both the naked eye and optical microscopy [50]. The microscopic textures of concentrated gels (Fig. 9) are typical nematic ones. However, the nematic-isotropic phase separation has only been achieved very exceptionally, which seems to be a typical feature of these systems. In contrast with V_2O_5 ribbons, as the clay concentration increases, the suspensions, initially isotropic-liquid, become isotropic-gel and finally birefringent-gel (Fig. 10a,b). Temperature seems to have no influence on the nematic organization; the system is athermal as expected from the Onsager description that also applies to discs [51]. The isotropic gels show very large pretransitional effects such as flow and shock birefringence (Fig. 10c). The question about the thermodynamic nature of the birefringence of these gels naturally arises. In other words, is this birefringence due only to the freezing of some accidental flow birefringence or is it really intrinsic? Some simple experiments point to the thermodynamic nature of the nematic ordering. First, for one system, Langmuir has reported the phase separation of these suspensions. Second, the optical textures of these birefringent gels still slowly evolve over a few weeks after their preparation because topological defects anneal. However, the birefringence of these gels does not de-

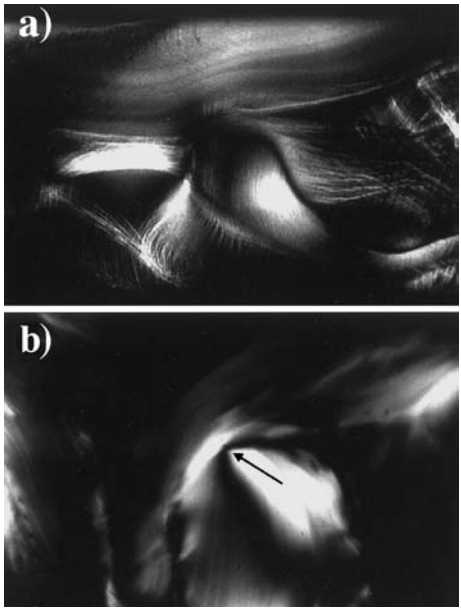

Fig. 9a,b. Microscopic observations in polarized light of the textures of the aqueous clay suspensions: **a** nematic threaded texture of a bentonite suspension (concentration 0.044 g/cm^3, magnification 50×); **b** detail of a 1/2 disclination line (*arrow*) in a laponite suspension (concentration 0.034 g/cm^3, magnification 100×) (Reprinted from [50], copyright (1996) from the American Chemical Society)

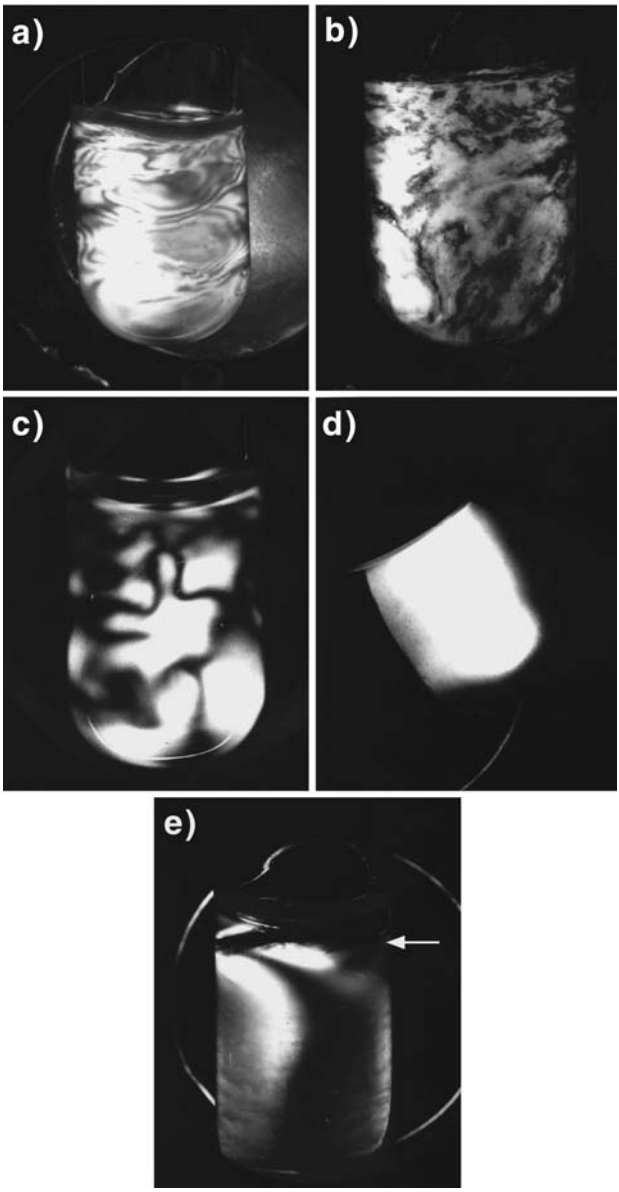

Fig. 10a–e. Tubes of aqueous clay suspensions observed between crossed polarizers: **a** bentonite suspensions of concentration 0.043 g/cm^3; **b** laponite suspensions of concentration 0.043 g/cm^3; **c** flow birefringence in a bentonite suspension of concentration 0.019 g/cm^3 – the test tube was previously vigorously shaken and was photographed during relaxation; **d** example of an oriented laponite suspension over a centimeter length scale – the sample looks bright because its principal axes are close to 45° with those of the polarizers; **e** an initially isotropic sample of bentonite gel (c=0.020 g/cm^3, bottom) in contact with brine (5 mol/l) turns birefringent. The *arrow* points to the interface between the gel and the brine. (Reprinted from [4b], copyright (2000) from John Wiley and Sons)

crease over many years. This means that, at least during the first weeks, the particles are not completely frozen and that any accidental flow birefringence could in fact relax. Third, birefringent gels may be prepared in test tubes by slowly concentrating isotropic sols over weeks. This process does not involve any flow. In this way, nematic single domains as large as a cubic centimeter were reproducibly prepared (Fig. 10d). Moreover, birefringence appears at the same concentration as that determined on samples prepared in the usual way. Then, the mechanical history of the sample seems irrelevant in this respect. Therefore, these studies show that a nematic order prevails in these suspensions over a distance that can be as large as 1 cm. Nevertheless, this discussion not only emphasizes that one should not confuse plain flow birefringence with true nematic ordering but also illustrates the difficulties of working with gels.

Very recently, well-aligned samples of laponite gels (c=0.02 g cm^{-3}) were prepared by slowly concentrating isotropic sols directly in Lindemann glass capillary tubes suitable for SAXS experiments, instead of test-tubes as described in the previous paragraph. The SAXS patterns observed are clearly anisotropic (Fig. 11a), which demonstrates the nematic orientational order at the particle scale over the whole sample [52]. Moreover, the SAXS patterns also show that the positional correlations of the clay particles are very weak, which is a well-known feature of these laponite gels [53]. This allows one to model easily the SAXS pattern (Fig. 11b) by only considering the particle form factor and the Maier-Saupe orientational distribution function that classically describes the nematic order [1]. By fitting the SAXS pattern, the nematic order parameter is obtained, S=0.55±0.05. This value compares quite well with those of usual liquid crystals (0.4–0.8) and shows that the nematic order of these materials should always been kept in mind when elaborating experimental procedures.

The phase diagram of these suspensions has been established versus clay volume fraction and ionic strength (Fig. 12) allowing the behavior of the sol-gel as well as the isotropic-nematic phase transitions to be followed. At high salt concentration (>0.3 mol l^{-1} for bentonite and >9×10^{-3} mol l^{-1} for laponite), the repulsive electrostatic interactions are screened sufficiently so that short-range attractive interactions can take over inducing the flocculation of the suspension. Very strikingly, in the case of bentonite (Fig. 12a), the nematic phase is stabilized upon increasing the ionic strength: an increase of the ionic strength induces both gelation and the isotropic-anisotropic phase transitions to occur at lower clay concentration. If one follows a vertical line on this diagram, and for example starts with a liquid suspension of bentonite (1.5 wt%) in pure water, at a concentration of [NaCl]=0.02 mol l^{-1} the suspension is an isotropic gel and at [NaCl]=0.1 mol l^{-1} it is a birefringent gel. Therefore, adding some brine on an isotropic gel of bentonite of concentration slightly under the isotropic/nematic transition allows one to induce the phase transition without any slightest flow, another hint at the thermodynamic origin of this transition (Fig. 10e). This effect, though unexpected, was still predicted by a statistical physics model incorporating electrostatic interactions [54]. Furthermore, a similar phase diagram was recently reported by Mourchid and Levitz on a closely related form of laponite, in a thorough and detailed study [55]. The same authors have fully discussed the relation between gelation and nematic ordering in this system. They

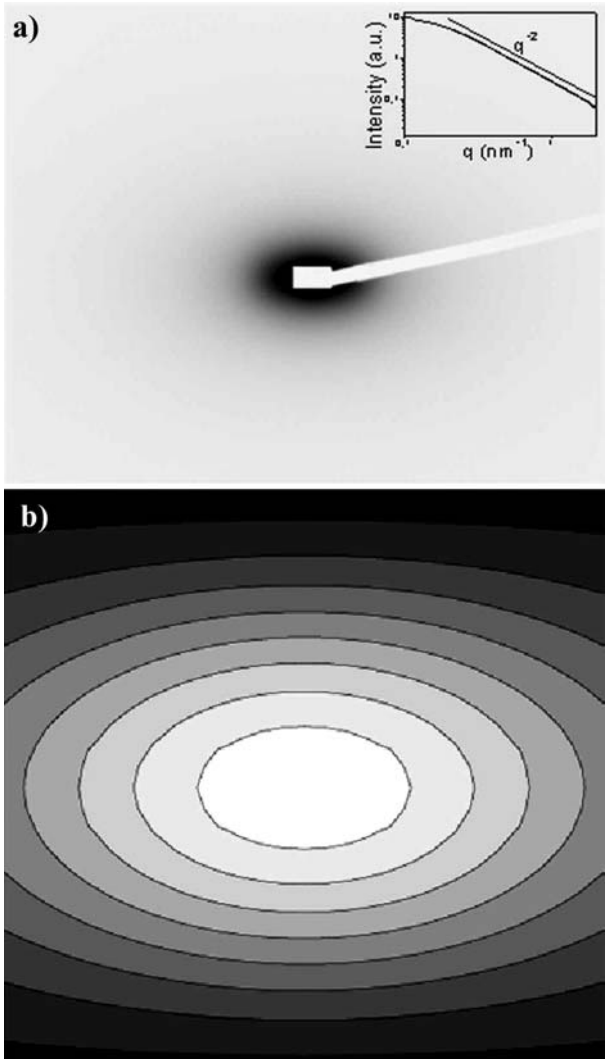

Fig. 11. **a** Anisotropic SAXS pattern of an aligned sample of clay gel in a horizontal capillary. Insert: SAXS intensity vs scattering vector modulus of an unoriented sample of the same concentration. (The *straight line* shows the q^{-2} dependence typical of the "intermediate regime" of plate-like particles). **b** Calculation of the SAXS pattern, with L=1 nm, R=15 nm, and S=0.55, that gives good agreement with the experimental one. (Reprinted from [52], copyright (2002) from EDP Sciences)

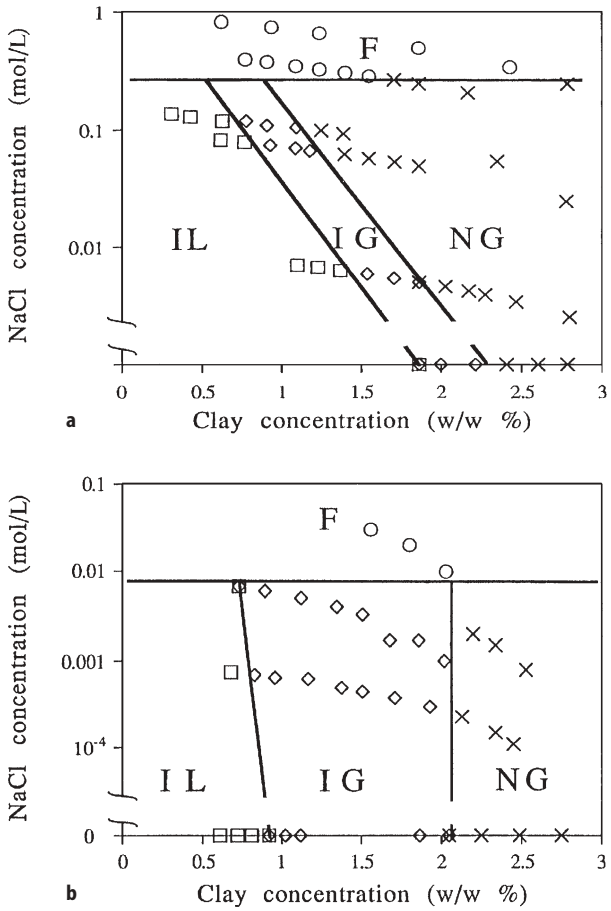

Fig. 12a,b. Phase diagram of clay suspensions vs clay and NaCl concentrations. (*circles*, F) Flocculated samples; (*squares*, IL) isotropic liquid samples (*lozenges*, IG) isotropic gel samples; (*crosses*, NG) nematic gel for: **a** bentonite; **b** laponite. (Reprinted from [4b], copyright (2000) from John Wiley and Sons)

have also explored the phase diagram at very low ionic strength and found the existence of a soft solid stabilized by long-range electrostatic repulsions [56].

In addition, it should be noted that there is now quite a few experimental studies that directly or indirectly document the existence of nematic order in clay gels [57]. Among them, let us particularly mention the direct visualization of aligned domains by X-ray fluorescence microscopy [58]. These clay-rich domains may arise from the nematic/isotropic phase separation that takes place at the micron length scale but does not extend to the macroscopic scale due to gelation, as discussed above. Another recent study leads to very similar conclusions [59]: Magnetic spherical colloidal particles of maghemite were incorporated as probes into laponite gels. A microscopic phase separation was also observed in

the region of the phase diagram where the nematic/isotropic phase separation was expected. Finally, all these various studies raise the same and yet open question: what is the interplay (if any) of the nematic/isotropic phase transition with the gelation of these clay suspensions [60]?

4.2 A Unique Liquid-Crystalline Lamellar Phase Comprised of Mineral Nanosheets: $H_3Sb_3P_2O_{14}$

Until very recently, a liquid-crystalline lamellar phase based on extended, covalent, solid-like sheets had never been reported, even in the huge field of organic lyotropic phases. However, the field of mineral compounds provides a wealth of original moieties that are not usually obtained from organic synthesis techniques. Any general chemistry textbook will show a wealth of low-dimensionality mineral compounds and among them, many are two-dimensional ones. The problem then is to try to disperse them in a suitable solvent without alteration. We have already discussed in a previous section the principles that lead to the successful dispersion of mineral moieties and this approach will be further illustrated with the following example [61]. The members of the series of solid acids $H_nM_nZ_2O_{3n+5}$ (with, for example, M=Sb, Nb, Ta; Z=P, As; n=1, 3) are known to display a crystalline lamellar structure [62][2]. Among them, $H_3Sb_3P_2O_{14}$ was found to disperse fully in water to yield homogeneous, transparent, colorless suspensions of extended covalent sheets of 1 nm thickness and at least 300 nm in diameter. The observation (Fig. 13) in polarized light of a series of test-tubes

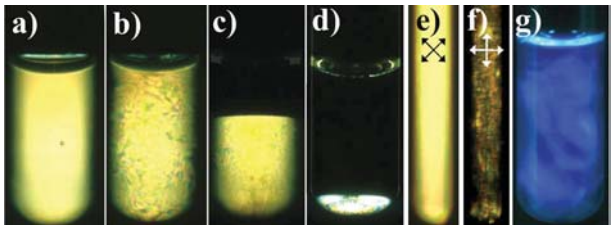

Fig. 13a–g. Naked-eye observation of samples. Test-tubes filled with aqueous suspensions of $H_3Sb_3P_2O_{14}$ single-layers, observed between crossed polarizers (a–e) (the isotropic phase appears dark): **a** 2 ml of birefringent gel phase (ϕ=1.98%) (topological defects are so dense that the texture appears homogenous at the scale of this photograph); **b** 2 ml of birefringent fluid phase (ϕ=0.93%); **c** 2 ml of a biphasic sample with an overall volume fraction ϕ_o=0.65%; **d** 2 ml of a biphasic sample with an overall volume fraction ϕ=0.03%; **e, f** magnetically aligned sample observed in a 5-mm NMR tube that has been immersed 10 min in a 18.7 T field at 50 °C, in two different orientations compared to the polarizer/analyzer system represented by *arrows* (ϕ=0.75%); **g** sample iridescence (ϕ=0.75%) observed in natural light and due to light scattering by the $H_3Sb_3P_2O_{14}$ layers stacked with a period of 225 nm. (Reprinted by permission from Nature [61], copyright (2001) Macmillan Publishers Ltd)

[2] In some cases, test tubes have shown temporarily a rainbow set of colors (see www graphical abstract) (induced by strong centrifugation for example), prior to reaching a single color equilibrium state.

filled with suspensions of decreasing volume fractions shows that: i) samples of high volume fractions (ϕ>1.78%) form birefringent gels; ii) for 1.78%>ϕ > 0.75%, the samples form a fluid birefringent phase; iii) for 0.75%>ϕ, the suspensions demix into a bottom birefringent fluid phase and a top isotropic one.

SAXS experiments (Fig. 14) have proved that the birefringent phase (sol and gel) has a lamellar structure and that its period can be continuously tuned from 1 to 225 nm according to dilution. In fact, very dilute samples are iridescent because the lamellar structure then has a period comparable to the wavelengths of visible light [62]. A large number (up to 10) of lamellar reflections were observed by SAXS, even at high dilutions, which shows the strength of the interactions between the mineral sheets. Further dilution leads to phase separation as excess water is expelled from the lamellar phase. Adding salt destabilizes the liquid-crystalline phase, eventually leading to flocculation of the colloid, indicating that these interactions are most probably of an electrostatic nature; this is hardly surprising as the sheets bear a rather large electrical charge. In addition, wide-angle X-ray scattering experiments have revealed the existence of sharp diffrac-

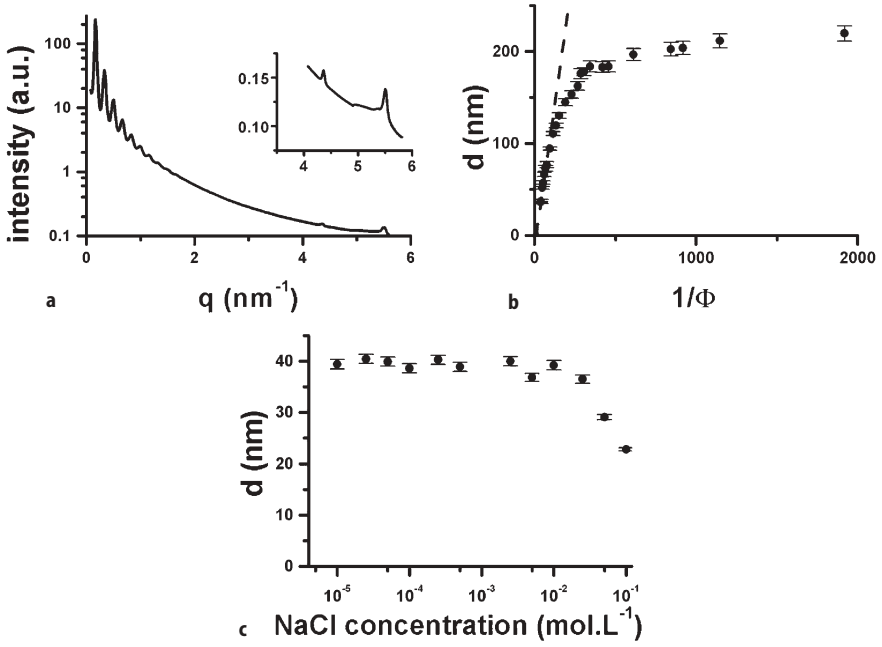

Fig. 14a–c. USAXS study of "powder" samples: **a** an example of scattered intensity vs scattering vector modulus q, showing ten orders of reflection due to the lamellar period as well as, in the inset, the thin diffraction lines due to the two-dimensional positional order within the covalent layers (ϕ=2.0%); **b** variation of the lamellar period, d, with inverse volume fraction (including two data points at very small d extracted from [62]) – the *dashed straight line* represents the one-dimensional swelling behavior of the lamellar phase d=δ/ϕ with δ=1.05 nm. A crossover from this law to a plateau is observed when entering the biphasic regime; **c** variation of the lamellar period d with salt molarity at constant volume fraction (ϕ=1.9%). (Reprinted from [61], copyright (2001) from Nature Publishing Group)

tion lines due to the crystalline order within the mineral sheets that do not fold or crumple but are fully preserved in suspension.

The mineral lamellar phase is readily aligned by shear in a Couette cell (Fig. 15) and the covalent sheets align parallel to the shearing surfaces. Dilute samples could be aligned at rather low shear rates (30 s^{-1}) and showed the best orientations. Moreover, the mesophase also aligns in high magnetic fields with the sheets perpendicular to the field, which provides a simple way to produce large (centimetric) oriented lamellar samples. This property was exploited by using the lamellar phase as a medium to induce a weak alignment of biomole-

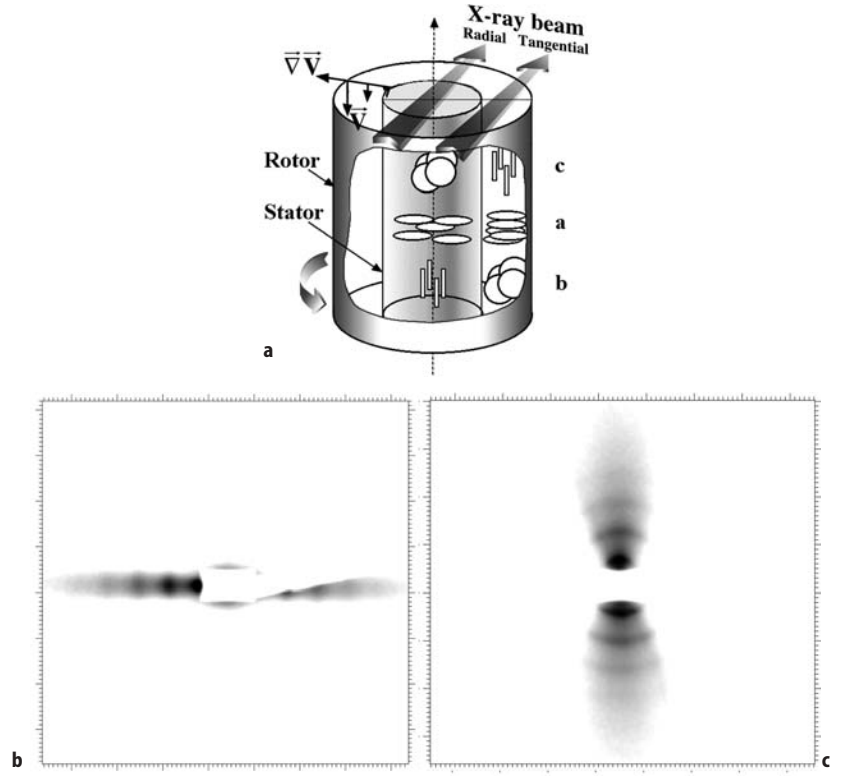

Fig. 15a–c. USAXS studies of aligned samples: **a** scheme of the Couette shear cell illustrating the radial and tangential geometries with respect to the X-ray beam (*flat arrows*). We also depict within the cell the three different types of lamellar orientations (a, b, and c) as seen by the X-rays in both geometries (the layers are sketched as *circular disks*); **b** USAXS 2-D scattering pattern obtained with a sample aligned in a Couette shear cell, in the tangential geometry, showing that the layers (d=175 nm) mostly belong to the c orientation; **c** USAXS 2-D scattering pattern of a vertical capillary filled with a suspension of $H_3Sb_3P_2O_{14}$ (ϕ=0.75%), obtained 20 min after its alignment using an 18.7-T magnetic field applied along its long axis. The vertical localization of the interference peaks (d=215 nm) indicates that the layers are oriented perpendicular to the magnetic field (in this case, since no mechanical shear is applied, the sample relaxes back to a powder within 1–2 h once removed from the magnetic field). (Reprinted from [61], copyright (2001) from Nature Publishing Group)

cules, which proves helpful when trying to determine their structure by NMR (see Sect. 6, Emerging Fields section).

5
Anisotropic Nanoparticles

5.1
Boehmite, a Model System to Test the Onsager Theory

The boehmite system (γ-AlOOH), originally studied by Zocher and Torök [63] and Bugosh [64] was further developed by Lekkerkerker and coworkers [65]. They extended the hydrothermal preparation pioneered by Bugosh [64] by starting from an aqueous aluminum alkoxide mixture acidified with hydrochloric acid [65a]. They studied the phase behavior of both charge stabilized aqueous dispersions of colloidal boehmite rods [65b,c] as well as sterically stabilized colloidal boehmite rods in an organic solvent (cyclohexane) [65d–f].

Using the aqueous suspensions as obtained from the hydrothermal treatment, the I–N transition was observed, but took a very long time (months) [65b]. On the other hand, by treating the boehmite dispersions with hydrolyzed aluminum polycations, the phase transition is complete in a few days [65c]. In retrospect, it appears that the boehmite suspensions prepared by Bugosh also contain aluminum polycations. The sterically stabilized boehmite dispersions undergo the I–N phase transition. The biphasic gap is much wider than predicted by the Onsager theory for a monodisperse sample [65e], but can be explained by taking into account the polydispersity [65f]. The rate of the I–N transition strongly depends on the concentration. Upon increasing concentration from c_i to c_n, polarization microscopy indicates a crossover from nucleation and growth to spinodal decomposition [66].

At this point, let us detail the conditions of validity and the main predictions of the Onsager theory. This model applies to very anisotropic rod-like (or disk-like) particles. An important quantity is the particle aspect ratio, L/D, defined as the ratio of its length L over its diameter D. The particles should only interact through a purely hard-core potential, which means that particles do not interact at all if they do not touch, but they also cannot interpenetrate each other. This statistical physics model is based on a balance of two kinds of entropies. As concentration of rod-like moieties increases, the system undergoes nematic ordering because its loss of orientational entropy is more than compensated by a gain in translational entropy. The predictions of the model are the following. The nematic/isotropic transition should be first-order, i.e., with phase coexistence. The concentrations of the coexisting nematic and isotropic phases are given by c_n=4.2D/L and c_i=3.3D/L respectively. The nematic order parameter should jump from 0 to 0.8 at the transition. Temperature has no effect on this transition and the system is called athermal. Thus, the predictions of the Onsager model and of more recent theories based on it were confirmed by the detailed and precise investigations using the suspensions of grafted boehmite rods dispersed in cyclohexane. Figure 16 illustrates the first-order nematic/isotropic phase transition of these grafted boehmite rods. The effect of controlled polydispersity was

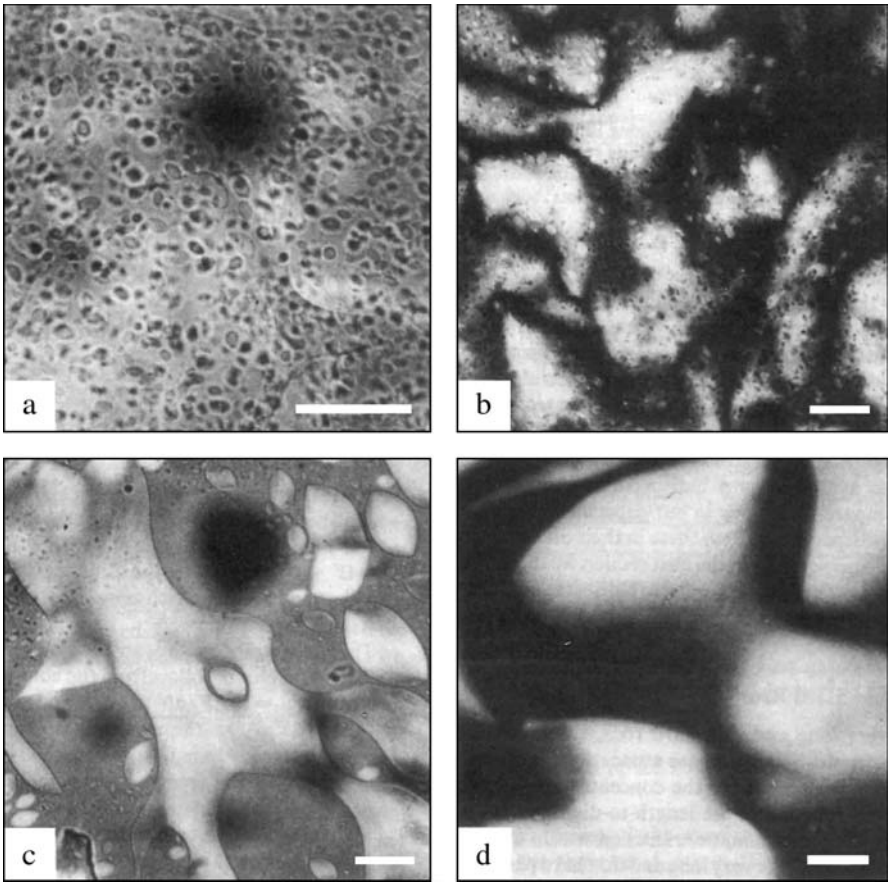

Fig. 16. **a** Optical micrograph of the nucleation of very small nematic droplets. **b** Nematic droplets and underneath a continuous nematic lower phase with Schlieren. **c** Grown-out tactoids. **d** Schlieren texture after completion of phase separation. All observations with crossed polarizers. The length of the *bar* represents 20 μm (Reprinted from [65e], copyright (1993) from the American Chemical Society)

also examined and the complex coexistence of two different nematic phases with the isotropic liquid phase, which is a consequence of polydispersity predicted by theory, was proved experimentally.

Non-grafted boehmite rods experience a much more complicated interaction potential as positive surface electrical charges now play an important role. In this case, the phase diagram has to be discussed in the frame of both the Onsager model of nematic ordering and the DLVO (named after: B.V. **D**eryagin, L. **L**andau, E.J.W. **V**erwey, and J.T.G. **O**verbeek) theory of colloidal stability, which describes colloidal stability as a balance between repulsive electrostatic and attractive van der Waals interactions [67, 68]. At low ionic strength, electrostatic repulsion dominates so that the phase stability is essentially described by the

Onsager model. However, at large ionic strength, these electrostatic repulsions are screened and van der Waals attractions come into play. Indeed, the strength of these latter interactions depends through the Hamaker constant on the electronic contrast between the mineral moieties and the solvent. Mineral moieties being electron rich are likely to show a large Hamaker contrast with the solvent. In the case of boehmite rods, these strong van der Waals attractions lead to the formation of dense space-filling isotropic gels. It should be noted at this point that the percolation threshold of very anisotropic rods is inversely proportional to their aspect ratio so that gels can be formed at rather low volume fractions. Note that a rather similar situation also prevails for the aqueous dispersions of V_2O_5 ribbons [69].

The same authors also investigated the dynamic properties of these suspensions by light scattering and rheology both in the isotropic liquid phase and in the nematic one. Even though this constitutes one of the most comprehensive studies of its kind for suspensions of rod-like moieties, we shall not further discuss their findings, as they are well described [68, 70].

5.2
Gibbsite and the Onsager Transition for Disks

In his seminal work of 1948, Onsager had already predicted the existence of a nematic phase for suspensions of disk-like particles. However, it was only fifty years later that Van der Kooij and Lekkerkerker clearly proved this conjecture by carefully investigating suspensions of gibbsite, $Al(OH)_3$, hexagonal platelets [71]. These particles were sterically stabilized by grafting them with a layer of polyisobutene before being dispersed in toluene. The aspect ratio of these moieties, defined as the ratio of their diameter (≈170 nm) to their thickness (≈15 nm), is approximately 11. In a given range of volume fraction (0.16–0.17), these suspensions spontaneously phase separate (Fig. 17) into a nematic and an isotropic phase as predicted by Onsager, and also more recently confirmed by computer simulations [72]. The birefringent nematic phase, being denser than the isotropic one, sediments at the bottom of the tube. Moreover, the relative proportion of the nematic phase increases linearly with the gibbsite volume fraction, as expected (Fig. 17a–d). The isotropic upper phase shows streaming birefringence when the tube is slightly shaken, indicating the presence of free alignable platelets. The lower phase is permanently birefringent due to nematic ordering and flows like a moderately viscous liquid when the tube is tilted, both properties proving its liquid crystalline nature. This phenomenon proves that the nematic order of gibbsite suspensions of volume fraction larger than 0.17 is really of a thermodynamic nature. In addition, the range of volume fraction of the biphasic gap is in relatively good agreement with the theory. This experimental study also proves that grafting particles with a polymer layer ensures that they strictly interact through a hard-core potential. Indeed, the thickness of the polymer layers prevents the particles from approaching each other at short range where electrostatic and van der Waals interactions come into play.

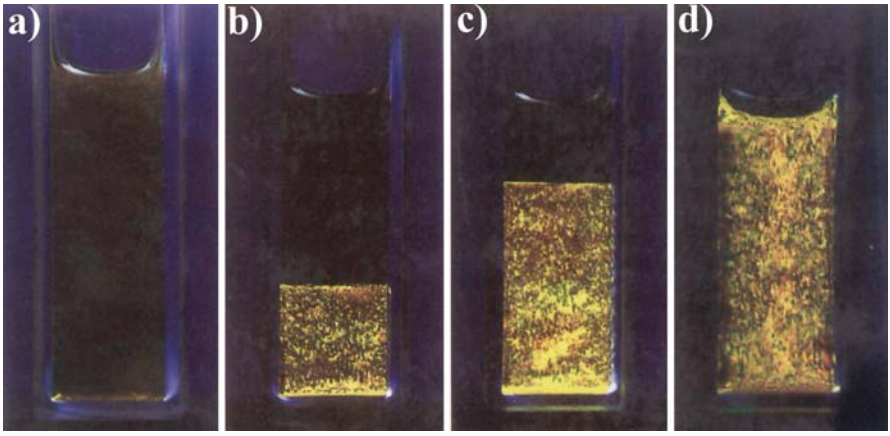

Fig. 17a–d. Isotropic-nematic phase separation as observed between crossed polarizers, at volume fractions ranging from; **a** 15.9; **b** 16.5; **c** 16.9; **d** 17.4 vol.%. (Reprinted from [71], copyright (1998) from the American Chemical Society)

5.3 Liquid Crystalline Hexagonal Phase of Disks: $Ni(OH)_2$

Liquid crystalline phases can show not only long-range orientational order as nematic phases do but also long-range positional order. When this positional order is one-dimensional, the mesophase is called lamellar or smectic; when it is two-dimensional, it is called columnar. The latter case is often found with thermotropic liquid-crystal disk-like molecules. Such molecules stack in columns that assemble on a 2-D lattice of hexagonal, rectangular, or oblique symmetry. The molecules in a given column only show 1-D liquid-like order and the uncorrelated columns are free to slide past each other, which ensures the mesophase fluidity [73].

Very recently, a hexagonal columnar mesophase has been reported in two different mineral systems. In the first example, nickel hydroxide ($Ni(OH)_2$) hexagonal plate-like particles have been grown by controlled precipitation [74]. They were then coated with a polyacrylate layer in order to avoid flocculation by steric repulsion. The bare particles are about 90 nm in diameter and about 10 nm thick, with an aspect ratio of 9:1. The polymer layer being about 4 nm thick, the particles, when coated, have an aspect ratio of about 5:1. The nickel hydroxide particles are charged and the strength of the electrostatic interactions can be tuned by adding salt. Observations of macroscopic samples with the naked eye, in polarized light, show, in a given range of concentration, the coexistence of two phases – a top isotropic phase and a bottom birefringent one. Small Angle Neutron Scattering (SANS) experiments on "powder" (i.e., unoriented) samples displayed five diffraction peaks. The first two, located at small scattering angles, in a ratio $1:3^{1/2}$, suggest the existence of a two-dimensional hexagonal lattice whereas the last three, located at wider angles, in a ratio 1:2:3, correspond to the stacking of the plates in columns. Very interestingly, this mineral phase looks therefore quite similar to the hexagonal columnar mesophase of usual disk-like organic mole-

cules. This interpretation was further confirmed by detailed SAXS experiments on aligned samples [75] and the experimental phase diagram was compared to that predicted by computer simulations for plate-like particles [76]. This system also allows one to balance delicately electrostatic and steric interactions by the control of the ionic strength, a possibility that was explored to some extent by the authors. The flow properties of this hexagonal phase, upon shear in a Couette cell, were also investigated [77]. It was found that, at low shear rates, the phase is aligned with columns in the flow direction but the particles have their normals tilted by 20° with respect to the flow direction. As the shear rate is increased, a kind of dynamical transition is observed to a layered state in which the layers and the particles are oriented with normals parallel to the shear gradient. The kinetics of alignment and relaxation were also investigated in detail.

The second example is found in the system of gibbsite disks that we already described in a previous section. In fact, this system shows not only an isotropic/nematic phase transition at a volume fraction of about 20% but also a nematic/columnar phase transition at around 40% [78]. The hexagonal phase is similar in nature to that of the $Ni(OH)_2$ particles but this system provides the additional opportunity to investigate the influence of polydispersity, a parameter that often plays a major role in determining whether a given phase will actually be observed. Two gibbsite systems were prepared that differ by their polydispersities. It was first found in the two systems that the coexisting nematic and columnar phases had different polydispersities. The columnar phase has a markedly smaller polydispersity than the nematic one so that the phase transition could be used to improve the size distribution of a suspension. It was then observed that, in the system of higher polydispersity, the hexagonal phase seemed to be replaced by a lamellar one at higher volume fraction. This nicely illustrates the disruptive effect of the diameter polydispersity, an effect that was indeed awaited. In fact, the relative stability of the nematic, columnar, and lamellar phases are not only controlled by the volume fraction but also by a subtle balance between plate diameter and thickness polydispersities.

Suspensions of colloidal gibbsite platelets of very large thickness polydispersity but of rather monodisperse diameter display a very unusual phenomenon [79]. In a limited range of volume fraction, these suspensions demix into a nematic *upper* phase in coexistence with an isotropic *bottom* phase. This is in stark contrast with the usual case where the nematic phase is denser than the isotropic one. This behavior was interpreted as due to a fractionation effect related to the strong thickness polydispersity as the thicker platelets are largely expelled from the nematic phase and preferentially occupy the isotropic phase. Note that a theoretical model was especially developed in order to account for these quite peculiar observations [80]. Moreover, this model predicts that the nematic phase may demix into two separate nematic phases of differing densities and compositions.

5.4
Mixtures of Rods and Plates

The liquid crystalline behavior of mixtures of rod-like and plate-like particles is intrinsically much richer than those of rods and plates considered separately.

This is nicely illustrated by mixing the suspensions of goethite rods and gibbsite plates already described in this review. One of the motivations to undertake this kind of study was to find a new type of nematic phase, called biaxial [1]. Even though this biaxial nematic was not found here, the mixtures do present a remarkably rich phase diagram with four different liquid crystalline phases [81]. Up to five phases coexist in a region of the phase diagram. Two of these mesophases are nematic but are rod-rich and plate-rich respectively, another one is the columnar phase already described above, the nature of the fourth mesophase is still unknown, and the last phase is the isotropic one. The observation of a five-phase equilibrium region implies that the phase diagram cannot be explained without explicitly taking into account the polydispersity of both rods and plates. Actually, the two nematic phases differ not only in rod/plate proportion but also in particle dimensions. Strong fractionation effects also occurred in the columnar phase, resulting in a more pronounced columnar ordering than observed with suspensions of plate-like particles only. A theory adapted from the Onsager model was successfully developed to account for the corner of the phase diagram that shows the isotropic phase, the rod-rich and plate-rich nematic phases, and all the possible equilibria between them [82]. Finally, it was observed that the formation of the rod-rich nematic phase proceeds by the mechanism of spinodal decomposition whereas that of the plate-rich nematic phase proceeds by a nucleation-growth process [83].

5.5
β-FeOOH, a Colloidal Smectic Phase

In his search for ordering phenomena in suspensions of mineral crystallites, Zocher and Jacobsohn observed, in 1929, iridescent layers at the bottom of a flask filled with a colloidal solution of β-FeOOH (akaganeite) [84]. He called these layers "Schiller layers", which means iridescent layers in German. β-FeOOH forms fairly well monodisperse nanorods 500 nm long and 100 nm in diameter. The iridescence is due to the sedimentation of these rod-like particles, which form layers at the bottom of the flask [85]. The thickness of each layer, roughly the particle length, is comparable to the wavelength of light, explaining the iridescence. A lamellar structure is thus formed which is similar to the molecular organization of thermotropic smectic phases, but here the periodicity is about 100 times larger. This colloidal liquid crystalline phase coexists with the supernatant phase, which is a dispersion of individual rods. The thermodynamics of this phase transition could also be understood in the frame of the DLVO theory. Again, temperature has very little influence on the phase stability, pointing to a purely steric potential. Moreover, detailed studies [86] of dried Schiller layers by atomic force microscopy has shown that the layers can have two types of internal structure: the rods can pack on a distorted square lattice and be tilted with respect to the layer normal or they can assume a liquid-like ordering within the layers. Similar phenomena seem to exist in suspensions of tungstic acid, but they are less well documented. Finally, this example proves that very monodisperse mineral particles can form a colloidal smectic phase.

5.6
Suspensions of Goethite Nanorods

Goethite (α-FeOOH), which should not be confused with akaganeite (β-FeOOH), is one of the most widespread iron oxides [87]. It is widely used as a pigment in industry. Aqueous suspensions of goethite nanorods are readily obtained by raising the pH of an aqueous $Fe(NO_3)_3$ solution. The resulting precipitate is aged at room temperature, centrifuged, and rinsed several times, and finally dispersed at pH 3. At this pH, which represents a compromise between chemical and colloidal stabilities, due to the large surface charge density (0.2 C m^{-2}), electrostatic interactions prevent flocculation. The nanorods are strongly polydisperse with average length of 150 nm, width of 25 nm, and thickness of 10 nm. Goethite suspensions display a liquid crystalline phase at volume fractions of approximately 10%.

Despite the fact that bulk goethite is a typical antiferromagnet, the nematic suspensions of goethite nanorods display quite unexpected magnetic properties [88]. For instance, they align in very weak magnetic fields as the alignment (Frederiks) transition takes place at 20 mT for samples 20 μm thick. This field intensity is at least an order of magnitude smaller than observed in usual thermotropic and lyotropic liquid crystals. This mineral liquid crystal is therefore extremely sensitive to a magnetic field. Moreover, nematic suspensions of

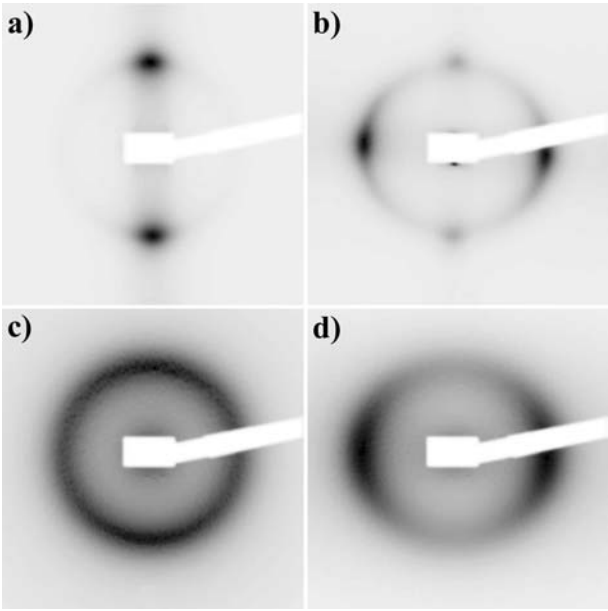

Fig. 18a–d. SAXS patterns of: **a** a nematic phase sample in a 30-mT field; **b** a nematic phase sample in a 625-mT field; **c** an isotropic phase sample in a 270-mT field; **d** an isotropic phase sample in a 900-mT field. (Reprinted from [88], copyright (2002) from the American Physical Society)

goethite align parallel to the field at low field intensities (≤350 mT) but, oddly enough, they reorient perpendicular to the field at large field intensities (≥350 mT) (Fig. 18). This behavior is again in sharp contrast with those of usual liquid crystals that align, at all field intensities, either parallel or perpendicular to the field, depending on their nature. It should also be noted that this property is also observed with initially isotropic goethite suspensions that show huge magnetic-field induced anisotropies and orientation reversal around 350 mT as well. Then, this phenomenon simply reflects the individual properties of the nanorods, even though they are probably enhanced by collective effects in the nematic phase. These quite peculiar magnetic properties probably arise from a competition between a nanorod remanent magnetic moment due to uncompensated surface spins and a negative anisotropy of its magnetic susceptibility.

6
Emerging Fields

6.1
Self Assembly of Nanorods and Nanowires

In the recent past, and following the discovery of nanotubes by Iijima [89], there has been an enormous increase in the number of groups and reports concerning the synthesis of nanorods, nanowires, as well as nanotubes. Most of the elements of the periodic table have now been used (N.B. the difference between nanorods and nanowires is that nanorods usually have a small aspect ratio when nanowires have a high one). These particles, which present a wide range of properties such as semiconducting or metallic behavior, could lead to numerous new liquid crystalline phases and by clever exploitation of their self-assembly properties, numerous new materials with a variety of applications could be synthesized. Since the number of such phases is increasing so rapidly, we have summarized the most studied systems and what we consider to be the most original in Table 1, although we must add that this is not an exhaustive list.

6.1.1
Synthesis

Dozens of methods to synthesize nanotubes, nanowires, and nanorods have been reported that can be found in the references included in Table 1. In addition to the most well known ones, such as hot plasmas, laser ablation, chemical vapor deposition, high temperature solid state and hydrothermal synthesis, filling/coating of carbon nanotubes and similar types of materials, three methods have been developed that enable the synthesis of a wealth of new anisotropic nanoparticles.

The first one makes use of the pores of membranes as templates for the electrolytic growth of metal nanorods. This technique consists of coating one side of a membrane with a metal electrode (such as gold or platinum) and then electrodepositing a metal or conducting polymer within the pores of the membrane [90]. This method controls more closely the filling of the pores compared to other

Table 1. A selection of the most common or original nanotubes, nanorods, and nanowires and their method of synthesis [131]

Composition	Synthesis method(s)	Type	Reference
C	Arc, laser ablation, CVD, templating etc.	NT	[98a, 130]
Ag	AAO templating	NW, NR	[131]
Au	AAO templating	NW, NR	[132, 133]
Bi	AAO templating	NW	[134]
C (diamond)	AAO templating	NW	[135]
Co	AAO templating	NW	[136, 137]
Cu	AAO templating	NW, NR	[95, 138]
Fe	AAO templating		[139]
Ni	AAO templating		[137]
Ge	Laser ablation		[140]
Si	Laser-assisted catalytic growth, laser ablation, catalytic growth, HT synthesis, thermal evaporation SiO, CVD		[141, 142]
Vanadium oxides(V_2O_5, VOx, $Na_2V_3O_7$)	Solution, hydrothermal, NT AAO templating, others	NT, NR	[143–145]
TiO_2	AAO templating, self assembly, sol-gel, wet chemistry	NT, NW	[144, 146, 147]
SnO_2	AAO templating	NW	[10, 148]
Al_2O_3	Anodisation	NT, NW	[141, 149]
In_2O_3	AAO templating	NW	[150]
ZnO	AAO templating, PVD	NW	[144, 147, 151, 152]
WO_3	AAO templating, NT templating	NW, NR	[144, 146, 147]
SiO_2	AAO templating (mesoporous), templated coprecipitation, wet chemistry, laser ablation, carbothermal reduction, sol-gel	NT, NW	[144, 153]
Co_3O_4	AAO templating,	NW	[144]
MnO_2	AAO templating,	NW	[144]
MoO_3	NT templating	NT, NR	[145]
Sb_2O_5	NT templating	NT, NR	[145]
MoO_2	NT templating	NT, NR	[145]
RuO_2	NT templating	NT, NR	[145]
IrO_2	NT templating	NT, NW	[145]
Ga_2O_3	High T, arc discharge, carbothermal reduction	NW	[152, 154]
CuO	Solid state (grinding)	NR	[155]
α-Fe_2O_3	Controlled precipitation	NR	[156]
BaCrO4	Reverse micelle templating	NW	[96]

Table 1 (continued)

Composition	Synthesis method(s)	Type	Reference
$BaWO_4$	Reverse micelle templating	NR	[157]
$YBa_2Cu_3O_7$	Laser ablation	NR	[158]
MoS_2	Catalyzed transport reaction, H_2 reduction, C60 and CNT templating, other	NT	[159–161]
WS_2	H_2 reduction of WS_3, WO_x+H_2S, other	NT	[160–162]
WSe_2	HT reaction	NT	[163]
$W_xNb_yS_2$	HT reaction	NT	[164]
$W_xMo_yC_zS_2$	$W_xNb_yO_z$+H_2S	NT	[165]
NbS_2	H_2 reduction of NbS_3	NT	[166]
TaS_2	H_2 reduction of TaS_3	NT	[166]
$FeTe_2$	Hydrothermal	NR	[167]
$SiSe_2$	Theoretical study	NW	[168]
Bi_2Te_3	AAO templating	NW	[169]
$LiMo_3Se_3$	HT synthesis+cation exchange	NW	[13, 170]
$NaNb_2PS_{10}$	HT synthesis	Nanotubules	[34]
Cu_2S	Cu (surfactant treated)+H_2S	NW	[171]
ZnS	HT conversion of ZnO	NR	[172]
CdS	Thermal decomposition	NR, NW	[173]
CdSe	AAO templating	NR, NW	[97, 174]
BN	Arc, laser ablation, CVD, templating etc.	NT	[175–180]
GaN	Use of growth promoter, CNT templating	NW	[152, 181]
AlN	HT synthesis	NW, NR	[152]
SiN	Si-SiO_2+N_2+2C (CNT templating)	NR	[182]
InP	Laser-assisted catalytic growth	NW	[183]
GaAs	Laser-assisted catalytic growth, laser ablation	NW	[184, 185]
SiC	Arc, HT reaction via CNT templating, carbothermal reduction, HFCVD	NW, NR	[186]
TiC	HT reaction	NW	[187]
MC (M=transition metals, Ge, Ta, Gd, Hf, La)	Various	NR	[188]

nanometer sized materials that have been used, such as the pores of membranes, zeolites, or mesoporous materials [91]. It even allows one, by changing the voltage during the electrodeposition, to synthesize nanowires made of periodically alternating metals [92]. Note that these "striped" metal nanoparticles, in which the stripes are comprised of different metals such as gold, silver, platinum, and nickel, can be visualized using bright-field optical microscopy, which allows them to be used as nano-barcodes [93]. Indeed, in an analogous fashion to conventional barcoding, this technology enables the creation of an extremely large numbers of unique and identifiable particles by varying the width and composition of the stripes. Individual particles can be identified by reading the striped pattern using an optical microscope. Nanobarcoded particles can be used to carry out simultaneously large numbers of biological assays in a small volume.

The second approach takes advantage of tools developed in the field of "*Chimie douce*" typically applied for synthesizing metal nanoparticles, semiconductors or oxides. By analogy to biomineralization, in which minerals are induced to form within an isolated space (a cell or a cell compartment), reverse micelles have been used [94]. In these complex fluids, small compartments of supersaturated aqueous solutions are stabilized within an oil using a surfactant (for example (2-ethylhexyl)sulfosuccinate, AOT) A precipitation is then induced inside each of these nanoreactors (either by chemical reaction of the precursors or by changing the temperature), which leads to the synthesis of nanoparticles whose size and shape is determined by the size and shape of the micelle. Anisotropic particles were grown by the addition of salts and/or co-surfactants that changed the micelle from spherical into roughly rod-like shapes [95]. A further development involved controlling the interfacial activity of the reverse micelles so that the nanoparticle synthesis and their self-assembly was coupled to give superlattices of shape controlled nanoparticles [96]. Face growth kinetics could even be used to tune the shape of the particles when the structure of the material targeted was highly anisotropic [97].

The third and most recent approach is an extension of the thoroughly studied carbon nanotube growth mechanism, namely the use of a growth promoter that helps in directing the growth of a material in a highly anisotropic manner [98]. The idea is to use a growth promoter nanoparticle (the diameter of which will drive the diameter of the nanowire) that can form a liquid alloy with the nanowire material of interest (Fig. 19). A careful study of the phase diagram allows the specific composition to be determined and the synthesis temperature necessary to achieve simultaneously the coexistence of the liquid alloy and the solid nanowire material. The liquid alloy nanoparticles act as preferred sites for the adsorption/dissolution of new reactant. When this alloy becomes supersaturated, it also acts as the nucleation site for recrystallization, leading to the growth of a nanowire.

6.1.2 Properties

However, apart from the examples developed above, the study of the self-assembly, in relation to the mesogenic properties for these suspensions of nanotubes,

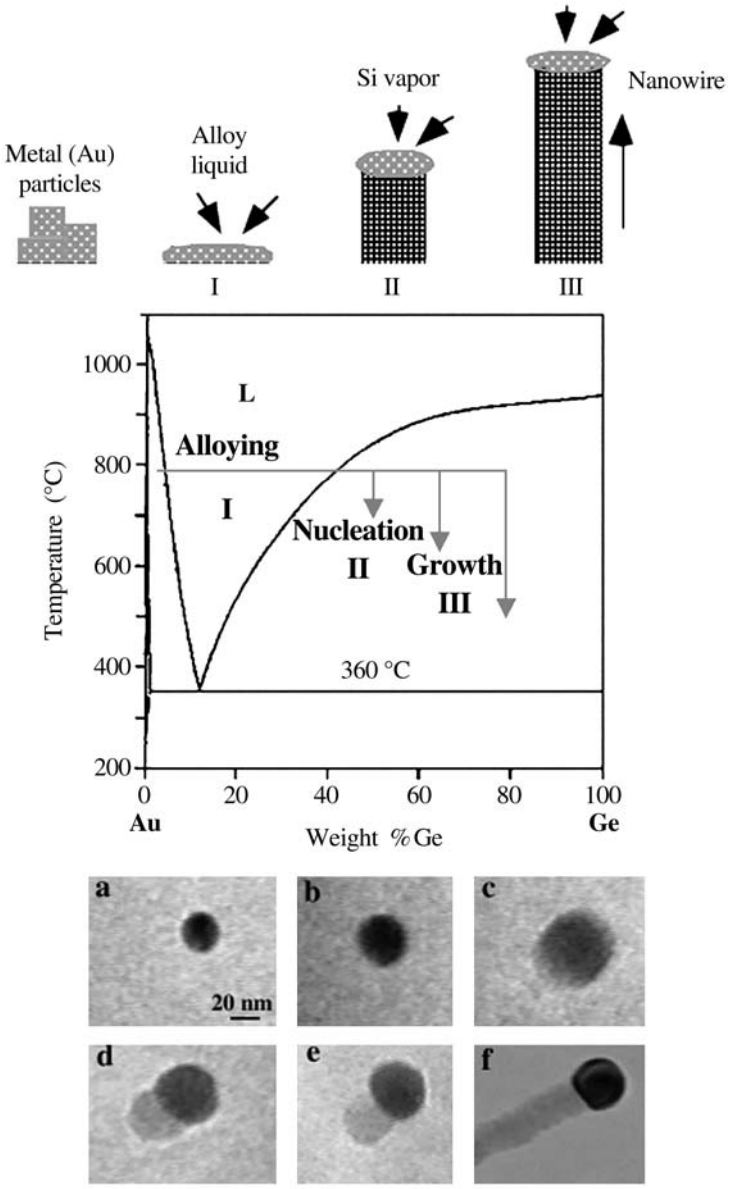

Fig. 19. Schematic illustration of vapor – liquid – solid nanowire growth mechanism including three stages: I) alloying, II) nucleation, and III) axial growth, as exemplified with the Au-Ge binary phase diagram (Au is a good solvent for the Ge nanowire growth because of the existence of the Au-Ge eutectic). This mechanism has been observed by in situ TEM that recorded images during the process of nanowire growth with: **a** Au nanoclusters in solid state at 500 °C; **b** alloying is initiated at 800 °C (Au now exists mostly in solid state); **c** liquid Au/Ge alloy; **d** nucleation of a Ge nanocrystal on the alloy surface; **e** Ge nanocrystal elongates with further Ge condensation; **f** eventually forms a wire. (Reprinted from [98b], copyright (2002) from John Wiley and Sons)

nanowires, and nanorods, is still in its infancy. A first challenge is to be able to reach a high enough concentration so as to obtain the Onsager nematic transition. We have seen that in the case of highly anisotropic charged particles, concentrations in the range of few percent by weight are usually necessary in order to observe such a transition. With much lower aspect ratio particles, such as nanorods or with uncharged moieties such as nanotubes, much higher concentrations are required. Also, many of these colloids are often too bulky and therefore do not form stable concentrated colloidal suspensions on their own. In most cases studied up to now, this problem has been overcome by stabilization of the suspension using either surfactants or by wrapping the colloids within a polymer therefore allowing highly concentrated suspensions to be obtained.

Another difficulty is that often only very small amounts of these anisotropic moieties can be synthesized at a time, limiting the study of the self-assembly properties to transmission electron microscopy analysis [135]. This makes it difficult to study in detail the phase diagram in concentration, usually a fairly sample consuming process. However, different approaches are currently being devised that give a taste of the huge potential that the self-assembly of these nanowires and nanorods can lead to.

A first way to circumvent the problem is to study the self-assembly of these anisotropic moieties within a 2-D Langmuir-Blodgett film. This was recently illustrated by P. Yang and co-workers using suspensions of $BaCrO_4$ nanorods synthesized by the reverse micelle approach [157]. Langmuir-Blodgett films obtained on the water surface and collected on a TEM grid display typical 2-D nematic and smectic organizations, and their topological defects. In Yang's report, a 2-D smectic to 3-D nematic transition is briefly mentioned that gives an insight into the bulk properties of such nanorods. However, as always in the case of TEM studies, it is difficult to determine exactly the role of drying. Note that in a related set of experiments, although the film was deposited by dip coating (directly from the bulk of the solution), the self-assembly properties of the carbon nanotubes bundles [99] allow the formation of fairly well oriented and therefore birefringent films of bundles. Such self-assembly of carbon nanotubes into a structure highly reminiscent of a nematic mesophase has been long awaited and discussed in meetings. Some alignment successes have even been reported when one combines nanotubes with some other liquid crystals, either lyotropic [100] or thermotropic [101]. Based upon our calculation using the Onsager model and our trials, in the case of bulk suspensions of neutral carbon nanotubes, we think that what has precluded the observation of a transition similar to what has been reported in the case of $Li_2Mo_6Se_6$ nanowire, imogolite or $NaNb_2PS_{10}$ nanotubes has been that the isotropic-nematic critical concentration is still higher than the highest concentration yet obtained. In the Zhou and co-workers' report, nanotube bundles have been shortened using a strong etching solution. The consequence is that the nanotubes are probably much more charged than the neutral pristine ones (due to the addition of carboxylic groups), which is known to decrease the critical transition concentration. We therefore expect for these suspensions that the pH of the solution should have a dramatic effect on the self-assembly properties reported.

Another method that has been developed for rapid screening of organic complex fluid phase diagrams consists of studying the drying of a suspension within

a capillary tube, directly on the beamline of a synchrotron. It is not an easy method for the quantitative determination of phase diagrams, but one may determine some phase transitions. Unfortunately, thermodynamic equilibrium is not usually reached and therefore this technique cannot be recommended.

Finally, a study of fairly monodisperse CdSe semiconducting nanorods functionalized with amphiphilic molecules in a suspension of cyclohexane has recently been published that shows preliminary results indicative of a typical nematic behavior [102]. Note that these nanorods have been synthesized by the pyrolysis of organometallic precursors of Cd and Se in hot surfactant mixture allowing a good control of the aspect ratio. This state of the art particle size and shape control method should allow one to customize accurately their semiconducting properties.

6.2 Use of MLC for the Structure Determination of Biomolecules by NMR

The first reported use of the mesogenic properties of MLC did not arise where one could have first expected it, i.e., liquid crystal displays, but in NMR. The classic NMR strategy for determining the conformation of a biomolecule [103] involves exploiting the combination of the scalar coupling, ^3J, to obtain dihedral angle information and the ^{1}H-^{1}H dipolar cross-relaxation rate, that has a $(1/r^6)$ dependence, where r is the internuclear distance. The limitation of this approach is that only short-range structural information is obtained (a few bonds for the scalar coupling and distances inferior to 5 Å for the relaxation). As a consequence, if only few constraints per nucleus can be detected (e.g., multi-domain proteins, oligosaccharides, or oligonucleotides), the accumulation of errors can lead to an imprecise overall structure. In order to circumvent this problem, a different approach has recently been proposed using, in addition, structural data that are defined relative to an absolute molecular frame [104, 105]. Particularly interesting are methods that exploit residual dipolar couplings [105, 106]. However, as dipolar couplings are almost averaged to zero (tenths of Hz) because of the almost isotropic overall tumbling of the solute molecule, it is therefore necessary to make this tumbling motion more anisotropic. This can be achieved by replacement of the aqueous phase by an anisotropic medium such as a magnetically oriented mesophase [106]. As a consequence new couplings, D, add to the usual scalar couplings, J, to split the signals by a few Hz. By using pairs of spins separated by well known distances (any C-H or N-H bond) one can finally extract more precise and longer range structural information.

A few organic/biological liquid crystals (LC) have been used successfully for this purpose: surfactant-based bicelles, purple membranes, phages, and cellulose microcrystals [107]. We recently proposed using MLC to generate an anisotropic medium. Their inherent advantages are numerous: (i) some MLCs can be easily aligned when a magnetic field is applied, using only very small amounts of mineral materials (1–3 wt%, to be compared with 5–30% for bicelles, 10% for purple membranes, 5% for phages, and 8% for cellulose); (ii) these MLCs, which are sometimes formed using polar solvents other than water, present nematic phases that are stable on a very long time scale (few years) and over

a wide temperature range (the liquid state temperature range of the solvent), in stark contrast with the organic LC systems whose stability is often an experimental problem for this type of NMR method [108]; (iii) the dissolved biomolecule can simply be recovered after the experiment by flocculation of the mineral colloid; (iv) finally, the absence of ^{1}H and ^{13}C nuclei renders isotope labeling of the studied molecule unnecessary, whereas, in the case of organic liquid crystals, the NMR signal is strongly dominated by the liquid crystal resonances due to the high ratio of LC molecules to biomolecules. This is obviously a major advantage especially for systems such as oligosaccharides or oligonucleotides for which labeling is chemically challenging and particularly expensive.

We therefore demonstrated the potential of such MLC for NMR structural characterization by reporting residual C-H dipolar couplings observed for nonlabeled saccharide containing the Lewis^{X} motif of various flexibility dissolved in aqueous suspension of V_2O_5 [109], as well as $H_3Sb_3P_3O_{14}$ [61, 110, 111].

6.3
Use of Flow Alignment and Pretransitional Effect Toward Applications

We have seen that it can be difficult to reach the critical concentration required to observe an isotropic-anisotropic transition because concentrated suspensions of colloids are not always stable. However, orientation of flexible polymers as well as of anisotropic particles in suspension can be induced by flow, a phenomenon that has long been observed, reported, and studied. This phenomenon is especially strong when a pretransitional effect exists, which can be easily observed by the naked eye on a sample that is shaken between crossed polarizers (see for example the section on clays). In these systems, birefringence is induced via mechanical forces, like the shear stresses in a laminar flow ("Maxwell-dynamo-optic effect").

One can therefore take advantage of this alignment effect when anisotropic materials are desired. In a first example, the mesomorphic properties of $Li_2Mo_6Se_6$ that we had previously demonstrated were used to synthesize: (i) highly oriented conducting thin films by spin coating the pure material (after solvent evaporation); (ii) oriented composites by extrusion [112].

Another example comes from the fact that up to recently one could not store beer in plastic bottles because gas diffusion (in and out) through the bottle walls was too large. Composites have now been developed by dispersing clay particles within a polymer. The particles are aligned by flow during extrusion, parallel to the bottle walls. Because of this orientation, the clay particles can play a barrier role and drastically reduce gas diffusion. The charge of the clay also allowed improvements of the mechanical properties of these composites materials [113]. Highly oriented extruded polymer-carbon nanotube composites have been obtained using flow orientation [114] that show very anisotropic properties, including electrical conductivity (with high conductivity only along the axis of extrusion). Such anisotropic conductivity can be useful for some applications but not for the conducting composites used in the new generation of reversible fuses that are widely employed nowadays by the semiconducting and electronic industry [115].

More recently, the flow alignment of suspensions of nanowires has been combined with microfluidic technology [116]. In this development, suspensions of nanowires/nanotubes are flowed within microchannels formed in a PDMS mold and deposited on a silicon wafer substrate (Fig. 20a,b). This allows parallel arrays of NW aligned along the flow direction when the mold is removed to be obtained. Multiply crossed NW arrays can then be built by changing the flow direction sequentially by iterating this process using a succession of molds with channels oriented along different axes (Fig. 20b).

6.4 Composites Materials

We have seen that only in a few cases have some composites materials based on MLC been made. Out of those only in the case of $Li_2Mo_6Se_6$ was the mesogenic

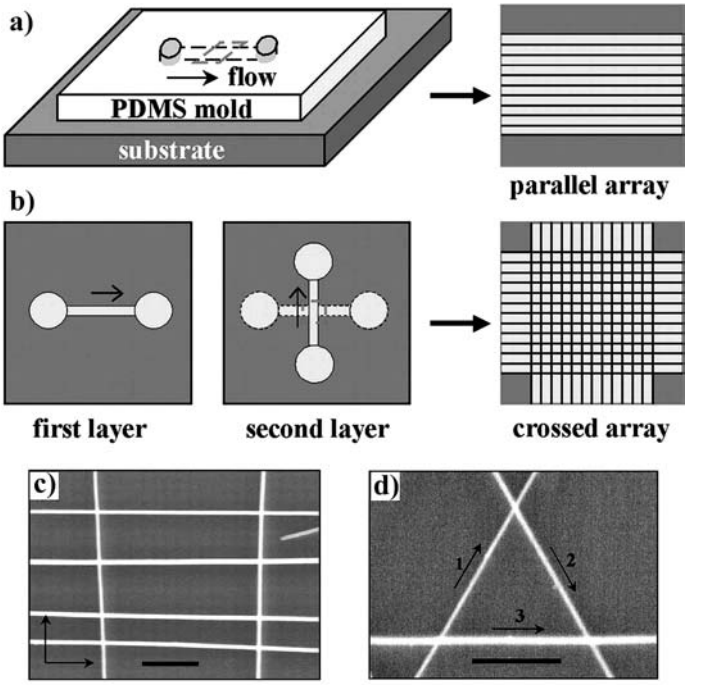

Fig. 20a–d. Schematic of fluidic channel structures for flow assembly and layer-by-layer assembly of crossed NW arrays: **a** NW assembly is carried out by controlling the flow of a NW suspension inside the channel (made from the mold-substrate assembly) – arrays of NWs are oriented parallel to the flow direction on the substrate (after removal of PDMS mold); **b** multiple crossed NW arrays are created by changing the flow direction sequentially in a layer-by-layer assembly process – typical SEM image of crossed arrays of NWs obtained in an assembly process (flow directions are highlighted by *arrows* in the images) comprising: **c** two sequential steps with orthogonal flow directions (InP NWs); **d** three sequential steps with 60° angles between flow directions (GaP NWs). The *scale bars* correspond to 500 nm in c and d. (Reprinted from [116], copyright 2001 American Association for the Advancement of Science)

property purposely used to organize the final material. We develop below two other recent examples.

6.4.1
Mesoporous Materials Based on MLC Templates

We recently showed that it is possible to synthesize a mesoporous composite material by direct assembly of anisotropic hollow objects [117]. In this study we used stable colloidal suspensions of well defined tubular structure made from the scrolling of the sheets themselves obtained by the exfoliation of the acid-exchange $K_4Nb_6O_{17}$ with tetra-(*n*-butyl)-ammonium hydroxide in water [118]. Detailed physicochemical studies of these colloidal suspensions at high concentration are still in progress [119]; however we thought they would be good candidates to make a silicate-nanotubule composite. The synthesis of our composite material (CMI-1) was adapted from the procedure of Goltsov et al. [120], but now using the organized nanotubules instead of an organic surfactant. Nitrogen physisorption experiments performed on this composite exhibited type IV behavior (hysteresis), typical of materials with large pores with restricted openings (ink bottle). This material has an N_2 Brunauer-Emmett-Teller (BET) surface area of 102 m^2/g, a mean pore size of 14.6 nm, and a single point (p/p0=0.965) pore volume of 0.32 cm^3/g. This mean pore size is in agreement with the mean inner diameter determined by TEM (15.5 Å). This use of mineral liquid crystals represents a new approach for the synthesis of composite porous materials and thus diversifies the types of objects that can be assembled in this way, offering the possibility of synthesizing new materials with a variety of properties.

This work has been further developed using V_2O_5 nanoribbons instead of the $[Nb_6O_{17}^{4-}]_n$ nanotubules [121]. The use of a magnetic field during the condensation of the silicate framework allowed us to obtained centimeter sized single-domain monoliths in which the nematic mineral liquid crystals are well aligned. Total removal of the MLC can also easily be achieved leaving transparent mesoporous birefringent silica with complete retention of the magnetically aligned channels director, even for centimeter sized samples.

6.4.2
Hybrid Organic-Inorganic Solar Cells

In a recent publication, Alivisatos and co-workers reported the making of hybrid nanorods-polymer solar cells and their properties [122]. These solar cells were made by spin casting of a solution of both poly(3-hexylthiophene) (hole acceptor) and CdSe nanorods (electron acceptor) onto indium tin oxide glass substrates coated with poly(ethylene dioxythiophene) doped with polystyrene sulfonic acid and aluminum as a top contact. Nanorods have been used in composites so as to improve the carrier mobility. Indeed, the latter can be high for some inorganic semiconductors, but it is typically extremely low for conjugated polymers [123]. The use of the nanorods supplies an interface for the charge transfer as well as a direct path for electrical transport. Also, because of their anisotropy, self-assembly of these nanorods is observed by electron microscopy. It shows

that the nanorods are partially aligned perpendicular to the substrate plane. The orientation of the nanorods as a function of their aspect ratio is predicted to play a crucial role in the properties of these new devices, as it should have a strong impact on the formation of percolation pathways for electron transport.

6.5 Hybrid Bio-Mineral Mesogens

A superb liquid crystal system was recently created by Belcher and co-workers that allowed them to produced a highly ordered composite material from genetically engineered M13 bacteriophage and zinc sulfide (ZnS) nanocrystals [124]. The mesogenic properties of the bacteriophage [125], which was selected for its specific recognition for ZnS crystal surfaces [126] (Fig. 21), were used to trigger the self-assembly. Indeed, bacteriophages were coupled with ZnS solution precursors and spontaneously evolved into a self-supporting hybrid film material that was ordered both at the nanoscale and at the micrometer scale and which was continuous over a centimeter length scale.

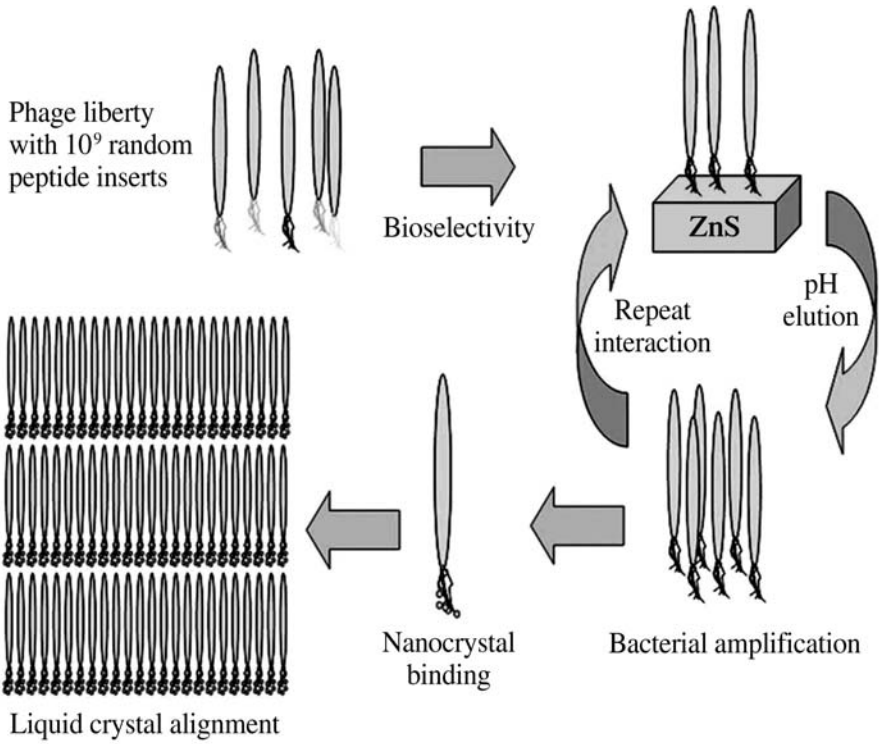

Fig. 21. Schematic diagram of the process used to generate nanocrystal alignment by the phage display method. (Reprinted with permission from [124], copyright 2000, American Association for the Advancement of Science)

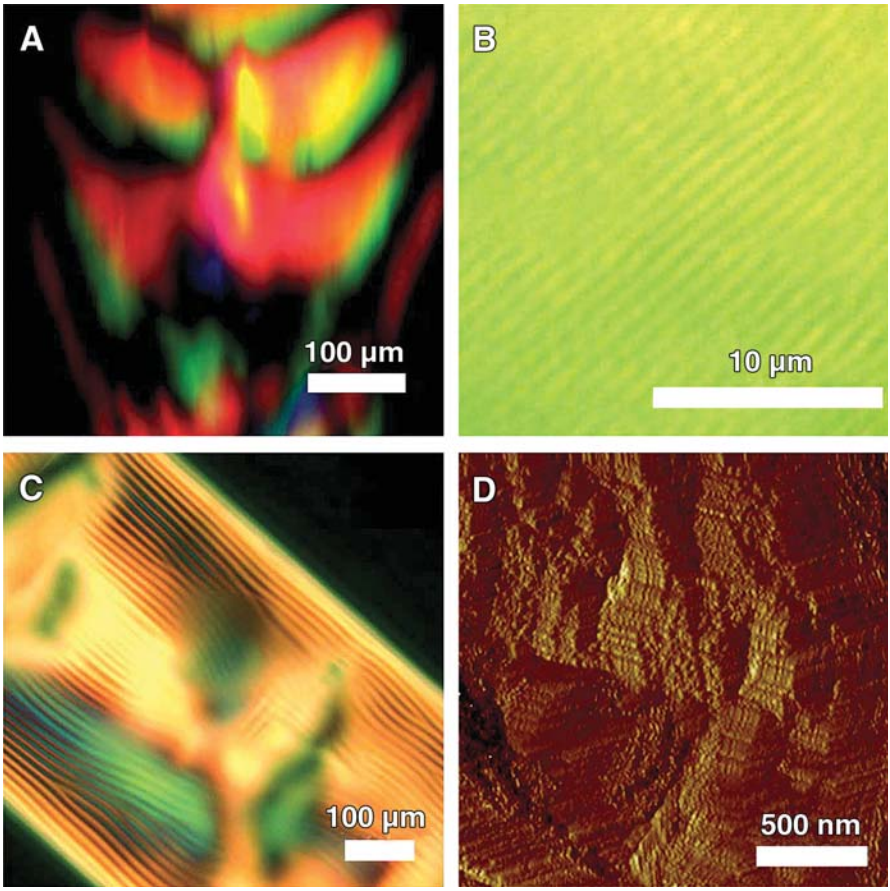

Fig. 22A–D. Characterization of the liquid crystalline suspensions of A7 phage-ZnS nanocrystals (A7-ZnS) and cast film: **A** POM texture of a suspension of A7-ZnS (127 mg/ml); **B, C** their constructive and destructive interference patterns generated from parallel aligned smectic layers when observed using a differential interference contrast filter; **D** texture of the cholesteric phase of an A7-ZnS suspension (76 mg/ml). (Reprinted with permission from [124], copyright 2000, American Association for the Advancement of Science)

In addition, the liquid crystalline phase behavior of these suspensions could be controlled by solvent concentration as well as by the use of a magnetic field. These suspensions and films observed by optical microscopy showed textures indicative of the smectic and cholesteric structure of the hybrid systems (Fig. 22).

7 Perspectives

Let us here briefly discuss a few guidelines useful for the search of new mineral liquid crystalline suspensions. This discussion tries to summarize the subtle balance between excluded volume interactions, electrostatic repulsions, and Van der Waals attractions that is needed to stabilize the nematic phase with respect to the isotropic one and flocculation or recrystallization.

An obvious criterion is that the mineral moieties of interest have to be able to be dispersed in a suitable solvent in large enough concentrations. We have seen several examples of how this can be achieved by exfoliation or by direct self-assembly from molecular precursors. This dispersion step is probably one of the most delicate points to fulfill.

Another related criterion is that the colloidal moieties should be as anisotropic as possible. This can be quantitatively predicted in the frame of the Onsager model. The volume fraction at which nematic ordering occurs is $\Phi \approx 4D/L$, which is 40% in the case of rods of aspect ratio 10 interacting through a purely hard-core potential. This is still quite a large volume fraction. In contrast, rods of aspect ratio 100 will order at a much more reasonable value of 4%. Moreover, both theory and numerical simulations show that particles of aspect ratio smaller than 3–4 never order in a nematic phase whatever their volume fraction. These orders of magnitude illustrate the need for fairly anisotropic moieties.

A parameter that cannot be over looked is the dispersity in size of the particles. Indeed, polydispersity usually prevents long range positional ordering. For example, it is crucial in order to obtain (i) smectic phases to have nanoparticles of fairly homogeneous length and (ii) hexagonal phases to have nanoparticles with diameters as monodisperse as possible.

The charge of the building blocks within mineral liquid crystalline suspensions should also be considered in detail since electrostatic repulsions play two important roles. First, these interactions often ensure colloidal stability against Van der Waals attractions. Second, the existence of clouds of counter-ions increase the effective volume fraction of anisotropic moieties in suspension, which helps to attain the phase transition threshold. Moreover, there is a large entropy gain associated with the release of the counter-ions in solution, which stabilizes the nematic suspension. Therefore, charged moieties are better candidates. However, in the case of neutral moieties, grafting with a polymer layer seems to be an efficient way of preventing particle aggregation.

Flexibility of the moieties is another important parameter because it was recently shown that flexible objects require larger volume fractions to undergo nematic ordering. Flexibility also reduces the nematic order parameter at the transition. Intuitively, very flexible mineral polymers should not show any orientational order at rest, but may display a strong flow birefringence. Thus, any soluble system where the structural unit in the solid state is anisotropic may not necessarily be a lyotropic liquid crystal. For example, in solution a polymer is much less constrained than in the solid state, and hence one must consider the elastic properties of the polymer chain and whether the anisotropic units still exist in solution. As shown recently for the case of the complex fluid with a min-

eral core based upon the 1-D polyelectrolyte $^{1}_{\infty}[MPS_4]^-$ (M=Ni, Pd) dissolved in DMF [6], the polymer chain is highly flexible and may even, depending upon the metal M and the temperature, fragment and lose its complex fluid properties. High flexibility does not however preclude self-assembly when folding of the polymer leading to unexpected superstructures [34].

We have only described here the mineral mesophases that have been fully and unambiguously characterized. This review article is therefore not exhaustive. Other less well-documented examples can be found in the literature, in particular in another review article [127, 128]. Nevertheless, the diversity of examples described here should draw the attention of the reader to the fact that suspensions based on anisotropic structural units may be liquid crystalline, a feature that could be used to obtain a better understanding/optimization of materials synthesis and processing conditions. Thus, the existence of a nematic domain in the phase diagram together with the possibility of growing reproducibly oriented single domains on the centimeter scale could be used, for instance, in the field of pillared materials to produce better structured materials.

The main interest of mesophases based on mineral moieties is, in contrast to their organic counterparts, that they can be electron rich and so have enhanced electrical, optical, and magnetic properties. In addition, mineral moieties are thermally very stable. Thus, combined with their typically very wide range of temperature stability of mesomorphic organization, it can be envisaged that they can be used for applications under extreme conditions. Another important and common asset of these MLC is their very low cost since some of them can even be found in a natural form. This will allow their use for massive material production.

Finally, since MLC are based on anisotropic nanosystems, the understanding of their collective properties, either pre- or post-transitional, is of prime importance to allow their manipulation and therefore for the development of applications in the field of nanotechnology.

Acknowledgements. We are deeply indebted to many colleagues for instructive discussions and to our coworkers whose listing would be too long. However, we particularly wish to express our gratitude to Patrick Batail and Jacques Livage who have persistently supported us in this new avenue of research, to our PhD students, Olivier Pelletier, Franck Camerel, and Bruno Lemaire as well as to H.N.W. Lekkerkerker and L.M. Bull for their critical review of the manuscript. Finally, we would like to thank Wiley-VCH Verlag GmbH & Co. who kindly granted us permission to use in this article parts of our previous review article [4b], copyright 2000

References

1. De Gennes PG, Prost J (1995) The physics of liquid crystals. Clarendon Press, Oxford
2. Tschierske C (1998) J Mater Chem 8:1485
3. Demus D, Goodby JW, Gray GW, Spiess HW, Vill V (eds) (1998) Handbook of liquid crystals. Wiley, Weinheim
4. a) Davidson P, Batail P, Gabriel JCP, Livage J, Sanchez C, Bourgaux C (1997) Prog Polym Sc 22:913; b) Gabriel JCP, Davidson P (2000) Adv Mater 12:9
5. Gabriel JCP, Uriel S, Boubekeur K, Batail P (2001) Chem Rev 101:2037

6. Sayettat J, Bull LM, Gabriel JCP, Jobic S, Camerel F, Marie AM, Fourmigué M, Batail P, Brec R, Inglebert RL (1998) Angew Chem Int Ed 37:1711
7. Oriol L, Serrano JL (1995) Adv Mater 7:348
8. Zocher H (1925) Z Anorg Allg Chem 147:91
9. Langmuir I (1938) J Chem Phys 6:873
10. Onsager L (1949) Ann NY Acad Sci 51:627
11. See, for instance, Samborski A, Evans GT, Mason CP, Allen MP (1994) Mol Phys 81:263
12. Guinier A, Fournet G (1955) Small angle scattering of X-rays. Wiley, New York
13. Synthesis of $M_2Mo_6Se_6$: a) M=Tl. In: Potel M, Chevrel R, Sergent M (1980) Acta Cryst B 36:1545; b) (M=Li, Na, K, Rb, Cs) Tarascon JM, Hull GW, DiSalvo FJ (1984) Mater Res Bull 19:915
14. Most members of the family, $M_2Mo_6Y_6$ (M=Na, In, K, Rb, Cs, Tl, Y=chalcogen), are pseudo-one-dimensional metals with even a superconductor at 3 K with $Tl_2Mo_6Se_6$: a) Armici JC, Decroux M, Fisher Ø, Potel M, Chevrel R, Sergent M (1980) Solid State Comm 33:607; b) Potel M, Chevrel R, Sergent M, Armici JC, Decroux M, Fisher Ø (1980) J Solid State Chem 35:286
15. Tarascon JM, DiSalvo FJ, Chen CH, Carrol PJ, Walsh M, Rupp L (1985) J Solid State Chem 58:290
16. Gabriel JCP (1993) PhD Thesis, University Paris XI, Orsay
17. a) Davidson P, Gabriel JC, Levelut AM, Batail P (1993) Europhys Lett 21:317; b) Davidson P, Gabriel JC, Levelut AM, Batail P (1993) Adv Mater 5:665
18. Fuhrer MS, Nygard J, Shih L, Forero M, Yoon Y, Mazzoni MSC, Choi H, Ihm J, Louie SG, Zettl A, McEuen PL (2000) Science 288:494
19. Messer B, Song JH, Huang M, Wu YY, Kim F, Yang PD (2000) Adv Mater 12:1526
20. Song JH, Messer B, Wu YY, Kind H, Yang PD (2001) J Am Chem Soc 123:9714–9715
21. Venkataraman L, Lieber CM (1999) Phys Rev Lett 83:5334
22. Bronger W, Müller P (1984) J Less Comm Met 100:241
23. Lu YJ, Ibers JA (1993) Comments Inorg Chem 14:229
24. For example, this was observed in the case of the series $Na_{2-x}Li_xMo_6Se_6$ (x=0–2) [15]
25. a) Farmer C, Fraser AR, Tait JM (1977) Chem Comm 462; b) Wada S-I, Eto A, Wada K (1979) J Soil Sci 30:347; c) Wada S-I (1987) Clays Clay Miner 35:379
26. Barett SM, Budd PM, Price C (1991) Eur Polym J 27:609; d) US Pats 4,252,779 and 4,241,035
27. Koenderink GH, Kluijtmans SGJM, Philise AP (1999) J Colloid Interface Sci 216:429
28. In the case of synthetic Imogolite, it seems that the diameter of the cylinder is 28 Å, slightly more that the natural one
29. a) Kajiwara K, Donkai N, Hiragi Y, Inagaki H (1986) Makromol Chem 187:2883; b) Kajiwara K, Donkai N, Fujiyoshi Y, Inagaki H (1986) Makromol Chem 187:2895; c) Donkai N, Kajiwara K, Schmidt M, Miyamoto T (1993) Makromol Chem Rapid Comm 14:611
30. Donkai N, Hoshino H, Kajiwara K, Miyamoto T (1993) Makromol Chem 194:559
31. a) Livolant F, Leforestier A (1996) Prog Polym Sc 21:1115; b) Giraud-Guille MM (1998) Curr Opin Solid State Mater Sci 3:221
32. a) Hoshino H, Yamana M, Donkai N, Sinigerski V, Kajiwara K, Miyamoto T, Inagaki H (1992) Polym Bull 28:607; b) Hoshino H, Ito T, Donkai N, Urakawa H, Kajiwara K (1992) Polym Bull 29:453
33. Ramos L, Molino F, Porte G (2000) Langmuir 16:5846
34. Camerel F, Gabriel JCP, Davidson P, Schmutz M, Gulik-Krzywicki T, Lemaire B, Bourgaux C, Batail P (2002) Nanoletters 2:403
35. Livage J (1991) Chem Mater 3:578
36. Bailey JK, Nagase T, Pozarnsky GA, MeCartney ML (1990) Mat Res Soc Symp Proc 180:759; b) Pozarnsky GA, McCormick AV (1994) Chem Mater 6:380; c) Livage J (1998) Coord Chem Rev 178/180:999; d) Pelletier O, Davidson P, Bourgaux C, Coulon C, Regnault S, Livage J (2000) Langmuir 16:5295

37. a) Davidson P, Garreau A, Livage J (1994) Liq Cryst 16:905; b) Davidson P, Bourgaux C, Schoutteten L, Sergot P, Williams C, Livage J (1995) Phys II (France) 5:1577; c) Pelletier O, Bourgaux C, Diat O, Davidson P, Livage J (2000) Eur Phys J E 2:191
38. Pelletier O, Bourgaux C, Diat O, Davidson P, Livage J (1999) Eur Phys J B 12:541
39. Commeinhes X, Davidson P, Bourgaux C, Livage J (1997) Adv Mater 9:900
40. Panar M, Beste LF (1977) Macromolecules 10:1401; b) Sridhar CG, Hines WA, Samulski ET (1974) J Chem Phys 61:947
41. Srajer G, Fraden S, Meyer RB (1989) Phys Rev A 39:4828
42. Davidson P, Petermann D, Levelut AM (1995) J Phys II (France) 5:113
43. Pelletier O, Davidson P, Bourgaux C, Livage J (1999) Europhys Lett 48:53
44. Pelletier O, Sotta P, Davidson P (1999) J Phys Chem B 103:5427
45. Lamarque-Forget S, Pelletier O, Dozov I, Davidson P, Martinot-Lagarde P, Livage J (2000) Adv Mater 12:1267
46. Van Olphen H (1977) An introduction to clay colloid chemistry. Wiley, New York
47. a) Burger J, Sourieau P, Combarnous M (1985) Thermal methods of oil recovery. Technip, Paris; b) Pinnavaia TJ (1983) Nature 220:365; c) Kojima Y, Usuki A, Kawasumi M, Okada A, Kurauchi T, Kagimaito O, Kaji K (1995) J Polym Sci B 33:1039
48. EmersonWW (1956) Nature 178:1248
49. a) Mourchid A, Delville A, Lambard J, Lécolier E, Levitz P, (1995) Langmuir 11:1942; b) Mourchid A, Lécolier E, Van Damme H, Levitz P (1998) Langmuir 14:4718; Pignon F, Piau JM, Magnin A (1996) Phys Rev Lett 76:4857; c) Pignon F, Magnin A, Piau JM (1997) Phys Rev Lett 79:4689; d) Pignon F, Magnin A, Piau JM, Cabane B, Lindner P, Diat O (1997) Phys Rev E 56:3281; e) Bonn D, Tanaka H, Wegdam G, Kellay H, Meunier J (1998) Europhys Lett 45:52; f) Bonn D, Kellay H, Tanaka H, Wegdam G, Meunier J (1999) Langmuir 15:7534
50. Gabriel JCP, Sanchez C, Davidson P (1996) J Phys Chem 100:11,139
51. a) Forsyth PA, Marcelja JS, Mitchell DJ, Ninham BW (1978) Adv Colloid Interface Sci 9:37; b) Eppenga R, Frenkel D (1984) Mol Phys 52:1303; c) Frenkel D (1989) Liq Cryst 5:929
52. Lemaire BJ, Panine P, Gabriel J-CP, Davidson P (2002) Europhys Lett (in press)
53. Morvan M, Espinat D, Lambard J, Zemb T (1994) Colloid Surf A 82:193
54. Forsyth PA, Marcelja JS, Mitchell DJ, Ninham BW (1978) Adv Colloid Interface Sci 9:37
55. Mourchid A, Levitz P (1998) Phys Rev E 57:R4887 and references cited therein
56. Levitz P, Lécolier E, Mourchid A, Delville A, Lyonnard S (2000) Europhys Lett 49:672
57. a) Saunders JM, Goodwin JW, Richardson RM, Vincent B (1999) J Phys Chem B, 103:9211; b) Ramsay JDF, Lindner P (1993) J Chem Soc Faraday Trans, 89:4207; c) Ramsay JDF, Swanton SW, Bunce J (1990) J Chem Soc Faraday Trans 86:3919; d) DiMasi E, Fossum JO, Gog T, Venkataraman C (2001) Phys Rev E, 64:061704; e) Porion P, Al Mukhtar M, Faugère AM, van der Maarel JRC, Delville A (2001) J Phys Chem B 105:10505
58. Bihannic I, Michot LJ, Lartiges BS, Vantelon D, Labille J, Thomas F, Susini J, Salomé M, Fyard B (2001) Langmuir 17:4144
59. Cousin F, Cabuil V, Levitz P (2002) Langmuir 18:1466
60. A new study of the salt-induced ordering in lamellar colloids appeared while this paper was in press: Rowan DG, Hansen JP (2002) Langmuir 18:2063–2068
61. Gabriel JCP, Camerel F, Lemaire BJ, Desvaux H, Davidson P, Batail P (2001) Nature 413:504
62. Piffard Y, Verbaere A, Lachgard A, Deniard-Courant S, Tournoux M (1986) Rev Chim Gen 23:766
63. Zocher H, Torök C (1960) Kolloid Zeit170:140; b) Zocher H, Torök C (1960) Kolloid Zeit 173:1; c) Zocher H, Torök C (1962) Kolloid Zeit 180:41
64. Bugosh J (1961) J Phys Chem 65:1789
65. a) Buining PA, Pathmamanoharan C, Jansen JBH, Lekkerkerker HNW (1991) J Ceram Soc 74:1303; b) Buining PA, Philipse AP, Lekkerkerker HNW (1994) Langmuir 10:2106; c) van Bruggen MPB, Donker M, Lekkerkerker HNW, Hugues TL (1999) Colloid Surf 150:115; d) Buining PA, Veldhuizen YSJ, Pathmamanoharan C, Lekkerkerker HNW (1992) Colloid Surf 64:47; e) Buining PA, Lekkerkerker HNW (1993) J Phys Chem 97:11,510; f) Vroege GJ, Lekkerkerker HNW (1993) J Phys Chem 97:3601
66. van Bruggen MPB, Dhont JKG, Lekkerkerker HNW (1999) Macromolecules 32:2256

67. a) Deryagin BV, Landau L (1941) Acta Physicochim URSS 333:55; b) Verwey E, Overbeek JW (1948) Theory of the stability of lyophobic colloids. Elsevier, Amsterdam
68. Israelachvili JN (1991) Intermolecular and surface forces. Academic Press, London
69. Pelletier O, Davidson P, Bourgaux C, Livage J (1999) Progr Colloid Polym Sci 112:121
70. a) van Bruggen MPB, Lekkerkerker HNW, Dhont JKG (1997) Phys Rev E 56:4394; b) Wierenga AM, Philipse AP, Reitsma EM (1997) Langmuir 13:947; c) Wierenga AM, Philipse AP, Lekkerkerker HNW, Boger DV (1998) Langmuir 14:55; d) van Bruggen MPB, Lekkerkerker HNW, Maret G, Dhont JKG (1998) Phys Rev E 58:7668
71. Van der Kooij F, Lekkerkerker HNW (1998) J Phys Chem B 102:7829
72. Bates MA, Frenkel D (1999) J Chem Phys 110:6553
73. Chandrasekhar S, Sadashiva BK, Suresh KA (1977) Pramana 7:471
74. Brown ABD, Clarke SM, Rennie AR (1998) Langmuir 14:3129
75. Brown ABD, Ferrero C, Narayanan T, Rennie AR (1999) Eur Phys J B 11:481
76. Veerman JAC, Frenkel D (1992) Phys Rev A 45:5632
77. Brown ABD, Rennie AR (2000) Phys Rev E 62:851
78. van der Kooij FM, Kassapidou K, Lekkerkerker HNW (2000) Nature 406:868
79. van der Kooij FM, van der Beek D, Lekkerkerker HNW (2001) J Phys Chem B 105:1696
80. Wensink HH, Vroege GJ, Lekkerkerker HNW (2001) J Phys Chem B 105:10,610
81. van der Kooij FM, Lekkerkerker HNW (2000) Phys Rev Lett 84:781
82. Wensink HH, Vroege GJ, Lekkerkerker HNW (2001) J Chem Phys 115:7319
83. van der Kooij FM, Lekkerkerker HNW (2000) Langmuir 16:10,144
84. Zocher H, Jacobsohn K (1929) Kolloid Beih 28:167
85. Heller W (1935) Compt Rend 201:831; b) Heller W (1980) Polymer colloids II. Fitch E (ed) Plenum Press, New York, and references cited therein
86. a) Maeda Y, Hachisu S (1983) Colloids Surf 6:1; b) Maeda H, Maeda Y (1996) Langmuir 12:1446
87. Cornell RM, Schwertmann U (1996) The iron oxides. VCH, Weinheim
88. Lemaire BJ, Davidson P, Ferre J, Jamet JP, Panine P, Dozov I, Jolivet JP (2002) Phys Rev Lett 88:125,507
89. Iijima (1991) Nature 354:56
90. a) Ozin GA (1992) Adv Mater 4:612; b) Martin CR (1994) Science 266:1961; c) Martin CR (1996) Acc Chem Res 28:61
91. Wu CG, Bein T (1994) Science 266:1013
92. a) Piraux L, George JM, Despres JF, Leroy C, Ferain E, Legras R, Ounadjela K, Fert A (1994) Appl Phys Lett 65:2484; b) Fert A, Piraux L (1999) J Magn Magn Mater 200:338
93. a) Martin BR, Dermody DJ, Reiss BD, Fang MM, Lyon LA, Natan MJ, Mallouk TE (1999) Adv Mater 11:1021; b) Nicewarner-Pena SR, Freeman RG, Reiss BD, He L, Pena DJ, Walton ID, Cromer R, Keating CD, Natan MJ (2001) Science 294:137
94. Lisiedki I, Pileni MP (1993) JACS 115:3887
95. a) Tanori J, Pileni MP (1995) Adv Mater 7:862; b) Tanori J, Pileni MP (1997) Langmuir 13:639; c) Filankenbo, Pileni MP (2000) Appl Surf Science 164:260
96. Li M, Schnablegger H, Mann S (1999) Nature 402:393
97. Peng X, Manna L, Yang W, Wickham J, Scher E, Kadavanich A, Alivisatos AP (2000) Nature 404:59
98. a) Hu J, Odom TW, Lieber CM (1999) Acc Chem Res 32:435; b) Wu Y, Yan H, Huang M, Messer B, Song JH, Yang P (2002) Chem Eur J 8:1261
99. Shimoda H, Oh SJ, Geng HZ, Walker RJ, Zhang XB, McNeil LE, Zhou O (2002) Adv Mater 14:899
100. Vigolo B, Penicaud A, Coulon C, Sauder C, Pailler R, Journet C, Bernier P, Poulin P (2000) Science 290:1331
101. Lynch MD, Patrick DL (2002) Nanoletters (in press)
102. Li LS, Walda J, Manna L, Alivisatos AP (2002) Nano Lett 2:557
103. Wüthrich K (1986) NMR of proteins and nucleic acids. Wiley Interscience, New York
104. Tjandra N, Garrett DS, Gronenborn AM, Bax A, Clore GM (1997) Nat Struct Biol 4:443

105. Tjandra N, Omichinski JG, Gronenborn AM, Clore GM, Bax A (1997) Nat Struct Biol 4:732
106. Tjandra N, Bax A (1997) Science 278:1111
107. For a quick review: Prestegard JH, Kishore AI (2001) Curr Opin Chem Biol 5:584 and references therein
108. Losonczi JA, Prestegard JH (1998) J Biomol NMR 12:47
109. Desvaux H, Gabriel JCP, Berthault P, Camerel F (2001) Angew Chem Int Ed 40:373
110. Berthault P, Jeannerat D, Zhang Y, Camerel F, Alvarez-Salgado F, Boulard Y, Sinaÿ P, Gabriel JCP, Desvaux H (submitted)
111. See www graphical abstract that represent biomolecules within $H_3Sb_3P_3O_{14}$ sheets
112. a) Golden JH, DiSalvo FJ, Fréchet JMJ (1995) Chem Mater 7:232; b) Golden JH, DiSalvo FJ, Fréchet JMJ, Silcox J, Thomas M, Ellman J (1996) Science 273:782
113. Here are few examples of patents of composites based on a dispersed clay with enhanced mechanical or gas barrier properties: US4472538, US4739007, US4889885, US4894411, EP0352042, EP0398551, WO9304117, WO9304118, WO9311190, US5385776, US5514734, EP0358415
114. Vigolo B, Penicaud A, Coulon C, Sauder C, Pailler R, Journet C, Bernier P, Poulin P (2000) Science 290:1331
115. Chang J. Personnal communication
116. Huang Y, Duan X, Wei Q, Lieber CM (2001) Science 291:630
117. Camerel F, Gabriel JCP, Batail P (2002) Chem Comm 1926
118. Saupe GB, Waraksa CC, Kim HN, Han YJ, Kaschak DM, Skinner DM, Mallouk TE (2000) Chem Mater 12:1556
119. A nice optical study of this MLC ($K_4Nb_6O_{17}$ sols) appeared while this paper was in Press: Miyamoto N, Nakato T (2002) Adv Mater 14:1267
120. Goltsov YG, Matkovskaya LA, Smelaya ZV, Il'in VG (1999) Mendeleev Commun 241
121. a) Camerel F (2001) PhD Thesis, Nantes University, France; b) Camerel F, Gabriel JCP, Batail P (2002) In Press, Adv Funct Mater
122. Huynh WU, Dimer JJ, Alivisatos AP (2002) Science 295:2425
123. Borazano L, Carte SA, Scott JC, Malliaras GG, Brock PJ (1999) Appl Phys Lett 74:1132
124. Lee SW, Mao C, Flynn CE, Belcher AM (2002) Science 296:892
125. a) Dogic Z, Fraden S (1997) Phys Rev Lett 78:2417; b) Dogic Z, Fraden S (2000) Langmuir 16:7820; c) Lapointe J, Marvin DA (1973) Mol Cryst Liq Cryst 19:269; d) Issaenko A, Harris SA, Lubensky TC (1999) Phys Rev E 60:578
126. It has been shown recently that engineered viruses can recognize specific semiconductor surfaces using the method of selection by combinatorial phage display: Whaley R, English DS, Hu EL, Barbara PF, Belcher AM (2000) Nature 405:665
127. Sonin AS (1998) Colloid J 60:129
128. A report of a possible new MLC appeared while this manuscript was in press: Backov R, Morgan AN, Lane S, Perez-Cordero EE, Williams K, Meisel MW, Sanchez C, Talham DR (2002) Mol Cryst Liq Cryst 376:127
129. A review of oxidic nanotubes and nanorods has been published while this manuscript was in press: Patzke GR, Krumeich F, Nesper R (2002) Angew Chem Int Ed 41:2446
130. Here are few examples of reviews on the subject: a) Sinnott SB, Andrews R (2001) Crit Rev Solid State Mater Sciences 26:145; b) Rao CNR, Satishkumar BC, Govindaraj A, Nath M (2001) Chem Phys Chem 2:78; c) Rakov EG (2000) Uspekhi Khimii 69:41; d) Ajayan PM (1999) Chem Rev 99:1787
131. a) Zhang QM, Li Y, Xu DS, Gu ZN (2001) J Mater Sci Lett 20:925; b) Zhu JJ, Liao XH, Zhao XN, Chen HY (2001) Mater Lett 49:91; c) Lin SW, Yue J, Gedanken A (2001) Adv Mater 13:656; d) Jana NR, Gearheart L, Murphy CJ (2001) Chem Comm 2001:617; e) Bhattacharyya S, Saha SK, Chakravorty D (2000) Appl Phys Lett 77:3770; f) Kyoung M, Lee M (1999) Opt Commun 171:145; g) Link S, El-Sayed MA (1999) J Phys Chem B 103:8410; h) Sloan J, Wright DM, Woo HG, Bailey S, Brown G, York APE, Coleman KS, Hutchison JL, Green MLH (1999) Chem Comm 1999:699; i) Zhou Y, Yu SH, Cui XP, Wang CY, Chen ZY (1999) Chem Mater 11:545; j) Korgel BA, Fitzmaurice D (1998) Self-assembly of

silver nanocrystals into two-dimensional nanowire arrays. Adv Mat 10:661; k) Han YJ, Kim JM, Stucky GD (2000) Chem Mater 12:2068
132. a) Jana NR, Gearheart L, Murphy CJ (2001) J Phys Chem B 105:4065; b) Mbindyo JKN, Reiss BD, Martin BR, Keating CD, Natan MJ, Mallouk TE (2001) Adv Mat 13:249; c) Wang BL, Yin SY, Wang GH, Buldum A, Zhao JJ (2001) Phys Rev Lett 86:2046; d) Ramsperger U, Uchihashi T, Nejoh H (2001) Appl Phys Lett 78:85; e) Yu JS, Kim JY, Lee S, Mbindyo JKN, Martin BR, Mallouk TE (2000) Chem Comm 2000:2445
133. Nikoobakht, Wang ZL, El-Sayed MA (2000) J Phys Chem B 104:8635
134. a) Wang XF, Zhang LD, Zhang J, Shi HZ, Peng XS, Zheng MJ, Fang J, Chen JL, Gao BJ (2001) J Phys D 34:418; b) Choi SH, Wang KL, Leung MS, Stupian GW, Presser N, Morgan BA, Robertson RE, Abraham M, King EE, Tueling MB, Chung SW, Heath JR, Cho SL, Ketterson JB (2000) J Vac Sci Technol A 18:1326
135. Masuda H, Yanagishita T, Yasui K, Nishio K, Yagi I, Rao TN, Fujishima A (2001) Adv Mater 13:247
136. a) Henry Y, Ounadjela K, Piraux L, Dubois S, George JM, Duvail JL (2001) Eur Phys J B 20:35; b) Cao HQ, Xu Z, Sang H, Sheng D, Tie CY (2001) Adv Mater 13:121; c) Yang SG, Zhu H, Ni G, Yu DL, Tang SL, Du YW (2000) J Phys D Appl Phys 33:2388; d) Puntes VF, Krishnan KM, Alivisatos AP (2001) Science 291:2115
137. Ounadjela K, Ferre R, Louail L, George JM, Maurice JL, Piraux L, Dubois S (1997) J Appl Phys 81:5455
138. a) Molares MET, Buschmann V, Dobrev D, Neumann R, Scholz R, Schuchert IU, Vetter J (2001) Adv Mater 13:62; b) Peng LQ, Ju X, Wang SC, Xian DC, Chen H, He YJ (1999) Chin Phys Lett 16:126; c) Setlur AA, Lauerhaas JM, Dai JY, Chang RPH (1996) Appl Phys Lett 69:345; d) Peng LQ, Ju X, Wang SC, Xian DC, Chen H, He YJ (1999) Chin Phys Lett16:126
139. Park SJ, Kim S, Lee S, Khim ZG, Char K, Hyeon TJ (2000) Am Chem Soc 122:8581
140. Zhang YF, Tang YH, Wang N, Lee CS, Bello I, Lee ST (2000) Phys Rev B 61:4518
141. Tang CC, Fan SS, Li P, de la Chapelle ML, Dang HY (2001) J Cryst Growth 224:1171
142. Gu Q, Dang HY, Cao J, Zhao JH, Fan SS (2000) Appl Phys Lett 76:3020; b) Wang N, Tang YH, Zhang YF, Lee CS, Bello I, Lee ST (1999) Chem Phys Lett 299:237; c) Wang N, Tang YH, Zhang YF, Lee CS, Lee ST (1998) Phys Rev B 58(N24):R16024
143. a) Krumeich F, Muhr HJ, Niederberger M, Bieri F, Nesper R (2000) Z Anorg Allg Chem 626:2208; b) Reinoso JM, Muhr HJ, Krumeich F, Bieri F, Nesper R (2000) Helv Chim Acta 83:1724; c) Niederberger M, Muhr HJ, Krumeich F, Bieri F, Gunther D, Nesper R (2000) Chem Mater 12:1995; d) Muhr HJ, Krumeich F, Schonholzer UP, Bieri F, Niederberger M, Gauckler LJ, Nesper R (2000) Adv Mater 12:231; e) Millet P, Henry JY, Mila F, Galy J (1999) J Solid State Chem 147:67678; f) Krumeich F, Muhr HJ, Niederberger M, Bieri F, Schnyder B, Nesper R (1999) J Am Chem Soc 121(N36):8324; g) Spahr ME, Stoschitzki-Bitterli P, Nesper R, Haas O, Novak P (1999) J Electrochem Soc 146:278,083; h) Spahr ME, Bitterli P, Nesper R, Muller M, Krumeich F, Nissen HU (1998) Angew Chem Int Ed 37:1263; i) Pillai KS, Krumeich F, Muhr HJ, Niederberger M, Nesper R (2001) Solid State Ionics 141:185
144. Lakshmi BB, Patrissi CJ, Martin CR (1997) Chem Mater 9:2544
145. Satishku BC, Govindaraj A, Nath M, Rao CNR (2000) J Mater Chem 10:2115–2119
146. a) Zhang M, Bando Y, Wada K (2001) J Mater Res 16:1408; b) Kasuga T, Hiramatsu M, Hoson A, Sekino T, Niihara K (1998) Langmuir 14:3160–3163; c) Hoyer P (1996) Langmuir 12:1411; d) Seo DS, Lee JK, Kim H (2001) J Cryst Growth 229:428; e) Li XH, Zhang XG, Li HL (2001) Chem J Chin Univ 22:130; f) Zhang M, Bando Y, Wada K (2001) J Mater Sci Lett 20:167; g) Zhang SL, Zhou JF, Zhang ZJ, Du ZL, Vorontsov AV, Jin ZS (2000) Chin Sci Bull 45:1533; h) Khitrov G (2000) MRS Bull 25:3; i) Imai H, Takei Y, Shimizu K, Matsuda M, Hirashima H (1999) J Mater Chem 9:2971; j) Lei Y, Zhang LD, Fan JC (2001) Chem Phys Lett 338:231; k) Lei Y, Zhang LD (2001) J Mater Res 16:1138; l) Lei Y, Zhang LD, Meng GW, Li GH, Zhang XY, Liang CH, Chen W, Wang SX (2001) Appl Phys Lett 78:1125; m) Hulteen JC, Martin CR (1997) J Mater Chem 7:1075; n) Kobayashi S, Hanabusa K, Hamasaki N, Kimura M, Shirai H, Shinkai S (2000) Chem Mater 12:1523
147. Lakshmi BB, Dorhout PK, Martin CR (1997) Chem Mater 9:857
148. Zheng MJ, Li GH, Zhang XY, Huang SY, Lei Y, Zhang LD (2001) Chem Mater 13:3859

149. a) Pu L, Bao XM, Zou JP, Feng D (2001) Angew Chem Int Ed 40:1490; b) Zheng MJ, Zhang LD, Zhang XY, Zhang J, Li GH (2001) Chem Phys Lett 334:298
150. Zheng MJ, Zhang LD, Zhang XY, Zhang J, Li GH (2001) Chem Phys Lett 334(N4/6):298
151. a) Li Y, Cheng GS, Zhang LD (2000) J Mater Res 15:2305; b) Huang MH, Wu YY, Feick H, Tran N, Weber E, Yang PD(2001) Adv Mater 13:113; c) Kong YC, Yu DP, Zhang B, Fang W, Feng SQ (2001) Appl Phys Lett 78:407–409; d) Li Y, Cheng GS, Zhang LD (2000) J Mater Res 15:2305; e) Li Y, Meng GW, Zhang LD, Phillipp F (2000) Appl Phys Lett 76:2011
152. Tang CC, Fan SS, de la Chapelle ML, Li P (2001) Chem Phys Lett 333:12
153. a) Zhang M, Bando Y, Wada K, Kurashima K (1999) J Mater Sci Lett 18:1911; b) Chang HJ, Chen YF, Lin HP, Mou CY (2001) Appl Phys Lett 78:3791; c) Wang LZ, Tomura S, Ohashi F, Maeda M, Suzuki M, Inukai K (2001) J Mater Chem 11:1465; d) Wu XC, Song WH, Wang KY, Hu T, Zhao B, Sun YP, Du JJ (2001) Chem Phys Lett 336:53; e) Liu ZQ, Xie SS, Sun LF, Tang DS, Zhou WY, Wang CY, Liu W, Li YB, Zou XP, Wang G (2001) J Mater Res 16:683–686; f) Wang ZL, Gao RPP, Gole JL, Stout JD (2000) Adv Mater 12:1938; g) Harada M, Adachi M (2000) Adv Mater 12:839; h) Lin HP, Mou CY, Liu SB (2000) Adv Mater 12:103; i) Zhang M, Bando Y, Wada K, Kurashima K (1999) J Mater Sci Lett 18:1911; j) Adachi M, Harada T, Harada M (1999) Langmuir 15:7097; k) Zhang M, Bando Y, Wada K (2000) J Mater Res 15:387
154. Park GS, Choi WB, Kim JM, Choi YC, Lee YH, Lim CB (2000) J Cryst Growth 220:494
155. Wang WH, Zhan YJ, Wang GH (2001) Chem Comm 2001:727
156. Vayssieres L, Beermann N, Lindquist SE, Hagfeldt A (2001) Chem Mater 13:233
157. Kwan S, Kim F, Akana J, Yang PD (2001) Chem Comm 2001:447
158. Zhang YF, Tang YH, Duan XF, Zhang Y, Lee CS, Wang N, Bello I, Lee ST (2000) Chem Phys Lett 323:180
159. a) Remskar M, Mrzel A, Skraba Z, Jesih A, Ceh M, Demsar J, Stadelmann P, Levy F, Mihailovic D (2001) Science 292:479; b) Hsu WK, Chang BH, Zhu YQ, Han WQ, Terrones H, Terrones M, Grobert N, Cheetham AK, Kroto HW, Walton DRM (2000) J Am Chem Soc122:10155; c) Seifert G, Terrones H, Terrones M, Jungnickel G, Frauenheim T (2000) Phys Rev Lett 85:146; d) Margulis L, Dluzewski P, Feldman Y, Tenne R (1996) J Microsc 181:68; e) Zhang Q, Huang RB, Liu ZY, Zheng LS (1995) Chem J Chin Univ16:1624; f) Feldman Y, Wasserman E, Srolovitz DJ, Tenne R (1995) Science 267:222; g) Mastai Y, Homyonfer M, Gedanken A, Hodes G (1999) Adv Mater 11:1010
160. Nath M, Govindaraj A, Rao CNR (2001) Adv Mater 13:283; b) Remskar M, Skraba Z, Stadelmann P, Levy F (2000) Adv Mater 12:814; c) Remskar M, Skraba Z, Sanjines R, Levy F (1999) Surf Rev Lett 6:1283; d) Feldman Y, Frey GL, Homyonfer M, Lyakhovitskaya V, Margulis L, Cohen H, Hodes G, Hutchison JL, Tenne R (1996) J Am Chem Soc 118:5362
161. Homyonfer M, Alperson B, Rosenberg Y, Sapir L, Cohen SR, Hodes G, Tenne R (1997) J Am Chem Soc 119:2693
162. a) Zhu YQ, Hsu WK, Terrones H, Grobert N, Chang BH, Terrones M, Wei BQ, Kroto HW, Walton DRM, Boothroyd CB, Kinloch I, Chen GZ, Windle AH, Fray DJ (2000) J Mater Chem 10:2570; b) Rothschild A, Sloan J, Tenne R (2000) J Am Chem Soc 122(N21):5169; c) Zhu YQ, Hsu WK, Grobert N, Chang BH, Terrones M, Terrones H, Kroto HW, Walton DRM, Wei BQ (2000) Chem Mater 12:1190; d) Mackie EB, Galvan DH, Adem E, Talapatra S, Yang GL, Migone AD (2000) Adv Mater 12:495; e) Seifert G, Terrones H, Terrones M, Jungnickel G, Frauenheim T (2000) Solid State Commun 114:245; f) Rothschild A, Frey GL, Homyonfer M, Tenne R, Rappaport M (1999) Synthesis of bulk WS2 nanotube phases. Mater Res Innovations 3:145
163. Tsirlina T, Feldman Y, Homyonfer M, Sloan J, Hutchison JL, Tenne R (1998) Fuller Sci Technol 6:157
164. Zhu YQ, Hsu WK, Terrones M, Firth S, Grobert N, Clark RJH, Kroto HW, Walton DRM (2001) Chem Commun 2001:121
165. a) Hsu WK, Zhu YQ, Firth S, Terrones M, Terrones H, Trasobares S, Clark RJH, Kroto HW, Walton DRM (2001) Carbon 39:1107; b) Hsu WK, Zhu YQ, Boothroyd CB, Kinloch I, Trasobares S, Terrones H, Grobert N, Terrones M, Escudero R, Chen GZ, Colliex C, Windle AH, Fray DJ, Kroto HW, Walton DRM (2000) Chem Mater 12:3541

166. Nath M, Rao CNR (2001) J Am Chem Soc 123:4841
167. Zhang WX, Yang ZH, Zhan JH, Yang L, Yu WC, Zhou GE, Qian YT (2001) Mater Lett 47:367
168. Li W, Kalia RK, Vashishta P (1996) Phys Rev Lett 77:2241
169. a) Sapp SA, Lakshmi BB, Martin CR (1999) Adv Mater 11:402; b) Prieto AL, Sander MS, Martín-González MS, Gronsky R, Sands T, Stacy AM (2001) J Am Chem Soc 123:7160
170. a) Davidson P, Gabriel JC, Levelut AM, Batail P (1993) Nematic liquid crystalline mineral polymers. Adv Mater 5:665; b) Davidson P, Gabriel JC, Levelut AM, Batail P (1993) Europhys Lett 21:317; c) Messer B, Song JH, Yang PD (2000) J Am Chem Soc 122:10,232
171. a) Wang SH, Yang SH (2000) Adv Mater Opt Electron 10:39; b) Wang SH, Yang SH (2000) Chem Phys Lett 322:567
172. Dloczik L, Engelhardt R, Ernst K, Fiechter S, Sieber I, Konenkamp R (2001) App Phys Lett 78:3687
173. Xu DS, Xu YJ, Chen DP, Guo GL, Gui LL, Tang YQ (2000) Chem Phys Lett 325; b) Li Y, Xu DS, Zhang QM, Chen DP, Huang FZ, Xu YJ, Guo GL, Gu ZN (1999) Chem Mater 11:3433
174. Shen CM, Zhang XG, Ki HL (2001) Mater Sci Eng A 303:19
175. a) Rubio A, Corkill JL, Cohen ML (1994) Phys Rev B 49:5081; b) Chopra NG, Luyken RJ, Cherrey K, Crespi VH, Cohen ML, Louie SG, Zettl A (1995) Science 269:966; c) Loiseau A, Willaime F, Demoncy N, Hug G, Pascard H (1996) Phys Rev Lett 76:4737; d) Suenaga K, Colliex C, Demoncy N, Loiseau A, Pascard H, Willaime F (1997) Science 278:653; e) Cumings J, Zettl A (2000) Chem Phys Lett 316:211
176. Shimizu Y, Moriyoshi Y, Komatsu S, Ikegami T, Ishigaki T, Sato T, Bando Y (1998) Thin Solid Films 316:178; b) Shimizu Y, Moriyoshi Y, Tanaka H, Komatsu S (1999) App Phys Lett 75:929
177. a) Han WQ, Bando Y, Kurashima K, Sato T (1998) Appl Phys Lett 73:3085; b) Han WQ, Bando Y, Kurashima K, Sato T (1999) Chem Phys Lett 299:368; c) Golberg D, Bando Y, Han W, Kurashima K, Sato T (1999) Chem Phys Lett 308:337; d) Han WQ, Redlich P, Ernst F, Ruhle M (1999) Chem Mater 11:3620; e) Golberg D, Bando Y, Bourgeois L, Kurashima K, Sato T (2000) Carbon 38:2017; f) Golberg D, Bando Y, Kurashima K, Sato T (2000) Chem Phys Lett 323:185
178. a) Chen Y, Gerald JF, Williams JS, Bulcock S (1999) Chem Phys Lett 299:260; b) Chen Y, Chadderton LT, FitzGerald J, Williams JS (1999) Appl Phys Lett 74:2960
179. Lourie OR, Jones CR, Bartlett BM, Gibbons PC, Ruoff RS, Buhro WE (2000) Chem Mater 12:1808
180. Terauchi M, Tanaka M, Suzuki K, Ogino A, Kimura K (2000) Chem Phys Lett 324:359
181. a) Li JY, Chen XL, Qiao ZY, Cao YG, He M, Xu T (2000) Appl Phys A 71:349; b) Chen CC, Yeh CC (2000) Adv Mater 12:738; c) Han WQ, Fan SS, Li QQ, Hu YD (1997) Science 277:1287; d) Chen et al. (2001) J Am Chem Soc123:2791; e) Li ZJ, Chen XL, Li HJ, Tu QY, Yang Z, Xu YP, Hu BQ (2001) Appl Phys A 72:629; f) He MQ, Minus I, Zhou PZ, Mohammed SN, Halpern JB, Jacobs R, Sarney WL, Salamanca-Riba L, Vispute RD (2000) Appl Phys Lett 77:3731; g) Chen XL, Li JY, Cao YG, Lan YC, Li H, He M, Wang CY, Zhang Z, Qiao ZY (2000) Adv Mater 12:1432; h) Tang CC, Fan SS, Dang HY, Li P, Liu YM (2000) Appl Phys Lett 77:1961; i) Peng HY, Zhou XT, Wang N, Zheng YF, Liao LS, Shi WS, Lee CS, Lee ST (2000) Chem Phys Lett 327:263; j) Cheng GS, Chen SH, Zhu XG, Mao YQ, Zhang LD (2000) Mater Sci Eng A 286:165; k) LilientalWeber Z, Chen Y, Ruvimov S, Washburn J (1997) Phys Rev Lett 79:2835; l) Li JY, Chen XL, Qiao ZY, Cao YG, Lan YC (2000) J Cryst Growth 213:408; m) Cheng GS, Zhang LD, Chen SH, Li Y, Li L, Zhu XG, Zhu Y, Fei GT, Mao YQ (2000) J Mater Res 15:347; n) Duan XF, Lieber CM (2000) J Am Chem Soc 122:188; o) Lee SM, Lee YH, Hwang YG, Elsner J, Porezag D, Frauenheim T (1999) Phys Rev B 60:7788; p) Zhu J, Fan S (1999) J Mater Res 14:1175; q) Lee SM, Lee YH, Hwang YG, Lee CJ (1999) J Korean Phys Soc 34:S253; r) Bedarev DA, Kogitskii SO, Lundin VV (1999) Tech Phys Lett 25:385
182. a) Han WQ, Fan SS, Li QQ, Gu BL, Zhang XB, Yu DP (1997) Appl Phys Lett 71:2271; b) Wu XC, Song WH, Zhao B, Huang WD, Pu MH, Sun YP, Du JJ (2000) Solid State Commun 115:683
183. Duan XF, Huang Y, Cui Y, Wang JF, Lieber CM (2001) Nature 409:66

184. Duan X, Lieber CM (2000) Adv Mater 12:298
185. Shi WS, Zheng YF, Wang N, Lee CS, Lee ST (2001) Appl Phys Lett 78:3304–3306
186. a) Pham-Huu C, Keller N, Ehret G, Ledoux MJ (2001) J Catal 200:400; b) Li YB, Xie SS, Wei BQ, Lian GD, Zhou WY, Tang DS, Zou XP, Liu ZQ, Wang G (2001) Solid State Commun 119:51; c) Gao YH, Bando Y, Kurashima K, Sato T (2001) Scr Mater 44:1941; d) Zhang YJ, Wang NL, He RR, Chen XH, Zhu (2001) J Solid State Commun 118:595; e) Wu XC, Song WH, Huang WD, Pu MH, Zhao B, Sun YP, Du JJ (2001) Mater Res Bull 36:847; f) Li YB, Xie SS, Zou XP, Tang DS, Liu ZQ, Zhou WY, Wang G (2001) J Cryst Growth 223:125; g) Shi WS, Zheng YF, Peng HY, Wang N, Lee CS, Lee ST (2000) J Am Ceram Soc 83:3228; h) Wang ZL, Dai ZR, Gao RP, Bai ZG, Gole JL (2000) Appl Phys Lett 77:3349; i) Liang CH, Meng GW, Zhang LD, Wu YC, Cui Z (2000) Chem Phys Lett 329:323; j) Pan ZW, Lai HL, Au FCK, Duan XF, Zhou WY, Shi WS, Wang N, Lee CS, Wong NB, Lee ST, Xie SS (2000) Adv Mater 12:1186; k) Hu JQ, Lu QK, Tang KB, Deng B, Jiang RR, Qian YT, Yu WC, Zhou GE, Liu XM, Wu JX (2000) J Phys Chem B 104:5251; l) Zhou XT, Wang N, Au FCK, Lai HL, Peng HY, Bello I, Lee CS, Lee ST (2000) Mater Sci Eng A 286:119; m) Tang CC, Fan SS, Dang HY, Zhao JH, Zhang C, Li P, Gu Q (2000) J Cryst Growth 210:595; n) Zhou XT, Lai HL, Peng HY, Au FCK, Liao LS, Wang N, Bello I, Lee CS, Lee ST (2000) Chem Phys Lett 318:58; o) Lai HL, Wong NB, Zhou XT, Peng HY, Au FCK, Wang N, Bello I, Lee CS, Lee ST, Duan XF (2000) Appl Phys Lett 76:294; p) Lu QY, Hu JQ, Tang KB, Qian YT, Zhou G, Liu XM, Zhu JS (1999) Appl Phys Lett 75:507; q) Zhou XT, Wang N, Lai HL, Peng HY, Bello I, Wong NB, Lee CS, Lee ST (1999) Appl Phys Lett 74:3942; r) Meng GW, Zhang LD, Mo CM, Zhang SY, Qin Y, Feng SP, Li HJ (1998) J Mater Res 13:2533; s) Han WQ, Fan SS, Li QQ, Liang WJ, Gu BL, Yu DP (1997) Chem Phys Lett 265:374
187. a) Liang CH, Meng GW, Chen W, Wang YW, Zhang LD (2000) J Cryst Growth 220:296; b) Qi SR, Huang XT, Gan ZW, Ding XX, Cheng Y (2000) J Cryst Growth 219:485; c) Gao Y, Liu J, Shi M, Elder SH, Virden JW (1999) Appl Phys Lett 74:3642
188. a) Fukunaga A, Chu S, McHenry MEJ (1999) Mater Sci Lett 18:431; b) Nesting DC, Kouvetakis J, Smith DJ (1999) Appl Phys Lett 74:958; c) Fukunaga A, Chu SY, McHenry ME (1998) J Mater Res 13:2465; d) Wong EW, Nor BW, Burns LD, Lieber CM (1996) Chem Mater 8:2041; e) Ata M, Hudson AJ, Yamaura K, Kurihara K (1995) Jap J Appl Phys 34:4207; f) Liu MG, Cowley JM (1995) Carbon 33:749; g) Dai HJ, Wong EW, Lu YZ, Fan SS, Lieber CM (1995) Nature 375:769; h) Liu MQ, Cowley JM (1995) Carbon 33:225; i) Ata M, Kijima Y, Hudson AJ, Imoto H, Matsuzawa N, Takahashi N (1994) Adv Mater 6:590; j) Seraphin S, Zhou D, Jiao J, Withers JC, Loutfy R (1993) Nature 362:503

C. Travaux sur la croissance de nanotubes de carbone, leur intégration et utilisation comme senseurs chimiques et biochimiques

De 2001 à 2007, mes travaux de recherche ont pris une nouvelle direction et se sont centrés sur la valorisation industrielle des nanomatériaux et notamment des nanotubes de carbone. J'ai en effet été embauché en Mars 2001 par une startup nouvellement créée, Covalent Materials Inc, qui est devenue deux ans plus tard, Nanomix Inc (www.nano.com). Avec un collègue Physicien, Keith Bradley, nous avons été les premiers scientifiques expérimentateurs à joindre la compagnie. Il a donc s'agit de créer les laboratoires, les programmes de recherche, de recruter les membres des équipes de recherche. Lors de mon séjour dans cette compagnie j'ai participé à la levée de plus de $34 Millions auprès de sociétés de capital risque ainsi que de plusieurs millions de dollars par le biais de projets déposés auprès d'agences gouvernementales américaines. Au bilan plus de 35 brevets ont été déposés dans lesquels je suis co-inventeur, dans le domaine du stockage de l'hydrogène ainsi que dans celui des applications des nanotubes de carbones, ainsi que 15 articles dans des revues internationales à forts facteurs d'impacts. Nous avons ainsi été les premiers à breveter l'utilisation de réseaux 2d désordonnés pour en faire des transistors et les utiliser comme capteurs chimiques.

D'un point de vue des ressources humaines, j'y ai participé au recrutement de plus de soixante dix employés, ce qui représente pour moi une riche expérience.

J'y étais aussi le Safety Officer ce qui m'a très tôt confronté aux problèmes de sécurités associés aux nanoparticules et nanotubes ainsi qu'à leur manipulation.

Six faits marquants peuvent être mis en avant :

1) L'intégration de CNTs sur des wafers Si de 100 mm en Aout 2002 qui a été suivi immédiatement après (en septembre 2002) par une levée de fonds de $9 millions (Round B). J'étais à ce moment le manager de l'équipe « Process Development ». J'ai dessiné et construit un réacteur CVD 100 mm, développé le catalyseur,le procédé de dépot et le procédé de croissance sur wafer 100 mm et dirigé l'équipe d'ingénieurs en charge du développement du procédé d'intégration.
2) La démonstration de la possibilité de faire des transistors à effet de champs à base de réseaux désordonnés de nanotubes et de leur utilisation comme senseur chimique. Cette structure a fait l'objet d'un dépôt de brevet et ce plus de six mois avant le premier papier dans le domaine publique sur le sujet.[2]
3) Le premier transistor flexible et transparent à base de nanotubes de carbone. Travaux publiés à Nanoletters, une semaine avant ceux de Lieber sur des transistors flexibles à base de nanofils de Si. Il est à noter que le brevet déposé sur ce sujet, en co-propriété avec UCLA, représente le brevet fondamental ayant permis la création de la Société Unidim Inc, rachetée récemment par Arrowhead Inc. et qui devrait mettre sur le marché d'ici quelques mois les premiers films plastiques conducteurs commerciaux à base de CNTs.
4) En Mai 2005, production des senseurs sur wafer de 150 mm et Nanomix met sur le marché les premiers senseurs commerciaux à base de CNTs ce qui lui vaut de boucler un troisième tour de financement de $14.5 Millions (Round C). J'étais à ce moment le « Project leader » de cet effort.
5) Nos travaux sur la détection d'ADN à l'aide des transistors à CNTs sont publiés dans les Proceeding of the National Academy of Science.

[2] "Random Networks of Single-Wall Carbon Nanotubes as an Electronic Material" ; E.S. Snow, J.P. Novak, P.M. Campbell, D. Park : Applied Physics Letters 82, 2145 (2003).

6) Les travaux de mon équipe aboutissent sur un prototype pre-produit pour la détection de NH_3 ainsi que sur un démonstrateur de la détection de NO au niveau du ppb (marqueur d'asthme). Ces travaux permettent la levée de ~$10 Millions (Round D). J'étais à ce moment Senior Director Product Development.

L'ensemble de mes activités dans ce domaine sont résumées dans une publication dans le journal de veille de l'OMNT dédié à l'électronique moléculaire, qui suit.

Réseaux 2D aléatoires à nanotubes de carbone

L'utilisation de nanotubes de carbone dans des applications électroniques se heurte au problème du control de leur chiralité. Très tôt les chercheurs et industriels ont contournés cet écueil avec une approche statistique et l'utilisation de réseaux aléatoires de nanotubes qui permettent de moyenner leurs différentes propriétés.
Après un rappel de l'historique du sujet, cet article se concentre sur les développements très rapides et récents du domaine, de façon complémentaire au dossier réalisé par l'OMNT en 2005[1].

Jean Christophe P. Gabriel, CEA-LETI, Ancien Senior Dir. Nanomix

Mise en œuvre

⊡ *Travaux préliminaires*

Suite à la re-découverte[2] des nanotubes de carbone multi-parois (MWNT) par **S. Iijima**[3], mono-paroi (SWNT) par **D.S. Bethune**[4] et à la publication du premier transistor à effet de champ à base de nanotube de carbone[5], de nombreux travaux ont été effectués sur des composants à base d'un ou quelques nanotubes de carbone.

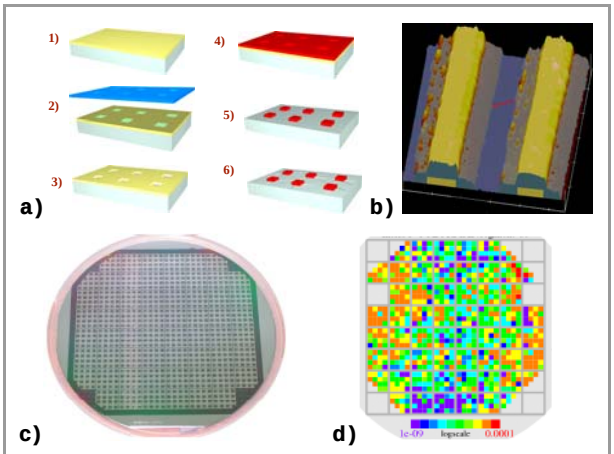

Figure 16 : a) Procédé de fabrication de transistors à nanotube unique utilisant la réalisation d'îlots de catalyseurs par lithographie suivi d'une croissance par CVD. b) Image AFM d'un nanocomposant à SWNT avec passivation des contacts. c) Wafer 100 mm obtenu à Nanomix selon ce procédé en Septembre 2002. d) Wafer map en conductance montrant une conductance variant sur plusieurs ordres de grandeurs.
Extrait avec la permission de "Large Scale Production of Carbon Nanotube Transistors: A Generic Platforms for Chemical Sensors" ; J.-C. P. Gabriel : Mat. Res. Soc. Symp. Proc. 776, Q.12.7.1 (2003).

Les premiers réseaux 2D aléatoires, hors buckypaper, ont ensuite été publiés par le groupe de **H. Dai** à l'**Université de Stanford** mais ces derniers étaient obtenus par croissance CVD directement sur une couche épaisse de catalyseur fait d'aluminosilicate poreux déposé sur un substrat à l'aide d'une tournette[6]. Des premières caractérisations électriques furent néanmoins publiées grâce au dépôt de contacts d'or directement sur le catalyseur. Ce procédé n'était cependant pas compatible avec la production à grande échelle de composant électronique[7].

La croissance des nanotubes par procédé CVD n'était et n'est toujours pas adaptée pour la production industrielle de nanocomposants à SWNT unique du fait du manque de contrôle de cette méthode. Notamment cette méthode ne permet pas la sélection de la chiralité des nanotubes synthétisés et de ce fait une grande polydispersité des distributions en conductance, transconductance et modulation des transistors obtenus est observée (Figure 16).

⊡ *Les premiers travaux*

Du fait de la nécessité de produire, à grande échelle et avec de bons rendements, des capteurs électroniques à base de nanotubes de carbone, l'idée de moyenner les propriétés des SWNTs est rapidement apparue comme une bonne solution à l'équipe de recherche de la start-up **Nanomix.** L'utilisation de nombreux SWNTs contactant la source et le drain d'un transistor en configuration parallèle a tout d'abord été étudiée mais cette disposition n'était pas entièrement satisfaisante car la modulation des transistors obtenus n'était pas adéquate du fait de la croissance indifférenciée de nanotubes semi-conducteurs et métalliques. Cette modulation pouvait certes être améliorée en détruisant les nanotubes conducteurs, par la méthode publiée par le groupe de **P. Avouris** à **IBM**[8], mais ce procédé était difficile à mettre en place dans une ligne de production à l'échelle du wafer sur des dizaines de milliers de transistors. C'est pourquoi **Nanomix** a été amené à étudier très tôt les réseaux 2D aléatoires (Figure 17).

La première méthode développée consistait tout simplement à soumettre à un plasma d'oxygène intense des îlots de catalyseurs. Sous l'effet du plasma, le catalyseur était projeté sous forme de nanoparticules sur l'ensemble du wafer. Par rapport à une calcination classique à haute température, ce procédé de calcination du catalyseur permettait d'éviter la diffusion des métaux catalytiques dans la couche de silice située en-dessous du catalyseur et servant de diélectrique au transistor à grille arrière. Cette diffusion est un problème car elle peut engendrer des courants de fuite importants. Les transistors à effet de champ (FETs) obtenus à partir de ces réseaux aléatoires ont permis l'obtention d'une très bonne reproductibilité des transistors ainsi que de leur modulation ($50 < Mod < 200$, en fonction de la géométrie du transistor et de la densité en nanotubes du réseau) et ce à l'échelle des wafers 100 mm sur lesquels **Nanomix** développait le procédé d'intégration. Ces travaux ont fait l'objet d'un dépôt de brevet dès juin 2002[9,10] (Figure 17).

Figure 17 : Image de microscopie électronique à balayage (couleurs artificielles) d'un réseau 2D aléatoire de nanotubes (rouge) entre deux contacts métalliques d'or (jaune) obtenue à Nanomix en 2002.
Extrait avec la permission de "Large Scale Production of Carbon Nanotube Transistors: A Generic Platforms for Chemical Sensors" ; J.-C. P. Gabriel : Mat. Res. Soc. Symp. Proc. 776, Q.12.7.1 (2003).

De façon indépendante à ces travaux, le groupe d'**E.S. Snow** au **Naval Research Laboratory** a aussi travaillé sur de tels transistors, produits sur de petits fragments de wafers. La croissance se faisait à partir d'un catalyseur déposé par tournette directement sur le wafer. La demande de brevet de **Nanomix** sur le sujet n'étant pas encore publique, c'est le papier publié par ce groupe en Mars 2003 qui a révélé à la communauté scientifique la faisabilité de FETs en utilisant ces réseaux 2D aléatoires[11] ainsi que leur intérêt comme capteur chimique[12].

La valeur ajoutée des réseaux aléatoires de nanotubes vis-à-vis des structures à nombreux nanotubes parallèles pour la réalisation de transistors provient de la meilleure reproductibilité et valeur en conductance et en modulation des composants obtenus. Notamment et de façon empirique, il a immédiatement été observé que la modulation des transistors s'améliore, en moyenne, avec l'augmentation de la distance entre la source et le drain. Trois composantes participent à cette amélioration. La première est que 2/3 des structures possibles de nanotubes ont la structure de bande d'un semi-conducteur. Ainsi, plus la distance entre la source et le drain est élevée par rapport à la longueur moyenne des nanotubes, plus la probabilité P qu'un chemin de conduction soit formé uniquement de nanotubes métalliques est faible ($P = (1/3)^n$ où n est le nombre de tubes formant la jonction entre la source et le drain). Deuxièmement, lors d'un croisement de nanotubes, la jonction nanotube-nanotube n'est pas de nature métallique. Enfin, la présence de défauts sur un nanotube métallique induit généralement l'ouverture d'un gap dans le diagramme de bande et ainsi rend le tube semi-conducteur[13]. Il a notamment été montré expérimentalement par **P.G. Collins** à l'**Université d'Irvine**[14] que la présence d'un seul défaut sur un SWNT est suffisante pour induire une transition vers un état semi-conducteur.

Notons enfin que les propriétés électroniques des FETs à réseau aléatoire de nanotubes de carbone ne cessent de s'améliorer. On peut notamment citer des travaux japonais qui ont utilisé des matériaux à haute constante diélectrique ($Ba_{0.4}Sr_{0.6}Ti_{0.96}O_3$, $\varepsilon_\sigma = 100$) comme isolant de grille, ce qui leur a permis de réduire de 90% le voltage de commutation, avec un ratio on/off de 10^5 ainsi qu'une réduction très significative de l'hystérésis[15]. L'hystérésis est en effet une composante importante des transistors à nanotubes utilisant la silice comme diélectrique de grille. Elle est, entre autres, reliée à la présence de charges mobiles sur la surface sur laquelle sont posés les nanotubes. Ainsi, toute stratégie tendant à réduire ces charges ou leur mobilité induit une réduction de cette hystérésis[16].

Enfin, un atout supplémentaire de ces réseaux est qu'ils apparaissent comme des structures pouvant résister à de fortes décharges électrostatiques ainsi qu'à de fortes irradiations[17].

⊡ *Les réseaux 2D aléatoires sur substrat flexible transparent*

Une fois que la possibilité de créer un transistor à effet de champ et grille arrière et à base d'un réseau aléatoire de SWNT fût démontrée, l'étape suivante était d'utiliser de tels réseaux sur un support flexible. Le premier transistor sur substrat flexible fut réalisé, publié et breveté par **Nanomix** en 2003[18] (Figure 18). On notera au passage la nature transparente de ce composant. Ces composants furent simplement réalisés par le transfert du système réseau de nanotubes de carbone + contacts métalliques : (i) par le dépôt d'un film de polyimide sur le dispositif développé précédemment sur wafer de silicium par photolithographie ; suivi (ii) d'une digestion du diélectrique silice sous jacent par du HF dilué, qui permet de libérer le réseau de nanotubes contactés et imbriqués dans le polymère. Même si ces tout premiers composants présentaient de piètres caractéristiques électroniques, l'intérêt pour l'électronique flexible, que représentaient ces réseaux aléatoires de SWNT vis-à-vis des molécules organiques ou organométalliques utilisées jusqu'alors dans les transistors organiques, reposait sur leur transparence et la très haute mobilité potentielle de tels transistors. En effet, la mobilité estimée pour les transistors présentés dans cette première publication était déjà de l'ordre de 10 ce qui à l'époque représentait une première mondiale.

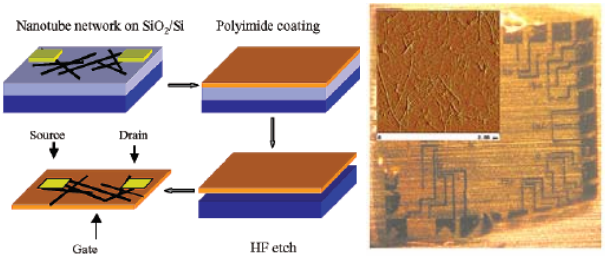

Figure 18 : a) Méthode de fabrication d'un transistor flexible.
b) Photographie du dispositif réalisé avec en insertion image AFM du réseau aléatoire de SWNT avant transfert.
Extrait avec la permission de Nano Letters 3, 1353 (2003). *Copyright 2003 American Chemical Society.*

Des études plus poussées ont ensuite été poursuivies et publiées par le groupe de **G. Grüner** à **UCLA** avec l'étude de la transparence, de la conductivité et du ratio on/off de ces composants en fonction de la densité du réseau en nanotube et notamment vis-à-vis du seuil de percolation. Les performances obtenues n'étaient cependant pas encore d'une qualité suffisante pour permettre une application transistor de ces composants pour les écrans plats, notamment d'un point de vue conductance et modulation[19] (Figure 19).

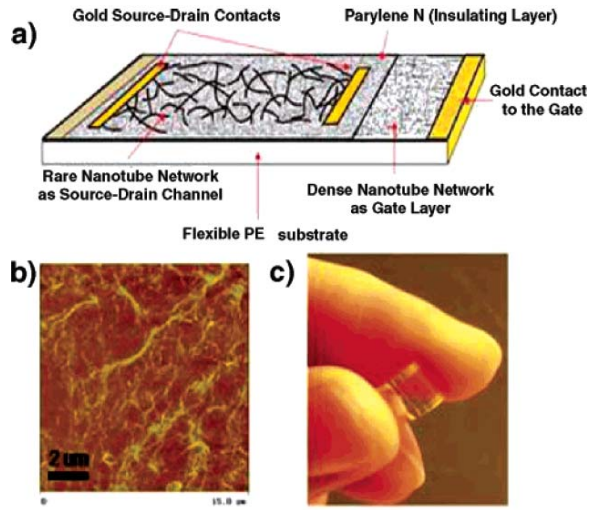

Figure 19 : Image AFM d'un réseau aléatoire de nanotubes déposé et photographie du film flexible transparent.
Extrait avec la permission de Nano Letters 5, 757 (2005).Copyright 2005 American Chemical Society.

⊡ *Méthodes de synthèse*

De nombreuses méthodes de croissance de tels réseaux, effectuées directement sur le substrat, ont été publiées. Parmi tous ces travaux on peut cependant citer l'utilisation comme catalyseur de croissance par le groupe de **H. Dai** à l'**Université de Stanford** d'une protéine à cluster de fer, la ferritine[20], ou encore l'utilisation de polyoxométallates[21]. Ce dernier article rapporte probablement la méthode de croissance permettant la croissance d'un réseau ayant une dispersion de diamètres des nanotubes de carbone monoparois la plus monodisperse et ce à partir d'un polyoxométallate relativement facile à synthétiser.

D'autres groupes se sont concentrés sur des méthodes de transfert ou de dépôt par voies liquides. On peut notamment citer les travaux du groupe de **R. Haddon** qui utilise des nanotubes purifiés et/ou fonctionnalisés (commercialisés par **Carbon Solutions Inc.**, une spin-off de son équipe) et qui les dépose par vaporisation d'un aérosol formé à partir d'une solution de ces nanotubes et ce, directement sur un substrat[22]. Le groupe de **V. Tsukruk** dépose les nanotubes par une méthode dérivée du dip-coating à partir de solutions mésogèniques (cristal liquide) à base de nanotubes, qui permet d'obtenir des réseaux à des degrés d'orientation modulable[23]. Quant au groupe de **J.A. Rogers**, il dépose les nanotubes par un procédé de transfert à partir d'un tampon[24]. Si toutes ces méthodes permettent effectivement d'obtenir des transistors, leurs propriétés électroniques sont encore très médiocres, notamment d'un point de vue ratio on/off, conductance et hystérésis. A cet effet, l'utilisation de nanotubes triés devrait permettre d'améliorer certaines de ces propriétés[25]. Une société, **NanoIntegris Inc.**, spin-off de l'**Université de Northwestern**, a notamment été créée récemment pour la commercialisation de nanotubes triés. Cette société devrait mettre ses produits sur le marché vers la fin 2008, d'après son fondateur, **M.C. Hersam** de l'**Université de Northwestern**[26].

Modélisation

Il a fallu attendre 2005 pour voir apparaître les premiers travaux de modélisation de ces réseaux aléatoires qui se sont révélés être d'excellents modèles d'études théoriques. Le groupe leader dans ce domaine est celui de **M.A. Alam** de l'**Université de Purdue**. Dans un premier article, un modèle a été développé permettant de simuler le comportement de ces réseaux en fonction de la densité des tubes et de leur longueur[27] (Figure 20).

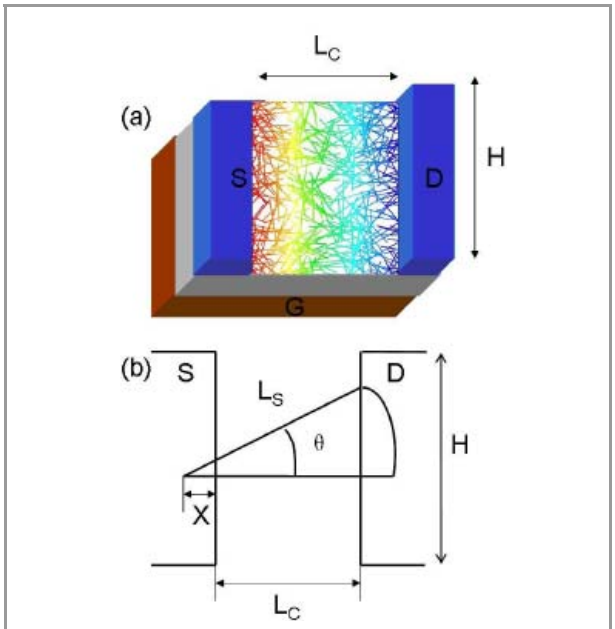

Figure 20 : a) Un transistor à réseau aléatoire de nanotubes (L_C: longueur du canal; H: largeur du canal; S: Source; D:drain) ; le code de couleur du réseau reflète de la distribution typique du potentiel électrique du réseaupour un canal L_C = 3 µm, H = 4 µm, L_S = 2 µm, cij = 5:0, and r = 3.5 µm^2. (b) Nomenclature utilisée
Extrait avec la permission de Physical Review Letters 95, 066802 (2005).Copyright 2005 American Physical Society.

Le modèle a par la suite été plus amplement développé pour prendre en compte divers effets comme celui du substrat et des charges de surface piégées[28], ou encore de l'influence d'une orientation partielle des nanotubes au sein du réseau[29]. Une dernière étude a porté sur la simulation de leurs propriétés de conduction thermique[30]. Ce modèle a permis à l'équipe de **M.A. Alam** de démontrer théoriquement puis expérimentalement la faisabilité d'augmenter de 5 ordres de grandeurs la conductance des composants grâce à l'optimisation théorique du taux d'orientation des nanotubes sans que cela se fasse au détriment de la modulation[31].

Applications

⊡ *Capteurs chimiques*

La sensibilité aux facteurs extérieurs des transistors à nanotubes a été observée dès 2000[32]. En première approximation, on peut dire que lorsque des molécules donneuses ou accepteuses d'électrons viennent à proximité d'un nanotube, il s'ensuit un transfert d'électrons qui peut être mesuré directement au niveau

de la caractéristique électronique du transistor. Dans le détail, il semble que la sensibilité puisse provenir de différentes contributions : (i) le dopage peut s'effectuer au niveau de la barrière de Schottky qui existe à l'interface des nanotubes semi-conducteurs et des métaux utilisés pour les contacts électriques (l'or est souvent utilisé)[33] ; le palladium a ainsi été introduit pour éviter cet effet[34] ; (ii) la détection peut s'effectuer au niveau du corps des nanotubes eux-mêmes[35] ; (iii) enfin elle peut s'effectuer au niveau des défauts des nanotubes[36].

Cette sensibilité semble avoir été conservée lors du passage de systèmes à nanotube unique vers ceux à réseaux aléatoires de SWNTs. Un mécanisme supplémentaire de détection est alors à étudier où la détection s'effectue au niveau des jonctions nanotubes-nanotubes.

Le mode de détection électrique peut se faire en mode résistif pur, en courant continu ou alternatif ou par la mesure d'un paramètre spécifique de la caractéristique IV_g (tension de seuil, impédance à une valeur de la tension de grille donnée), etc. La détermination des meilleurs modes de mesure est d'ailleurs l'objet de prises de propriétés intellectuelles. Dans le cadre de la mesure d'impédance, une autre méthode publiée, ici aussi, par le groupe d'**E.S. Snow**, est d'utiliser le réseau aléatoire comme l'une des deux électrodes d'un condensateur, l'autre étant la grille en face arrière[37]. Cette méthode est complémentaire de la précédente car elle permet la détection de molécules à nuage électronique polarisable. Cette stratégie a permis à **Nanomix** le développement d'une stratégie de détection des molécules utilisées dans le domaine de l'anesthésie, qui sont en général riches en halogène et sont facilement polarisables[38] (Figure 21).

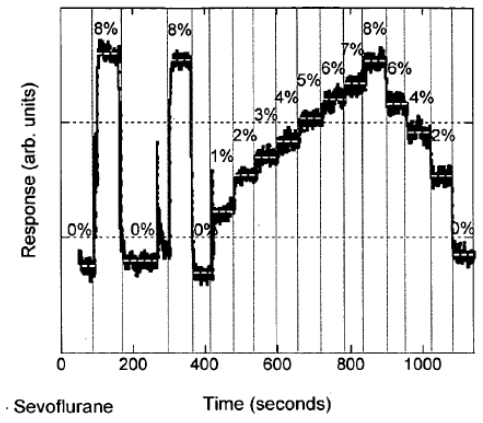

Figure 21 : Réponse en mode capacitif d'un capteur à réseau aléatoire de nanotube au gaz d'anesthésie Sevoflurane dans le domaine typique d'utilisation de ce composant lors d'une procédure d'anesthésie (0 à 8%).
Extrait avec la permission de US 20080021339 du 26/10/2006, "Anesthesia monitor, capacitance nanosensors and dynamic sensor sampling method" ; J.C.P. Gabriel, V. Joshi, J.L. Passmore, S. Skarupo, A. Star, C. Valcke.

Ces transistors peuvent aussi être utilisés immergés, en solution aqueuse ou non, et notamment avec l'utilisation, non plus d'une grille en face arrière, mais d'une grille immergée, ce qui permet de réduire les voltages de grille nécessaires d'un ordre de grandeur[39]. Cette configuration est très utile pour le développement de capteurs en phase aqueuse et notamment de biocapteurs[40, 41] (Figure 22).

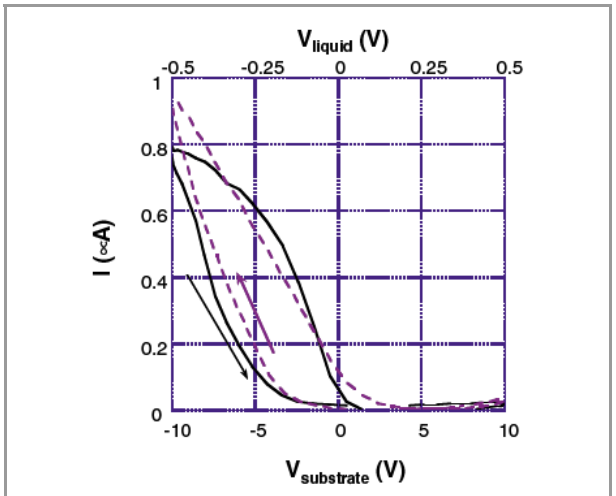

Figure 22 : Caractéristique électronique d'un NT-FET dans l'air (ligne continue) en utilisant une grille face arrière et dans l'eau (ligne discontinue) en utilisant une grille immergée. Les flèches indiquent le sens du balayage. Les échelles des abscisses sont différentes pour les deux configurations.
Extrait avec la permission de Physical Review Letters 91, 218301 (2003).Copyright 2003 American Physical Society.

Si de tels FETs présentent une bonne sensibilité à de nombreuses molécules, il s'agit aussi de leur talon d'Achille car elles ne sont pas spécifiques. Or, la plupart des cahiers des charges de capteurs commerciaux nécessitent l'absence de faux positifs et négatifs qui tous deux peuvent avoir de lourdes conséquences. Il s'agit donc de développer des stratégies de fonctionnalisation de ces capteurs permettant de réaliser une bonne spécificité dans l'environnement prévu par le cahier des charges[42]. En cela les capteurs à nanotubes de carbone ne diffèrent pas des autres types de capteurs, et le coût associé au développement de ces stratégies ne doit pas être sous estimé. Ainsi pour la réalisation du détecteur à hydrogène commercialisé par **Nanomix** en mai 2005, premier produit mis sur le marché intégrant des nanotubes de carbone dans un composant électronique silicium[43], c'est un alliage à base de palladium qui a permis d'obtenir la bonne spécificité du capteur[44]. Dans le cas du développement d'un détecteur de dioxyde de carbone pour les applications dans le domaine de la capnographie (mesure du dioxyde de carbone dans l'haleine) c'est une formulation complexe à base de polyéthylèneimine qui a joué ce rôle[45]. D'autres stratégies ont été développées comme la mise en place de barrières de diffusions[46].

Lorsqu'il n'est pas possible de trouver une fonctionnalisation induisant une haute spécificité, une autre approche est possible. Dans ce cas, on utilise plusieurs capteurs, chacun ayant une fonctionnalisation propre. Si les matériaux de fonctionnalisation sont bien choisis, c'est-à-dire qu'ils donnent des réponses différentes les unes des autres pour les différentes classes de molécules à détecter, c'est la réponse collective de tous les capteurs qui permet de différencier les molécules les unes des autres. Cette approche est typique de celle utilisée dans les nez artificiels[47]. Il faut cependant noter que la raison de

l'échec de la plupart des tentatives de commercialisation de ce type de systèmes réside dans le problème de leurs déviations. En effet, chaque capteur représente une dimension de mesure et lorsque l'on veut mettre en place des procédures de compensation des différents facteurs de déviation (tout capteur dévie que ce soit dans le temps, en température ou en fonction des fluctuations en humidité, pour ne citer que les paramètres les plus courant) on se retrouve à devoir mettre en place des algorithmes de compensation ayant plusieurs dizaines voire centaines de dimensions. La mise au point de ces algorithmes est soit mathématiquement, soit économiquement impossible. Pour ce type d'application il est donc primordial de viser des applications qualitatives et non quantitatives, c'est-à-dire reconnaissance de la présence d'une molécule et non mesure de sa concentration.

Au bilan, de nombreux travaux sont maintenant dans la littérature sur le sujet, qui pour la plupart en restent à l'observation d'une variation de comportement lors de l'exposition du composant à un stimulus extérieur (lumière[48], gaz[49], molécules en solution, bio-molécules[41,50] – glucose, ADN[51], protéines[52], dérivés benzeniques[53]-, et même mécaniques).

Par contre, l'utilisation de ce type de composants dans des capteurs commerciaux nécessite de lourds investissements (y compris dans le développement des bancs de tests et des méthodologies) afin de les amener sur le marché sous une forme qui réponde au cahier des charges et à l'attente du client. Seuls les produits à grande diffusion et à très forte valeur ajoutée peuvent être étudiés en vue d'une possible production même si, en principe, cette structure peut se voir appliquée dans de nombreux domaines. Dans cette optique, **Nanomix** a développé avec succès jusqu'au stade du prototype produit un détecteur d'ammoniaque fonctionnant en atmosphère résiduelle d'ammoniaque, un gaz à effet de serre, ce qu'aucun capteur commercial actuel ne permet de faire. **Nanomix** recherche un distributeur pour la fabrication et la commercialisation de ce produit (Figure 23).

Figure 23 : Le prototype pré-production de Nanomix pour la détection de NH_3 en milieu avicole.
Reproduit avec la permission de Nanomix.

Les efforts commerciaux de **Nanomix** se concentrent à l'heure actuelle sur la mesure de monoxyde d'azote dans l'haleine comme traceur d'asthme, une maladie qui touche 20 millions d'américains. Cette application issue d'une collaboration avec l'**Université de Pittsburg**[54] nécessite la mesure de concentration de monoxyde d'azote à hauteur de quelques ppb.

⊡ *Composants électroniques*

De nombreux brevets ont été pris par la société **Nantero Inc.** (Woburn, Massachusetts) qui s'est initialement lancée sur le développement d'une mémoire réinscriptible et capable de conserver des données sans alimentation électrique, ce qui en fait potentiellement une mémoire universelle, utilisable dans une multitude d'applications. Ce type de mémoire, appelée NRAM par **Nantero Inc.**, exploite la stabilité bimodale d'une matrice de nanotubes de carbone déposée dans un sillon préalablement gravé[55]. Ce réseau positionné généralement au dessus d'un via peut se déformer sous l'application d'un champ électrique, et ainsi venir au contact d'une électrode située en dessous du réseau. Il s'agit là d'un nanocommutateur qui peut être intégré dans des composants et architectures variés tels que des mémoires, switchers, émetteurs de lumière, récepteurs, transistors électromécaniques, circuits logiques (Figure 24). En avril 2006, **Nantero Inc.** a annoncé avoir fabriqué et testé avec succès un commutateur de mémoire en technologie 22 nm[56]. Une sortie commerciale était alors annoncée pour 2007 mais des problèmes de production semblent retarder cette mise sur le marché.

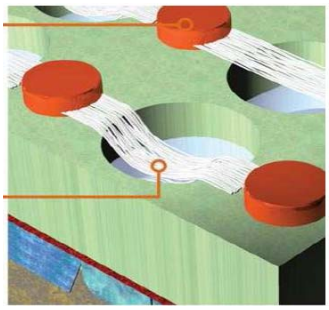

Figure 24 : Source : Site web de Nantero
Extrait avec la permission de Nantero (http://www.nantero.com/).

⊡ *Film conducteur comme électrode flexible*

L'utilisation des réseaux désordonnés de nanotubes comme conducteur électronique est aussi très avancé d'un point de vue industriel.

Un premier domaine est dans le remplacement des couches de carbone amorphe utilisées dans les bandelettes de mesure du taux de glucose dans le sang. En effet, la reproductibilité de ces couches n'est pas excellente, ce qui force les industriels à de coûteuses phases de calibration. Le remplacement de cette couche par un film de nanotubes en réseau désordonné a été proposé et son utilisation est en cours d'étude. L'avantage principal serait une meilleure conductance ainsi qu'une meilleure reproductibilité.

Une deuxième application est étudiée par plusieurs industriels : le remplacement de l'ITO (Indium-Tin-Oxyde) qui est utilisé comme couche conductrice et transparente dans de nombreuses applications comme les écrans tactiles, les affichages cristaux liquides, les écrans souples, etc. Les prix des matières premières et

la faiblesse des stocks d'indium et d'étain favorisent la recherche d'alternative.

On peut notamment citer les travaux initiés et brevetés par **Nanomix** puis développés à **UCLA** par **G. Grüner** qui a étudié l'influence de la densité et de l'épaisseur du réseau en nanotubes sur la conductance et la transparence de ces films. Ces travaux ont permis la création d'une start-up, **Nanodym Inc.**, qui a depuis été rachetée par **Arrowhead** et qui est sur le point de mettre sur le marché des films PET (polyéthylène téréphtalate) à couche conductrice à base de réseaux aléatoires de nanotubes de carbone. Ces films sont destinés à être intégrés dans des écrans tactiles[57].

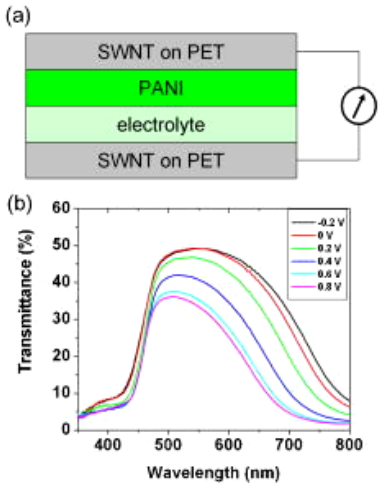

Figure 25 : (a) Architecture d'une fenêtre "intelligente" dont la couleur peut être modulée.
(b) Transmission optique du composant pour différentes valeurs de voltage appliqué.
Extrait avec la permission de Journal of Applied Physics 101, 016102 (2007). Copyright 2007 American Institute of Physics.

D'autres travaux semblent indiquer que ces films pourraient aussi être intégrés un jour dans des OLED[58], des cellules photovoltaïques[59], ou encore comme électrode dans des applications électrochromiques de type écrans flexibles[60] (Figure 25). Pour ces applications, la combinaison de la haute transparence, la faible résistance électrique des couches, leur caractère mécaniquement robuste, leur stabilité environnementale et la facilité de leur dépôt de façon industrielle sont mis en avant comme atouts clés.

Enfin, la société **Nantero Inc.** a récemment annoncé une collaboration avec **Hewlett Packard** pour la réalisation d'électronique souple combinant leur savoir faire en dispersion des nanotubes et celui d'**Hewlett Packard** en technologie Ink-Jet[61].

Une dernière application possible a récemment été proposée pour l'utilisation de ces réseaux de nanotubes comme collecteur de charge, dans l'architecture de batteries souples[62] (Figure 26).

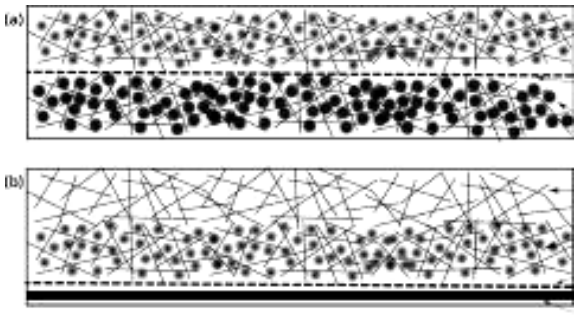

Figure 26 : (a) Proposition de design d'une batterie incorporant le matériau de l'électrode active et celui du collecteur en une seule couche. (b) Design d'un démonstrateur construit à partir d'un collecteur de charge à base d'un film de nanotubes de carbones et d'un matériau actif à base d'un mélange de MnO_2 et de nanofils.
Extrait avec la permission de Applied Physics Letters 91, 144104 (2007). Copyright 2007 American Institute of Physics.

⊡ *Santé et sécurité.*

La réalisation des réseaux aléatoires 2D de nanotubes peut, selon les méthodes de fabrication utilisées, être une source d'exposition des personnels aux nanotubes. Même si les études cherchant à évaluer la toxicité des nanotubes sont loin d'être complètes, on sait que certains nanotubes peuvent avoir des effets néfastes sur la santé. Cependant, en raison de ce manque de données, il n'existe pas encore de réglementation déterminant des niveaux d'exposition aux nanotubes. Le principe de précaution doit donc s'appliquer. A ce titre, de nombreuses compagnies ont mis en place des procédures très spécifiques et draconiennes (sous peine de licenciement) qui interdisent l'ouverture à l'air libre de tout objet ayant des nanotubes de carbone exposés (Intel par exemple).

Figure 27 : Film de très grande surface à base de nanotubes dont la faisabilité a fait l'objet d'un communiqué de presse de la part de la société Nanocomp technologies. On notera la présence d'un employé seulement muni d'une blouse et d'une paire de gant au voisinage immédiat du film.
Extrait avec la permission de (http://www.nanocomptech.com/press/pr_02-22-08.htm).

Dans ce contexte il parait aberrant de voir une société comme **Nanocomp** communiquer sur un film de nanotube de grande surface qu'elle a réalisé en montrant un de ses employé allongé à ses cotés sans protection particulière (Figure 26). A sa décharge, cette

compagnie affirme que les nanotubes sont inclus dans une matrice conçue pour éviter la dissémination des nanotubes dans l'atmosphère. Cependant, il n'y aucune allusion à ce sujet dans le communiqué de presse auquel est associée cette image.

La communauté scientifique doit donc être très vigilante sur la sécurité des procédés de manipulation des nanotubes mis en place ainsi que sur la façon de communiquer sur ses travaux.

⊡ *Les acteurs industriels*

La demande mondiale en nanotubes de carbone augmente rapidement du fait de la maturation de ses applications. En effet, le marché global des nanotubes de carbone devrait dépasser les 1,9 milliards de dollars en 2010 d'après un récent rapport de **Global Industry Analysts Inc.**[63]. On commence d'ailleurs à voir les premières consolidations s'effectuer avec, par exemple, l'acquisition par **Arrowhead** de **Unidym Inc.** suivi plus récemment de l'acquisition de **Carbon Nanotechnologies Inc.**, société initialement créée par le lauréat du prix Nobel, le professeur **R. Smalley** de l'**Université de Rice**, USA.

Une liste des acteurs commerciaux principaux dans le domaine des nanotubes est donnée dans le tableau 1.

Conclusions

Les réseaux aléatoires à nanotubes de carbone représentent la première réponse des industriels au problème de la polydispersité en propriétés physiques des transistors à nanotubes. Ils vont permettre l'intégration des nanotubes dans des produits complexes à haute valeur ajoutée comme l'illustre la mise sur le marché des premiers produits électroniques à base de nanotubes et le grand nombre d'applications en cours de développement. Le remplacement de l'ITO par les nanotubes représenterait notamment une percée majeure, à forts volumes, pour l'obtention de films plastiques conducteurs à intégrer dans les écrans tactiles qui ne devraient pas présenter de problème de fatigue mécanique. Une amélioration importante des propriétés électroniques des films déposés par voie humide est cependant nécessaire pour que ces réseaux percent dans le milieu des composants électroniques flexibles de type transistor à effet de champ.

Organisation	Méthode de production / Produit	Statut
Matériaux		
SouthWest NanoTechnologies, Norman, Okla. (www.swnano.com)	Production par la technique de CVD	Production
Ahwahnee Technology (USA)	Pas d'information sur la méthode de production	Production
Apex Nanomaterials (USA)	Production par la technique de l'arc électrique	Production
Arry International Group Ltd. (Germany)	Production par la technique de CVD ; purification ; fonctionnalisation	Production
Bayer MaterialScience AG (Germany)	Pas d'information sur la méthode de production	Production
BuckyUSA (USA)	Production par la technique de l'arc électrique	Production
CarboLex Inc. (USA)	Productions par les techniques de l'arc électrique et de dépôt en phase vapeur (CVD)	Production
Carbon Nanotechnologies Inc. (USA)	Productions par les techniques de CVD à partir de ferrocène et monoxyde de carbone et ablation laser	Production (racheté par Arrowhead, Avril 2007)
carbon NT&F 21.. (Austria)	Pas d'information sur la méthode de production	Production
Carbon Solutions, Inc. (USA)	Production par la technique de l'arc électrique, purification et modification chimiques	Production
Catalytic Materials LLC (USA)	Production par la technique de CVD ;	Production
Cheap Tubes Inc. (USA)	Purification ; Fonctionnalisation	Distributeur
Chengdu Organic Chemicals Co., Ltd.(China)	Production par la technique de CVD ;	Production
Heji, Inc. (Hong Kong)	Pas d'information sur la méthode de production, probablement CVD ; purification ; fonctionnalisation	Production
Helix Material Solutions (USA)	Production par la technique de CVD ;	Production
Idaho Space Materials, Inc. (USA)	Production par la technique de l'arc électrique, sans catalyseur métallique	Production
Iljin Nanotech Co., Ltd. (Korea)	Productions par les techniques de l'arc électrique et de dépôt en phase vapeur (CVD)	Production
M.E.R. Corp. (USA)	Productions par les techniques de l'arc électrique et de dépôt en phase vapeur (CVD)	Production
MicrotechNano (USA)	Pas d'information sur la méthode de production, probablement CVD	Production
Nano-C (USA)	Production par la technique de CVD	Production
NanoCarbLab (Russia)	Production par la technique de l'arc électrique, purification et modification chimiques	Production
Nanocomp Technologies, Inc. (USA)	Longs nanotubes par CVD	Production
Nanocs (USA)	Productions par les techniques de l'arc électrique et de dépôt en phase vapeur (CVD) ; purification et modification chimiques	Production
Nanocyl S.A. (Belgium)	Production par la technique de CVD	Production

Organisation	Méthode de production / Produit	Statut
NanoIntegris (www.nanointegris.com)	Nanotubes triés par fonctionnalisation suivi de centrifugation successives (spin-off de l'université de Northwestern)	Production prévue pour fin 2008
NanoLab (USA)	Production par la technique de CVD et Plasma enhanced CVD (PE-CVD pour les films de CNTs alignés verticalement)	Production
Nanoledge (France)	A arrêté la production de CNT par la méthode de l'arc électrique, se focalise sur la formulation de composites pour applications à haute valeur ajoutée	Production et R&D (en cours de délocalisation au Canada)
Nanostructured & Amorphous Materials, Inc. (USA)	Production par la technique de CVD	Production
NanoTechLabs, Inc. (USA)	Production par la technique de CVD	Production
Nanothinx S.A. (Greece)	Production par la technique de CVD	Production
n-Tec (Norway)	Production par la technique de l'arc électrique	Production
Raymor Industries Inc. (Canada)	Production par la technique de la torche à plasma	Production
Rosseter Holdings Ltd. (South Cyprus)	Production par la technique de l'arc électrique à bas voltage en phase liquide	Production
SES Research (USA)	Production par la technique de CVD	Production
Shenzhen Nanotechnologies Co. Ltd. (China)	Pas d'information sur la méthode de production, probablement CVD	Production
Sun Nanotech Co Ltd. (China)	Production par la technique de CVD	Production
Thomas Swan & Co. Ltd. (England)	Production par la technique de CVD, hauts volumes	Production
Xintek, Inc. (USA)	Production par la technique de CVD	Production
21st Century NanoTechnologies, Inc (China)	Production par la technique de CVD	Production
Ironbark Composites (Australia)	Pas d'information sur la méthode de production, probablement CVD	MWNTs, Production ($500 / kg au 22/01/2008)
Films Tranparents		
Battelle Memorial Institute, Columbus, Ohio (www.battelle.org)	Dépôt de couche mince transparente	R&D
Eikos, Franklin, Mass. (www.eikos.com)	Encres pour dépôts de films conducteurs ; formulation	Production, développement de produits et R&D
Eastman Kodak, Rochester, N.Y. (www.kodak.com)	Dépôt de couche mince transparente	R&D, prototype
Unidym, Menlo Park, Calif. (www.unidym.com)	Films transparents conducteurs pour écrans tactiles, cellules photovoltaïques et diodes électroluminescentes	Produits en cours de développement, premier produit attendu courant 2008 (racheté par Arrowhead en 2006)
Composants		
DuPont, Wilmington, Del. (www.dupont.com)	Electronique transparente	R&D
IBM, Armonk, N.Y. (www.ibm.com)	Transistors et interconnections	R&D
Intel, Santa Clara, Calif. (www.intel.com)	Transistors et interconnections	R&D
Motorola, Schaumburg, Ill. (www.motorola.com)	Capteurs chimiques et biochimiques	Prototype

Organisation	Méthode de production / Produit	Statut
Nanomix, Emeryville, Calif. (www.nano.com)	Capteurs chimiques et biochimiques	Production, prototypes, R&D
Nantero, Woburn, Mass. (www.nantero.com)	NRAM; encre et formulation; électronique flexible	Prototype
Samsung, Seoul, South Korea (www.samsung.com)	Ecrans, interconnections	R&D
Unidym (see above)	Electronique imprimée pour écrans, écrans tactiles, OLED, batterie et électronique souple	Prototypes pré-production ; Proof of concept
Xintek, Inc. (USA)	Cathode, tube à rayons X, pointes AFM	Production

Tableau 1 : Acteurs commerciaux principaux dans le domaine des nanotubes

Références

[1] "L'avancée de l'année : Les films de nanotubes de carbone non ordonnés" ; G. Bidan : *Electronique Moléculaire synthèse de l'année* 2005, 21 (2006).

[2] "Who should be given the credit for the discovery of carbon nanotubes?" ; M. Monthioux, V.L. Kuznetsov : ***Carbon*** **44**, 1621 (2006).

[3] "Helical microtubules of graphitic carbon" ; S. Iijima : ***Nature*** **354**, 56 (1991).

[4] "Cobalt-catalysed growth of carbon nanotubes with single-atomic-layer walls" ; D.S. Bethune, C.H. Klang, M.S. de Vries, G. Gorman, R. Savoy, J. Vazquez, R. Beyers. : ***Nature*** **363**, 605 (1993).

[5] "Room-temperature transistor based on a single carbon nanotube" ; S.J. Tans, A.R.M. Verschueren, C. Dekker : ***Nature*** **393**, 49 (1998).
"Single- and multi-wall carbon nanotube field-effect transistors" ; R. Martel, T. Schmidt, H.P. Shea, T. Hertel, P. Avouris : ***Applied Physics Letters*** **73**, 2447 (1998).

[6] "Synthesis of individual single-walled carbon nanotubes on patterned silicon wafers" ; J. Kong, H.T. Soh, A.M. Cassell, C.F. Quate, H. Dai : ***Nature*** **395**, 878 (1998).
"Directed Growth of Free-Standing Single-Walled Carbon Nanotubes" ; A.M. Cassell, N.R. Franklin, T.W. Tombler, E.M. Chan, J.Han, H.Dai : ***Journal of the American Chemical Society*** **121**, 7975 (1999).

[7] Brevet US 5578543 du 5/06/1995, "Carbon fibrils, method for producing same and adhesive compositions containing same" ; H.G. Tennent, J.J. Barber, R. Hoch (Hyperion).

[8] "Engineering carbon nanotubes and nanotube circuits using electrical breakdown" ; P.G. Collins, M.S. Arnold & P. Avouris : ***Science*** **292**, 706 (2001).

[9] Demande de brevet WO2004040671 du 20/06/2003, "Dispersed growth of Nanotubes on a substrate" ; J.-C.P. Gabriel, K. Bradley, P.G. Collins (Nanomix).

[10] "Large Scale Production of Carbon Nanotube Transistors: A Generic Platforms for Chemical Sensors" ; J.-C.P. Gabriel : ***Materials Research Society Symposium Proceeding*** **762**, Q.12.7.1 (2003).

[11] "Random Networks of Single-Wall Carbon Nanotubes as an Electronic Material" ; E.S. Snow, J.P. Novak, P.M. Campbell, D. Park : ***Applied Physics Letters*** **82**, 2145 (2003).

[12] "Nerve Agent Detection Using Networks of Single-Wall Carbon Nanotubes" ; J.P. Novak, E.S. Snow, E.J. Houser, D. Park, J.L. Stepnowoski, R.A. McGill : ***Applied Physics Letters*** **83**, 4026 (2003).

[13] "Crossed Nanotube Junctions" ; M.S. Fuhrer, J. Nygård, L. Shih, M. Forero, Y.G. Yoon, M.S.C. Mazzoni, H.J. Choi, J. Ihm, S.G. Louie, A. Zettl, P.L. McEuen : ***Science*** **21**, 494 (2000).

[14] "Identifying and counting point defects in carbon nanotubes" ; Y. Fan, B.R. Goldsmith, P.G. Collins : ***Nature Materials*** **4**, 906 (2005).
"Electronic fluctuations in nanotube circuits and their sensitivity to gases and liquids" ; D. Kingrey, O. Khatib & P.G. Collins : ***Nano Letters*** **6**, 1564 (2006).

[15] "Improvements in the device characteristics of random-network single-walled carbon nanotube transistors by using high-κ gate insulators" ; M. Ohishi, M. Shiraishi, K. Ochi, Y. Kubozono, H. Kataura : ***Applied Physics Letters*** **89**, 203505 (2006).

[16] "Influence of Mobile Ions on Nanotube Based FET Devices" ; K. Bradley, J. Cumings, A. Star, J.-C.P. Gabriel, G. Grüner : ***Nano Letters*** **3**, 639 (2003).

[17] "Radiation hardness of the electrical properties of carbon nanotube network field effect transistors under high-energy proton irradiation" ; W.K. Hong, C. Lee, D. Nepal, K.E Geckeler, K. Shin, T. Lee : ***Nanotechnology*** **17**, 5675 (2006).

[18] "Flexible nanotube electronics" ; K. Bradley, J.-C.P. Gabriel, G. Grüner : ***Nano Letters*** **3**, 1353 (2003).
Demande de brevet US 20050184641 A1 du 14/05/2004, "Flexible nanostructure electronic devices" ; P.N. Armitage, K. Bradley, J.-C.P. Gabriel, G. Grüner.

[19] "Transparent and Flexible Carbon Nanotube Transistors" ; E. Artukovic, M. Kaempgen, D.S. Hecht, S. Roth, G. Grüner : ***Nano Letters*** **5**, 757 (2005).
"Percolation in Transparent and Conducting Carbon Nanotube Networks" ; L. Hu, D.S. Hecht, G. Grüner : ***Nano Letters*** **4**, 2513 (2004).

[20] "Growth of Single-Walled Carbon Nanotubes from Discrete Catalytic Nanoparticles of Various Sizes" ; Y. Li, W. Kim, Y. Zhang, M. Rolandi, D. Wang, H. Dai : ***Journal of Physical Chemistry B*** **105**, 11424 (2001).

[21] "Synthesis of Nearly Uniform Single-Walled Carbon Nanotubes Using Identical Metal-Containing Molecular Nanoclusters as Catalysts" ; L. An, J.M. Owens, L.E. McNeil, J. Liu : ***Journal of the American Chemical Society*** **124** 13688 (2002).

[22] "Electronic Properties of Single-Walled Carbon Nanotube Networks" ; E. Bekyarova, M.E. Itkis, N. Cabrera, B. Zhao, A. Yu, J. Gao, R.C. Haddon : ***Journal of the American Chemical Society*** **127**, 5990 (2005).

[23] "Liquid-Crystalline Processing of Highly Oriented Carbon Nanotube Arrays for Thin-Film Transistors" ; H. Ko, V.V. Tsukruk : ***Nano Letters*** **6**,1443 (2006).

[24] "Solution Casting and Transfer Printing Single-Walled Carbon Nanotube Films" ; M.A. Meitl, Y. Zhou, A. Gaur; S. Jeon, M.L. Usrey, M.S. Strano, J.A. Rogers : ***Nano Letters*** **4**, 1643 (2004).

[25] "Intrinsic current gain cutoff frequency of 30 GHz with carbon nanotube transistors" ; A. Le Louarn, F. Kapche, J.-M. Bethoux, H. Happy, G. Dambrine, V. Derycke, P. Chenevier, N. Izard, M.F. Goffman, J.P. Bourgoin : ***Applied Physics Letters*** **90**, 233108 (2007).
"Sorting carbon nanotubes by electronic structure using density differentiation" ; M.S. Arnold, A.A. Green, J.F. Hulvat, S.I. Stupp, M.C. Hersam : ***Nature Nanotechnology*** **1**, 60 (2006).

[26] M.C. Hersam, communication personnelle, Février 2008.

[27] "Percolating Conduction in Finite Nanotube Networks" ; S. Kumar, J.Y. Murthy, M.A. Alam : ***Physical Review Letters*** **95**, 066802 (2005).

[28] "Theory of transfer characteristics of nanotube network transistors" ; S. Kumar, N. Pimparkar, J.Y. Murthy : ***Applied Physics Letters*** **88**, 123505 (2006).

[29] "Experimental and Theoretical Studies of Transport through Large Scale, Partially Aligned Arrays of Single-Walled Carbon Nanotubes in Thin Film Type Transistors" ; C. Kocabas, N. Pimparkar, O. Yesilyurt, S.J. Kang, M.A. Alam, J.A. Rogers : ***Nano Letters*** **7**, 1195 (2007).

[30] "Effect of percolation on thermal transport in nanotube composites" ; S. Kumar, M.A. Alam, J.Y. Murthy : ***Applied Physics Letters*** **90**, 104105 (2007).
"Computational Model for Transport in Nanotube-Based Composites With Applications to Flexible Electronics" ; S. Kumar, M.A. Alam, J.Y. Murthy : ***Journal of Heat Transfer*** **129**, 500 (2007).

[31] "Limits of Performance Gain of Aligned CNT Over Randomized Network: Theoretical Predictions and Experimental Validation" ; N. Pimparkar, C. Kocabas, S.J. Kang, J. Rogers, M.A. Alam : ***IEEE Electron Device Letters*** **28**, 593 (2007).

[32] "Extreme Oxygen Sensitivity of Electronic Properties of Carbon Nanotubes" ; P.G. Collins, K. Bradley, M. Ishigami, A. Zett : ***Science*** **287**, 1801 (2000).

[33] "Carbon Nanotubes as Schottky Barrier Transistors" ; S. Heinze, J. Tersoff, R. Martel, V. Derycke, J. Appenzeller & Ph. Avouris : ***Physical Review Letters*** **89**, 106801 (2002).

[34] "Ballistic carbon nanotube field-effect transistors" ; A. Javey, J. Guo, Q. Wang, M. Lundstrom, H. Dai : ***Nature*** **424**, 654 (2003).

[35] "Short-channel effects in contact-passivated nanotube chemical sensors" ; K. Bradley, J.-C.P. Gabriel, A. Star, G. Grüner : ***Applied Physics Letters*** **83**, 3821 (2003).

[36] "Role of defects in single-walled carbon nanotube chemical sensors" ; J.A. Robinson, E.S. Snow, S.C. Badescu, T.L. Reinecke, F.K. Perkins : ***Nano Letters*** **6**, 1747 (2006).

[37] "Chemical Detection with a Single-Walled Carbon Nanotube Capacitor" ; E.S. Snow, F. Perkins, E.J. Houser, S.C. Badescu, T.L. Reinecke : ***Science*** **307**, 1942 (2005).

[38] Demande de brevet US 20080021339 du 26/10/2006, "Anesthesia monitor, capacitance nanosensors and dynamic sensor sampling method" ; J.C.P. Gabriel, V. Joshi, J.L. Passmore, S. Skarupo, A. Star, C. Valcke.

[39] "Electrochemical carbon nanotube field-effect transistor" ; M. Krüger, M.R. Buitelaar, T. Nussbaumer, C. Schönenberger, L. Forró : ***Applied Physics Letters*** **78**, 1291 (2001).
"High Performance Electrolyte Gated Carbon Nanotube Transistors" ; S. Rosenblatt, Y. Yaish, J. Park, J. Gore, V. Sazonova, P.L. McEuen : ***Nano Letters*** **2**, 869 (2002).

[40] "Charge Transfer from Ammonia Physisorbed on Nanotubes" ; K. Bradley, J.C.P. Gabriel, M. Briman, A. Star, G. Grüner : ***Physical Review Letters*** **91**, 218301 (2003).

[41] "Carbon Nanotube Field-Effect-Transistor-Based Biosensors" ; B.L. Allen, P.D. Kichambare, A. Star : ***Advanced Materials*** **19**, 1439 (2007).

[42] Demande de brevet US 20050279987 du 5/09/2003, "Nanostructure sensor device with polymer recognition layer" ; A. Star, J.C.P. Gabriel, G. Grüner.
Brevet US 6905655 du 14/06/2005 "Modification of selectivity for sensing for nanostructure device arrays arrays" ; J.C.P. Gabriel, P.G. Collins, K. Bradley, G. Grüner.
Demande de brevet US 20070208243 du 14/11/2005, "Nanoelectronic glucose sensors" ; J.C.P. Gabriel, S. Gandhi, A. Star, C. Valcke (Nanomix).
US20070178477 A1, "Nanotube sensor devices for DNA detection" ; C.S. Joiner, J.C.P. Gabriel, G. Grüner, A. Star.
Demande de brevet US 20070048181 du 18/07/2006, "Carbon dioxide nanosensor, and respiratory CO2 monitors" ; D.M. Chang, Y.L. Chang, J.C.P. Gabriel, V. Joshi, W. Mickelson, J. Niemann, J.L. Passmore, A. Star, C. Valcke.
Demande de brevet US 20060228723 du 25/10/2005, "System and method for electronic sensing of biomolecules" ; K. Bradley, J.C.P. Gabriel, G. Grüner, A. Star, E. Tu, C. Valcke (Nanomix).
Brevet US 7312095 du 25/12/2007, "Modification of selectivity for sensing for nanostructure sensing device arrays" ; J.C.P. Gabriel, P.G. Collins, K. Bradley, G. Grüner.

[43] (http://www.nano.com/news/archives/press_releases_and_articles/000082.html).

[44] Demande de brevet US 20060263255 du 14/02/2006, "Nanoelectronic sensor system and hydrogen-sensitive functionalization" ; T.R. Han, A. Star, J.C.P. Gabriel, S. Skarupo, J.L. Passmore, P.G. Collins, K. Bradley, D. Olson.

[45] Demande de brevet US 20080021339 du 26/10/2006 "Anesthesia monitor, capacitance nanosensors and dynamic sensor sampling method" ; J.C.P. Gabriel; V. Joshi, J.L. Passmore, S. Skarupo, A. Star, C. Valcke.

[46] Demande de brevet US 20060078468 du 27/05/2005, "Modification of selectivity for sensing for nanostructure sensing device arrays".

[47] "Gas Sensor Array Based on Metal-Decorated Carbon Nanotubes" ; A. Star, V. Joshi, S. Skarupo, D. Thomas, J.C.P. Gabriel : ***Journal of Physical Chemistry B*** **110**, 21014 (2006).

[48] "Nanotube optoelectronic memory devices" ; A. Star, Y. Lu, K. Bradley, G. Grüner : ***Nano Letters*** **4**, 1587 (2004).

[49] "Chemical vapor detection using single-walled carbon nanotubes" ; E.S. Snow, F.K. Perkins, J.A. Robinson : ***Chemical Society Reviews*** **35**, 790 (2006).

[50] "Carbon Nanotubes for Electronic and Electrochemical Detection of Biomolecules" ; S.N. Kim, J.F. Rusling, F. Papadimitrakopoulos : ***Advanced Materials*** **19**, 3214 (2007).

[51] "Label-free detection of DNA hybridization using carbon nanotube network field-effect transistors" ; A. Star, E. Tu, J. Niemann, J.C.P. Gabriel, C.S. Joiner, C. Valcke : ***Proceedings of the National Academy of Sciences*** **103**, 921 (2006).

[52] "Charge transfer from adsorbed proteins" ; K. Bradley, M. Briman, A. Star, G. Grüner : ***Nano Letters*** **4**, 253 (2004).

[53] "Interaction of Aromatic Compounds with Carbon Nanotubes: Correlation to the Hammett Parameter of the Substituent and Measured Carbon Nanotube FET Response" ; A. Star, T.R. Han, J.C.P. Gabriel, K. Bradley, G. Grüner : ***Nano Letters*** **3**, 1421 (2003).

[54] "Carbon nanotube sensors for exhaled breath components" ; O. Kuzmych, B.L Allen, A. Star : ***Nanotechnology*** **18**, 375502 (2007).

[55] Brevet US 7138832 du 21/11/2006, "Nanotube-based switching elements and logic circuits" ; C.L. Bertin, T. Rueckes, B.M. Segal (Nantero).
Brevet US 6,706,402 du 16/04/2004 "Nanotube films and articles" ; T. Rueckes, B.M. Segal (Nantero).
(http://en.wikipedia.org/wiki/Nano-RAM).

[56] (http://nantero.com/pdf/Release_0406.pdf).

[57] G. Grüner, communication personnelle, Sept. 2007.

[58] "Organic Light-Emitting Diodes Having Carbon Nanotube Anodes" ; J. Li, L. Hu, L. Wang, Y. Zhou, G. Grüner, T.J. Marks : ***Nano Letters*** **6**, 2472 (2006).

[59] "Carbon nanotubes: a multi-functional material for organic optoelectronics" ; R.A. Hatton, A.J. Miller, S.R.P. Silva : ***Journal of Materials Chemistry*** **18**, 1183 (2008).

[60] "Patternable transparent carbon nanotube films for electrochromic devices" ; L. Hu, G. Grüner, D. Li, R.B. Kaner, J. Chech : ***Journal of Applied Physics*** **101**, 016102 (2007).

[61] (http://nantero.com/pdf/Press_ReleaseC7F35.pdf)

[62] "Carbon nanotube based battery architecture" ; A. Kiebele, G. Gruner : ***Applied Physics Letters*** **91**, 144104 (2007)

[63] Carbon Nanotubes - Global Strategic Business Report, Publisher: Global Industry Analysts, Inc. USA (www.StrategyR.com), Juillet 2007.

V. PROGRAMMES DE RECHERCHE ACTUELS

Mon rôle de Responsable Programme au CEA/LETI n'est actuellement pas un rôle de recherche opérationnel. De ce fait je ne dispose, pour l'instant, pas de moyens de recherche humain ou matériel propre. Il est cependant clair que dans le cadre de mes fonctions de montage de projets je suis amené à proposer des axes ou sujets de recherches. Mon association à ces projets peut donc régulièrement intervenir ou niveau d'une co-direction de travaux de thèses. Il est d'autre part probable qu'un rôle plus opérationnel m'incombe d'ici un an ou deux. Mon inscription pour l'HDR s'effectue dans cette optique.

Un résumé des associations en cours sont listées ci-dessous.

2009 -2012 : Développement de d'applications à partir d'une plateforme NEMS.

Dans le cadre des travaux de collaboration avec Caltech, une plateforme NEMS a été développée par le groupe de Philippe Andreucci. Cette plateforme peut avoir de multiples applications, notamment dans le domaine de la détection chimique (liquide ou gazeuse) ou de la spectrométrie de masse intégrée, ultra-sensible.

Du fait de mon expérience importante acquise dans le domaine du développement de capteurs gas je vais encadrer à partir de Septembre 2009 une thèse en recherche technologique sur la réalisation de capteurs chimiques à base de NEMS. La direction sera partagée avec J. Arcamone (non HDR), du CEA. Ces capteurs sont notamment dédiés aux applications capteurs de masse ultra sensibles. En effet, utilisés en oscillateur haute fréquence, leur masse extrêmement faible devrait permettre d'atteindre des résolutions de l'ordre du zeptogramme (10^{-21}g). La masse est évaluée en suivant le décalage du pic de résonance mécanique de l'oscillateur au fur et à mesure que les molécules se déposent à sa surface. Divers types de transduction électrique, soit piézorésistive soit capacitive, permettent de convertir ces oscillations mécaniques en une grandeur électrique mesurable.

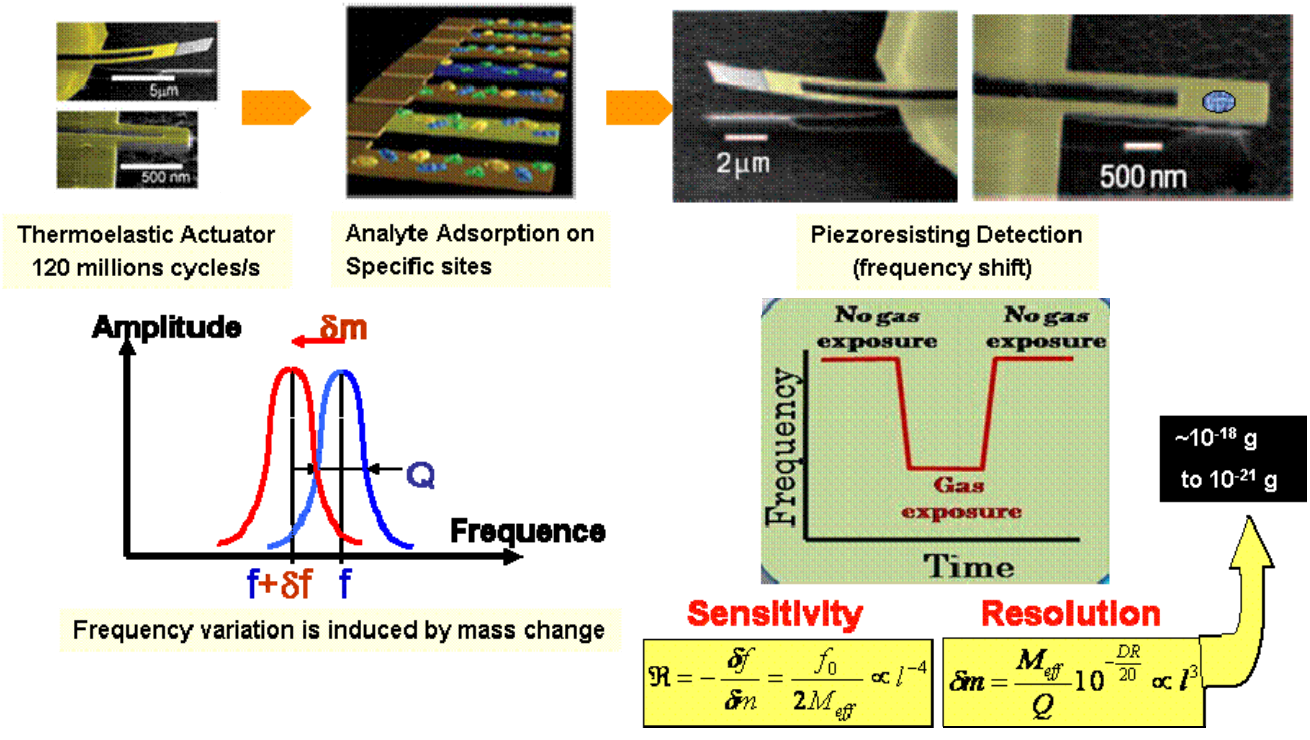

Pour cette application, les nanofils, doivent être associés à des éléments de circuit CMOS afin d'amplifier le signal in situ et de les adresser individuellement. Des composants NEMS associés à un circuit d'amplification sont déjà disponibles et d'autres à base de nanofils sont en cours de

fabrication. Leur fonctionnalité en tant que capteur gaz devra être testée sur un gaz test à l'aide d'un banc de mesure dédié à mettre en place. La sélectivité du capteur sera apportée par une fonctionnalisation chimique de sa surface développée par un laboratoire du LETI-DRT/DTBS.

Cette proposition de thèse s'inscrit à la fois dans le cadre d'un projet européen ambitieux faisant collaborer les principaux centres de recherche du secteur (EPFL et IMEC), d'un projet ANR PNano 2009 avec Total (soumission 17/03/2009) sur la détection d'H_2S, et dans la collaboration bilatérale CEA-LETI MINATEC / Caltech portant sur l'intégration large échelle de NEMS (VLSI). Il permettra une valorisation du savoir faire acquis à Nanomix sur le développement de capteurs chimiques.

Autres projets potentiels :

- Un projet de recherche sur le transport thermoelectrique dans des matériaux complexes est en cours de montage avec Natalio Mingo de l'INAC. Se sujet se donne comme objectifs d'étudier l'utilisation de nanogaps dans des dispositifs thermoélectriques et d'étudier l'influence de paramètres tels que la rugosité des surfaces, la géométrie des nanogaps, la distance entre les surfaces. Des discussions sont en cours et devraient déboucher sur le dépôt d'un sujet de thèse.
- Intégration de graphène dans des dispositifs NEMS : Co-inventeur d'un brevet en cours de dépôt. Une demande de financement est en cours de montage pour permettre la réalisation d'un démonstrateur.
- Participation à de nombreux groupes de travail du CEA dédiés à l'électronique souple, aux procédés de fonctionalisation, aux capteurs chimiques , aux mémoires.